THERMAL CONDUCTIVITY OF PHENOLIC-CARBON CHARS

Wilson A. Clayton, et al

Boeing Company
Seattle, Washington

December 1969

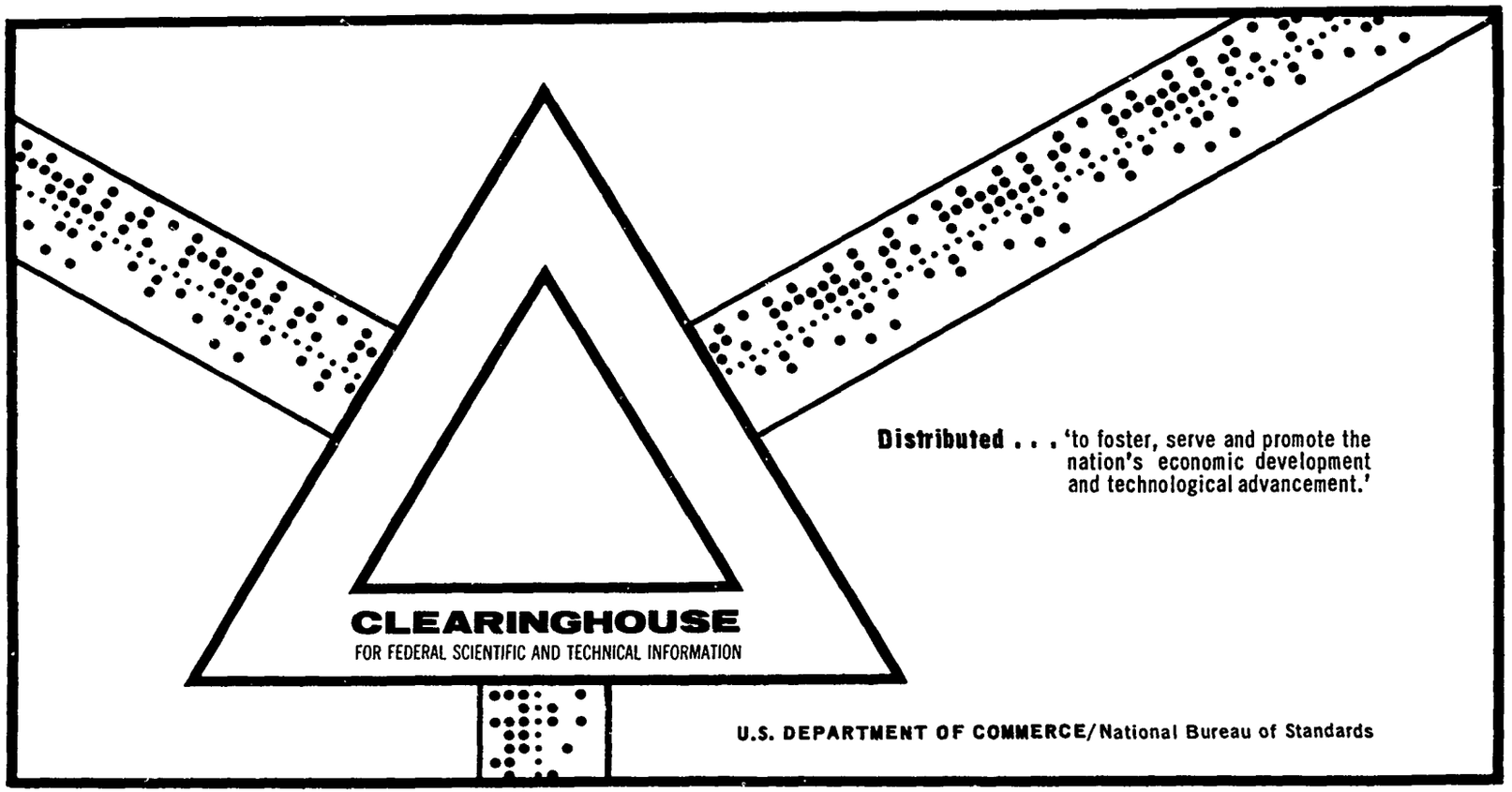

AFML-TR-69-313

THERMAL CONDUCTIVITY OF PHENOLIC-CARBON CHARS

W. A. Clayton

THE BOEING COMPANY
AEROSPACE SYSTEMS DIVISION

T. J. Fabish, J. F. Lagedrost

BATTELLE MEMORIAL INSTITUTE
COLUMBUS LABORATORIES

TECHNICAL REPORT AFML-TR-69-313
December 1969

AIR FORCE MATERIALS LABORATORY
AIR FORCE SYSTEMS COMMAND
WRIGHT-PATTERSON AIR FORCE BASE, OHIO

NOTICE

When Government drawings, specifications, or other data are used for any purpose other than in connection with a definitely related Government procurement operation, the United States Government thereby incurs no responsibility nor any obligation whatsoever, and the fact that the Government may have formulated, furnished, or in any way supplied the said drawings, specifications, or other data, is not to be regarded by implication or otherwise as in any manner licensing the holder or any other person or corporation, or conveying any rights or permission to manufacture, use, or sell any patented invention that may in any way be related thereto.

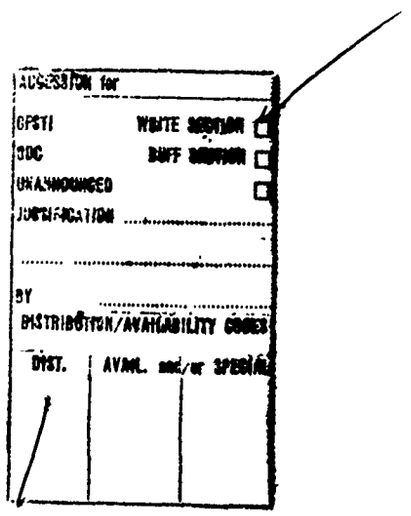

Copies of this report should not be returned unless return is required by security considerations, contractual obligations, or notice on a specific document.

Distribution of this document is unlimited.

THERMAL CONDUCTIVITY OF PHENOLIC-CARBON CHARS

W. A. Clayton
THE BOEING COMPANY

T. J. Fabish, J. F. Lagedrost
BATTELLE MEMORIAL INSTITUTE

FOREWORD

This report was prepared by the Aerospace Systems Division of The Boeing Company under USAF Contract Number F33615-68-C-1416, Project Number 7381. The work was administered under the direction of the Air Force Materials Laboratory, Materials Support Division, Task 738106, "Design Information Development", with Dr. Merrill L. Minges (MAAS) acting as Project Engineer. Gary L. Denman provided valuable technical assistance and performed comparative thermal diffusivity measurements at AFML.

The Boeing Company Program Manager and principal investigator was W. A. Clayton. The program was conducted in the Environmental Protection Group under the management of F. N. Breslich and Dr. E. E. Bauer, Manager, Materials Research and Development. A. C. Francisco prepared the thermal conductivity specimens and developed computerized data reduction methods. L. H. Hillberg conducted computer predictions of reentry ablation using the correlated thermal conductivity results. The contributions of G. W. Way in photomicrography, I. L. Brower in X-ray diffraction analysis, and G. Johanknecht, Dr. M. E. Taylor, and A. D. VonVolkli in other measurements is greatly appreciated.

Thermal conductivity, electrical resistivity, and porosity characterization measurements with comparison to hard carbon were conducted at the Battelle Memorial Institute Columbus Laboratories by T. J. Fabish and J. F. Lagedrost, Project Manager. These gentlemen provided the written discussion of their measurements in Sections IV, V, and VI and the appendices. Battelle acknowledges the assistance of the following staff members: W. A. Schmitt, A. R. Noe, L. Porter, A. S. Lower, L. Hildebrand, W. Keigley, L. Dillinger, A. Skidmore, and C. Brockway.

The authors wish to acknowledge the contributions of W. T. Barry of Aerospace Corporation, who supplied R-6300 chars for characterization, and of Haveg Industries, Inc./ Reinhold Aerospace Division, who supplied molded FM-5055A for this program.

This report covers work conducted from April 1, 1968 through September 30, 1969.

This report was submitted by the authors on November 10, 1969.

This technical report has been reviewed and is approved.

L. N. HJELM, Chief
Space and Missiles Systems Support Branch
Materials Support Division
AF Materials Laboratory

ABSTRACT

The thermal conductivity of several phenolic-carbon and phenolic-graphite ablative composites was established as a function of layup angle and temperature for ablation heating or cooling from -10°F to over 5000°F. Conductivity was measured on virgin and charred FM-5055A phenolic-carbon as a function of layup angle and heating or cooling temperature to 5000°F. These measurements, plus new measurements on charred MX-4926 phenolic-carbon and FM-5014 phenolic-graphite were made by the steady-state, unidirectional, comparative disk method. Furnace charred conductivity specimens were shown to represent ablation chars by detailed characterization and by comparative thermal diffusivity measurements. Theory relating the constituent (cloth and matrix) and composite conductivities was used to correlate the new conductivity data and literature data on composites having the same reinforcements. The procedure provides correlated constituent conductivities for CCA-1 standard and high purity carbon cloth, WCA and WCB graphite cloth, and carbon powder filled and unfilled 91-LD and SC 1008 virgin or charred phenolic resins, from which the conductivity of virgin or charred composites is obtained within the accuracy of composite conductivity measurements. All results are expressed as equations for direct substitution in ablation computer programs, which was demonstrated for ballistic reentry ablation of FM-5055A phenolic carbon. The thermal conductivity of all carbon or graphite cloth reinforced phenolics increases versus layup angle and reinforcement volume fraction, is reduced by pyrolysis generated porosity, and increases in the mature char versus temperature and the degree of graphitization. Char characteristics and electrical resistivity measurements showed hard carbon behavior at all temperatures, as did thermal conductivity except for the reinforcements, which became graphite-like at high temperatures.

CONTENTS

FIGURES

TABLES

NOMENCLATURE

SYMBOLS

A	=	Area, ft^2
A,B,C	=	constants defined for equation (33)
C	=	constant of integration
C_D	=	drag coefficient
C_p	=	specific heat, BTU/lbm R
E	=	electrical potential, volts
I	=	current flow, amps
K	=	thermal conductivity, BTU in/hr-ft^2R
L	=	distance between measurement points
P	=	Volume fraction of discontinuous phase, used without subscript for pores
Q	=	Heat flow, BTU/hr
R	=	Roughness factor defined by equation (4)
T	=	Temperature, R
W	=	Weight, lbm
x	=	Dimension parallel to heat flow, inches
X	=	Pore shape factor
y,z	=	Dimensions perpendicular to heat flow, inches
X_p	=	Pyrolyzed resin fraction defined by equation (34)
Y	=	$K_0/K_{c_\perp}$ from equation (13)
α	=	Thermal diffusivity, ft^2/hr
β	=	Belle pore shape factor defined by equation (4)
ρ	=	Density, lb/ft^3
ρ	=	Electrical resistivity, ohm-cm
θ	=	Layup angle, degrees

Subscripts

a	=	Apparent or bulk property
ad	=	Apparent property on dry material
c	=	continuous phase constituent
c	=	Mature char value
d	=	Discontinuous phase
f	=	Reinforcement fibers
i	=	A single item or class
m	=	Mature char state
p	=	Pore conductivity
pr	=	Porous pyrolysis residue excluding reinforcement
r	=	Solid pyrolysis residue excluding reinforcement
s	=	solid material
v	=	virgin material value
//	=	Conductivity parallel to fiber axis
$\perp$	=	Conductivity perpendicular to laminate plane
1,2	=	Phase 1 or 2 in mixture equations
0,90	=	Principle layup angle property

SECTION I

INTRODUCTION

Analytical predictions of ablation performance require accurate values of thermophysical properties of ablators at the temperatures and states of decomposition encountered during ablation. Design of carbon or graphite cloth reinforced phenolic resin ablation systems for large rocket motors and reentry vehicles has been uncertain because of lack of char thermal conductivity values in over 80 percent of the ablation temperature range. In a previous program[1,23], it was shown that stable, furnace charred specimens could duplicate chars recovered from tested hardware. Accurate, steady state thermal conductivity measurements on furnace chars representing several stages of ablation could then be correlated to predict the conductivity for all stages of ablation. An initial correlation of thermal conductivity and specific heat data to 4500°F was obtained for MX-4926 phenolic-carbon and FM-5014 phenolic-graphite rocket nozzle materials. Characterization of plasma ablation chars of FM-5055A phenolic-carbon was also obtained.

The objective of this program was to extend the techniques developed on the previous program[1,23] to establish the thermal conductivity for all stages of ablation encountered to 5000°F in FM-5055A phenolic-carbon composites typical of those used on high performance ballistic reentry vehicles. Stable conductivity specimens were to be produced by Boeing for measurement of thermal conductivity by Battelle Memorial Institute. Thermal conductivity parallel and perpendicular to the laminate and across 30-degree layup composites was to be obtained for virgin material, partially pyrolyzed char, ungraphitized char, and chars having intermediate and high levels of graphitization. Extensive specimen characterization was to be conducted before and after the conductivity tests. Electrical resistivity measurements parallel and perpendicular to the laminate were to be made by Battelle for additional insight into the charred material behavior.

All FM-5055A thermal conductivity results were to be correlated for use in ablation analysis on the basis of material characteristics, ablation theory, and heat transport theory. Available data on similar materials was to be considered to determine if any correlation was applicable to phenolic-carbon materials as a class. A preliminary characterization of R-6300 chars exposed to severe environments was to be made, and available thermal conductivity data on this material was to be correlated. The correlation procedure finally adopted was to be demonstrated in a typical reentry ablation analysis.

The accomplishment of the program objectives presented in this report provides the thermal conductivity of several related phenolic-carbon and phenolic-graphite materials for ablation applications.

SECTION II

SUMMARY

This final report to the Materials Support Division summarizes work on Contract No. F33615-68-C-1416. Thermal conductivity between room temperature and 5000°F was measured on virgin and charred FM-5055A phenolic-carbon, and correlated along with available conductivity data on other materials for use in ablation analysis. The Boeing Company prepared and characterized the thermal conductivity specimens and Battelle Memorial Institute performed conductivity and porosity distribution measurements.

Thermal conductivity data was obtained parallel to the phenolic-carbon cloth laminations, representing ablators with laminations perpendicular to the char surface (90° layup angle material), perpendicular to the laminations representing ablators laid up parallel to the char surface (0° layup angle material), and across material with a layup angle of 30° to the char surface. Uniformly charred conductivity specimens were produced in argon in an induction heated graphite retort at maximum temperatures of 825, 1800, 3000 and 5000°F, corresponding to one-half pyrolyzed, fully pyrolyzed, moderately graphitized, and highly graphitized ablation chars. The term graphitization is used to describe the increase in carbon char crystallinity with temperature that approaches the characteristic crystal spacing of graphite. Specimens were produced from dense virgin FM-5055A phenolic-carbon precursor produced by Haveg/Reinhold to reentry vehicle specifications. 1800°F chars at 0- and 90-degree layup angles were also produced from low density virgin material to give data on chars having the higher porosity found in post-ablation chars(1).

Thermal conductivity was determined under vacuum by the steady state, unidirectional comparative disk method with an estimated precision of ±10%. Most measurements were made at temperatures below the furnace charring temperature where the specimens were stable, while measurements on the low density 1800°F chars were made at increasing temperatures up to 5000°F to determine the effect of graphitization versus temperature. New conductivity data was also obtained on graphitized chars of MX-4926 phenolic-carbon and FM-5014 phenolic-graphite composites studied on a previous program(1).

The correspondence of the FM-5055A furnace-charred conductivity specimens to charazterized post-ablation chars(1) was demonstrated by conductivity specimen characterization, and by thermal diffusivity measurements performed by the Air Force Materials Laboratory on both furnace chars and post-ablation chars. Bulk density, solid density determined in helium, and total porosity obtained before and after the conductivity measurements below the furnace charring temperatures showed that no changes had occurred. X-ray diffraction intensity measurements on furnace

chars agreed well with values obtained previously[1] on post-ablation chars. Polarized light photomicrographs and X-ray diffraction measurements showed that the crystal density in chars increased with temperature, and that the reinforcing fiber, with an adhering pyrolytic deposit, was the most highly ordered constituent as noted in post-ablation chars[1]. Conductivity values derived from AFML diffusivity measurements on both furnace chars and post-ablation chars demonstrated directly the correspondence between the two sources of char, and were in general agreement with the steady state conductivity results.

A detailed study of porosity characteristics in the conductivity specimens showed that pore size, shape and orientation factors were extremely complex, and that pyrolysis residue pore size distribution varied versus temperature in the same manner as hard or glasslike carbons. Pore size distribution changes accompanied graphitization during initial heating in chars, and were shown to influence the solid density measurements in helium. Measurements of electrical resistivity versus initial heat treatment and lower, ambient temperatures on both 0- and 90-degree layup material showed that hard carbon behavior was obtained, and that changes in electronic properties in chars occurred at high rates. The analogy to hard carbon behavior was also noted in most of the thermal conductivity results; the exceptions being 90-degree layup graphitized chars where the composite conductivity is controlled by the graphitized reinforcement.

All of the thermal conductivity data obtained on this program and the previous one[1], plus literature data on virgin materials with the same reinforcements[31], were successfully correlated for use in ablation analysis. The correlation was accomplished by applying new theory[22] that relates composite and constituent (fiber and matrix) thermal conductivities for all layup angles. The theory was extended to demonstrate that virgin material constituents must be isotropic to obtain a correlation, but that fiber axial conductivity and pyrolysis residue crossply conductivity were sufficient for chars having anisotropic constituents. A closed form expression for the theory applicable for all normal laminates was obtained for application in in-depth computer ablation predictions.

To correlate thermal conductivity data, the theory was applied to predict the conductivities of the reinforcements, the virgin resins, and the resin pyrolysis residues from the measured composite conductivities. The reinforcement conductivities were not affected by resin pyrolysis. The predicted constituent conductivities were then correlated with temperature, including graphitization effects, and expressed as equations applicable to either heating or cooling conditions accompanying ablation. The equations for correlated constituent conductivities are then combined in the closed form theoretical expression to describe the composite conductivity behavior versus temperature during ablation. The success of this approach was demonstrated by accurate predictions of phenolic resin conductivity, which had been independently

measured[31], and by the agreement among constituent conductivities predicted from several sources of composite conductivity data. Composite conductivities for ablation analysis are obtained within the accuracy of the measured values and the reproducibility of thermal conductivity specimens; ±12% for all virgin material and ±25% for chars having layup angles greater than 20-degrees. Large uncertainties in the thermal conductivities of lower layup angle chars remain, due primarily to the variable influence of delaminations.

The expression that provides composite conductivity for ablation analysis from correlated constituent conductivities is equation (33) near the end of Section III in the text. Correlated constituent conductivities for use in this equation are given as functions of temperature for heating or cooling by equations (38) through (44) in Section VII. Composite conductivity in the pyrolysis zone during ablation is estimated by using the pyrolysis fraction weighted average of the virgin resin and mature char pyrolysis residue conductivities. This is expressed by equations (34) and (35) at the end of Section III. Equations (33) through (35) together with the applicable expressions for constituent properties may be incorporated directly in ablation computer programs. Alternately, composite conductivity versus temperature for the virgin and mature char states can be calculated using equation (33), and substituted in existing computer programs utilizing pyrolysis fraction weighted composite conductivities in the pyrolysis zone. Both approaches were demonstrated in Section IX for ablation of 20-degree layup FM-5055A phenolic-carbon on a high-performance ballistic reentry vehicle. There was no difference in predicted overall ablation performance, but pyrolysis zone conductivity was slightly higher, and the pyrolysis zone thickness tended to be greater using the new procedure.

The conductivity correlation procedure based on constituent conductivities should enable prediction of the conductivity of any composite for which the constituent conductivities have been established. The influence of composite variables such as resin content is also provided. Equations are provided in Section VII for Hitco CCA-1 standard or high purity carbon cloth (from FM-5055A and MX-4926 data), National Carbon WCA and WCB graphite cloth (FM-5014 and others), carbon powder filled CTL 91-LD (FM-5055A and FM-5014) and Monsanto SC 1008 (MX-4926) phenolic resins and their pyrolysis residues, and unfilled SC 1008 resin (R-6300 and others). Attempts to establish the high temperature behavior of 3M Pluton B-1 carbon cloth used in R-6300 composites discussed in Section VIII were unsuccessful due to lack of suitable literature data. Extensive graphitization of CCA-1 carbon fiber raised its conductivity above that of WCA or WCB graphite fibers at high temperatures.

The thermal conductivity of all carbon or graphite cloth reinforced phenolic ablators increases versus layup angle and reinforcement volume fraction, is reduced by pyrolysis generated porosity, and increases in the mature char versus temperature and the degree of graphitization. No evidence of rate controlled graphitization was obtained, and no significant radiation component of thermal conductivity was detectable in the data from this program.

SECTION III

THEORY FOR THERMAL CONDUCTIVITY OF CARBON AND GRAPHITE REINFORCED CHARRING ABLATORS

Classical one-dimensional thermal conductivity is the material property required for the in-depth analysis of the ablation process using available ablation computer programs. In the heterogeneous, anisotropic ablators, the fundamental hypothesis of thermal conductivity for the isotropic solid embodied in Fourier's law is generalized to apply at each point in the material, but the resultant overall heat flow and temperature gradient vectors may not be parallel as in the case of the isotropic solid [8]. The desired property is then the thermal conductivity normal to the isotherms. This is the thermal conductivity measured in this program, discussed in Section IV, and the thermal conductivity considered in the theory summarized in this section.

In a recent thesis, Clayton [22] presented a review of available relationships for thermal conductivity in multiphase solids and developed new relationships specifically for cloth reinforced ablators. Employing a simplified thermal model for refractory reinforced ablators and a new, generalized variable dispersion equation for the effect of high conductivity reinforcement fibers perpendicular to the heat flow, Clayton obtained relationships for the conductivity of the composite ablator in terms of the conductivities of the major constituents; a continuous resin or pyrolysis residue constituent and a discontinuous reinforcement fiber constituent. Accounting for the effects of constituent changes during ablation, e.g. the pyrolysis of a continuous phenolic resin constituent to a continuous carbon char constituent with included voids, and graphitization in both the pyrolysis residue and carbon fiber constituents, provided a basis for describing the behavior of the composite thermal conductivity during ablation.

The approach described above provides a new method for predicting, from measured thermal conductivities obtainable only at stable states, the conductivity of all stable and unstable states encountered during ablation as required for ablation performance predictions. Measured composite conductivities are used to predict constituent conductivities, which are correlated with temperature and then recombined to describe the composite conductivity behavior during ablation in any desired direction through the laminated composite.

A rather large body of relationships have been developed to describe thermal conductivity in heterogeneous solids of interest in engineering. Typically these equations describe the conductivity of materials consisting of two discrete components, a continuous phase of one conductivity with included particles (i.e. voids or fibers in the case of chars) of a discontinuous phase of another conductivity.

Most equations are derived for a given geometrical distribution of the constituents and are derived in terms of solid conduction only. As long as solid conduction is dominant, radiarion transport may be handled as a simple, additive term [22,24]. Convection transport or radiation absorption by pyrolysis gases are assumed not to be included in the thermal conductivity as it is applied in ablation analysis. A thermal model of the ablators in terms of the geometries of the constituents for which available theory can be applied was developed as follows.

THERMAL MODELS FOR CARBON AND GRAPHITE FIBER REINFORCED ABLATORS

The phenolic-carbon and phenolic-graphite ablation materials and the basic changes that occur when they ablate were described previously in References 1, 22 and 23. Additional detailed characterization of the FM-5055A phenolic-carbon material of this study is presented in Section VI. These results show that the only significant geometrical change accompanying ablation is the development of porosity in the pyrolyzed phenolic resin phase. This is accompanied by up to 5% shrinkage in the crossply direction of unrestrained laminates. Two measurable chemical changes occur, pyrolysis of the phenolic to form carbon, and graphitization or ordering in the solid carbon constituents at high temperatures. While it was possible to obtain a reasonable description of the effect of these changes in terms of measured thermal conductivities [1,23], no generalized quantitative description of the behavior of composite conductivity between the states of material where conductivity was measured was possible. To do this utilizing the available theory requires separate consideration of the behavior of the various solid constituents of the material. Constituent geometry in terms of simple configurations is required.

Detailed ablator characterization studies have emphasized high magnification examination of the virgin and charred materials to illustrate the nature of the porosity and graphitization developed during ablation. Additional analysis of the available photomicrographs and low magnification inspection of charred samples indicated the following points significant in developing a description of the constituent geometries in carbon and graphite cloth reinforced phenolics:

1) All fibers in the cloth yarn bundles are separated either by virgin resin or by porous pyrolysis residue. The fibers are a discontinuous phase.

2) Yarn bundles are made up of untwisted fibers. The fibers can be considered to be parallel.

3) The fiber cross-section is serated, but the serations are not deep and the fiber cross-section can be considered to be circular. The fibers can be considered to be cylinders.

4) All large pores in reinforced areas are elongated in the fiber direction. This was noted previously[1].

5) Large pores may combine in the cross-fiber direction to form platelet shaped pores or cracks in random directions across the yarn fiber bundle.

6) The maximum length of cracks is the width of the yarn fiber bundle at the location it occurs, except those between cloth layers may continue to form a delamination.

7) All pyrolysis residue is porous, even in small spaces around closely packed fibers.

8) Carbon powder filler in the virgin phenolic resin or its carbon pyrolysis residue cannot be distinguished by optical techniques due to its small size. No agglomerated powder was visible, so it is assumed that all powder filler was uniformly distributed.

9) As noted previously [1], graphitized material visible in polarized light photomicrographs lies primarily along fiber surfaces, particularly in the areas of major cracks.

Except for delaminations, if they occurred, all of the above observations suggest that the reinforcing fibers and oriented porosity and graphitization must be the contributors to the directional dependence of thermal conductivity in phenolic carbon and phenolic graphite. Only a portion of the porosity is nonspherical, so the high concentrations of reinforcing fibers must be the major contributor to the directional dependence of thermal conductivity. This is, of course, expected.

Concentrated graphitization visible adjacent to fiber surfaces (see also Section VI) may be treated in this study as a change primarily in the fiber properties rather than in the pyrolysis residue properties. This is an assumption for convenience, since the available equations for conductivity in heterogeneous materials do not in general provide for either a cylindrical inclusion (fiber) coating of a different conductivity, or for more than two phases, one continuous and one discontinuous, of different conductivities. While the presence of an apparently distinct graphitized phase limits the ability to obtain from the conductivity data an estimate of the conductivities of either the fiber or continuous surrounding phase conductivities, the

above assumption does provide a basis for estimating the effects of graphitization on the overall conductivity. The carbon powder filler in the continuous resin or pyrolysis residue phase need not be treated separately. Since it is uniformly dispersed powder very small in size relative to the discontinuous phase fibers, it can simply be considered as a portion of the isotropic continuous phase.

Application of equations for the effect of the constituents on thermal conductivity requires a geometrical model for the discontinuous phase of the phenolic carbon and phenolic graphite ablators. The above observations show the reinforcing fibers to be the major discontinuous phase applicable to all states of the materials encountered during ablation. A thermal model of this phase was obtained by consideration of the construction of the woven cloth reinforcement and by low magnification observation of the samples on which thermal conductivity was obtained.

The thermal model obtained for FM-5055A and MX-4926 phenolic-carbon, both containing CCA-1 carbon cloth reinforcement, is illustrated in Figure 1. The model is equally applicable to all similar untwisted yarn reinforcements woven in the eight harness satin pattern. The significant feature of this weave is that yarns in one direction cross over only every eighth yarn in the other direction. The crossovers occur at shallow angles so that the departure from a straight path is slight, besides involving only about 1/8 of the volume of each ply. Some compression occurs at each crossover, leaving a rectangular dip filled with resin on each side of the ply that is one yarn width wide, two yarn widths long (in opposite directions on each side of the ply) and about 0.1 ply thickness deep. The shallow angle of the fibers at the crossover plus greater fiber concentration due to compression will tend to slightly raise the conductivity perpendicular to the ply in the local area of the crossover. The shallow depression filled with lower conductivity continuous phase material will be in series for heat flow perpendicular to the laminate (0-degree layup material), and if this is considered to be a platelet inclusion it will tend to lower the conductivity in the local area of the crossover. Local effects on conductivity at the crossover are therefore partially self-compensating, and since the crossovers occupy a minor portion of the total ply volume, their effects will be assumed to be negligible. Crossovers can be expected to have even less effect on conductivity parallel to the ply direction, since all available relationships predict that elongated inclusions such as the fibers or the platelets described above show the most influence due to orientation when they are nearly normal to the heat flow rather than nearly parallel.

With the effect of crossovers in the eight harness satin weave considered to be negligible, a minimum repeating reinforcement unit cell was defined as shown in Figure 1. The cloth ply is seen to be modeled as two layers of parallel yarns, one layer perpendicular to the other. For CCA-1 reinforcement, each yarn consists of

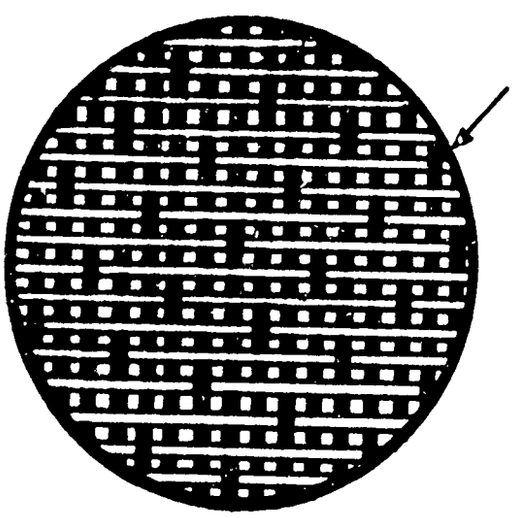

EIGHT-HARNESS SATIN WEAVE CARBON CLOTH
(not to scale)

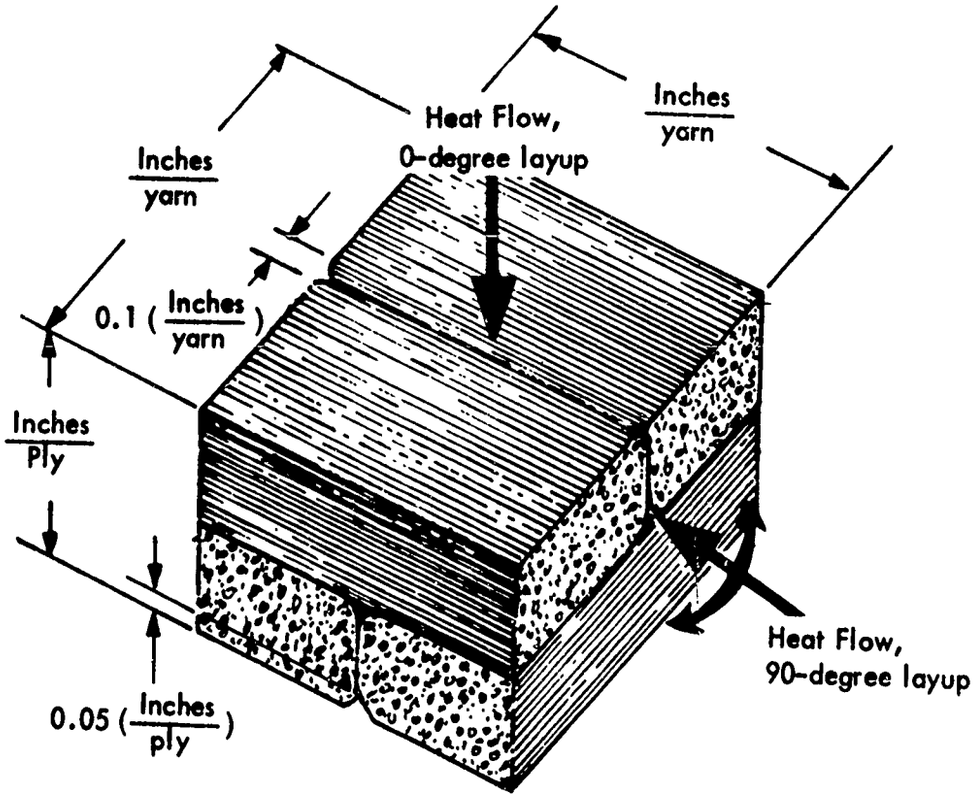

SATIN WEAVE UNIT CELL
(~ to scale)

FIGURE 1 PHENOLIC CARBON THERMAL MODEL

720 parallel fibers or filaments[1], which for heat transfer purposes are modeled as straight cylinders. The yarn bundles are flattened considerably by the high pressure (1000 psi) molding process (Reference 1 and Section VI) used on these materials. The unit cell is illustrated approximately to scale in Figure 1. Also illustrated is the slight rounding that occurs at the corner of each yarn and the fact that there is a physical separation around each yarn consisting of up to one mil of the continuous phase. These effects occupy less than five percent of the volume and can be neglected for analytical purposes within the accuracy of the data. Of course, the boundaries between parallel yarn bundles are usually not straight as indicated. This has no effect on the analysis since under the above assumptions the reinforcement fibers, not the yarn bundles, are considered to be the describable dispersed phase. Unit cell dimensions are obtained by counting the number of yarns per inch and the number of plys per inch in the conductivity samples, as indicated. These values are discussed later.

The thermal model obtained for FM-5014 and other phenolic-graphite materials having square weave graphite cloth reinforcement is illustrated in Figure 2. The square weave cloth, consisting of yarns having 1440 untwisted fibers or filaments in FM-5014[1], is not as simply modeled as the eight harness satin weave since every yarn must cross over to the other side of each perpendicular yarn it encounters. The resulting minimum repeating unit cell for this reinforcement is also illustrated in Figure 2. Drawn approximately to scale, the unit cell illustrates that the yarn bundles are flattened to an even greater extent than in the eight-harness satin weave and that the angles formed in the crossovers are reasonably shallow, on the order of 13° average, though not as shallow as in the less restrained eight harness satin weave. Also a fairly substantial depression exists at the center of each unit cell. If this area is considered to be an oblate ellipsoid or platelet of the continuous phase in series with the portion including angled reinforcement, then the overall effect approaches that modeled by the unit cell for phenolic-carbon due to the self-compensating effects described previously. On this basis, plus the fact that no exact expressions are available for a one-dimensionally continuous dispersed phase that is not straight, the model for satin weave phenolic-carbon will be adopted for square weave phenolic-graphite for analytical purposes. This model is obviously a much poorer representation of the square weave cloth reinforced phenolic-graphite. While it was found to be beyond the scope of this study to derive exact expressions for this case of extensive yarn crossovers, the model neglecting crossovers is expected to provide useful results for this case where the crossover angles are shallow and some compensating effects exist.

The actual sizes of the unit cells are not required for analytical purposes unless they vary between states of material encountered during ablation. The number of plys per inch in MX-4926 phenolic-carbon studied previously [1] increases

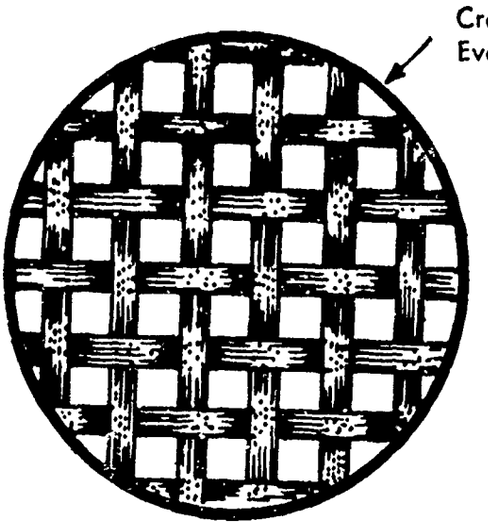

SQUARE WEAVE GRAPHITE CLOTH
(not to scale)

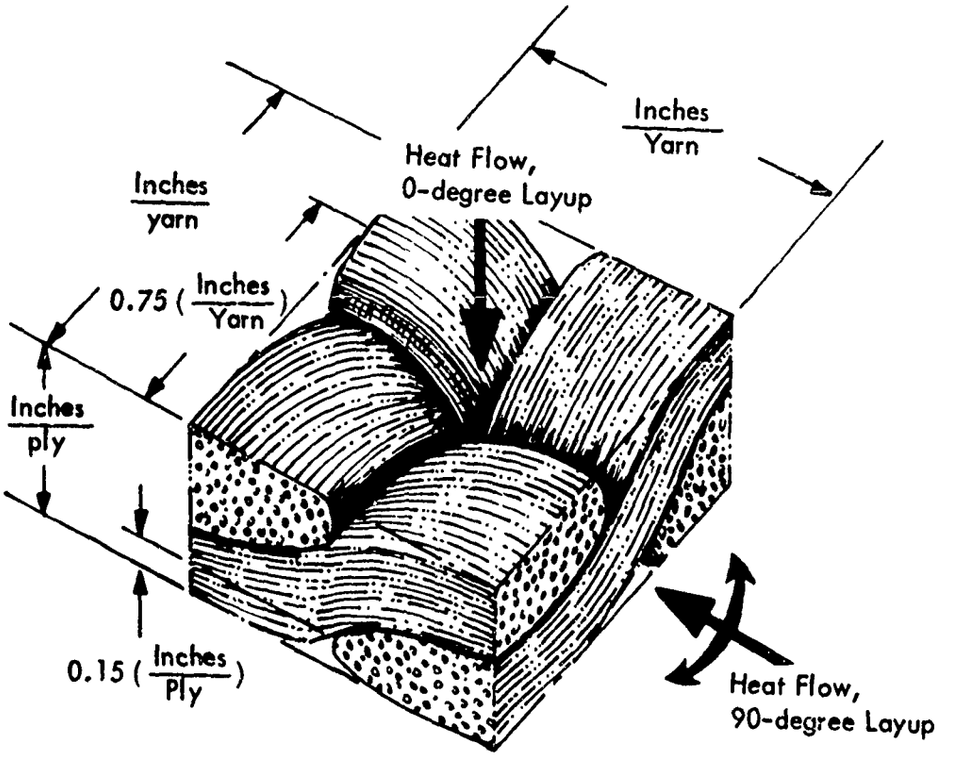

SQUARE WEAVE UNIT CELL
(~ to scale)

FIGURE 2 PHENOLIC GRAPHITE THERMAL MODEL

from 76 in the virgin material to 80 in fully charred material. In FM-5014 phenolic-graphite the number of plys per inch increases from 60 in the virgin material to 62 in fully charred material. These values correspond to total crossply shrinkages of 5.5% and 3.2% respectively that were noted previously for pyrolysis of these materials [1]. Yarn per inch counts in the cloth plane were constant at 48 and 27, respectively, for the two materials. These measurements showed that a minor change due to crossply direction shrinkage is the only measurable change that occurs in the unit cell size during ablation. All of this change occurs during pyrolysis, once the materials are fully charred they are stable. The FM-5055A phenolic-carbon investigated in this study behaves the same way, but total shrinkage is about the same as the FM-5014studied previously, probably because the same carbon powder filled resin system is used in both materials. Yarn counts per inch in all materials investigated were the same in both yarn directions in the cloth plane. Therefore, if the yarn directions are considered as principal directions for heat flow in the cloth plane (90-degree layup material) the conductivity in each of these principal directions would be the same. On this basis, equation (1) presented later for the effect of layup angle shows that if the conductivities in two principal orthogonal directions in a plane are equal, the conductivity is the same for all directions in the plane [8]. The fact that heat flow was in the cloth bias direction in 90-degree layup FM-5055A phenolic-carbon specimens on this study and in MX-4926 conductivity specimens studied previously [1] and in different directions along each cloth plane in FM-5014 phenolic-graphite studied previously [1] is then immaterial. The heat flow direction for the 90-degree layup case has been illustrated as along one of the principal directions in the cloth plane in Figures 1 and 2 for convenience in the development of mathematical relationships relative to the thermal model.

Since shrinkage occurs during the production of charred conductivity specimens by slow heating rather than during rapid heating accompanying ablation [1], it becomes one of the factors to be considered in relating the measured conductivities to conditions existing during active ablation pyrolysis. Correlation of the measured conductivity data itself can be carried out on the basis of the stable volume after shrinkage. The effect is that the volume concentration of reinforcing fibers is slightly higher in furnace charred material than in virgin material or in active ablation charred material. Also, as shown in Reference 1 , the porosity is lower in furnace charred material used for the conductivity measurements than in active ablation charred material. It will be seen later than such minor effects as a small difference in porosity can not be resolved within the certainty of the available data.

INFLUENCE OF REINFORCEMENT ORIENTATION AND LAYUP ANGLE

In the development of the thermal models it was shown that the major discontinuous phase common to all states of material during ablation is the reinforcement. This was the constituent modeled in Figures 1 and 2, and the simple model of Figure 1 is to be used to represent all carbon or graphite cloth reinforced ablators. Because the reinforcement is continuous in one dimension, it is also the major contributor to a strong directional dependence of thermal conductivity in the ablator composites. The requirements for any theory relating the composite conductivity to the conductivity of the constituents are given by the requirements for describing the directional dependence of the composite thermal conductivity.

The laminated chars, as represented by the thermal model in Figure 1, can be considered as an orthotropic solid which has different conductivities in three mutually perpendicular directions. Since yarn counts were the same in both yarn directions and oriented nonspherical pores did not form in a way to prefer one yarn direction over the other, then the conductivity in the two mutually perpendicular yarn directions is the same. For the moment, it is then assumed that conductivity in the plane of the cloth laminate is then independent of direction in the plane. In this case, conductivity, K_θ, across any plane oriented at a layup angle, θ, to the laminate is given by:

$$K_\theta = K_0 \left[1 + \left(\frac{K_{90}}{K_0} - 1 \right) \sin^2 \theta \right] \qquad (1)$$

where subscripts 0 and 90 refer to the heat flow normal ($\theta = 0$) and parallel ($\theta = 90$) to the laminate plane. If K_{90} and K_0 referred to orthogonal planes perpendicular to the laminate plane and extending in the fiber directions, then $K_{90} = K_0 = K_\theta$ and the assumption that conductivity is independent of direction in the laminate plane is substantiated by equation (1).

Equation (1) describes the directional dependence of thermal conductivity, and will describe all possible conductivities for the ablators if expressions for K_0 and K_{90} are obtained. These expressions are what is required from any theory describing the effect of the material constituents.

It should be noted that equation (1) is derived for conductivity perpendicular to isotherms[8], the property required for ablation analysis. Equation (1) was derived in Reference 8 from basic heat transport theory applied to isotropic, but homogeneous, material. The reinforced ablative composites are obviously heterogeneous rather than homogeneous in the usual sense. However, equation (1) has been shown to apply for phenolic-carbon materials previously[1], and is also shown to apply to the FM-5055A thermal conductivity data versus layup angle of this study in Section VII.

RELATIONSHIPS FOR THE INFLUENCE OF FIBERS AND VOIDS NOT CONTINUOUS IN THE HEAT FLOW DIRECTION

It was shown above that if the influence of the constituents on thermal conductivity can be obtained for the principal layup angles, 0 and 90 degrees, then the constituent influence at any other layup angle can be obtained using equation (1). Figure 1 showed that the major discontinuous constituent, the reinforcing fibers, can be considered as either parallel or perpendicular to the heat flow. The fibers can be described as cylinders. Another significant discontinuous phase is the voids produced during pyrolysis. Investigation of void geometry is discussed in detail in Section VI, where it is shown that many void shapes and orientations occur and the graphitization affects the voids. For fibers parallel to the heat flow Ohms law for parallel conductors applies, but for all other orientations of fibers and voids, the general relationships reviewed below are required. The simple solution offered by Ohms law for series constituents does not apply because the constituents are not true series lamina perpendicular to the heat flow[22].

Three general classes of relationships are available to describe the influence of a discontinuous phase on composite conductivity[14]. One type is the exact solutions for dilute dispersions where there is no particle interaction, or for higher concentrations where the influence of particle interaction is accounted for. The second type is variable dispersion solutions, which are a semi-empirical mathematical extension of exact dilute dispersion solutions to higher concentrations where particle interaction occurs. The third type is the mixture equations, which are empirical equations derived on the basis of the assumption that the discontinuous phase, in an unspecified manner, becomes the continuous phase as its concentration is increased. Derivations of each type of equation except the generalized variable dispersion equation have been reviewed previously by Powers[14]. The derivation of the generalized variable dispersion equation[22] is given in Appendix H.

Each type of equation is presented below. In each equation, K is the conductivity of the composite, K_c is the conductivity of the continuous phase, K_d is the conductivity of the discontinuous phase of specified geometry, P is the volume fraction of the discontinuous phase, and β or X is the factor that accounts for the shape and orientation of the discontinuous phase. Only equations of interest in this study are presented. Other equations are given by Powers[14] and in the more recent review by Clayton[22].

The exact relationships begin with a derivation by Maxwell for the effective conductivity of a heterogeneous body composed of spheres of one conductivity so far apart that they have no influence on one another, embedded in a matrix of another conductivity. Eucken[15] first applied the Maxwell equation to thermal conductivity and showed that the discontinuous phase may consist of different sizes and kinds of

spherical particles. The applicable equation, for i kinds of spherical particles in the discontinuous phase, is the Maxwell-Eucken dilute dispersion equation written as:

$$\frac{K}{K_c} = \frac{1 - 2\sum_i P_i \left(\frac{1 - K_i/K_c}{1 + 2K_i/K_c}\right)}{1 + \sum_i P_i \left(\frac{1 - K_i/K_c}{1 + 2K_i/K_c}\right)} \qquad (2)$$

Of course, if all K_i are identical, the summation is removed and K_i is simply K_d, making equation (2) identical to the original Maxwell equation. To account for particle interactions, a specific particle arrangement, usually a cubic array, must be specified. Exact solutions for a cubic array of uniform spheres at any concentration up to the closest packed cubic condition are available[14], but are of little interest for application to the nonuniform porosity in chars. These solutions are nearly identical to equation (2) for concentrations $P < 0.25$ of uniform spheres; and particle interaction effects are not large until the closest packing condition is approached[14].

For uniformly sized cylinders perpendicular to the heat flow, an accurate description of the reinforcement fibers, Lord Rayleigh[25] derived an exact solution for the case of a square array that applies for all concentrations of fibers up to the closest packed square array. This equation is:

$$K/K_c = 1 - \frac{2P}{\frac{1 + K_d/K_c}{1 - K_d/K_c} + \frac{P - 0.3058P^4}{\frac{1 + K_d/K_c}{1 - K_d/K_c}} - \frac{0.135P^8}{\frac{1 + K_d/K_c}{1 - K_d/K_c}}} \qquad (3)$$

At low P, the higher order terms are negligible and equation (3) reduces to a dilute dispersion form similar to equation (2) without the summation. The higher order terms in equation (3) actually increase K/K_c by only about 2% at a $P = 0.5$ fiber concentration typical of phenolic-carbon or phenolic-graphite. The major difficulty with equation (3) is the restriction to a square array of the fibers, which gives the minimum effect of possible interactions due to adjacent fibers. Application of equation (3) is demonstrated later.

For the special case of low concentration, P, combined with $K_d = 0$, applicable to a dilute dispersion of pores, equations (2) and (3) were written by Belle[26] in 1967 in the form:

$$K/K_c = \frac{1 - P}{1 + \beta P} \quad ; K_d = 0 \qquad (4)$$

where β = pore shape factor
= 1/2 for spheres, from equation (2)
= 1 for cylinders $\perp$ to the heat flow, from equation (3)
= 0 for cylinders or lamina // to the heat flow, from Ohm's law.

From consideration of the known values of β for spherical and oriented cylindrical pores given above, Belle[26] generalized β to the three dimensional case of oriented ellipsoidal pores in a form that also yields the correct β values listed above. The resulting empirical expression for β has been shown by Clayton[22] to be a very good approximation of the cumbersom pore shape factor expression for oriented ellipsoidal pores derived from exact theory. The empirical expression for β is:

$$\beta = R \frac{\frac{1}{x}}{\frac{1}{y} + \frac{1}{z}} \qquad (5)$$

where:

x = ellipsoidal pore axis perpendicular to the heat flow

y, z = the other two axes

R = a roughness factor for departure from ellipsoidal pore shapes; assumed = 1 within engineering accuracy[26]

Equations (4) and (5) were used previously to correlate char thermal conductivity data assuming that the development of porosity accompanying pyrolysis was a major variable describing the behavior of thermal conductivity during pyrolysis[1]. The total porosity of the laminated composite was used, whereas consideration of the major constituents separately suggests that the effects of porosity development during pyrolysis are confined to the continuous resin matrix. In this case the porosity values based on the volume of the matrix alone may be very high, and equation (4) for dilute dispersions would be expected to underestimate the effect of porosity.

To obtain an expression for the effect of a discontinuous phase at high concentrations without the restrictions to one size of particles in a square array, the exact solutions for dilute dispersions can be extended to high concentrations mathematically to yield the semi-empirical variable dispersion solutions. The derivation of a generalized variable dispersion equation[22] following the method used by Bruggeman[27] for the special case of spherical discontinuous phase particles, is given in Appendix VIII. The result is:

$$1 - P = \frac{K_d - K}{K_d - K_c}\left(\frac{K_c}{K}\right)^{\frac{1}{X+1}} \qquad (6)$$

where:

X = shape factor for discontinuous phase

= 2 for spheres

= 1 for cylinders $\perp$ heat flow

= $1/\beta$ for oriented ellipsoids; $K_d = 0$

= complex expressions from Reference 22 for randomly oriented or finite conductivity ellipsoids.

For the case of interest where the discontinuous phase consists of spherical or oriented ellipsoidal pores having $K_d = 0$, equation (6) becomes simply:

$$K/K_c = (1-P)^{\frac{X+1}{X}} = (1-P)^{1+\beta} \quad ; K_d = 0 \qquad (7)$$

For the case of interest where the discontinuous phase consists of cylinders (fibers) oriented perpendicular to the heat flow, equation (6) may be solved to give[22] (see Appendix VIII):

$$\left(\frac{K}{K_c}\right)^{1/2} = \frac{\left[(1-P)^2\left(\frac{K_d}{K_c}-1\right)^2 + 4\,K_d/K_c\right]^{1/2} - (1-P)\left(\frac{K_d}{K_c}-1\right)}{2} \qquad (8)$$

Equation (8) is applied later in the correlation of thermal conductivity data for this study. The results indicate equation (8) to be the most successful of the available relationships for describing the effect on thermal conductivity of reinforcing fibers perpendicular to the heat flow.

Both dilute dispersion and variable dispersion classes of relationships are derived on the basis that one phase is discontinuous with conductivity K_d and specified particle shape, and is completely surrounded by the second phase which is continuous with conductivity K_c. Both types of equations yield two curves, one for $K_d/K_c > 1$ and one for $K_d/K_c < 1$.[14]

if the discontinuous phase is not physically constrained, however, it is quite likely that coalescence of particles will occur as the volume fraction of the discontinuous phase, P, is increased. Coalescence has no effect on the dilute or variable

dispersion solutions if the same particle shape is maintained and the dispersed phase remains discontinuous. Coalescence outside these restrictions is normally represented by assuming that K_d becomes K_c as P is increased. How this happens in physical terms is not specified.. Relationship derived from dilute dispersion equations on this basis are classified as mixture equations. Mixture equations yield a single curve for all K_d/K_c that turns out to be the transition curve between the two curves for the corresponding dilute dispersion equation.

Many mixture equations are available which give substantially identical results even though the specific assumption used to describe the behavior of the mixture is not always the same as that given above. Whatever the form of the basic assumptions on the formation of the mixture, the derived mixture equations must be considered to be empirical in comparison to the equations for dilute and variable dispersions. This is due to the fact that any assumption concerning the formation of the mixture probably cannot be substantiated, plus the fact that a great degree of mathematical approximation is employed in the derivations. The general form for the mixture equations developed by Bruggeman[27] can be made to cover all of the cases of interest in this study. The equation, which applies only to isotropic phases, but to mixtures of many sizes of particles, is:

$$P_1 \frac{K_1 - K}{K_1 + XK} + P_2 \frac{K_2 - K}{K_2 + XK} = 0 \qquad (9)$$

where:

$P_1 + P_2 = 1$

P_1 = volume fraction of phase 1 having K_1

P_2 = volume fraction of phase 2 having K_2

X = shape factor for nominally discontinuous phase, with same values as in equation (6)

For the special case of pores occupying volume fraction P_1, where we may assign $K_1 = 0$, equation (9) reduces to:

$$\frac{K}{K_2} = 1 - P_1 \left(\frac{X + 1}{X}\right) ; K_1 = 0 \qquad (10)$$

Equation (10) is not considered satisfactory for general use; low density foams would have zero conductivity in vacuum if this equation applied.

One other special case of interest in this study is a Bruggeman derived mixture equation for platelets (oblate ellipsoids) with one diametric axis oriented normal to the flux while the other is randomly oriented. This corresponds to the description of cracks across yarn bundles given for the development of the thermal models when the heat flow is normal to the yarn. The equation is

$$K = \sqrt{\left(K_{x//Q}\right)\left(K_{y,z//Q}\right)} \quad ; \text{ platelet axis } x < y = z \qquad (11)$$

Input values for equation (11) can be obtained from the previous relationships for oblate ellipsoids. It is simply the geometric mean of the conductivities for a medium including platelets oriented perpendicular ($x//Q$), or parallel ($y,z//Q$), to the heat flow, Q.

As stated previously, all of the above equations were derived by consideration of solid conduction only. All of the equations are insensitive to the size of the particles of the discontinuous phase (fibers or pores in the case of chars), but depend on the total volume fraction of particles and their shape and orientation. Application of the available relationship to carbon or graphite reinforced phenolic abiators on the basis of the thermal model in Figure 1 is presented below.

DEVELOPMENT OF SOLUTIONS FOR THE EFFECTS OF MODELED CHAR CONSTITUENTS

The conductivities of the various components of the char may be indicated as follows:

K = overall conductivity, as before

K_c = conductivity of continuous phase resin or pyrolysis residue

K_s = conductivity of all solid material except pores

K_v = conductivity of virgin phenolic resin

K_f = conductivity of all pyrolysis residue except reinforcing fibers, including pores and carbon powder filler

K_{pr} = conductivity of all pyrolysis residue except reinforcing fibers, including pores and carbon powder filler

K_r = conductivity of above pyrolysis residue not including pores

K_p = conductivity of pores = 0, except for radiation across pores treated separately

$//$ or $\perp$ = additional subscripts noting whether heat flow in any phase is parallel or perpendicular to the fiber direction

All of the detailed characterization data available from reference 1 and the investigations of this study in Section VI indicate that the reinforcing fibers which make up the untwisted woven yarn should be considered as a dispersed phase. This is not surprising in a high quality laminate material, where good physical properties depend on thorough wetting and surrounding of all fiber bundles by the resin matrix. The most convincing evidence was high magnification photomicrographs, several of which are shown in reference 1 and Section VI, and all of which show the fibers to be clearly separated by a continuous matrix of virgin phenolic or porous pyrolysis residue.

The reinforcing fibers are physically constrained by the nature of the reinforced phenolic material to be a discontinuous phase and the carbon powder filled phenolic resin or its pyrolysis residue is constrained to be a continuous phase. These two constituents, then, form one natural pair for application of the available relationships for heterogeneous materials consisting of two phases. Since the volume fraction of reinforcing fibers, designated P_f, falls in the range 0.4 to 0.6 for the materials of interest, the dilute dispersion equations do not apply. Mixture equations do not apply because the fibers are all physically separated. The fibers can be represented as cylinders, so the applicable equations are the Ohms law equation for parallel conductors for fibers oriented parallel to the heat flow and either Rayleigh's equation (3) or the variable dispersion equation (8) for fibers oriented perpendicular to the heat flow. Note that in Rayleigh's equation all cylinders must be the same diameter, a test that is met in the case of the reinforcing fibers.

For fibers oriented parallel to the heat flow, Ohms law gives:

$$K_{//} = P_f K_{f_{//}} + (1 - P_f) K_{c_{//}} \qquad (12)$$

Of course, equation (12) and all others to follow can be written in terms of K_f and K_v or K_{pr} as well. For fibers oriented perpendicular to the heat flow, which describes all of the fibers for heat flow perpendicular to the laminate, the condition obtained in conductivity measurements on 0-degree layup specimens, we may write:

$$K_0 = Y K_{c_\perp} \qquad (13)$$

where:

$Y = \frac{K_0}{K_{c_\perp}}$ for cylindrical particle dispersions from equation (3) or (8)

On the basis of the thermal model, the conductivity of 90-degree layup specimens where the heat flow is parallel to the laminate direction can be represented by Ohms law for parallel conductors with half of the area represented by a dispersion containing fibers parallel to the flow and half containing fibers perpendicular to the flow. Adding these parallel conductivities using Ohms law gives:

$$K_{90} = \frac{1}{2} K_{//} + \frac{1}{2} K_0 \tag{14}$$

The basic relationship for K_{90} in terms of the constituents conductivities K_f and K_c is obtained by substituting equations (12) and (13) into equation (14):

$$K_{90} = \frac{P_f}{2} K_{f//} + \left(\frac{1 - P_f}{2}\right) K_{c//} + \frac{Y}{2} K_{c\perp} \tag{15}$$

In terms of the constituent conductivities and the experimentally determined conductivity K_0, the relationship for K_{90} is obtained by substituting only equation (12) into equation (14). We also at this time include the empirical concept that K_c may be different in the 90-degree direction than in the 0-degree direction by parameters, $\frac{K_{c//}}{K_{c\perp}} = n$, due to oriented nonspherical porosity. Also, possible fiber anisotropy is introduced by the parameter $\frac{K_{f//}}{K_{f\perp}} = m$.

$$K_{90} = \frac{P_f}{2} m K_{f\perp} + \left(\frac{1 - P_f}{2}\right) n K_{c\perp} + \frac{K_0}{2} \tag{16}$$

Equations (13) and (16) give both principal direction composite conductivities, K_0 and K_{90}, in terms of the two unknown constituent conductivities, $K_{f\perp}$ and $K_{c\perp}$. A solution for the unknown constituent conductivities is now possible, and the knowledge of the constituent conductivities so provided gives insight into their influence on the conductivities K_0 and K_{90} of the composite. A general solution for $K_{f\perp}$ and $K_{c\perp}$ is most conveniently expressed in terms of the ratio $K_{f\perp}/K_{c\perp}$ as a function of the ratio K_{90}/K_0 obtainable from the experimental data. Equation (16) may be solved for $K_{f\perp}/K_{c\perp}$ by the following manipulations.

Collecting terms and forming the ratio K_f/K_c in the P_f term from $mK_f - nK_c = \left(\frac{mK_f}{K_c} - n\right) K_c$

$$K_{90} = \frac{1}{2} K_0 + \frac{1}{2} n K_{c\perp} + \frac{P_f}{2}\left(\frac{mK_{f\perp}}{K_{c\perp}} - n\right) K_{c\perp} \tag{17}$$

Dividing by K_0 and further collecting terms:

$$\frac{K_{90}}{K_0} = \frac{K_{c_\perp}}{2K_0}\left[P_f\left(\frac{mK_{f_\perp}}{K_{c_\perp}} - n\right) + n\right] + \frac{1}{2} \qquad (18)$$

Equation (18) is a form useful in exact solutions illustrating how K_{90}/K_0 is influenced by $K_{f_\perp}/K_{c_\perp}$. Equation (18) or equation (17) may be solved for $K_{f_\perp}/K_{c_\perp}$. Dividing equation (17) by $K_{c_\perp}/2$ gives:

$$2\frac{K_{90}}{K_{c_\perp}} = \frac{K_0}{K_{c_\perp}} + n + P_f\left(\frac{mK_{f_\perp}}{K_{c_\perp}}\right) - n P_f \qquad (19)$$

Solving for $K_{f_\perp}/K_{c_\perp}$ gives:

$$\frac{mK_{f_\perp}}{K_{c_\perp}} = \frac{2K_{90}}{P_f K_{c_\perp}} - \frac{K_0}{P_f K_{c_\perp}} - \frac{n}{P_f} + n \qquad (20)$$

Collecting terms:

$$\frac{mK_{f_\perp}}{K_{c_\perp}} = \frac{1}{P_f K_{c_\perp}}(2K_{90} - K_0) + n\left(\frac{P_f - 1}{P_f}\right) \qquad (21)$$

Forming the ratio K_{90}/K_0:

$$\frac{mK_{f_\perp}}{K_{c_\perp}} = \frac{K_0}{P_f K_{c_\perp}}\left[\frac{2K_{90}}{K_0} - 1\right] + n\left[\frac{P_f - 1}{P_f}\right] \qquad (22)$$

The unknown on the right in equation (22) is $K_0/K_{c_\perp}$. The preferred expression for $K_0/K_{c_\perp}$ is obtained from the variable dispersion equation (8) for cylinders perpendicular to the heat flow. Unfortunately, substitution of equation (8) into equation (22) does not give a result for $K_{f_\perp}/K_{c_\perp}$ in terms only of the known quantities K_{90}, K_0 and P_f, and parameters m and n. In addition, no combination of any equations (15) through (22) with any form of the variable dispersion equation in Appendix VIII gave this desired result.

The best procedure appears to be to obtain values of $K_0/K_{c_\perp}$ from equation (8), substitute these into equation (18) along with the same values of $K_{f_\perp}/K_{c_\perp}$, and form a plot of K_{90}/K_0 versus K_f/K_{pr}. This plot can then be used to find K_f/K_{pr} from measured values of K_{90}/K_0.

Solutions to equations (8) and (22) by the above procedure are very tedious by hand calculations. Therefore a computer was used to obtain values of K_0/K_c and K_{90}/K_0 for isotropic constituents (m=n=1 and the subscript $\perp$ is unnecessary) over a range of P_f from 0.36 to 0.63 and K_f/K_c from 5 to 1000. The results, tabulated in Appendix VII for use in data reduction, cover nearly all of the data that has been encountered on phenolic-carbon or phenolic-graphite materials. Solutions for some values of the constituent anisotropy parameters m and n were obtained by hand, as well as solutions using the Rayleigh equation (3) and the mixture equation (9) for K_0/K_c in place of the variable dispersion equation.

Figure 3 illustrates the behavior of the theoretical solutions for a nominal fiber volume fraction of 0.5. The influence of the continuous constituent anisotropy factor, n, and the fiber constituent anisotropy factor, m, is shown for the variable dispersion case.

Both the exact Rayleigh solution and the variable dispersion solution show similar behavior. As the fiber conductivity increases relative to the continuous phase, an asymptotic limit is reached in K_0, and K_{90} increases linearly. The Rayleigh solution reaches its limit sooner. The effect of the higher order terms in equation (3) due to fiber interaction in the Rayleigh solution is only about 2% for the 0.5 concentration of fibers, so the solution shown is practically identical to a dilute dispersion solution. The mixture equation solution fails completely to describe the behavior of the conductivity data, and is shown only to demonstrate this point.

The variable dispersion solution was selected for data correlation in this study for the following reasons:

1) The Rayleigh solution predicts the minimum effect of fiber conductivity, K_f, of all of the available relationships. A choice of this solution is a choice to operate at one extreme of the theory.

2) The restrictions to a square array and to equal size cylinders in the Rayleigh solution are the reason it gives the minimum effect of K_f. The square array restriction, in particular, may be violated by the arrangement of fiber in phenolic-carbon and phenolic-graphite.

3) The variable dispersion solution imposes no restrictions except that the fibers are, in fact, dispersed as a discontinuous phase. Isolated fiber contacts, which cause a local shape factor change, would have little effect as long as they were in random directions and dispersed[14].

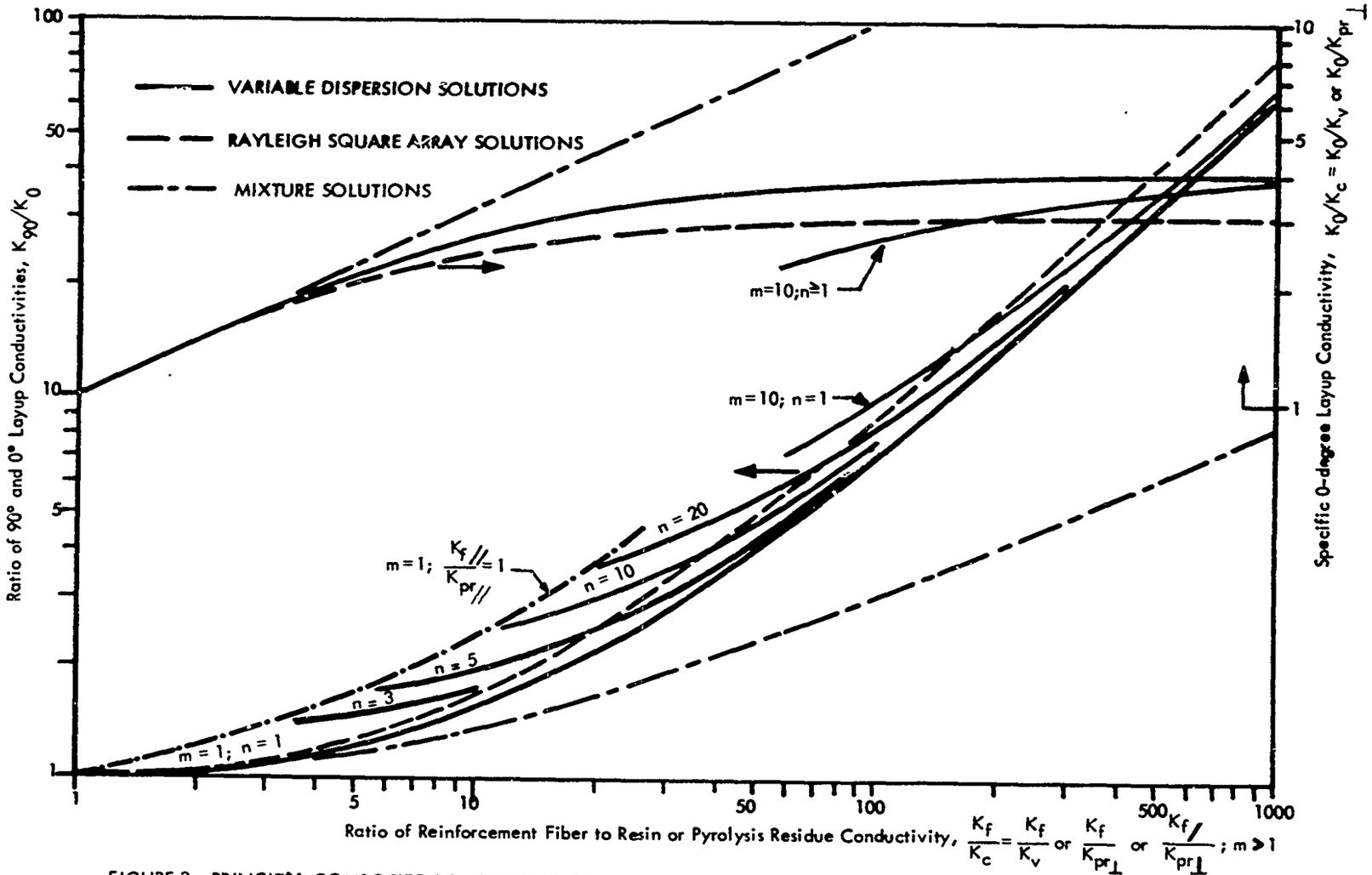

FIGURE 3 PRINCIPAL COMPOSITE CONDUCTIVITIES VERSUS RELATIVE CONSTITUENT CONDUCTIVITIES FOR $P_f = 0.5$

4) As discussed later, accurate simplified equations are available for the variable dispersion case, offering usable working relationships for development of the final data correlation. Adequate simplified solutions for the Rayleigh case have not been found[22].

5) The variable dispersion solution gives the most accurate prediction of the resin constituent conductivity from the measured composite conductivity in comparison with independent resin conductivity measurements. Results are shown in Section VII. The Rayleigh solution predicts slightly high values for the resin conductivity, consistent with its prediction of the minimum effect of fibers perpendicular to the heat flow.

Solutions for several values of the continuous phase anisotropy parameter, $K_{pr_{/\!/}}/K_{pr_{\perp}} = n$, are shown for the variable dispersion solution in Figure 3. Figure 3 includes a line showing the solution limit where the continuous phase conductivity parallel to the fiber equals the fiber conductivity. The parameter is written for the pyrolysis residue phase to emphasize that anisotropy is expected to result from oriented nonspherical porosity in the char. The virgin resin phase is expected to be isotropic. It is apparent that the influence of the anisotropy parameter, n, is significant only at low K_f/K_{pr}. Furthermore, estimates of the parameter using equations (7) and (11) to predict the effect of 4:1 prolate or oblate pores elongated in the fiber direction show that values of $n > 5$ are unlikely for all but the extreme cases of all of the pores being the oriented, highly nonspherical type at very high concentrations[22]. The effects of oriented porosity on the pyrolysis residue conductivity and the corresponding anisotropy factors are shown in Figure 4. Since the probable range of n is not large and its effects are limited to K_f/K_{pr} lower than values corresponding to the chars of this study, continuous phase anisotropy can be safely neglected in the data correlation. The physical reason for this is that the fiber almost completely dominates the conductivity of 90-degree layup chars, and even if the pyrolysis residue conductivity parallel to the fibers is much higher than the conductivity perpendicular to the fibers, it makes little difference in K_{90}/K_0. The solutions were developed above using the conductivity perpendicular to the fiber as the basis. This is the pyrolysis residue constituent property of interest, since it controls K_0, and this is the property predicted by the data reduction procedure described later.

The effect of possible anisotropy in the fiber conductivity is shown for $K_{f_{/\!/}}/K_{f_{\perp}} = m = 10$ in Figure 3. The results for both $K_0/K_{pr_{\perp}}$ and K_{90}/K_0 are plotted versus $K_{f_{/\!/}}/K_{pr_{\perp}}$ to emphasize that if m is neglected, the results still give a good estimate based on the fiber axial conductivity for high $K_{f_{/\!/}}/K_{pr_{\perp}}$. As noted above, this controls K_{90}, and is the property of interest, while the actual value of the fiber conductivity perpendicular to the fiber axis has little effect on K_0 if K_f/K_{pr} is high enough. No information has been found to indicate that $m > 1$ need be considered for the reinforcing fibers. The tendency for pyrolytic deposits to form on fiber surfaces during ablation could give an effective value of $m > 1$.

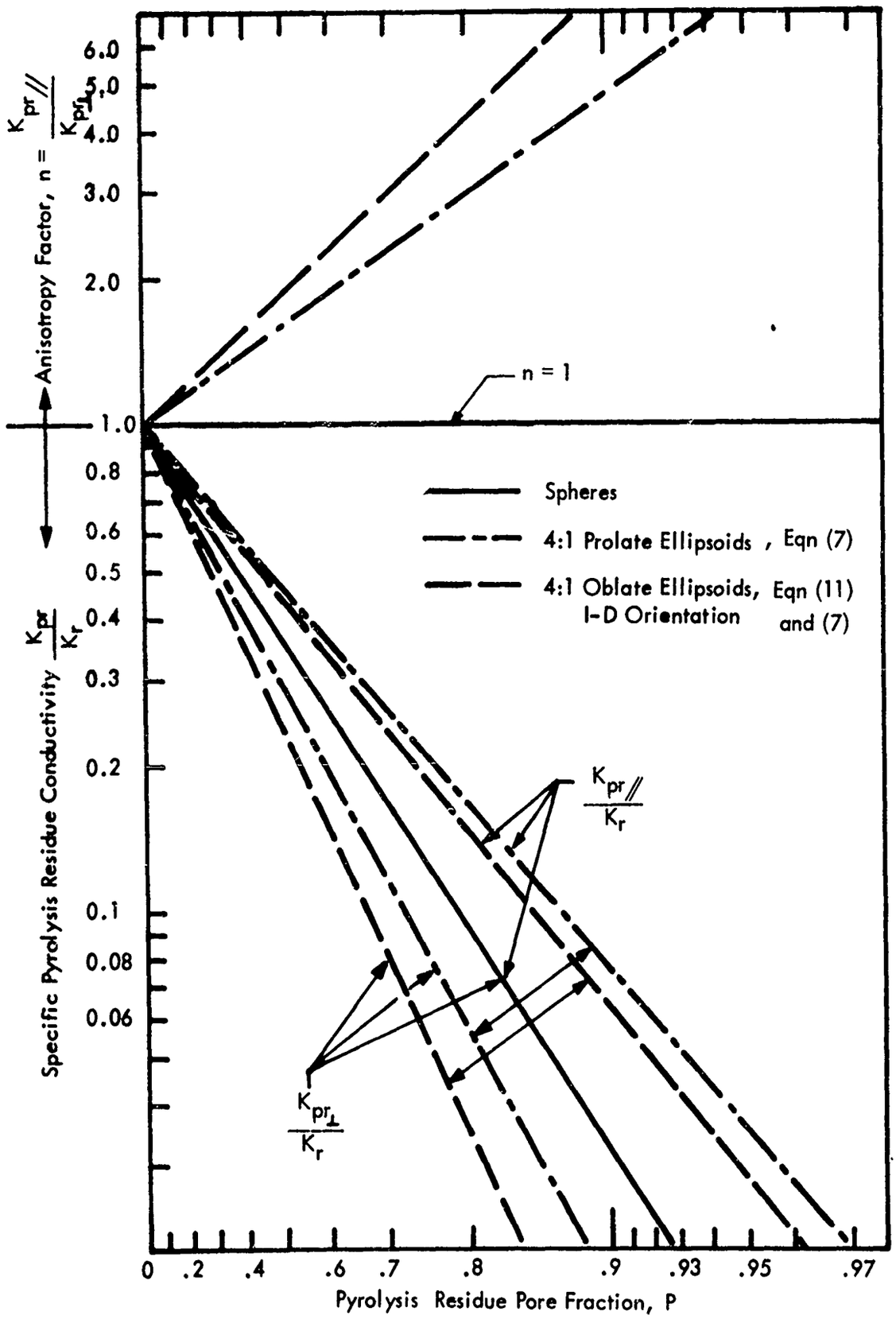

FIGURE 4 EFFECT OF ORIENTED ELLIPSOIDAL PORES

Neglecting m and n in the data reduction procedure described later has the effect that K_f may be overpredicted and K_{pr} may be underpredicted when constituent conductivities are predicted from composite conductivities. Regardless of the values of m and n, $K_{f//}$ should be predicted to better than + 20% accuracy, however the influence on predicted K_{pr} could be more than -50% in low temperature chars. The data reduction procedure tends to concentrate the errors in the prediction of K_{pr}. However, it will be seen in Section VII that K_{pr} predictions are somewhat uncertain anyway, since they are influenced primarily by measured K_0 values which are highly variable due to a tendency for delamination in the chars. The treatment of the data in this case to obtain a correlation is presented in Section VII. Delaminations lower the measured K_0 and the predicted K_{pr}, which depends on K_0, by the same amount. Predicted K_f is lowered slightly, on the order of 20% if K_0 and K_{pr} are lowered by a factor of four, for example.

It is apparent from the above discussion that delaminations counteract constituent anisotropy influences on the prediction of K_f, and that the fiber axial conductivity will be predicted accurately. Both delaminations and constituent anisotropy tend to lower predicted K_{pr} values, with the largest uncertainty from anisotropy effects confined to the region below $K_f/K_{pr} = 100$. Since even very extensive conductivity sample characterization studies (see Reference 1 and Section VI) have not yielded a quantitative estimation of anisotropy parameter values, and some delaminations are inevitable, the theory is applied ignoring these effects. In practice, this makes little difference, since predicted constituent properties are recombined in the same manner to obtain composite properties, and measured composite conductivities are automatically reproduced. The effect of the uncertainties due to anisotropy and delaminations is that the fiber axial conductivity and virgin resin conductivity should be accurately predicted and comparable to independently measured fiber or resin conductivities, but the pyrolysis residue conductivity may not be accurately predicted. The simple procedure for obtaining predicted constituent conductivities from the measured composite conductivity data is outlined below.

APPLICATION OF THEORY FOR PREDICTION OF CONSTITUENT CONDUCTIVITIES

Values of K_f and K_v or K_{pr} are easily determined from the composite thermal property data with the aid of plots such as Figure 5. Figure 5 demonstrates the behavior of the variable dispersion solution, neglecting constituent anisotropy, for the range of fiber volume fractions, P_f, of interest in phenolic-carbon or phenolic-graphite materials. The theoretical relationships for other values of P_f are tabulated in Appendix VII.

The procedure for predicting the dispersed fiber conductivity, K_f, and the continuous phase resin or pyrolysis residue conductivity, K_v or K_{pr}, from measured composite conductivities for the 90-degree, K_{90}, and 0-degree, K_0, layup angles is as follows.

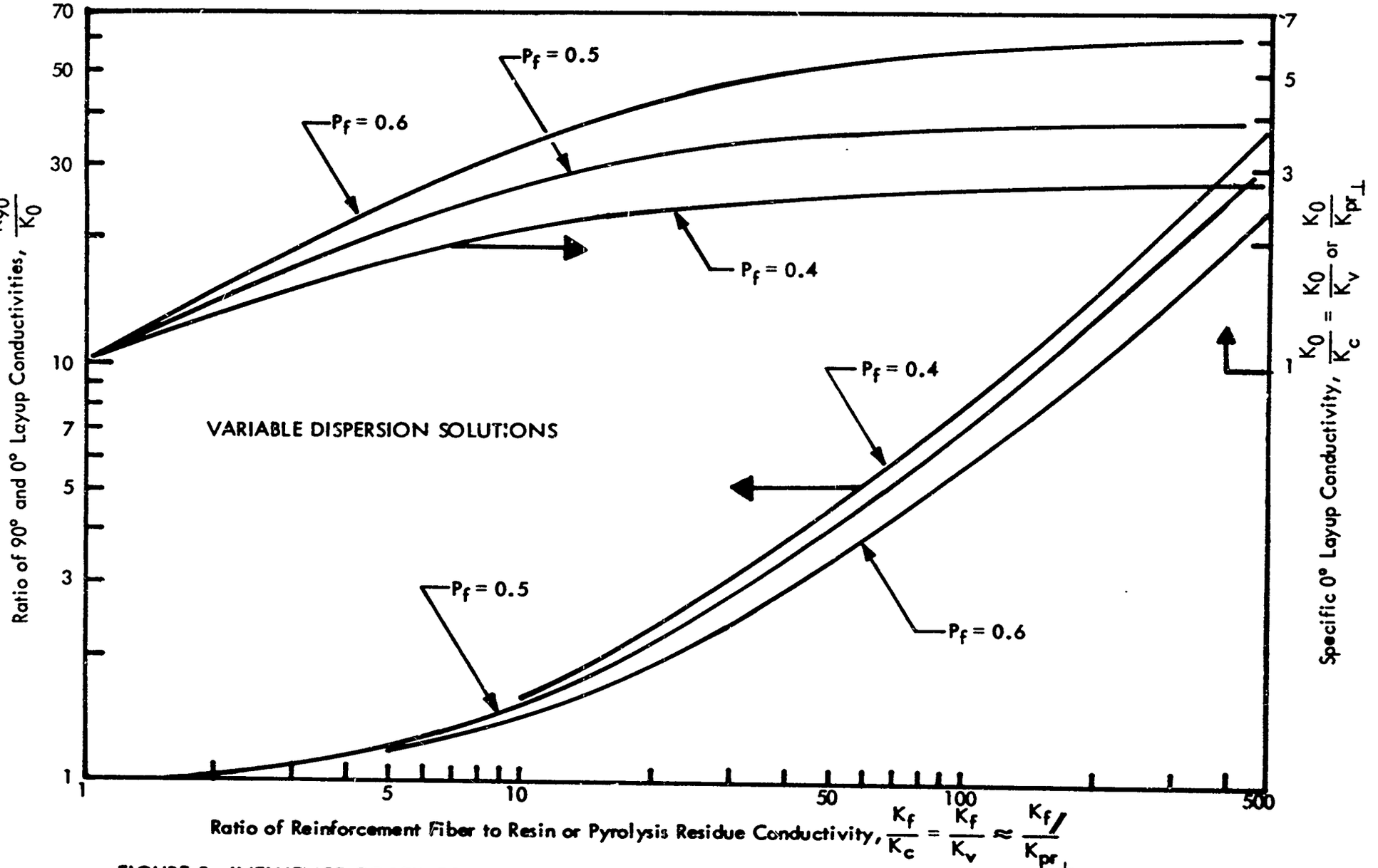

FIGURE 5 INFLUENCE OF REINFORCEMENT VOLUME FRACTION, P_f, ON COMPOSITE CONDUCTIVITIES VERSUS CONSTITUENT CONDUCTIVITIES

1) The fiber volume fraction, P_f, for the composite is obtained experimentally or by a material balance based on known resin content, resin and fiber densities, and composite apparent density and porosity.

2) A plot such as Figure 5 is made for the P_f value of interest using the theory values tabulated in Appendix VII. Nearest bounding values may be plotted for interpolation if required.

3) Ratios of K_{90}/K_0 are calculated from the measured composite conductivities at each temperature of interest.

4) Ratios of K_{90}/K_0 are entered in the theory plot to find the corresponding values of K_f/K_c and K_0/K_c.

5) $K_c=K_v$ or K_{pr} values are found from the measured values of K_0 by the multiplication $K_0\ (K_c/K_0)$.

6) K_f values are obtained from $K_f = (K_f/K_c)K_c$.

The above data reduction procedure compensates for neglecting m and n to give accurate predictions of fiber axial conductivity in the following way. In Figure 3 it can be seen that neglecting m or $n>1$, K_{f/K_c} based on K_{90}/K_0 will be too high. However, K_0/K_c will also be too high, so use of this ratio to obtain K_c from K_0 will give low values of K_c. The low values of K_c multiplied by high values of K_f/K_c are self compensating to the extent that accurate predictions of $K_{f//}$ are obtained. Emphasis on accurate predictions of $K_{f//}$ is proper, since this property controls the composite conductivity at all but very low layup angle of little practical interest, and since K_c in the chars, K_{pr}, can be highly variable due to the influence of delaminations, and anisotropy factors.

Predicted constituent properties for phenolic-carbon and phenolic-graphite materials studied on this program and previous programs are presented in Section VII and VIII. The above procedure was used. If a very large volume of data were to be reduced, the entire procedure could be automated to reduce data directly using the theoretical relationships presented previously.

If the above procedure is followed using the Rayleigh equation or mixture equation solutions in Figure 3, the influence of the theory used can be demonstrated. This was done for the MX-4926 phenolic-carbon and FM-5014 phenolic graphite studied previously[1, 22], both of which have a nominal $P_f=0.5$. The variable dispersion theory solutions for these materials are included in Section VII. Compared to the variable dispersion solution, the other solutions predict the same values for K_f,

within a few percent. This is consistant with the fact noted previously that even gross delamination or constituent anisotropy effects have little influence on the prediction of K_f. The physical reason is that the fibers parallel to the heat flow so dominate K_{90} that it makes little difference what the assumed effect is for the portion of the fibers perpendicular to the flow. This being the case, independently determined fiber conductivities could then be used to check the adequacy of the thermal model, the controlling theoretical consideration being that for K_{90} half of the fiber can be considered as parallel and half as perpendicular to the heat flow.

The differences in the three types of solutions show up in the prediction of K_v or K_{pr}. Compared to the variable dispersion solution, the Rayleigh solution predicts slightly high values and the mixture solution predicts very low values, by as much as an order of magnitude. These results are consistent with the theoretical expectations discussed previously. The mixture equation solution does not apply, and the variable dispersion solution is prefered to the Rayleigh solution on the basis of a better representation of actual material geometry and on the basis of the results obtained for predicted virgin resin conductivity compared to independently determined resin conductivity as shown in Section VII.

While predicted constituent properties are easier to correlate than composite conductivities over all of the changes that accompany ablation, and assist in understanding the behavior of thermal conductivity during ablation, they must be recombined to give the composite conductivity needed for ablation performance predictions. The exact variable dispersion solution is cumbersome, and a simplified direct solution for composite conductivity from constituent conductivities is desired both for hand calculations and computer calculations employing minimum machine time.

DEVELOPMENT OF WORKING RELATIONSHIPS TO OBTAIN COMPOSITE CONDUCTIVITIES FROM CONSTITUENT CONDUCTIVITIES

When K_f/K_c becomes sufficiently large, solutions for K_f/K_c in terms of K_0, K_{90}, and P_f, and solutions for K_{90} and K_0 in terms of K_f/K_c and P_f were obtained as follows. Variable dispersion equation (8) for the effect of fibers perpendicular to the heat flow was obtained in Appendix VIII by a quadratic solution of:

$$\frac{K_\theta}{K_{c_\perp}} = \frac{K_{f_\perp}}{K_{c_\perp}} - (1 - P_f)\left[\frac{K_{f_\perp}}{K_{c_\perp}} - 1\right]\left[\frac{K_0}{K_{c_\perp}}\right]^{\frac{1}{2}} \qquad (23)$$

Formulating equation (23) to give K_f/K_c as a separate factor on the right gives:

$$\frac{K_0}{K_{c_\perp}} = \frac{K_{f_\perp}}{K_{c_\perp}}\left[1 + (1 - P_f)\left(\frac{K_0^{1/2}}{K_{c_\perp}{}^{1/2}} \cdot \frac{K_{c_\perp}}{K_{f_\perp}} - \frac{K_0^{1/2}}{K_{c_\perp}{}^{1/2}}\right)\right] \qquad (24)$$

Substituting equation (24) into equation (22), gives:

$$\frac{m K_{f_\perp}}{K_{c_\perp}} = \frac{K_{f_{/\!/}}}{K_{c_\perp}} = \frac{K_{f_\perp}}{K_{c_\perp}}\left[1 + (1-P_f)\left(\frac{K_0^{1/2}}{K_{c_\perp}^{1/2}} \cdot \frac{K_{c_\perp}}{K_{f_\perp}} - \frac{K_0^{1/2}}{K_{c_\perp}^{1/2}}\right)\right]\left[\frac{1}{P_f}\left(\frac{2K_{90}}{K_0} - 1\right)\right] + n\left(\frac{P_f - 1}{P_f}\right) \quad (25)$$

Equation (25) can be considered as the exact expression that was solved indirectly to give the values in Appendix VII and in Figures 3 and 5. For $K_f/K_c > 100$, $P_f > 0.4$ and $n < 5$, the limit on n demonstrated previously, the terms

$$\frac{K_0^{1/2}}{K_{c_\perp}^{1/2}} \cdot \frac{K_{c_\perp}}{K_{f_\perp}} \quad \text{and} \quad n\left[\frac{P_f - 1}{P_f}\right] \quad \text{are negligible.}$$

That n can be neglected was demonstrated in Figure 3. Equation (25) also shows that under these conditions the fiber conductivity in the ratio on the left is actually close to the desired fiber axial conductivity even though the fiber anisotropy factor m is unknown. This is also demonstrated in Figure 3 and in the approximate relations to follow. The reason for this, as discussed previously, is that $K_0/K_{c_\perp}$ and K_0 become constant for high $K_{f_\perp}/K_{c_\perp}$, and the results are controlled by the experimental K_{90} values, which vary directly with $m K_f = K_{f_{/\!/}}$. The procedure for predicting constituent properties further compensates for neglecting m.

For equation (25) to hold neglecting the terms listed above, the multiplier on $K_{f_\perp}/K_{c_\perp}$ on the right must be m. It is then possible to write the following relationship where the negligible terms are omitted:

$$1 + (P_f - 1)\left(\frac{K_0}{K_{c_\perp}}\right)^{1/2} = \frac{m P_f}{\frac{2K_{90}}{K_0} - 1} \quad (26)$$

Solving for $(K_0/K_{c_\perp})^{1/2}$, squaring the result, and combining $(2K_{90}/K_0 - 1)$ terms gives:

$$K_0/K_{c_\perp} = \frac{\left(\frac{2K_{90}}{K_0} - 1 - m P_f\right)^2}{(1 - P_f)^2\left(\frac{2K_{90}}{K_0} - 1\right)^2} \quad (27)$$

Equation (27) is interesting for its ability to predict $K_0/K_{c_\perp}$ directly from experimental data as long as $K_{f_\perp}/K_{c_\perp} > 100$

Substituting equation (27) into equation (22) where the term including n is neglected as above, and combining $(2K_{90}/K_0-1)$ terms gives:

$$\frac{m K_{f_\perp}}{K_{c_\perp}} = \frac{K_{f_{/\!/}}}{K_{c_\perp}} = \frac{\left(\frac{2K_{90}}{K_0} - 1 - m P_f\right)^2}{P_f (1-P_f)^2 \left(\frac{2K_{90}}{K_0} - 1\right)} \qquad (28)$$

For $K_{f_\perp}/K_{c_\perp} > 100$ and $P_f > 0.4$, equation (28) yields $K_{f_{/\!/}}/K_{c_\perp}$ relative to the cloth reinforced material model entirely from experimentally determined quantities. Equation (28) also illustrates that it is the fiber axial conductivity that is predicted, the error in neglecting m being confined to the $m P_f$ term. The somewhat circular path in the development of this equation was necessary to identify the terms that could be neglected under the assumed conditions.

Equations (27) and (28) have the same form, and comparing the two shows that we may write:

$$\frac{K_0}{K_{c_\perp}} = \frac{P_f \cdot \frac{m K_{f_\perp}}{K_{c_\perp}}}{\frac{2K_{90}}{K_0} - 1} \qquad (29)$$

Equation (28) may be written as a quadratic in $(2K_{90}/K_0-1)$ as follows:

$$\left(\frac{2K_{90}}{K_0} - 1\right)^2 - \left(\frac{2K_{90}}{K_0} - 1\right)\left[2mP_f + P_f(1-P_f)^2 \frac{m K_{f_\perp}}{K_{c_\perp}}\right] + (m P_f)^2 = 0 \qquad (30)$$

Neglecting the small $(m P_f)^2$ term at high $K_{f_\perp}/K_{c_\perp}$, equation (30) yields:

$$\frac{2K_{90}}{K_0} - 1 = 2m P_f + P_f (1-P_f)^2 \frac{m K_{f_\perp}}{K_{c_\perp}} \qquad (31)$$

Equations (29) and (31) agree with exact solutions within a few percent, even for high values of m and n, for all $K_{f_{\perp}}/K_{c_{\perp}} > 50$. This range covers nearly all of the phenolic-carbon or phenolic-graphite char constituent properties presented in Sections VII and VIII. Equation (31) then provides a simple solution for K_{90}/K_0 in terms of constituent properties and equation (31) substituted into equation (29) provides K_0. In this later case m cancels out as it should, since K_0 is a function of constituent conductivities perpendicular to the fiber axis only. Since $m\, K_{f_{\perp}} = K_{f_{/\!/}}$, equation (31) emphasizes that the fiber axial conductivity controls K_{90}/K_0, and hence controls K_{90}, as noted previously. Furthermore, m in the first P_f term on the right in equation (31) can be neglected. Then equations (29) and (31) should be written as functions of $K_{f_{/\!/}}$, which has been shown previously to be the fiber property that is predicted for measured composite data.

Extension of equations (29) and (30) to low values of $K_{f_{/\!/}}/K_{c_{\perp}}$ was done by comparing the results to exact solutions and making empirical adjustments on the $K_{f_{/\!/}}/K_{c_{\perp}}$ terms. In this case, if m and n are large, the predicted values of $K_{c_{\perp}}$ are low, but the results of combining predicted $K_{f_{/\!/}}$ and $K_{f_{\perp}}$ to obtain K_0 and K_{90} are still correct since the same theory is used in going from K_0 and K_{90} to $K_{f_{/\!/}}$ and $K_{c_{\perp}}$ for correlation, and then back to K_0 and K_{90}. In the virgin laminates, the constituents are expected to be isotropic, so both $K_{f_{/\!/}}$ and $K_{c_{\perp}} = K_v$ are expected to be accurately predicted. This is seen to be the case in Section VII.

The empirical adjustments extending equations (29) and (30) to low $K_{f_{/\!/}}/K_{c_{\perp}}$ were developed as a function of P_f to provide K_{90} and K_0 from constituent properties to within 1% of the exact solution for all $K_{f_{/\!/}}/K_{c_{\perp}} > 5$ and all P_f in the range 0.4 to 0.6. The composite conductivity, K_θ at all intermediate layup angles is then given by equation (1).

K_0 for use in equation (1) may be obtained from equations (29) and (31) and $(K_{90}/K_0 - 1)$ may be obtained from equation (31). The results of these substitutions in equation (1) are written below, including the empirical adjustments to low K_f/K_c. The directional designations which show that $K_f/K_c \approx K_{f_{/\!/}}/K_{c_{\perp}}$ are dropped in the equation below which holds within 1% down to $K_f/K_c = 5$ where anisotropy effects would not be negligible if present. This is done with the understanding that $K_{f_{/\!/}}$ and $K_{c_{\perp}}$ are the constituent properties that are predicted and are required at high K_f/K_c in the chars, where anisotropy can be neglected.

$$K_\theta = \frac{K_c\, P_f \left(\frac{K_f}{K_c} + 0.24\, P_f^{-2} \right)}{2\, P_f + P_f\,(1 - P_f)^2 \left(\frac{K_f}{K_c} - 25\, P_f^4 \right)} \left[1 + \left[P_f + \frac{P_f}{2}\,(1 - P_f)^2 \left(\frac{K_f}{K_c} - 25\, P_f^4 \right) - \frac{1}{2} \right] \sin^2 \theta \right] \tag{32}$$

Equation (32) may be written as follows where the constituent conductivities are separated.

$$K_\theta = \frac{K_f + AK_c}{B\,K_f + CK_c}\left[K_c + \left[\left(C - \frac{1}{P_f}\right)K_c + B\,K_f\right]\frac{P_f}{2}\sin^2\theta\right] \qquad (33)$$

For cloth reinforced laminates:

$$K_f/K_c \geq 5\,;\; 0.4 \leq P_f \leq 0.6$$

where:

P_f = Dispersed reinforcement fiber volume fraction

K_f = Reinforcement fiber isotropic or axial conductivity, $K_{f/\!/}$

K_c = Continuous phase resin, K_v, or pyrolysis residue isotropic or crossply conductivity, $K_{pr\perp}$

θ = Layup angle measured $\perp$ to cloth plane

$A = 0.24\,P_f^{-2}$

$B = (1 - P_f)^2$

$C = 2 - 25\,P_f^4\,(1 - P_f)^2$

In the pyrolysis zone during ablation it is necessary to make a transition between K_c=K_v predicted for virgin resin and K_c=$K_{pr\perp}$ predicted for pyrolysis residue. Since there is insufficient data on partially pyrolyzed material to make a quantitative correlation for partially pyrolyzed resin conductivity (see Section VII), continuous phase conductivity is assumed to follow the pyrolysis fraction weighted average of the virgin and mature char pyrolysis residue values. Typical pyrolysis fraction versus temperature curves for phenolic-carbon and phenolic-graphite were presented in Reference 1. Pyrolysis fraction, the fraction of the resin that is pyrolyzed, is defined as:

$$Xp = \frac{P_v - P_a}{P_v - P_m} \qquad (34)$$

where:

P_v = virgin ablator composite apparent density

P_a = instantaineous apparent density

P_m = mature char apparent density

Pyrolysis fraction weighted properties are commonly employed in computer predictions of ablation performance. The expression for K_c that incorporates all of the virgin resin and mature char matrix conductivity values is the commonly used form:

$$K_c = K_v (1 - X_p) + X_p K_{pr_\perp} \quad (35)$$

Equations (33) and (35) yield phenolic-graphite or phenolic-carbon thermal conductivity during ablation for any layup angle from constituent properties K_f, K_v and $K_{pr_\perp}$, correlated versus temperature in Sections VII and VIII. Equations (33) and (35) together with constituent properties expressed as functions of temperature may be incorporated directly in ablation computer programs. Alternately, conductivity versus temperature for the virgin and mature char states can be calculated from these relationships and substituted in existing computer programs utilizing pyrolysis fraction weighted composite conductivities in the pyrolysis zone. Both approaches are demonstrated in Section IX. Differences in conductivity during heating, or cooling, due to material changes accompanying ablation are incorporated in the correlation of constituent conductivities. Equation (33) should also be very useful in estimating the effect on conductivity of changes in ablation heat shield parameters such as reinforcement, resin content, layup angle, resin filler, and resin porosity (Figure 4).

SECTION IV

THERMAL CONDUCTIVITY MEASUREMENTS

MEASUREMENT TECHNIQUE

Thermal conductivity of the FM-5055A phenolic-carbon chars was measured by a steady-state, one-dimension heat flow, comparative method. In this technique, heat is transferred axially from a source through the specimen and a heat flow meter in series to a sink. The heat flux common to the specimen and meter is determined on the basis of the known conductivity of the meter, and conductivity of the specimen is calculated using the form of the Fourier equation:

$$K = \frac{Q}{A} \frac{L}{\Delta T} \qquad (36)$$

where:

Q = measured heat flux

A = cross section area of measurement zone

L = distance between temperature measurement points

ΔT = temperature difference across L .

As used in this program, the technique utilized disk-shaped specimens nominally 3 inches in diameter by 1/4 to 1/2 inch thick. Heat flow during measurement is axial. The central 1 inch diameter is considered to be the conductivity measurement section, and the remainder of the disk guards against radial heat flow from this section. Hence, the term "self-guarding disk" is appropriate. The effectiveness of this feature is enhanced as the specimen diameter-to-thickness ratio is increased, but the thickness must be great enough to permit establishment of a reasonable (from the standpoint of accuracy) temperature gradient during measurement, and also must be representative of the material in the measurement direction.

The heat flow meter has a diameter equal to that of the specimen measurement section; radial heat flow from it is minimized by guard cylinders which have an axial temperature gradient equivalent to that of the meter.

Temperatures and temperature gradients along the axis of the specimen and meter are measured by thermocouples or optical pyrometer.

This measurement technique is appropriate for reinforced carbon phenolics. The steady-state feature minimizes the number of variables in the measurement, thus enhancing accuracy, and the one-dimension feature is a requirement for anisotropic

materials. In such materials, the local heat flux vector is not necessarily normal to the local isotherm. In order to allow interpretation of data, it is desirable to employ a measurement technique that provides information on the direction of either the heat flux vector or isotherms. The technique described here is designed to promote development of isothermal planes parallel to the faces of the disk specimen. Therefore, the measured thermal conducitivity coefficient is related to the principal conductivity coefficients through the direction cosines between the normal to the isotherms and the principal conductivity axes.

The heat soak period at temperature for each specimen range from 2 to 4 hours per equilibrium (data point) depending on the absolute temperature. These time-at-temperature intervals are considered long compared with the time scales for ordering processes in carbonaceous materials, and each data point should represent an equilibrium condition in the sample.

Apparatus Description

Two apparatus were used for this program; they are referred to as high-temperature and low-temperature apparatus. The low-temperature unit (Reference 1) employs a Pyroceram 9606 heat flow meter and a conduction-type heater element. It was used for measurements in the range 70 to 1800°F. The high-temperature unit, employs a Type 347 stainless steel meter and a radiant (graphite) heater element. It was used for measurements in the range from 1500°F upward. This apparatus is illustrated schematically in Figure 6.

Measurement Procedure

For each measurement, the three-inch-diameter specimen was machined to a thickness appropriate for the desired measurement boundary conditions (temperature range, temperature gradient, anticipated thermal conductivity, etc.) and set up with necessary instrumentation, insulation, and environment control. Thermal equilibria were established and conductivity calculated at several temperatures in the range of interest. Data were recorded in the order of ascending temperatures for all specimens, and additional measurements were made on cooling and subsequent reheating of selected samples.

The high-temperature measurements required at least two setups to cover the extensive ranges of temperature gradient and heat flux. All measurements were made under dynamic vacuum; system pressures ranged generally from 10^{-3} to 10^{-5} torr.

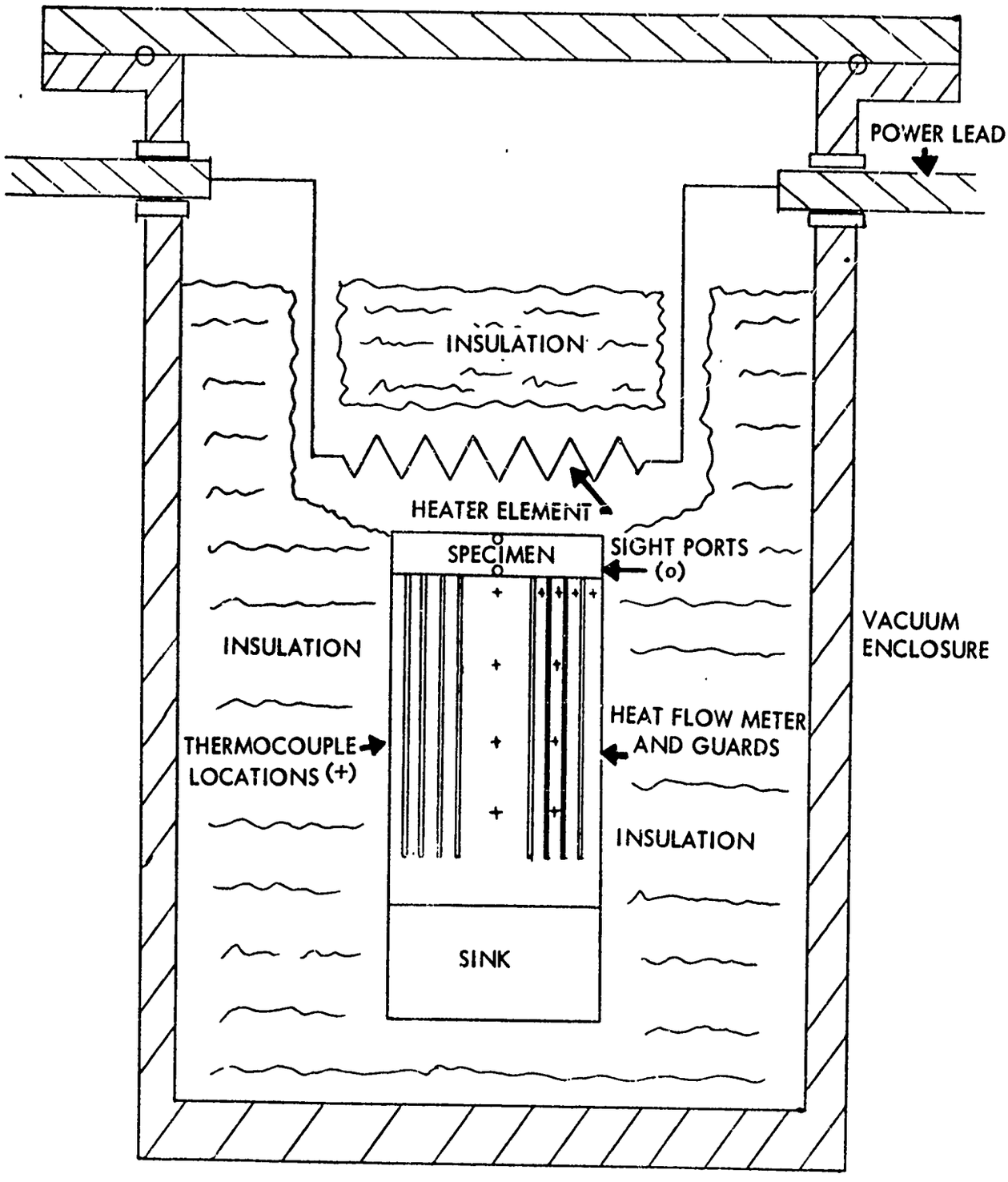

FIGURE 6 SCHEMATIC OF THERMAL CONDUCTIVITY MEASUREMENT APPARATUS

Precision and Accuracy

The precision of conductivity measurements by this technique is defined as the limits within which measurement results can be reproduced. In this program, reproducibility generally was in the range ±2 to ±4 percent, except in two cases of the higher-conductivity specimens as will be discussed later.

The accuracy of results by any comparative conductivity measurement is dependent primarily on the accuracy of the heat meter conductivity, and how efficiently heat flow is regulated during the measurement. The material for the Pyroceram meter was obtained from the National Bureau of Standards; its conductivity was reported by Robinson and Flynn (Reference 2). Since there are no good comparative standards with conductivity in the range of Pyroceram 9606, no separate measurements of the conductivity of this meter were made. Instead, the NBS data were used directly. On this basis, error limits are set conservatively at ±10 percent for the low-temperature measurements.

The conductivity of the Type 347 stainless steel meter of the high-temperature apparatus was measured in a longitudinal flow (cut-bar type), comparative apparatus against an Armco iron standard. The conductivity of this iron has been measured extensively at Battelle and at four other laboratories by both absolute and comparative (using NBS freezing point lead) techniques. In general, results of these measurements were in excellent agreement; standard deviations in the data are of the order of 1.5 percent or less. (Reference 3). Therefore, the conductivity of the stainless steel meter is assumed to be known to within ±2 percent, and errors attributable to this factor in the program measurements are conservatively set at ±5 percent.

The ability of the apparatus to sustain one-dimension heat flow through the specimen measurement section was judged on how effectively temperature gradients in the radial direction in the heat flow meter and its guard tubes could be minimized, and on the ability to match axial heat fluxes in the meter with those in its guard tubes. Both conditions were achieved to a satisfactory degree with proper choice of insulation in the apparatus. Errors attributable to lack of control of radial heat flow are judged to be less than ±5 percent.

Another source of potential error, especially at higher temperatures in the high-conductivity materials, is specimen temperature gradient measurement. The temperatures were measured by optical (Pyro-Optical) pyrometer, and distances between measurement points (sight holes) by micrometer. The magnitude of error depends on temperature range, temperature gradient, etc., and cannot be evaluated generally for the whole program.

Obviously, the only way to evaluate total potential errors in the technique employed, particularly in the high-temperature range, is to make conductivity measurements with it on a reference standard material. Unfortunately, there are no well-established standards for the range above 1000°C. However, results of measurements in the high-temperature apparatus on a sample of AXM-5Q graphite, a proposed standard (Reference 4), were in agreement with those reported tentatively by other laboratories, and also with calculated conductivity values based on results of thermal diffusivity measurements at Battelle. Figure 7 shows results of these measurements, and of the calculated values by diffusivity measurement. As the figure shows, steady-state measurements were made both before and after measurements on the program materials. The values indicate that overall errors in this measurement technique probably can be less than ±5 percent, and that the apparatus performed well throughout the program. However, insofar as the specimens of this program are concerned, the error limit is assigned conservatively at ±10 percent for the high-temperature and low temperature measurements.

MEASUREMENT PLAN

The program objectives included thermal conductivity measurement of specimens representing the phenolic carbon material in the virgin and various char states as a function of heat flow direction in the anisotropic structure, of density, and of extent of graphitization. The specimens were cut from molded blocks of U.S. Polymeric FM-5055A material, and were furnace charred at Boeing. Most of the specimens were prepared from a high quality virgin precursor which is referred to as high-density material. However, to evaluate the effect of higher porosity, some specimens were prepared from a low density precursor, and are referred to as low-density materials.

Table I lists the various specimen conditions prior to, and parameters for, measurement, and defines the specimen identification code utilized throughout this report.

All of the char specimens prepared from the high density virgin precursor were heat treated to form specific char states which were presumed to be stable, i.e., that further heat treatment at temperatures below the previous maximum would have no effect on thermal properties. Certain characterization tests were performed by Boeing, such as TGA on the lower two char states, 800°F and 1800°F, and X-ray diffraction intensity scans on the virgin and three higher char states, 1800°F, 3000°F, and 5000°F, to investigate the effects of time-at-temperature on weight loss and relative amounts of graphite-like crystallinity for times at maximum temperature which were much greater than those experienced in the usual oblation cycle. Generally, these characterization tests indicated that the

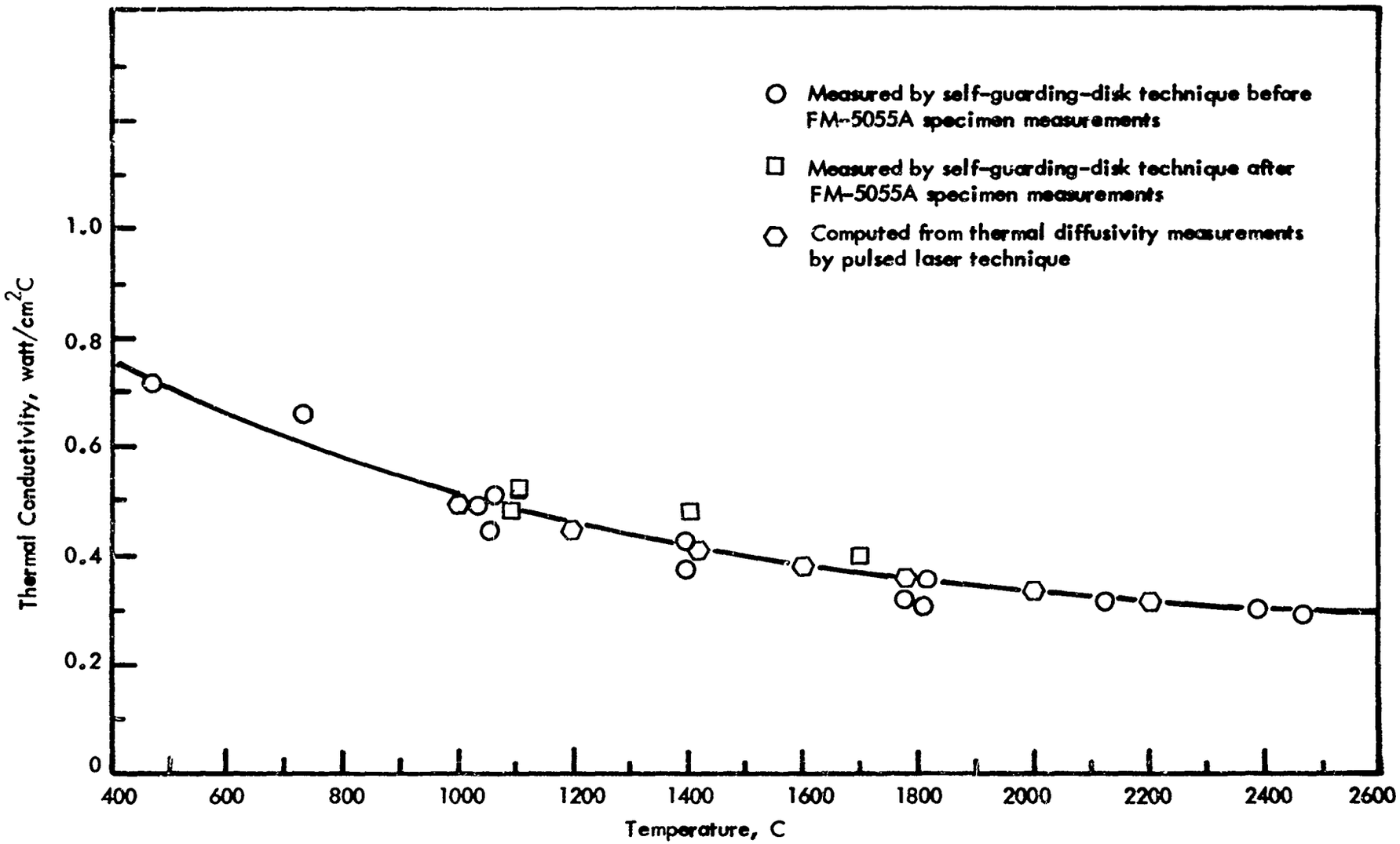

FIGURE 7 THERMAL CONDUCTIVITY OF AXM-5Q GRAPHITE

TABLE I THERMAL CONDUCTIVITY SPECIMEN IDENTIFICATION

[1] Specimen Number	Description	Initial Heat Treatment degrees F	Nominal Layup Angle degrees	Precursor Density	Measurement Temperature Range, °F
V-0-H	Virgin	--	0	high	70 - 500
V-30-H		--	30	high	70 - 500
V-90-H		--	90	high	70 - 500
800-0-H	Slightly pyrolyzed,	825	0	high	70 - 800
800-30-H	low porosity	825	30	high	70 - 800
1800-0-H	Fully pyrolyzed,	1825	0	high	70 - 1800
1800-30-H	High porosity,	1800	30	high	70 - 1800
1800-90-H	ungraphitized	1800	90	high	70 - 1800
1800-0-L	Fully pyrolyzed,	1800	0	low	70 - 1800
1800-90-L	Maximum porosity, ungraphitized	1800	90	low	70 - 1800
3000-0-H	High porosity	3025	0	high	1000 - 3000
3000-30-H	low graphitization	3025	30	high	1000 - 3000
3000-90-H		3025	90	high	1000 - 3000
5000-0-H	High porosity,	5000	0	high	1000 - 5000
5000-30-H	high graphitization	5000	90	high	1000 - 5000
5000-90-H, No. 1		5000	90	high	1000 - 5000
5000-90-H, No. 2		5000	90	high	1000 - 5000
5000-0-L	Maximum porosity,	1800	0	low	1000 - 5000
5000-90-L	graphitized during measurement	1800	90	low	1000 - 5000

[1] The first number gives heat treatement temperature (V=virgin), the second gives nominal layup angle in degrees (0°= heat flow normal to cloth plane, 90°= heat flow parallel to cloth plane), and the third indicates precursor density (high or low).

char levels were stable in regard to the test parameters. The thermal conductivity measurements on the high density chars were performed such that the temperature of the hot face of the specimen did not exceed the maximum heat treatment temperature. Therefore, the measurements give the conductivities of the high density chars as functions of ambient temperature, and should be reproducible. Exceptions are discussed in Section VI, where all specimen characteristics before and after thermal conductivity tests are discussed.

The thermal conductivities of two of the four char specimens prepared from the low density virgin precursor were measured as a function of ambient temperature below their maximum heat treatment of 1800°F, the same as for the high density chars. Two others, having identical 1800°F initial heat treatments, were graphitized during measurement to 5000°F. These latter measurements give conductivity as a function of heat treatment and so provided almost continuous information on the effects temperature dependent ordering on thermal conductivity.

FM 5055A THERMAL CONDUCTIVITY RESULTS

Data from the conductivity measurements are plotted in Figures 8 through 20. Where appropriate, the data are characterized by symbols which give information relative to measurement conditions. Several sets of overlapping data indicate that comparable results for a given specimen were obtained regardless of the apparatus (low or high temperature) or means of temperature measurement (thermocouples or optical pyrometer). Tabulated data point values are given in Appendix III.

Figure 21 presents a composite of the smoothed conductivity curves for the high density chars, illustrating the effects of anisotropy and prior heat treatment (HT) on conductivity through the temperature range. The cross-ply conductivity is seen to decrease with HT to minimum values at the 800°F HT, increase just slightly at the 1800°F level, and increase by about an order of magnitude between the 1800°F and 3000°F char levels. Whatever the HT, the slope of conductivity with ambient temperature remains positive. This is a characteristic feature of hard (poorly graphitizable) carbons.

The conductivity in the ply direction appears to increase continuously with HT, while the slope of conductivity with ambient temperature changes from the positive values found at and below 1800°F HT, to zero or negative at 3000°F HT and above. The variation of conductivity with ambient temperature above 3000°F HT invites comparison as much with bulk graphites as with hard carbon, reflecting the higher degree of ordering achieved in the reinforcement cloth fiber (and possibly the pyrolysis residue matrix adjacent to the fibers) relative to that in the hard carbon matrix.

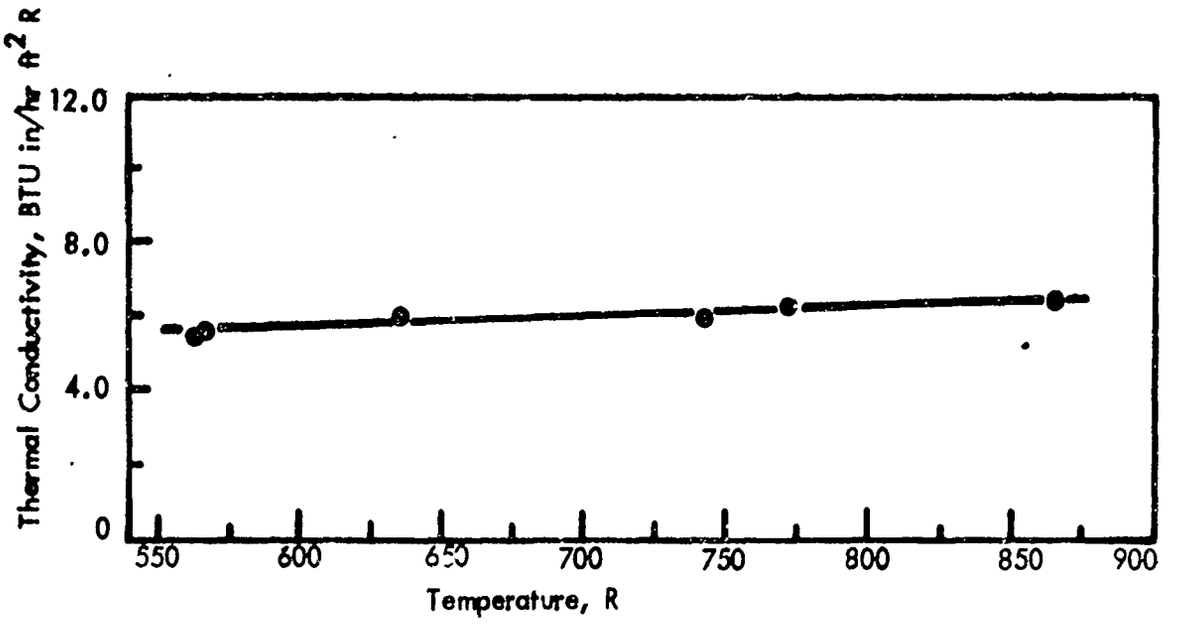

FIGURE 8 THERMAL CONDUCTIVITY OF SPECIMEN V-0-H

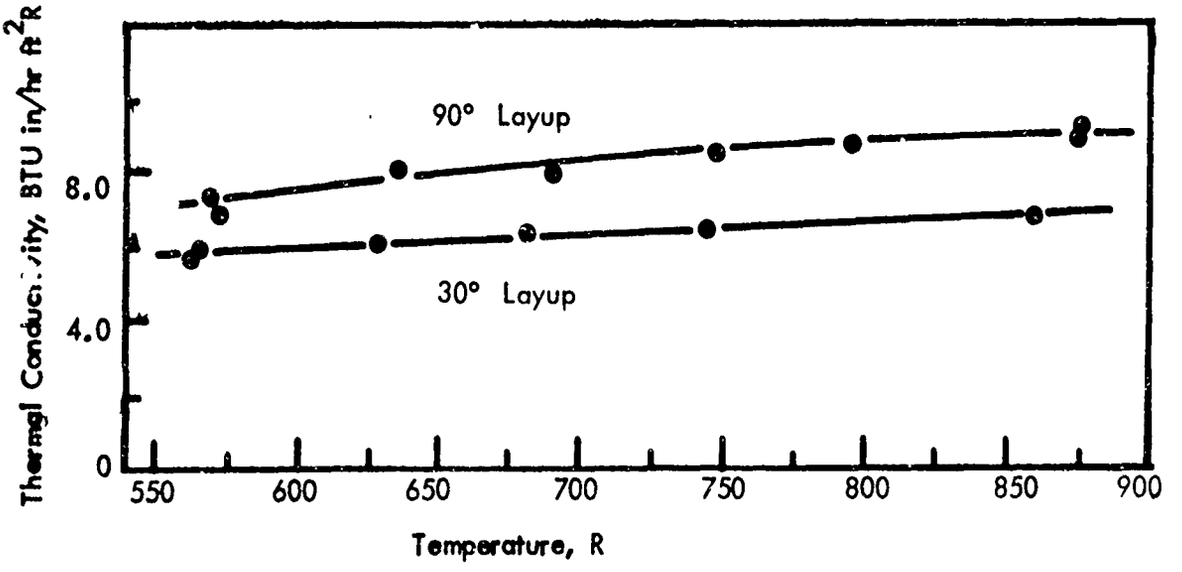

FIGURE 9 THERMAL CONDUCTIVITY OF SPECIMENS V-30-H and V-90 -H

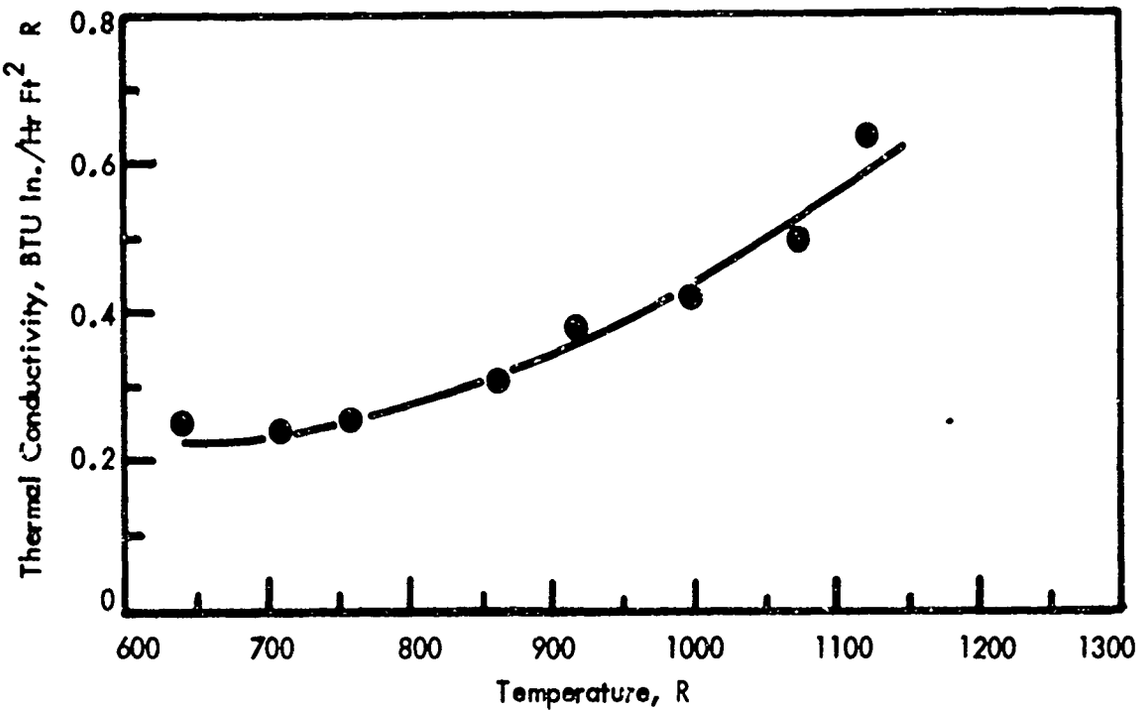

FIGURE 10 THERMAL CONDUCTIVITY OF SPECIMEN 800-0-H

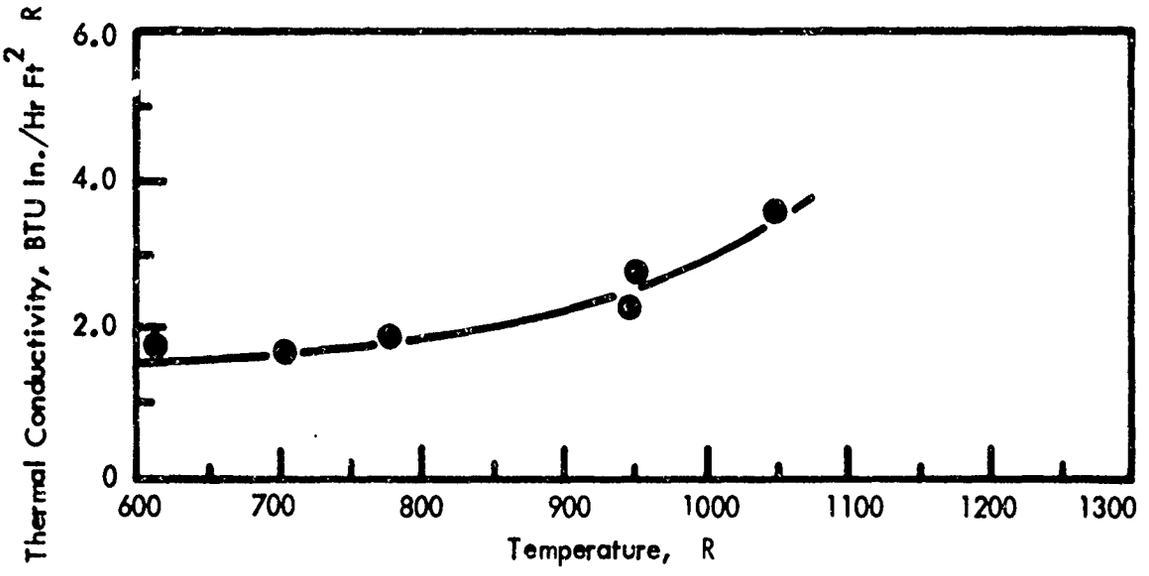

FIGURE 11 THERMAL CONDUCTIVITY OF SPECIMEN 800-30-H

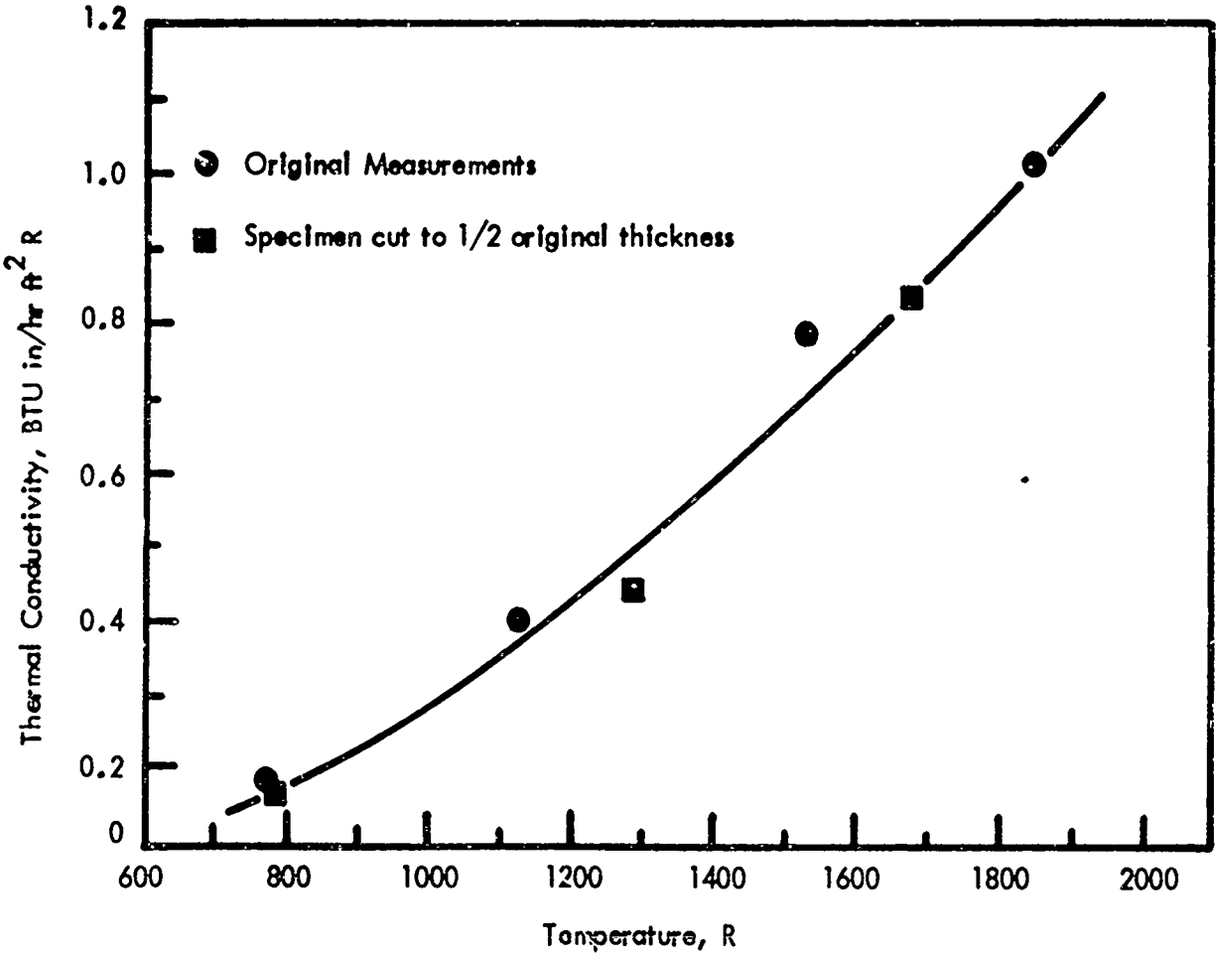

FIGURE 12 THERMAL CONDUCTIVITY OF SPECIMEN 1800-0-H

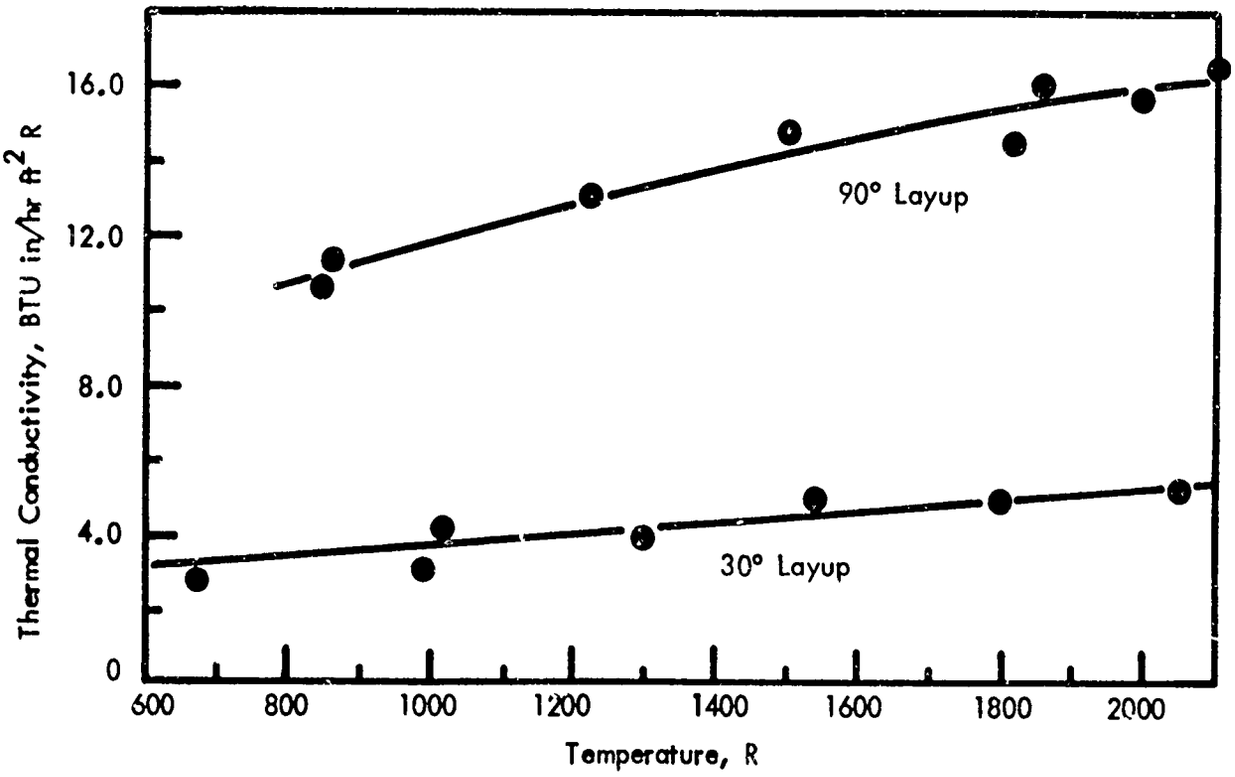

FIGURE 13 THERMAL CONDUCTIVITY OF SPECIMENS 1800-30-H AND 1800-90-H

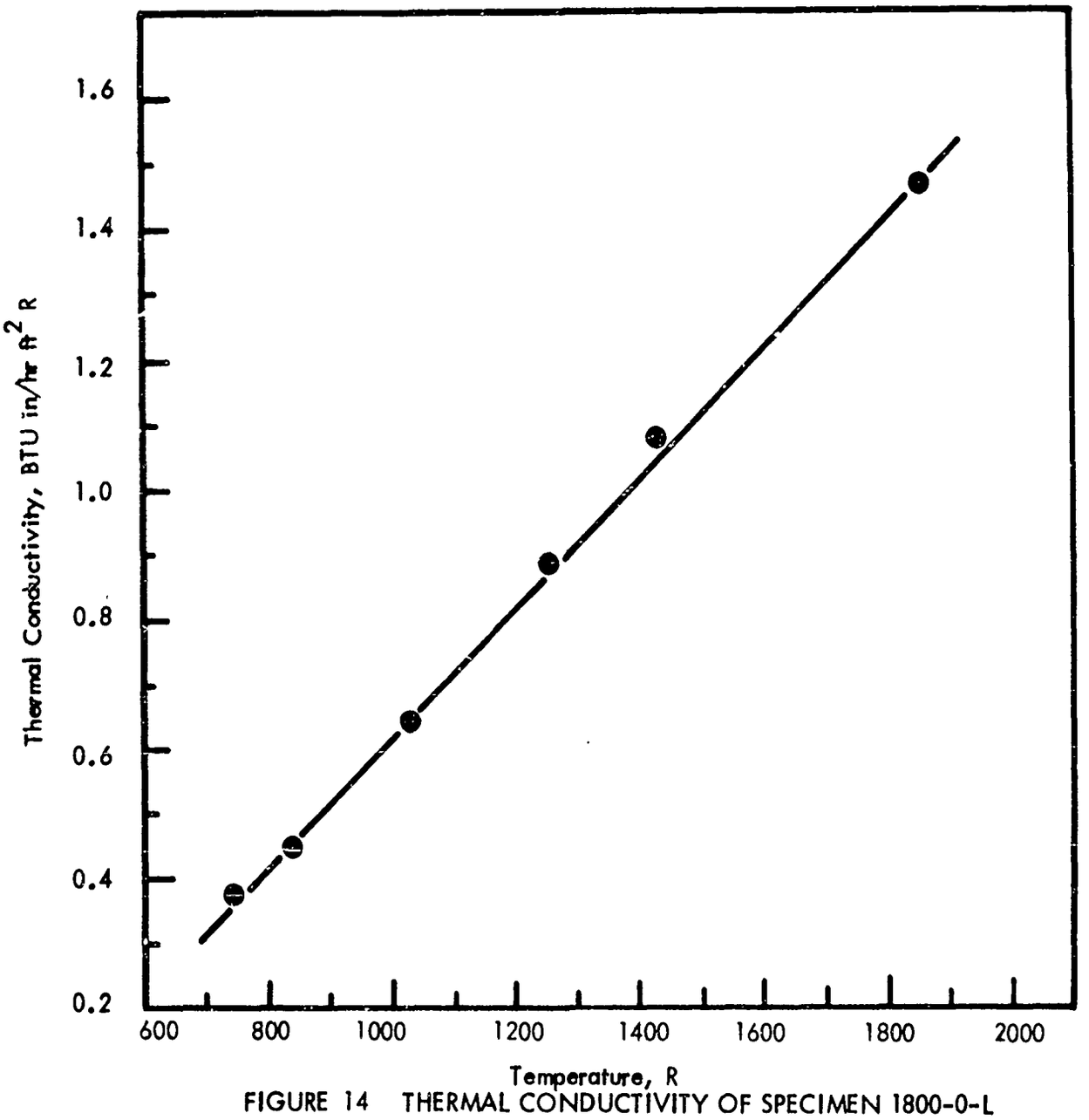

FIGURE 14 THERMAL CONDUCTIVITY OF SPECIMEN 1800-0-L

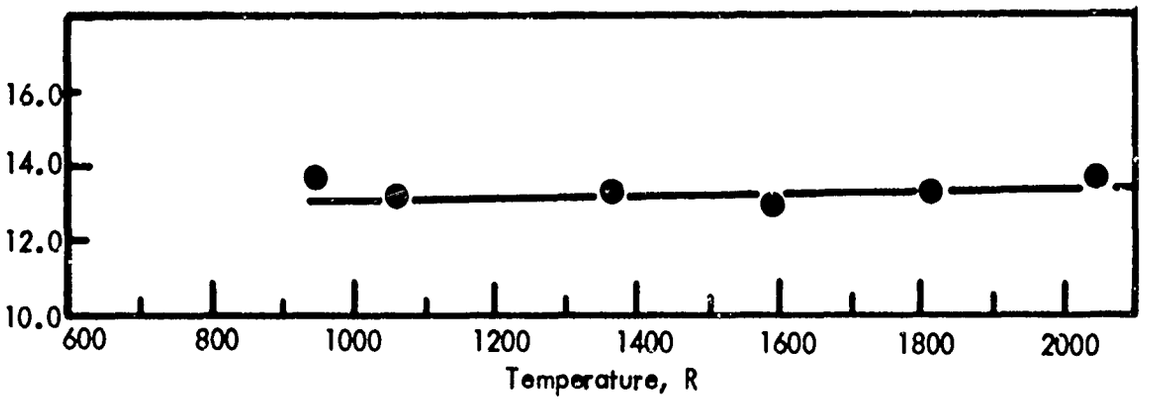

FIGURE 15 THERMAL CONDUCTIVITY OF SPECIMEN 1800-90-L

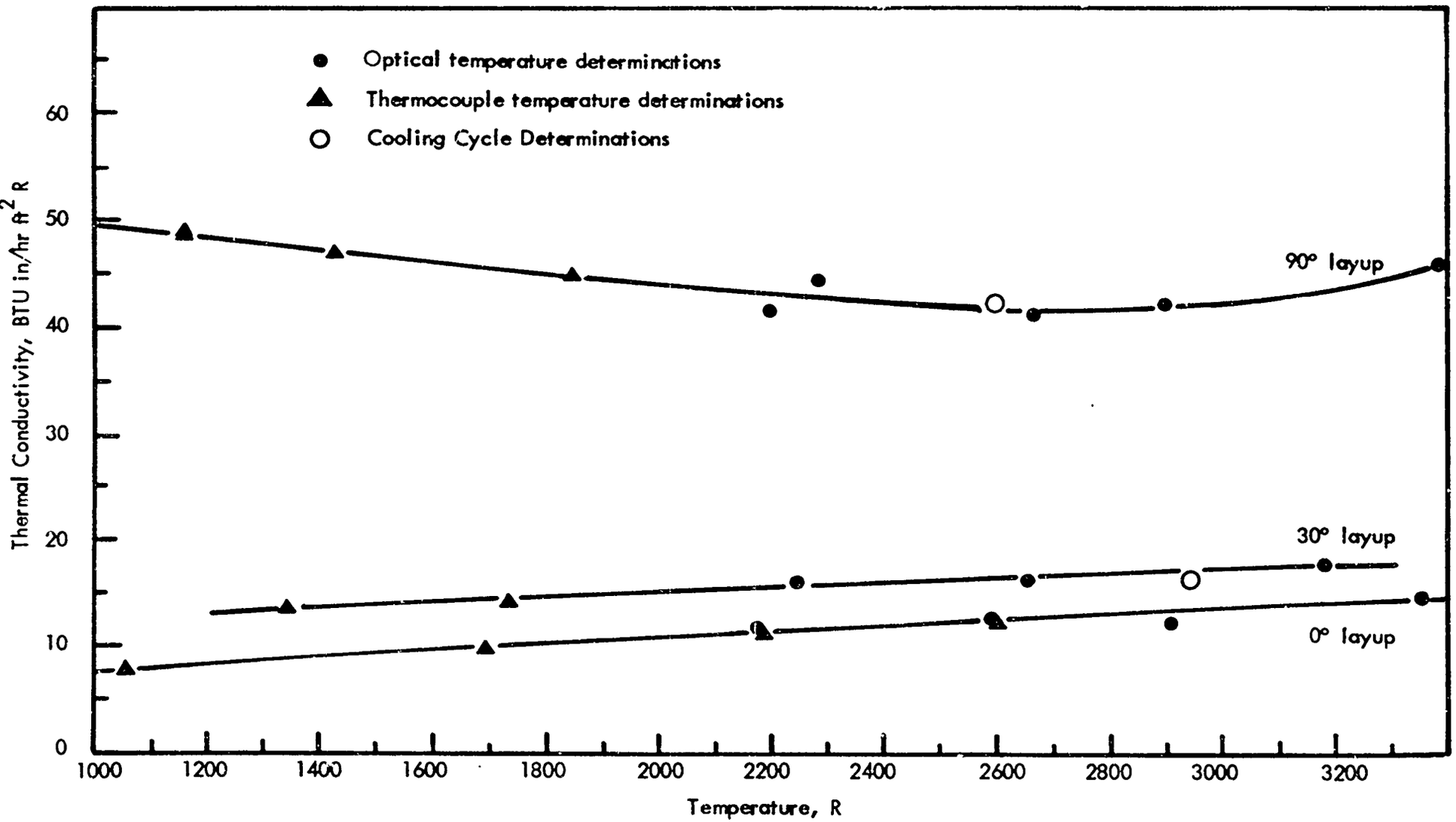

FIGURE 16 THERMAL CONDUCTIVITY OF SPECIMENS 3000-0-H, 3000-30-H, AND 3000-90-H

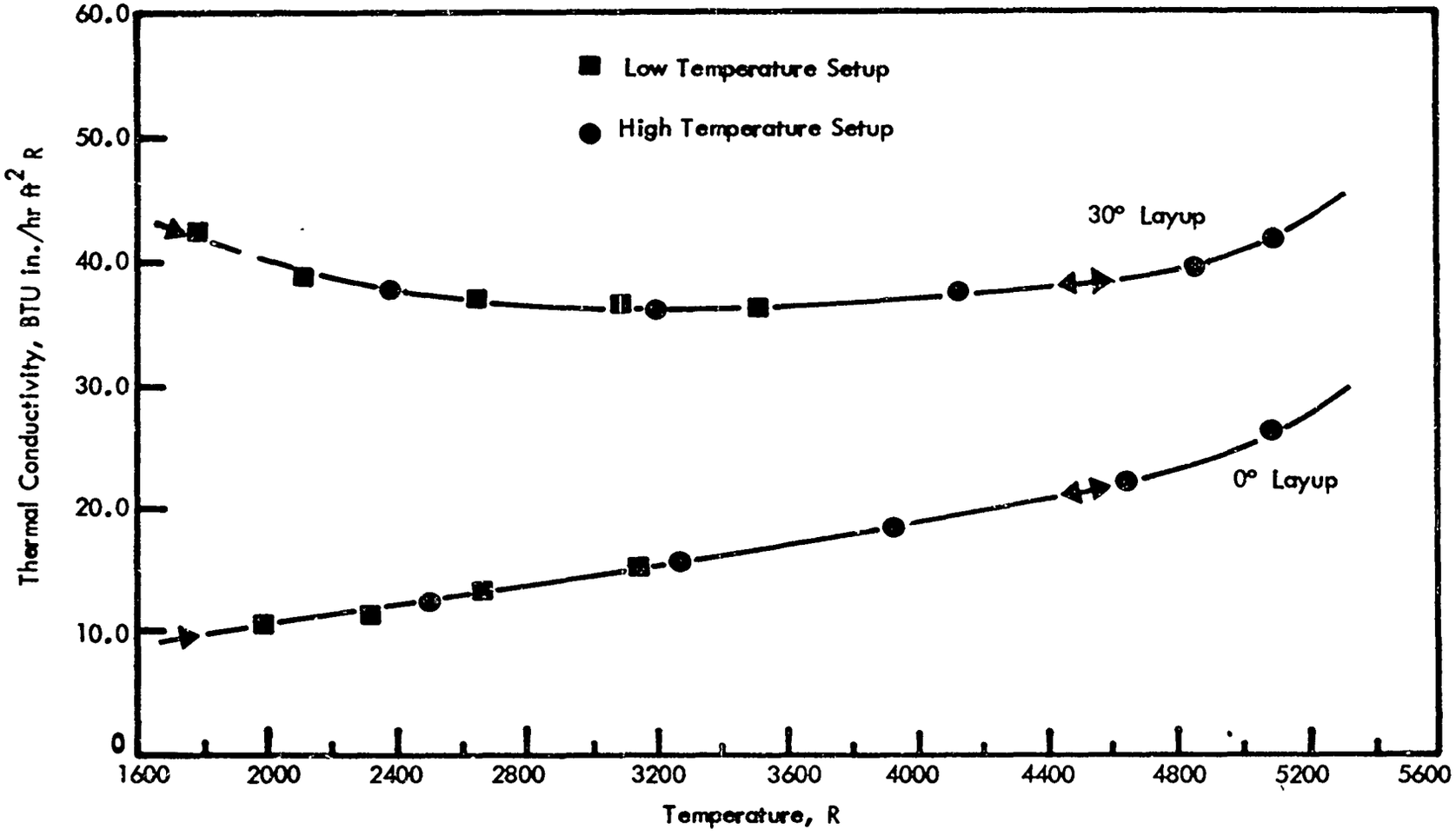

FIGURE 17 THERMAL CONDUCTIVITY OF SPECIMENS 5000-0-H AND 5000-30-H

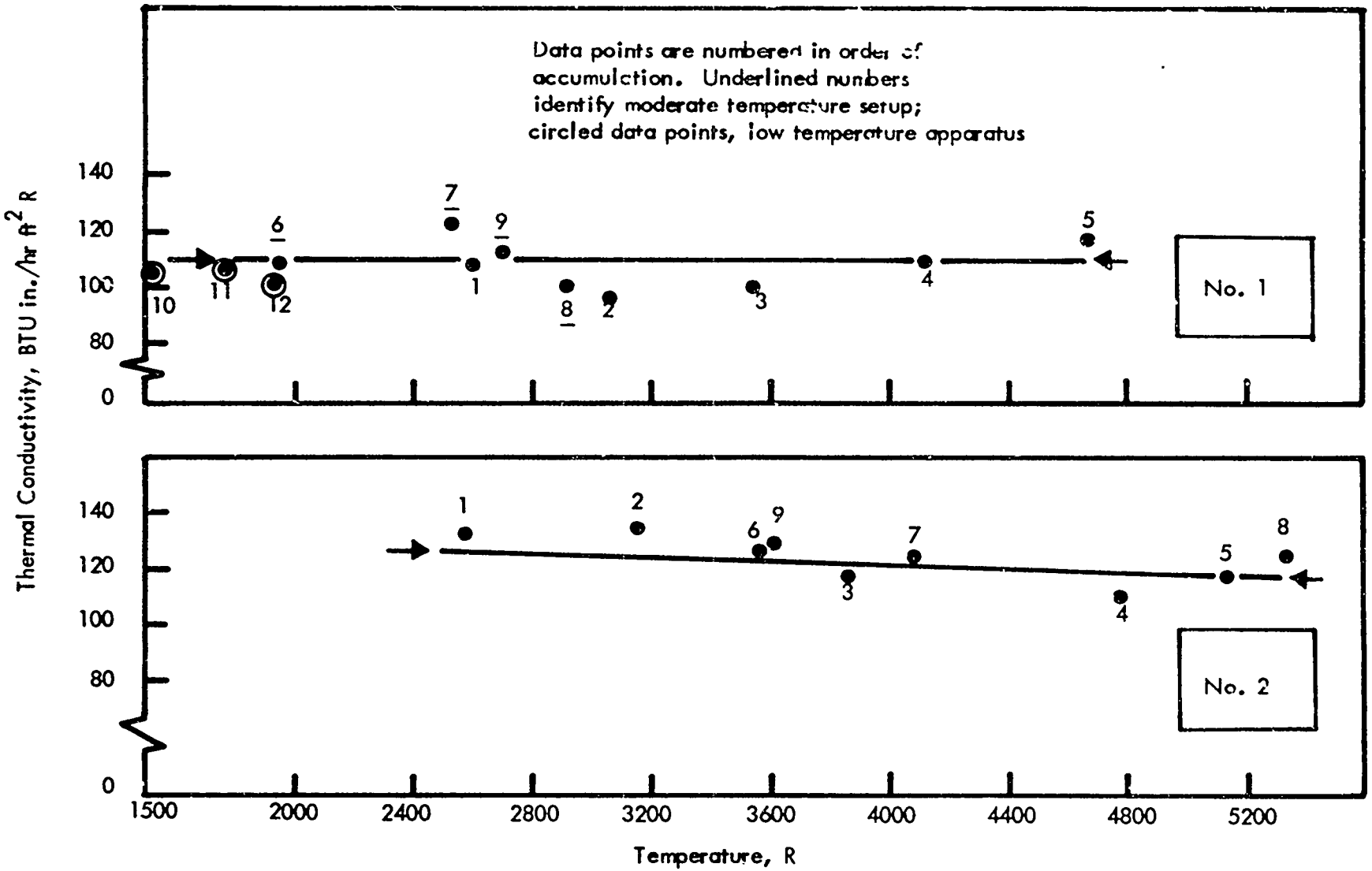

FIGURE 18 THERMAL CONDUCTIVITY OF SPECIMENS 5000-90-H No.1 and 5000-90-H No.2

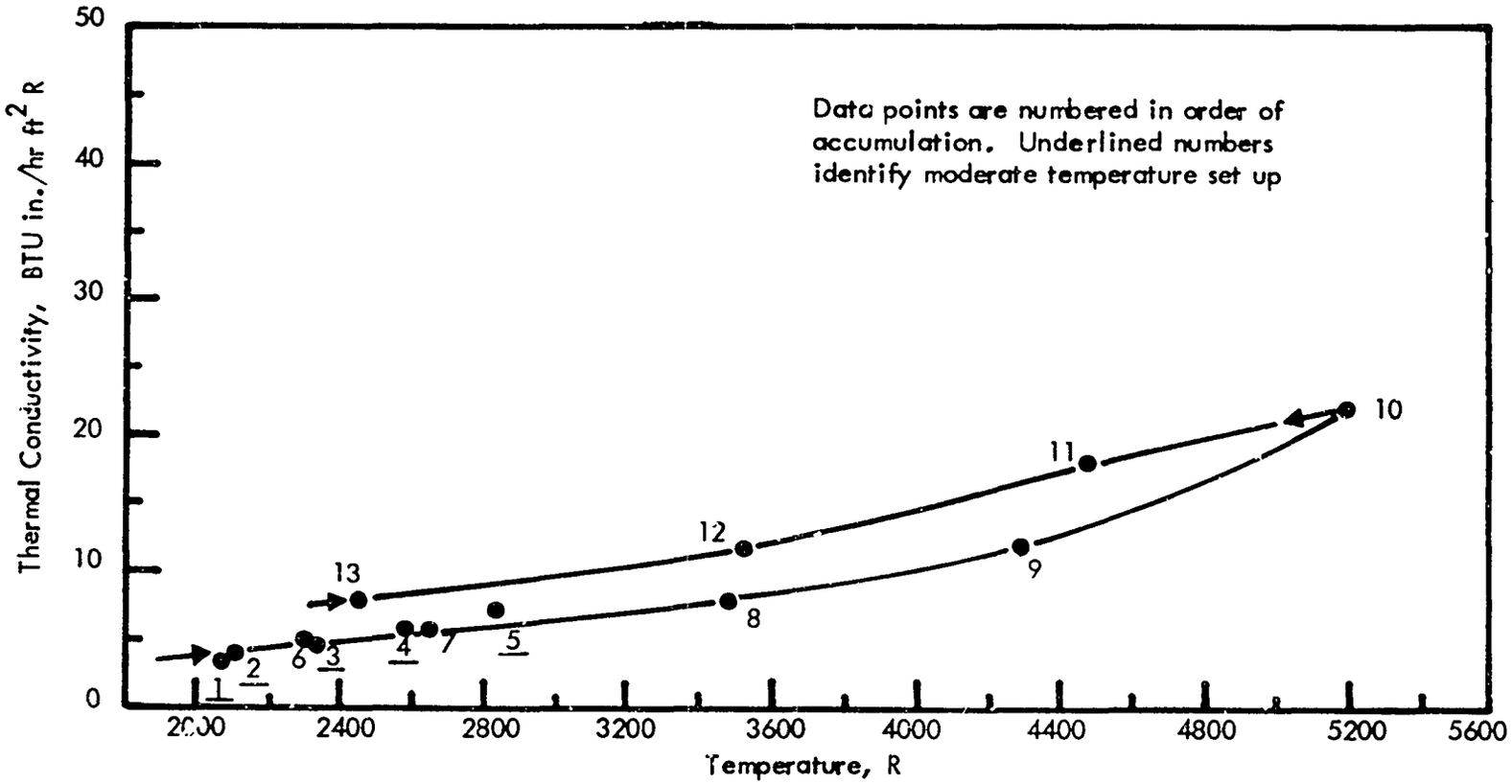

FIGURE 19 THERMAL CONDUCTIVITY OF SPECIMEN 5000-0-L - GRAPHITIZED DURING MEASUREMENT

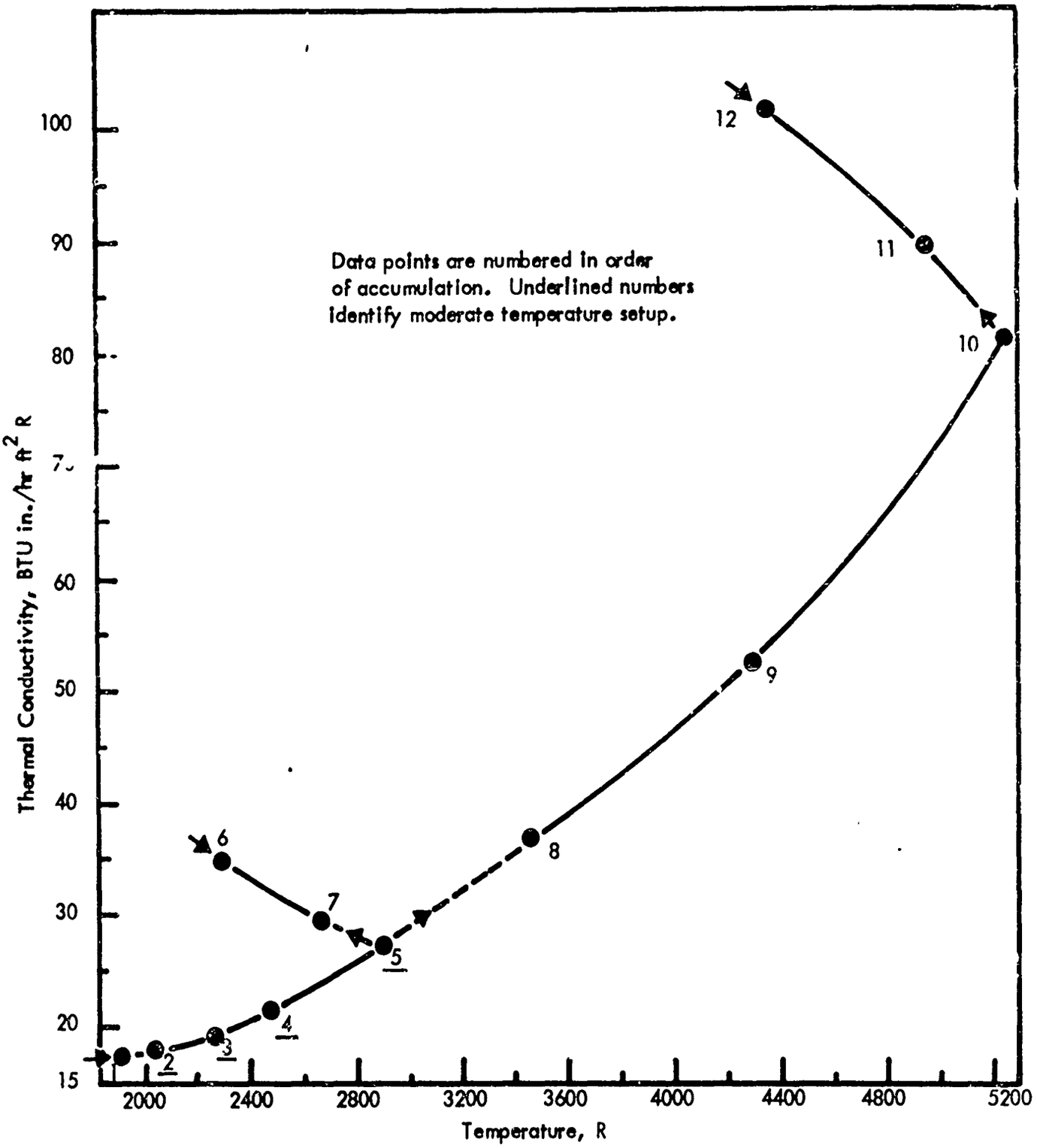

FIGURE 20 THERMAL CONDUCTIVITY OF SPECIMEN 5000-90-L - GRAPHITIZED DURING MEASUREMENT

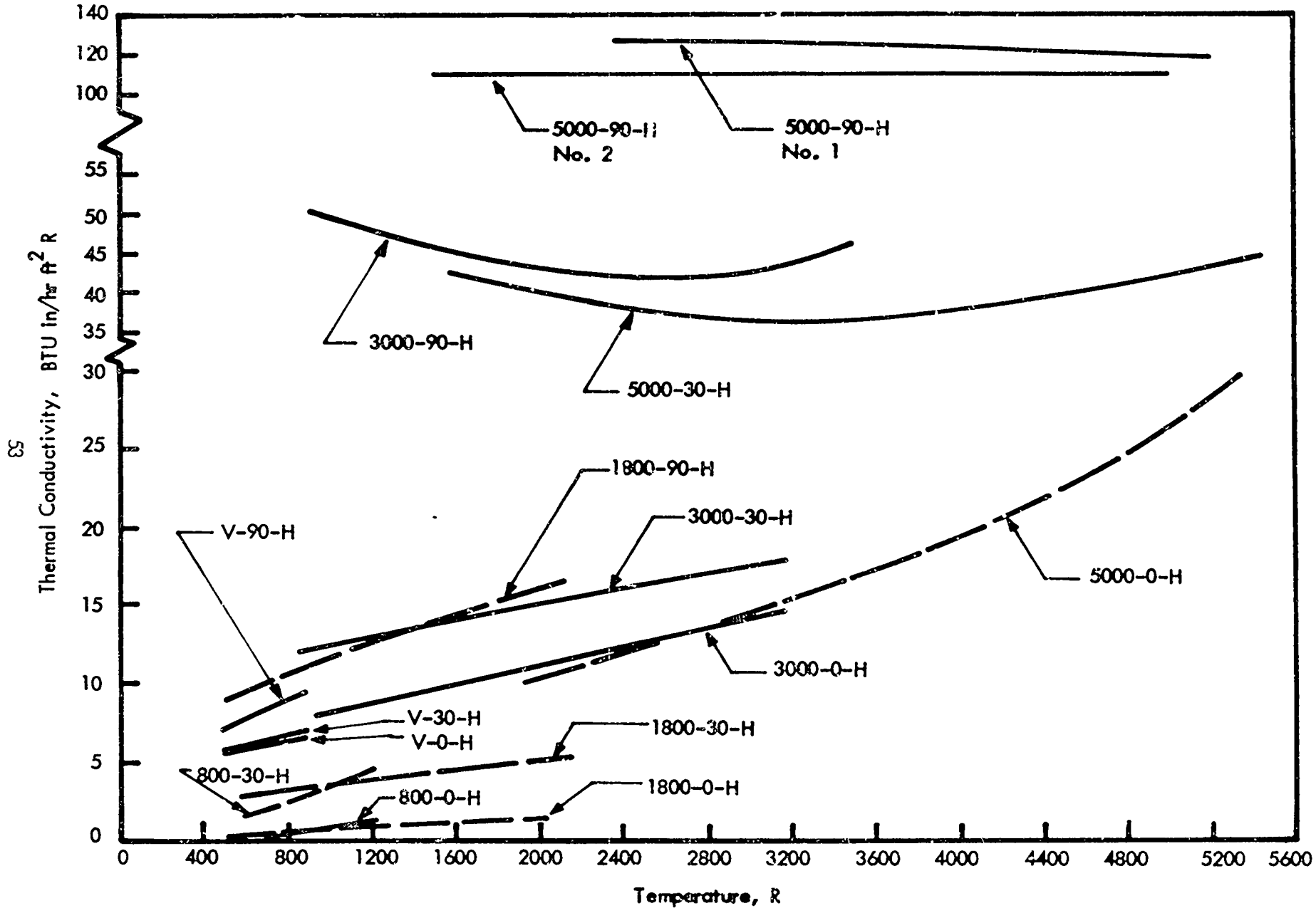

FIGURE 21 COMPOSITE OF SMOOTHED CONDUCTIVITY CURVES FOR HIGH DENSITY CHARS

The large differences in the levels and temperature dependencies of the ply and cross-ply conductivities may be explained on the basis of the simplified model for the composites presented in Section III. The highly oriented reinforcement cloth possesses a high, in-plane conductivity in relation to the carbon matrix, so that thermal energy is efficiently transported in the ply direction by conduction through the fiber bundles which are continuous in the ply direction. The cloth planes are discontinuous in the cross-ply direction, however, being separated from intimate contact by the resin or its pyrolysis residue which is the continuous matrix material in this direction. Thus, thermal properties in the ply direction are dominated by the properties of the continuous phase in the ply direction, the cloth. Similarly, the thermal properties in the cross-ply direction are dominated by the matrix. The properties at intermediate cloth layup angles are an admixture of the dominant features of the matrix and reinforcement cloth described by equation (1) in Section III.

Time-at-Temperature Effects on Measured Thermal Conductivities

The steady-state measurement technique utilized in this program required that the specimen remain at temperature for about two hours to allow the entire system to reach thermal equilibrium prior to accumulation of the data for a thermal conductivity calculation. The furnace-prepared chars experienced times-at-temperature on the order of minutes in their initial charring cycle, specifically, about five minutes at the highest heat treatment temperature, 5000°F. The investigations of Noda[5], and Yokokawa, et al [6, 7], give evidence that the time scales for certain of the ordering processes occurring in carbon to advance to near completion may indeed be on the order of hours, the rate constants being temperature dependent. Therefore, some concern for the stability of the furnace-prepared thermal conductivity specimens over the time-at-temperature periods involved in the program measurements is justifiable.

Specimen 5000-90-H No. 2 was measured under a plan designed to investigate effects of time-at-temperature on conductivity in the ply direction of the 5000°F material. The data, numbered to indicate the order of measurement, are given in Figure 18. The fact that Points 5 and 8 are within about 6 percent of each other, even though Point 8 involved several hours additional heat treatment, indicates little if any effect of time-at-temperature. A similar comparison of Points 6 and 9, approximately 2 percent apart, yields the same conclusion.

It will be noted in comparison of Specimens 1 and 2 in Figure 18 that the average conductivity of No. 2 is about 8 percent higher than that of No. 1, and its curve with temperature has a slightly negative slope compared to zero slope for No. 1. This difference might be related to prior low-temperature heat treatments. Specimen No. 1 was initially treated at 900°F, then taken directly to 5000°F. Specimen No. 2, however, was initially treated at 1800°F, so that it was exposed more extensively at this temperature than was No. 1.

Although there is considerable scatter in both sets of data in Figure 18, due to the lack of good precision in measurement of these higher-conductivity specimens, the difference between the two is believed to be real. The curve positions reflect a nominal 10 percent precision in the individual data points, and thus do not follow precisely the curvature indicated by the data.

Because of the dominating effect of structure on thermal conductivity in this material, the existence of time-at-temperature stability in the ply direction does not imply similar stability in the cross-ply direction. In fact, results for Specimen 5000-0-H might illustrate a time-temperature effect on conductivity in this direction. The conductivity of this specimen, previously heat treated to 5000°F, is proportional to the absolute temperature raised to the power 0.9 in the range 2000 R to 4400 R. Above 4400 R, the conductivity is not proportional to temperature to a constant power, and in the range 5200 R to 5300 R, the exponent is approximately 3.0. As will be pointed out later, an exponent of this order is appropriate to describe the effects of temperature-dependent ordering during measurement (Specimen 5000-0-L) during initial heating.

By analogy, it is possible that temperature dependent ordering proceeded beyond the level achieved in the original furnace preparation cycle during the thermal conductivity measurement of Specimen 5000-0-H. In this event, the conductivity temperature curve given in Figure 17 would not be reproduced upon remeasurement. The arrows on the curve define what is felt to be the temperature region in which the as-received specimen was stable against change caused by ordering processes which were slow relative to the residence times spent at char preparation temperature. The same argument is applied to Specimen 5000-30-H in Figure 17.

The conclusion appears to be that, under the conductivity measurement conditions of this program, time-at-temperature stability is achieved much more rapidly in the ply than in the cross-ply direction. This conclusion is tentative. It will be shown in Section VII that, when the data is reduced to predicted constituent properties using the theory of Chapter III, there is a tendency for both the fiber and the continious pyrolysis residue matrix conductivities to curve up near the heat treatment temperature and become asymptotic to a line representing the change in constituent conductivity versus heat treatment temperatures. This behavior would appear to be a permanent change as discussed above, and the two types of behavior are difficult to distinguish for any specimen where return data from the highest temperature were not obtained.

Effects of Structural Flaws on Measured Thermal Conductivities

In the thermal conductivity measurement plan there existed several opportunities to cross-check results for high and low density specimens which should be comparable providing heat treatment and composition are similar, and allowance is made for the

difference in porosity. It was shown in the theoretical development in Section III that structural flaws can be expected to have a major effect on measured conductivities of 0-degree layup specimens and relatively minor effect on conductivities of 90-degree layup specimens. Comments on several comparisons follow.

Comparison of the conductivities for the low and high density, 1800°F, 0-degree layup angle specimens 1800-0-H and 1800-0-L show that the values are in agreement over the entire temperature range of the measurements. For the 90-degree layup angle specimens 1800-90-H and 1800-90-L, the average values of the conductivities over the temperature range of the measurements are in agreement, but the temperature dependencies for the two chars are different. However, non-homogeneity of specimen 1800-90-L, evidenced in the thermal conductivity measurements, probably caused this difference. A similar fault was not indicated for specimen 1800-0-L. Therefore, it is concluded that the conductivities for the low and high density 1800°F chars are equivalent. It will be seen in Section VII that both the low and high density chars had about the same fiber volume fractions, so from the theoretical standpoint they should be equivalent.

Specimens 5000-0-L and 5000-90-L were initially heat treated to 1800°F. Therefore, the thermal conductivity values for these specimens before heat treatment above 1800°F should essentially equal those for specimens 1800-0-L and 1800-90-L, respectively, in the temperature region wherein the values overlap. Comparison of the ply conductivity value from Figure 20 (5000-90-L) with those from Figures 13 (1800-90-H) and 15 (1800-90-L) at 1800 R show that the former is 10 percent greater than that of specimen 1800-90-H, and 30 percent greater than that of specimen 1800-90-L. These differences are not considered especially significant.

In contrast, the cross-ply conductivity value for specimen 5000-0-L, Figure 19, is almost twice the value for specimens 1800-0-L and 1800-0-H, extrapolated to 1900R. Delamination, a problem most severe for the 0-degree layup angle specimens (see Appendix II) is the most probable reason for this difference. All 0-degree specimens for measurement above 1800°F were obtained by slicing in half the original 1/2 inch thick disks. For this reason, specimen 5000-0-L may have been expected to contain fewer series delaminations than the 1800°F specimen. However, specimen 1800-0-H was measured in its original 1/2 inch thickness and then cut and remeasured at one-half its original thickness, and the data from the two measurements agreed within experimental error. The discrepancies between the conductivities of specimen 5000-0-L and specimen 1800-0-L cannot be explained on the basis of any single observed structural difference in the two specimens, or the experimental error in the measurements. It is surmised that variations in interlaminar bonding and effective layup angle, non-homogeneity, (see Appendix II) and uncertainty in the measurements combine to account for the observed inconsistency. The greater inconsistency in the cross-ply data is not surprising from the theoretical standpoint. It is also reflected in predicted pyrolysis residue conductivities in Section VII.

Effect of Graphitization During Conductivity Measurements (Low-Density Chars)

The thermal conductivites of two low-density specimens (0- and 90-degree) which had been previously heat treated to only 1800°F were measured through the range to 5000°F to note the effects of ordering in the material on conductivity during heat treatment. In addition to this prime objective, results of these measurements were also examined to establish a comparison with those on high density material, insofar as heat treatment effect on conductivity is concerned. Low density chars were selected for these measurements to give a better approximation of actual ablation char porosities on the basis of the Reference 1 characterization studies. The results are of most interest when presented in terms of predicted constituent conductivities in Section VII, but some observations can be made directly from the measured composite conductivities.

Figures 19 and 20 are plots of thermal conductivity data for the low-density 0-degree and 90-degree chars graphitized during measurement. As indicated, the points are numbered in the order measured, and dwell times at each equilibrium were on the order of two hours. The consistency of data under two experimental setups for each specimen is very good; two setups were required to cover the entire temperature range with comparable accuracy. The dominance of the cloth and matrix on the conductivity in the ply and cross-ply directions, respectively, are again evident, and the ordering effects which results in irreversibility of the curves are illustrated dramatically in the 90-degree specimen.

To provide basis for comment on the effects of the ordering processes, the curves of Figures 19 and 20 are presented on log-log scales in Figure 22. If conductivity is explicitly proportional to absolute temperature raised to a constant power, the exponent of temperature can be obtained from the slope of conductivity-versus-temperature curve on the log-log plot. For the initial heat-up of the 0-degree layup angle char the temperature exponent of the conductivity is reasonably constant at 1.2 between 2500 R and 3500 R, and increases continuously above 3500 R, reaching the value 3.7 between 5000 R and 5200 R. Upon cooling from 5200 R, the temperature exponent reduces to 1.3 between 5200 R and 5000 R, while the entire cooling curve may be reasonably approximated by a straight line of slope 1.2 on the log-log plot. Evidently, the higher values of the exponent are associated with temperature-dependent ordering in the pyrolysis matrix which progresses when the ambient temperature exceeds the maximum HT previously experienced by the char components. Based upon the accumulated results for all the program chars, the cooling curve in Figure 19 should be repeatable upon subsequent reheating of the specimen.

The conductivity-temperature relation for the 90-degree layup angle, low density char appears almost linear between 2500 R and 5200 R on the log-log plot, Figure 22. The temperature exponent of the conductivity between 2500 R and 3500 R is 1.7, increasing to 2.6 between 5000 R and 5200 R. A reasonable approximation to the entire conductivity HT curve between 2500 R and 5200 R in Figure 22 is attained with a straight line of slope 1.8.

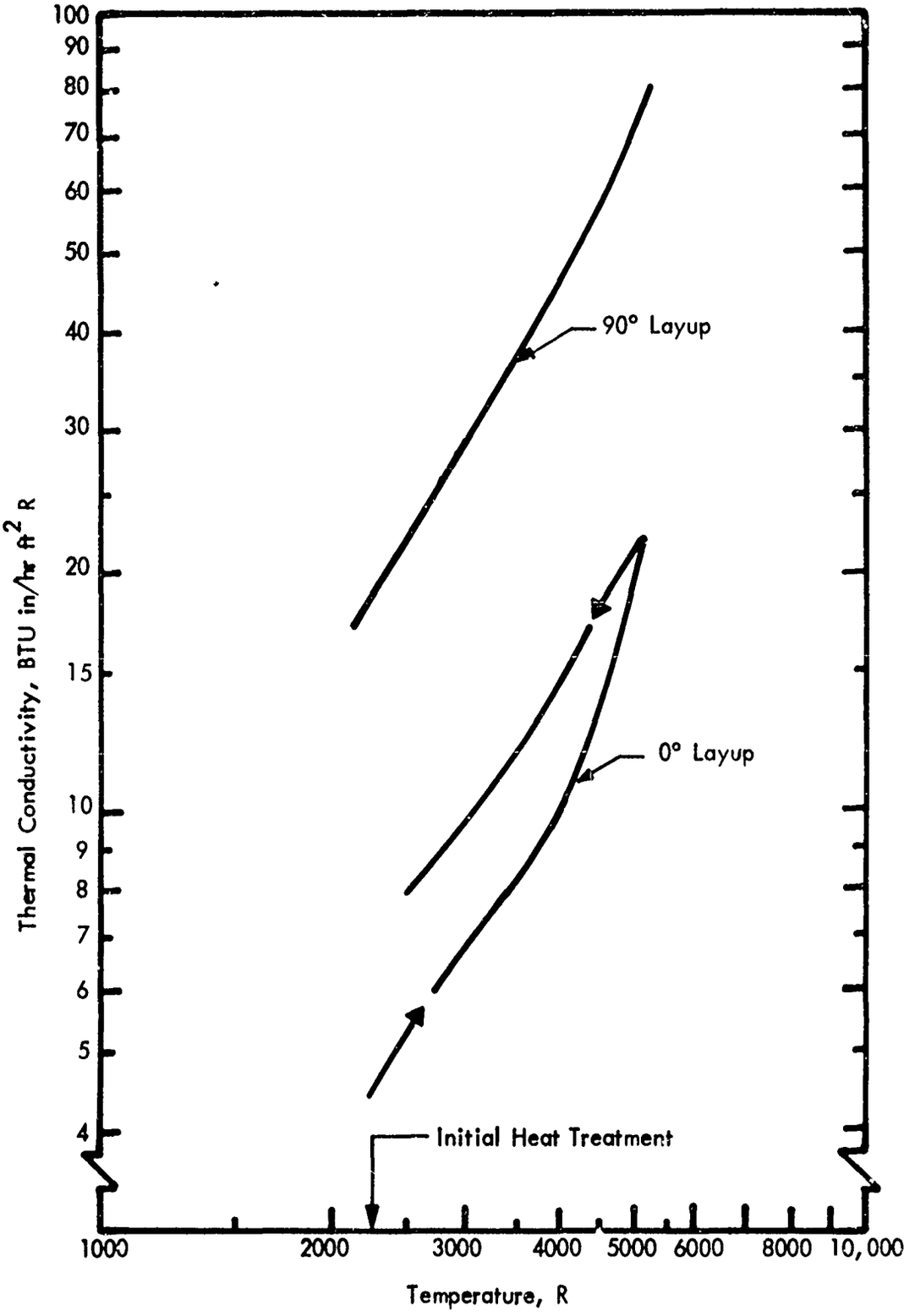

FIGURE 22 THERMAL CONDUCTIVITY OF SPECIMENS 5000-0-L AND 5000-90-L

Note that the conductivity slope between 2500 R and 3500 R is lower in the cross-ply direction and above 3500 R the slope is lower in the ply direction. The difference below 3500 R is much more dramatic if the effect of the apparent variation in total void fraction between these temperatures (see Section Vi) is included. X-ray diffraction intensity measurements presented in Section VI, which provide a relative measure of the amount of graphite-like crystallinity present, show a factor of 2 increase in this temperature range in both the ply and cross-ply directions. In addition, polarized light photomicrographs in Section IV reveal the presence of ordered material in the matrix adjacent to the fibers at the 3500 R char level. Consideration of these results together with the relative increases in ply and cross-ply conductivities suggests that the sites of the ordered material generated in the temperature range 2500 R to 3500 R are localized within, and/or about, the reinforcement fibers. The possibility of catalytic graphitization of the hard carbon matrix adjacent to the fibers should be noted. It is reported (Appendix I) that a variety of elements including graphite, added to certain hard carbons, enhance the tendency of the carbon to order to a much greater degree than it normally would without the additives.

Between 3500 R and 5200 R the ply and cross-ply conductances increase by 111 and 175 percent, respectively. The behavior of the cross-ply conductivity with ambient temperature in Figure 19 after exposure to maximum HT shows that the temperature sensitivity of the conductivity of specimen 5000-0-L is somewhat greater than that for the corresponding high density specimen 5000-0-H (below 4500 R); the conductivity of the former (cooling cycle) is about 38 percent less than that of the latter at 2400 R, and 15 percent less at 4400 R. Similarly the conductivity of specimen 5000-90-L is about 33 percent less than that of the corresponding high density specimen 5000-90-H No. 2 at 5200 R. Interestingly, the slopes of the ply conductivity with ambient temperature at 2900 R and 5200 R, Figure 19, are negative and much greater for specimen 5000-90-L than for the corresponding high density chars, specimens 3000-90-H and 5000-90-H No. 2. A full explanation of this behavior has not been found, and comparative results from thermal diffusivity measurements presented later show positive rather than negative slopes.

The above comments, based on the measured composite conductivities, are illustrated more clearly by consideration of predicted constituent conductivities in Section VII. Constituent conductivities are also easier to generalize for application to ablation calculations on the basis of the theory in Section III.

NEW CONDUCTIVITY DATA FOR MX-4926 AND FM-5014

The thermal properties of MX-4926 phenolic-carbon and FM-5014 phenolic-graphite were investigated in a previous program, and the results reported in Reference 1. The same self-guarding disk technique was used in the thermal conductivity measurements of MX-4926 and FM-5014 as in the present program for FM-5055A phenolic-carbon materials.

Because of advances in materials, techniques, and experience, the reliability in the thermal conductivity measurements for anisotropic materials above 2000°F has been greatly improved since the original data were generated. For this reason, several of the MX-4926 and FM-5014 chars were re-measured as a part of the FM-5055A measurement program. New conductivity-temperature relationships are suggested for these materials in some areas based upon this new data.

The conductivity of a Zone II (Reference 1, 2500°F initial heat treatment), 90-degree layup angle, MX-4926 char was measured in a program to establish the conductivity as a function of ambient temperature below the initial heat treatment temperature (HT). Then the specimen was advanced in temperature to obtain the conductivity as a function of HT to near 4000°F, the Zone I limit in Reference 1. Two cooling cycles were interposed during the heat treatment cycle above 2500°F; one near 2700°F, and again after reaching maximum HT. The data are given in Figure 23.

The conductivity of a Zone I (4000°F initial heat treatment), 45-degree layup angle, MX-4926 char was measured as a function of increasing temperature to about 4350°F, followed by a cooling cycle. These data are also given in Figure 23.

Finally the conductivity of a Zone II, 90-degree layup angle, FM-5014 specimen was measured as a function of ambient temperature within the Zone II HT boundary, followed by heat treatment to about 4060°F and establishment of the conductivity ambient temperature relationship below the maximum HT. The data are given in Figure 24.

All data points in Figures 23 and 24 are numbered in the order in which they were determined. Of special note are the results for the 90-degree layup angle, FM-5014 specimen obtained subsequent to maximum HT. The repetitious measurements within the temperature region 2500°R to 4500°R show that long time-at-temperature exposures at temperatures below the maximum HT do not further change the thermal conductivity of this specimen, within experimental uncertainty.

Smoothed recommended conductivity-temperature curves based upon the new data for the MX-4926 and FM-5014 materials are given in Figures 25 and 26 where they are also compared with the curves originally reported in Reference 1 for the Zone II and I materials. The new recommended curves in these figures include consideration of experimental uncertainty and precision as well as the results of the present measurements on the FM-5055A materials. The temperature regions in which the specimens are felt to be stable, i.e., the conductivity values are repeatable upon cooling and reheating of the specimen, are indicated by arrows placed on the curves.

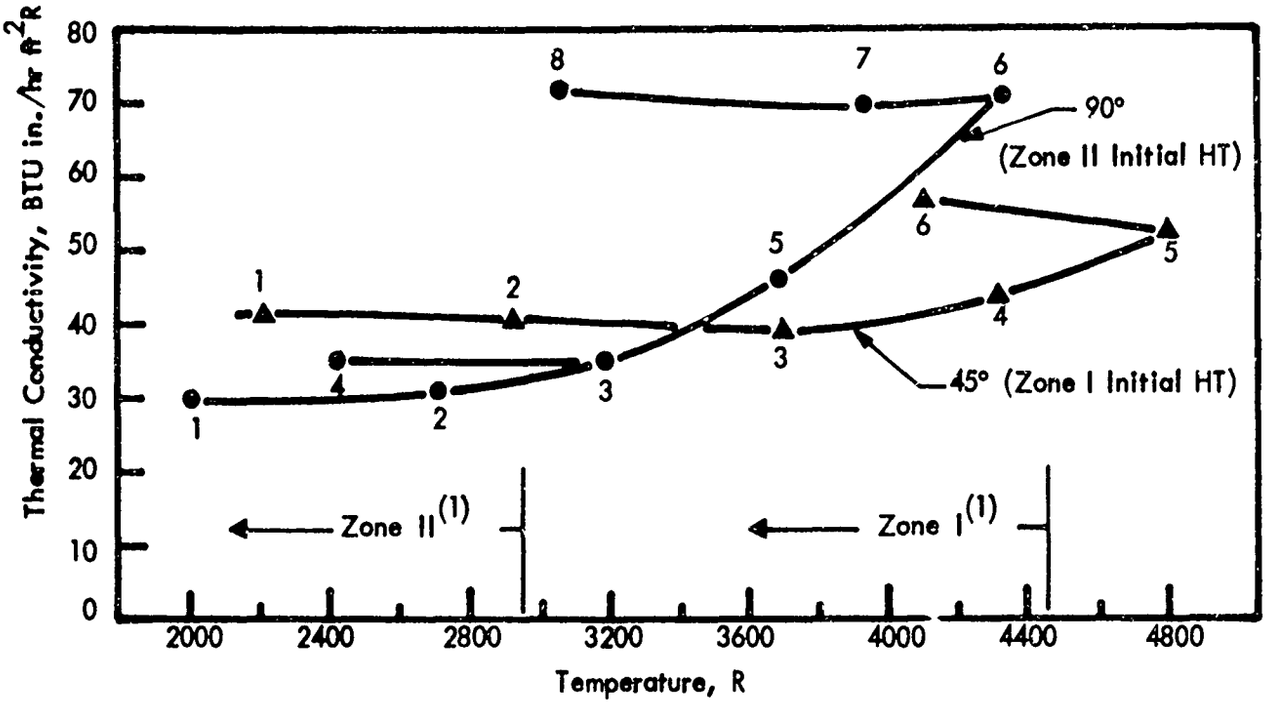

FIGURE 23 THERMAL CONDUCTIVITY OF MX-4926 90° AND 45° LAYUP CHARS

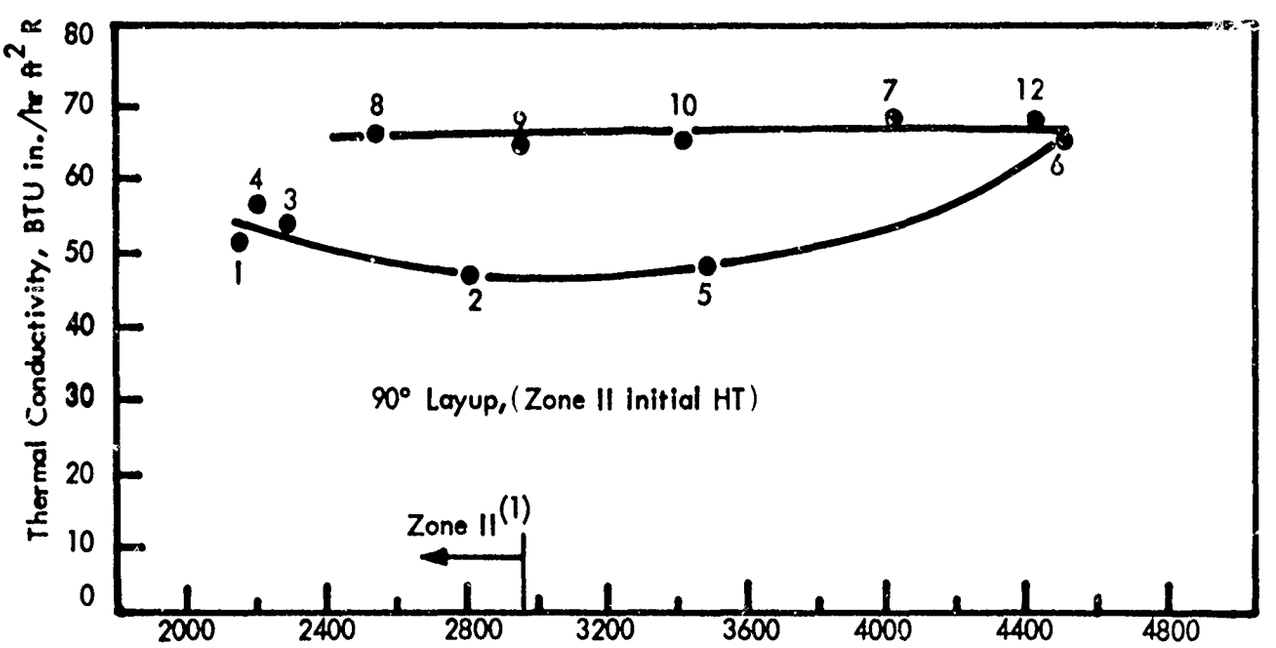

FIGURE 24 THERMAL CONDUCTIVITY OF FM-5014 90° LAYUP CHAR

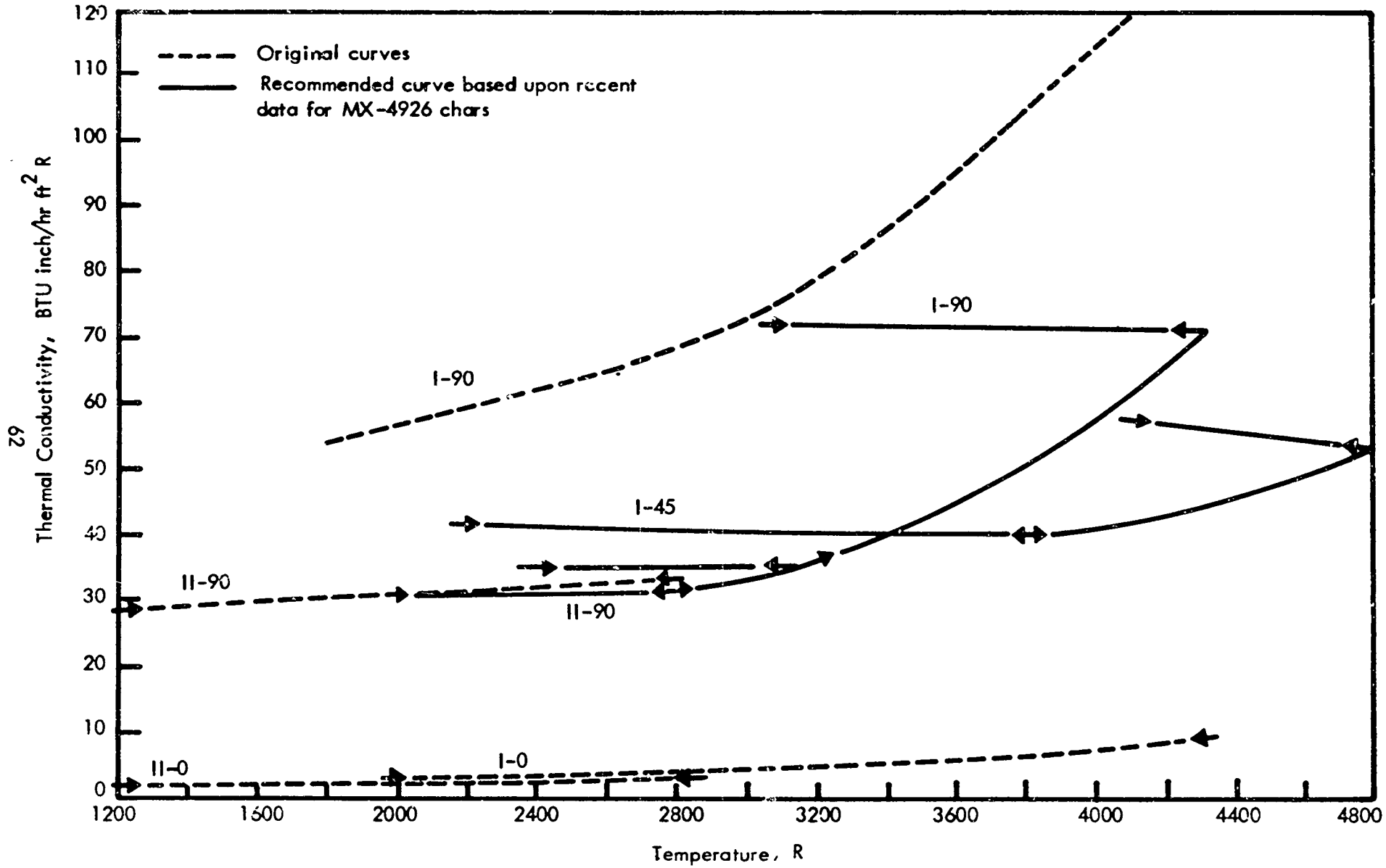

FIGURE 25 THERMAL CONDUCTIVITY OF MX-4926 PHENOLIC CARBON CHARS - RECOMMENDED CURVES FOR ZONES II AND I

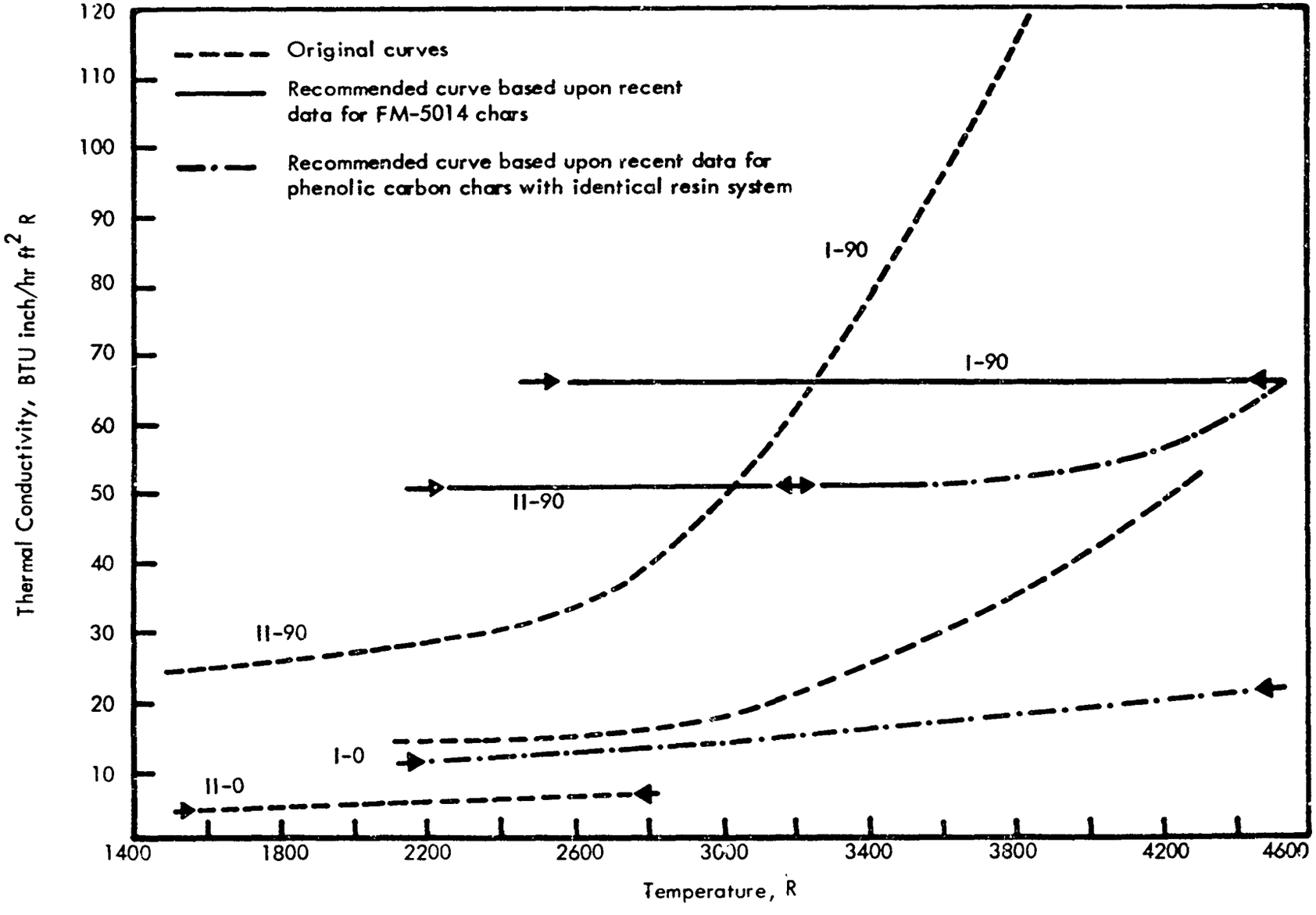

FIGURE 26 THERMAL CONDUCTIVITY OF FM-5014 PHENOLIC GRAPHITE CHARS-RECOMMENDED CURVES FOR ZONES II AND I

Although no 0-degree layup angle specimens were re-measured (specimens were not available), there is good reason to suggest a new conductivity temperature relation for the 0-degree layup angle, Zone I, FM-5014 specimen. As pointed out in Section III, the cross-ply char conductivity varies in direct proportion to the conductivity of the pyrolysis residue. The resin systems in FM-5014 and FM-5055A are identical and specimens of both materials were pyrolyzed in the same manner. On this basis, cross-ply conductivities in the two materials should behave similarly. Since some doubt remained as to the validity of the original[1] FM-5014 cross-ply conductivity values, the recommended zone 1, 0-degree layup curve (I-O) in Figure 26 was derived from the equivalent FM-5055A data.

The new recommended curves for MX-4926 and FM-5014, together with the Reference 1 data at lower temperature, has been used for additional constituent property predictions for phenolic-carbon materials in Section VII. There it is shown that the CCA-1 reinforcement behaves similarly in the two phenolic-carbon systems and the resin and pyrolysis residue predicted conductivities from FM-5014 are similar to those for the same resin system from the FM-5055A data. It should be noted that the 90-degree layup data on virgin FM-5014 was plotted incorrectly in Reference 1. The conductivity scale should have been four BTU in/ft^{2}sec.R greater than was shown. The correct values were used in obtaining predicted constituent conductivities in Section VII. Tabulated values are given in Appendix V.

The behavior of the graphite reinforcement conductivity in FM-5014 has been presented previously in Reference 22 and is also shown in Section VII. In general, the graphite fiber conductivity starts out at higher values in the virgin material than the carbon fiber conductivity, but increases much less with increasing heat treatment temperature. As a consequence, high temperature values of ply direction conductivity in FM-5014 are lower than in either MX-4926 or FM-5055A, and low temperature values are higher. Cross-ply conductivity values in the two materials are similar, as would be expected from theoretical considerations.

COMPARATIVE THERMAL DIFFUSIVITY MEASUREMENTS ON ABLATION CHARS AND FURNACE CHARS

The thermal conductivity data obtained on this program and a previous program[1], as well as most of the available published data, were obtained by steady state thermal conductivity measurements on stable furnace-charred samples which represented major stages of ablation. On this program and the previous one[1], detailed characterization of the conductivity samples has been employed to demonstrate their relationship to the same characteristics defined in actual post-ablation chars[1]. Thermal conductivity values derived from thermal diffusivity measurements on small samples of actual ablation chars were conducted at the Air Force Materials Laboratory to demonstrate the correspondence between data on post-ablation chars and furnace

prepared chars. Comparative results from diffusivity measurements were also obtained on selected furnace chars. Results for MX-4926 phenolic-carbon and FM-5014 phenolic-graphite studied on the previous program[1] have been published previously[23]. This discussion compares these previous diffusivity derived conductivities with the revised steady state conductivities on MX-4926 and FM-5014 presented above, and presents a comparative measurement on 90-degree layup FM-5055A char (5000-90-L) graphitized during the diffusivity measurements at temperatures exceeding the initial 1800°F furnace charring heat treatment. In general, the two types of measurements agree within about 30%.

Thermal diffusivity measurements were made using the pulse technique over the temperature range of 600 R to 5200 R. In this technique thermal diffusivity was obtained from the half time of the back face temperature response of a thin disk sample held on knife edges in an evacuated tube furnace and exposed to an energy pulse at the front face. A 15-joule normal mode ruby laser was used as the pulse energy source with about 4 to 6 joules absorbed by the sample. The back-face temperature response was obtained by photographing an oscilloscope display of the signal from an indium arsenide infrared detector. After correcting for any transient losses,[28,29] the accuracy of the thermal diffusivity data is estimated to be about ±10%, with sample thickness irregularities being the major source of error.

Post-ablation char samples for the thermal diffusivity measurements were machined directly from the nozzle throat sections using the same definition of char zones[1] developed for the previous thermal conductivity measurements on MX-4926 and FM-5014. The dimensions of the disk samples were 0.270 inches in diameter by 0.040 to 0.070 inches thick. For samples with the disk axis approximately normal to the nozzle char layer (90-degree layup angle samples), the sample mid-plane was located approximately in the center of the particular zone, which results in the total sample volume being representative of average conditions in the zone. However, for samples with axis approximately parallel to the nozzle char layer (0-degree layup angle samples), the samples overlapped the zones to a slight extent since the sample diameter was greater than the zone thickness. Several thermal diffusivity samples were also machined from the MX-4926 thermal conductivity specimens following the conductivity measurements. The FM-5055A sample was taken from the same furnace charred slab as the corresponding thermal conductivity sample. All samples were taken from areas free of delaminations.

The thermal diffusivity results, α, were converted to thermal conductivity using specific heat, C_p, data from Reference 1 for the nozzle char and using density values, ρ, determined for each thermal diffusivity sample. Specific heats determined for both nozzle chars and furnace chars in Reference 1 were the same. The standard relation, $k = \alpha \rho C_p$, was used for the calculations. The use of transient technique data for calculation of thermal conductivity for porous and

heterogeneious materials, like those used in this study, is always suspect. Although adequate theory is not available to predict this effect, it is felt that errors greater than about 25% are unlikely.

The conductivity results derived from diffusivity measurements are shown in Figures 27, 28 and 29 along with the comparable results from the steady state thermal conductivity measurements presented previously. For MX-4926 and FM-5014, the data is shown for heating cycles only; however, measurements were made on cooling from maximum temperature and with only a few exceptions, the heating values were reproduced. The maximum furnace charring heat treatment (HT) temperature corresponding to the nozzle char zones I, II and III defined in Reference 1 is indicated for the data on furnace chars. In the nozzle chars, Zone I included all definately graphitized chars that had reached temperatures from 3300 R to 5100 R during ablation, Zone II was fully pyrolyzed but nominally ungraphitized char between 2300 R and 3300 R, and Zone III was almost completely pyrolyzed, ungraphitized char between 1600 R and 2300 R. The results from each of the two methods of establishing thermal conductivity are self consistent but differences between the two types of data are apparent at high temperatures. All of the measured conductivity data is within about 30% of the conductivity values derived from diffusivity data except for 0-degree layup angle Zones I and II in MX-4926 and Zone II in FM-5014. In addition, the curves from each type of measurement are converging versus temperature except for the Zone II 0-degree layup chars in MX-4926 and FM-5014 and the cooling data on FM-5055A. With these exceptions, the conductivity values derived from diffusivity data on nozzle chars are close enough to the directly measured conductivities on furnace chars (within the combined measurement uncertainties) to validate the approach of establishing properties from measurements on simulated chars.

In the ply direction (90-degree layup) Zone I chars of MX-4926 phenolic-carbon, values from diffusivity measurements on nozzle chars are lower and similar values on furnace chars are equal to the directly measured conductivities on furnace chars. Low nozzle-char values are consistent with the fact that the Zone I nozzle char diffusivity specimens are obtained below the char surface in a region of low graphitization level relative to the furnace chars. Zone I values derived from diffusivity measurements on furnace chars show good agreement and are believed to reflect both the uniformly high level of graphitization in the samples and the fact that even though the diffusivity samples were selected from regions of slightly higher average density where no delaminations had occurred, this had little effect on K_{90}. Similar effects are believed to have occurred in the Zone II laminate-direction data on MX-4926.

The good agreement of all MX-4926 and FM-5014 cross-ply (0-degree layup) data in Zone III and the poor agreement in Zones II and I mentioned previously

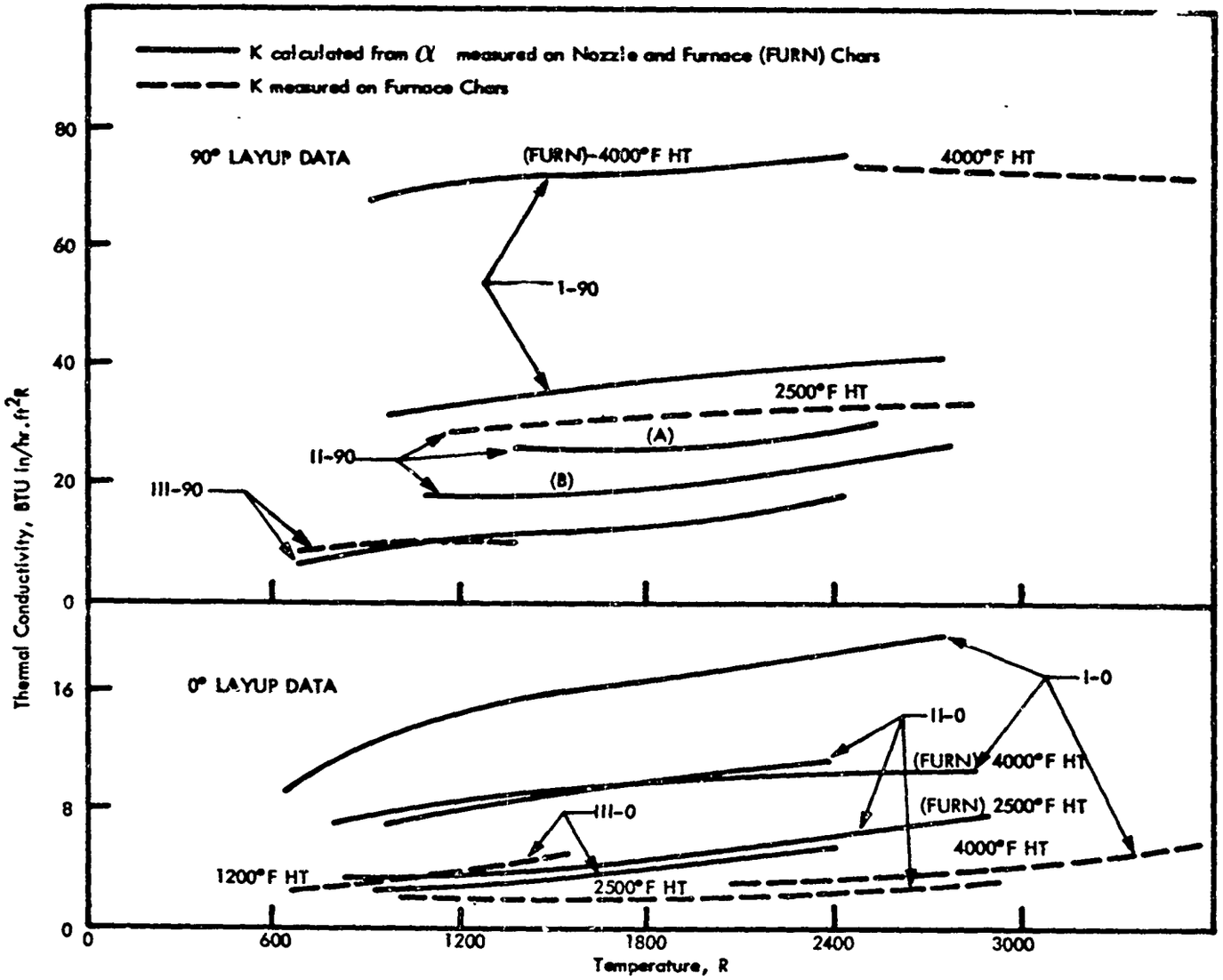

FIGURE 27 MX-4926 NOZZLE AND FURNACE CHAR CONDUCTIVITY

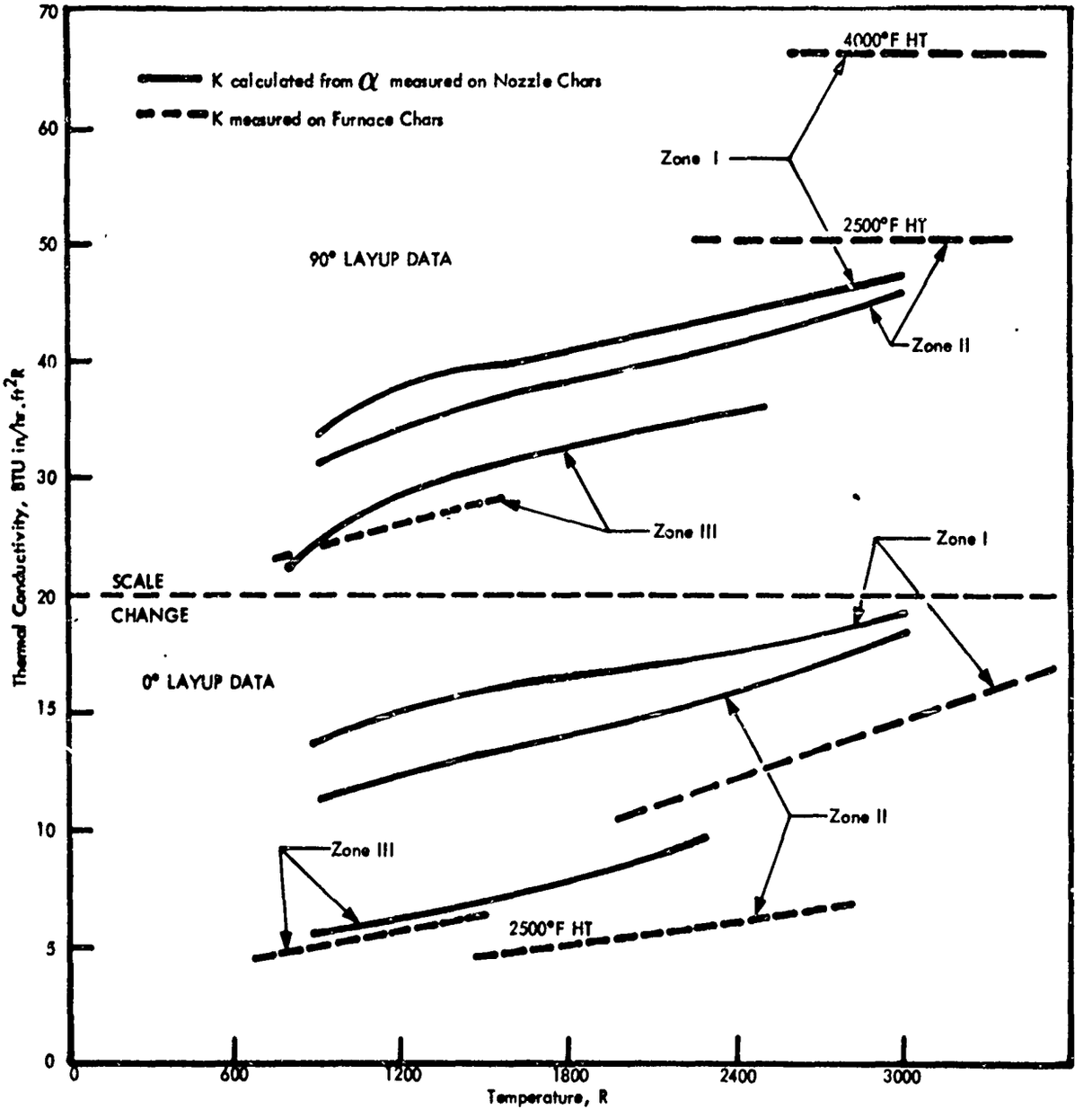

FIGURE 28 FM-5014 NOZZLE AND FURNACE CHAR CONDUCTIVITY

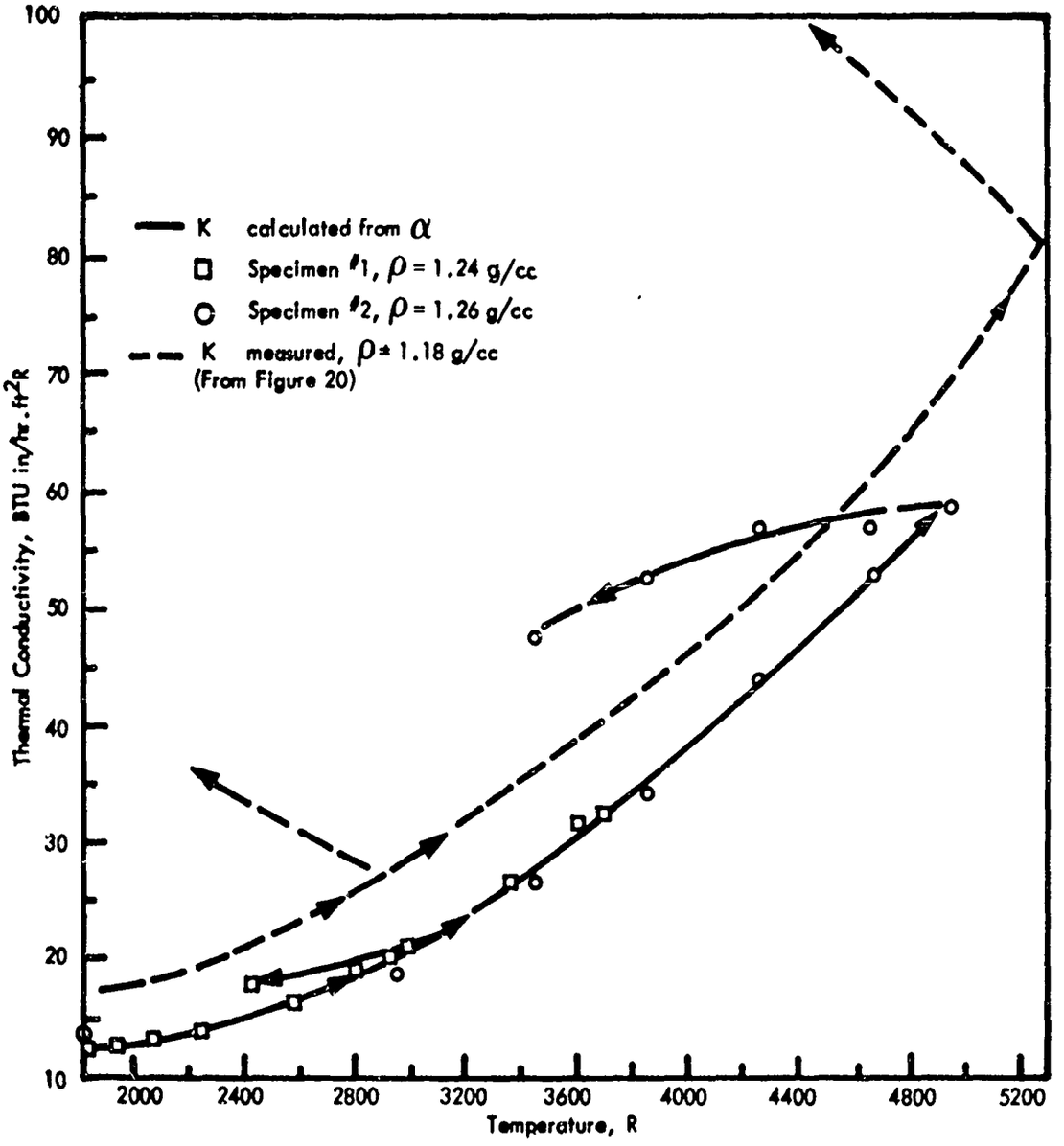

FIGURE 29
FM-5055A COMPARATIVE CONDUCTIVITY RESULTS, SPECIMEN 5000-90-L

have special significance in establishing an overall correlation of the behavior of thermal conductivity during ablation. 0-degree nozzle-char conductivities in Zones II and I may be increased by the presence of extra pyrolysis deposition products left during cool-down[1] and carbonized during the measurements, that would tend to bridge delaminations. Such extra deposited material may also diffuse the strong orientation of graphitization in MX-4926[1], thereby contributing to low nozzle char values in the 90-degree direction as well. Lack of strongly directional graphitization effects in FM-5014[1] is consistent with the nozzle char data in both directions. Bias toward high values of 0-degree layup nozzle-char conductivity is caused by selection of diffusivity samples to avoid delamination. In contrast, Zone III nozzle specimen data was obtained up to temperatures high enough to insure pyrolysis of the small amount of remaining resin without opportunity for any redeposition of pyrolysis products, and no large discontinuities are noted in the results. This observation leads to the conclusion that, for initial-ablation heating, the conductivity measurements on furnace chars are more applicable than those on quenched nozzle-ablation chars. The uncertainty shown by the 0-degree-layup Zones II and I results would then be restricted only to rapid cool-down periods and following reheat periods, which are of concern in relatively few of the applications of these materials. This uncertainty in 0-degree-layup data does indicate a strong effect of inter-laminar contact resistance in the char crossply conductivity, making the results very sensitive to any small difference between samples.

The diffusivity measurements on specimen 5000-90-L in Figure 29 were obtained to compare results on material graphitized during the measurement. The diffusivity measurement also included an intermediate and final cooling curve analogous to the steady state conductivity data to see if the negative slope of the steady state data was reproduced. Figure 29 clearly demonstrates that the cooling curve slopes were not reproduced; the diffusivity tests gave the opposite slope. The conclusion is that neither cooling curve slope has special significance, and in particular, the high negative slope of the steady state measurements should not influence the overall data correlation in Section VII. The difference between the two heating curves in Figure 29 is larger than expected, particularly at low temperatures, and is not explained by the differences in specimen density noted on Figure 29. The slopes of the two heating curves are in excellent agreement however, indicating that the results obtained during heating of the specimen that is graphitizing versus heat treatment are a valid representation of the effect of temperature on the conductivity of fully pyrolyzed char.

SECTION V

ELECTRICAL RESISTIVITY MEASUREMENTS

Electrical resistivity was measured on specimens representing 0-degree (cross-ply) and 90-degree (ply) directions in the FM-5055A material. The specimens were cut from a single, good quality slab of high density material which had been heat treated to 1800°F. Measurements were made in the temperature range 1650°F to 4500°F, with graphitization during measurement. The data is significant primarily as an indicator of the hard carbon-like behavior of FM-5055A.

During measurement, each specimen, nominally 0.5 in. diameter by 0.7 in. long and cemented between graphite electrodes, was a.c. resistance-heated in a vacuum chamber. Adequate insulation and baffling were provided to insure an essentially isothermal gauge section. The current through the specimen was determined by measuring the voltage drop across a standard resistor in series with it. Probes sensed the voltage drop across the gauge length of the specimen. The resistivity was calculated from the relation:

$$\rho = \frac{\Delta E}{I} \quad \frac{A}{x} \tag{37}$$

where:

ρ = electrical resistivity, ohm-cm

ΔE = voltage drop across specimen gauge length, volts

I = current flow, amps

A = specimen across section area, cm^2

x = specimen gauge length, cm

Specimen temperatures were measured by optical pyrometer.

Total uncertainties in the resistivity measurement values by this technique are estimated to be ±10 percent; precision is estimated to be ±3 percent.

The measurement plans consisted of determining the electrical resistivities in the ply and cross-ply directions as functions of heat treatement temperatures (HT) and ambient temperature at selected HT's. The data are tabulated in Appendix VI, wherein the individual points are listed in the order of determination.

The data show that resistivities in both directions decrease with advancing HT, and that they are quite dissimilar. Throughout the temperature region below 3920°F HT, the cross ply resistivity is about four times greater than the ply resistivity, reflecting the dominance of the cloth on this property. For comparison, the ratio of ply to cross-ply thermal conductivity values varied with HT as follows: 10 at 1800°F, 3 at 3000°F, and 4 near 5000°F. The corresponding thermal conductivity ratios for the low density chars which were graphitized during measurement were approximately 4, 3, and 4, respectively. Thus, except for the high density chars at 1800°F HT, the ratios of ply to cross-ply electrical and thermal conductivities are about equal.

Above 3920°F HT, the rate of decrease of the cross-ply resistivity with advancing HT lessens considerably, suggesting that the resistivity values will remain comparable to those reported for hard carbons heat treated to 5500°F (Yamada, et al. [13] and Yamada [9].

The resistivity data are presented on Arrhenius plots in Figure 30 . These plots illustrate the vehavior of electrical resistivity with HT and with ambient temperature below HT. The arrows on the curves define the regions in which the materials are stable, i.e., the measurement results are repeatable.

The appearance of linearity with ambient temperature in these plots suggest an interpretation of the slopes in terms of activation energies for the electrical conduction process. The slopes and associated activation energies for the cross-ply and ply directions are given on the following table.

TABLE II ELECTRICAL CONDUCTION ACTIVATION ENERGIES

Direction	Heat Treatment K	Heat Treatment F	Slope K	Activation Energy, electron volts[a]
cross-ply	1255,	1800	854.7	0.15
	1665,	2538	575.4	0.10
	2108,	3335	967.9	0.17
	2438,	3929	1159	0.20
ply	1255,	1800	266.7	0.05
	2099,	3319	1095	0.19
	2437,	3927	1088	0.19

(a) The activation energy was computed using the relationship $\rho = Ae^{\frac{E}{2kT}}$

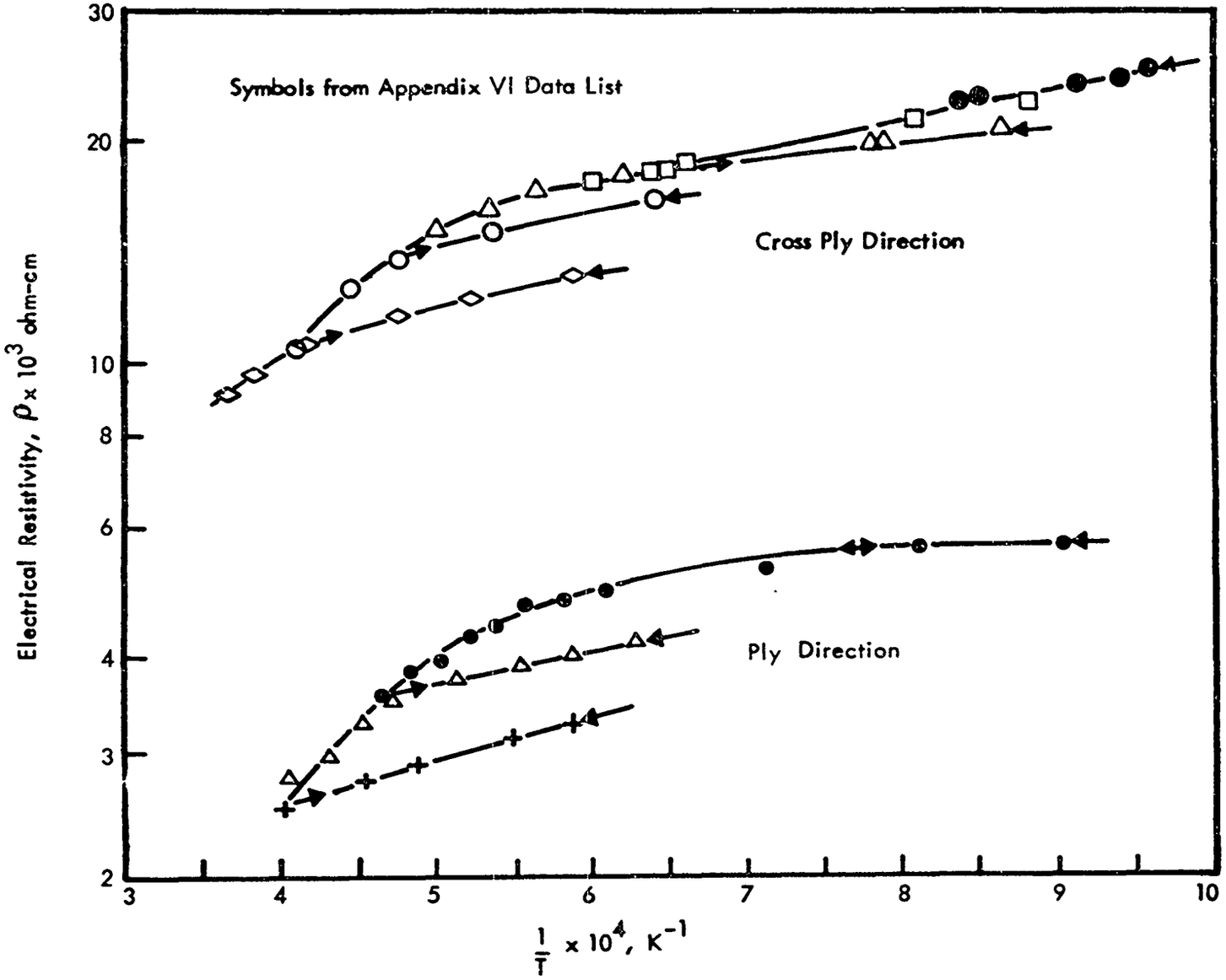

FIGURE 30 ELECTRICAL RESISTIVITY OF FM-5055A

The above values are in general agreement with those reported for condensed, aromatic compounds which behave like intrinsic semiconductors (Inokuchi and Akamatu[21]), and for glassy carbon (Yamada, et al.[13].)

The slopes and associated activation energies for the ply and cross-ply resistivities become approximately equal at HT's greater than 3300°F suggesting that the electronic conduction processes active in the reinforcement cloth and matrix are similar above this HT.

It is interesting to note that the resistivity changes with temperature observed in these measurements occurred in relatively short times at temperature. Generally, values recorded approximately one minute after reaching a new HT temperature were constant for long periods. For example, the 90-degree (ply) specimen was held at 2000°F for 12 hours with a resistivity value change of less than 3 percent. Therefore, rate dependent ordering processes which affect the electronic properties of the chars appear to reach completion in less than one minute residence time at temperature.

SECTION VI

FM-5055A THERMAL CONDUCTIVITY SPECIMEN CHARACTERISTICS

Blocks of high density virgin FM-5055A material, hydroclave molded according to existing ablative heat shield specifications, were used for most of the specimens in this program. In addition, a block of low density material, press molded at low pressure to specification requirements except for density, was used to obtain higher porosity 1800°F furnace chars. Previous experience [1] had shown that furnace charred dense material exhibited lower porosity than corresponding active ablation chars due to shrinkage accompanying slow furnace pyrolysis without the restraint due to attached virgin material. Chars produced from low density precursor material were investigated in an attempt to counteract this effect, and investigate the effect of porosity on thermal conductivity in chars.

Table I in Section IV listed all of the specimens produced from the above material on which thermal conductivity was obtained. This section includes all of the production and characterization data obtained on these specimens plus several additional specimens designated as spares on which thermal conductivity was not run.

VIRGIN MATERIAL DESCRIPTION

Virgin material for production of thermal conductivity specimens was obtained from Haveg Industries, Inc./Reinhold Aerospace Division, Santa Fe Springs, California. Dense, hydroclave cured material laminated on the bias relative to the block sides was received in three blocks of 4.5" x 5.5" x 10" and one block of 4.5" x 5.5" x 13". One 4" x 6" x 8" low density, press cured, bias laminated block for production of maximum porosity char samples was also procured. The material received was of good quality.

A description of the U. S. Polymeric FM-5055A phenolic-carbon prepreg material, applicable specification values, and laminated material characterization has been reported in Reference 1. This material consists of HITCO-CCA-1 (1641) high purity carbon cloth reinforcement with approximately 34% by weight of CTL 91-LD phenolic resin and 13% by weight of carbon powder filler. Dense virgin material for this program was produced to the requirements of General Electric Specification RSD-9049-A. Material received for this program was laminated from prepreg batch No. C-7532, impregnated on 4/9/68, and characterized as follows:

Resin Content	34.4%
Flow	6.6%
Volatile Content	3.7%

All processing was in accordance with the requirements of Haveg/Reinhold Process Specification H-PS-189. The cure was accomplished by heating at a rate of 1°F per minute maximum to 310°F ± 10°F, holding at temperature for 3 hours, and then cooling. Hydroclave pressure of 1000 ± 100 psig was maintained from below 200°F through the time at the curing temperature, and maintained above 200 psig during cool-down. Tensile properties of the cured material in the laminate warp direction per the G.E. specification were determined by the supplier. The results from five tests are given in Table III below.

TABLE III– DENSE FM-5055A TENSILE PROPERTIES

	Range	Average	Requirement
Tensile Strength, psi	13,155 — 16,330	15,029	4,500 min.
Tensile Modulus, 10^6 psi	2.00 — 2.27	2.16	1.5 — 3.2
Elongation, %	.83 — 2.46	1.69	0.40 min.

All specific gravity values, on coupons by Haveg/Reinhold and on the blocks by Boeing, were in the range of 1.49 — 1.52. Resin content determined by Haveg/Reinhold was 35.41%.

The low density, U.S. Polymeric FM-5055A was laminated from prepreg batch No. C-7577, impregnated on 6/5/68, and characterized as follows:

Resin content	33.5%
Flow	10.5%
Volatile content	4.4%

The low density block was produced to the requirements of General Electric Specification RSD-9049-A, except density, with processing in accordance with Haveg/Reinhold Process Specification H-PS-189. After debulking, the block was press cured by heating at a rate of 1°F per minute to 310°F ± 10°F, holding at temperature for 8 hours, and then cooling. Press pressure of 15 psi was maintained from below 200°F through the time at the curing temperature, and maintained above 15 psig during cool down. Tensile properties in the laminate warp direction per the G. E. specification were determined by the supplier. The results from five tests are given in Table IV below. The values are similar to those for dense laminates.

TABLE IV — LOW DENSITY FM-5055A TENSILE PROPERTIES

	Range	Average	Requirement
Tensile Strength, psi	13,200 — 16,726	15,297	4,500 min.
Tensile Modulus, 10^6 psi	2.00 — 2.16	2.11	1.5 — 2.7
Elongation, percent	1.30 — 1.50	1.35	0.20 min.

Specific gravity determined on coupons by Haveg/Reinhold was 1.34. Block specific gravity determined by Boeing was 1.30 and slabs cut from this block were in the range 1.22 tc 1.41 specific gravity. The low pressure press cured block was denser at the faces than in the center. Since blocks produced with greater uniformity were almost as dense as hydroclave cured material, it was necessary to accept some non-uniformity to obtain high porosity virgin material. This does not effect 1/2 inch thick 0-degree layup slabs cut from the block, which are individually quite uniform, but does cause an unavoidable density gradient in 90-degree layup slabs. Final resin content determined by Haveg/Reinhold was 31.9 percent.

The virgin FM-5055A blocks were cut into 4" x 6" x 0.6" slabs, coded relative to their location in the original block, giving the desired 0, 30 and 90-degree layup angles relative to the slab faces. The lamination angles are defined along the bias direction in uniformly oriented carbon cloth reinforcement to provide properties applicable to tape-wrapped construction. Virgin thermal conductivity specimens were machined from the appropriate layup angle slabs, with the remainder used for virgin material characterization. Most charred samples were obtained by charring the entire slab and then machining out the 3" diameter x 0.5" conductivity specimen, leaving the remainder for characterization representing the pre-test state of the samples. All cutting was done dry to avoid contamination, using a radial cut-off saw with an aluminum oxide blade, and final finishing was done by grinding with a carbide wheel.

CHAR SAMPLE PRODUCTION

Charred thermal conductivity samples were obtained from virgin slabs charred in an argon atmosphere using an induction heated graphite retort. The retort, illustrated in Figure 31 , was similar to that used for char sample production in Reference 1 , with modifications to reduce heat losses for 5000°F operation. The induction coil and method of operation were the same as described in Reference 1.

The states of charred material to be produced were selected on the basis of FM-5055A plasma test char characterization results on the previous program at Boeing, Reference 1. Charred specimens used in thermal conductivity measurements are listed in Table 1 , Section IV. Additional specimens, designated as spares, are included in some of the presentations of sample characteristics in the following subsections. The effect of layup angle was investigated for the various states of charred material by including samples of 0, 30, and 90-degree layup angles. The intermediate layup angle of 30 degrees minimizes the number of measurements required to establish layup angle effects, since it gives a sensitive test of any of the layup angle relationships that have been proposed.

A charring temperature of 825°F to produce approximately 50% pyrolyzed material was selected by trial after an initial selection of 850°F on the basis of TGA data and a trial run at 900°F. These specimens were produced to give insight into the

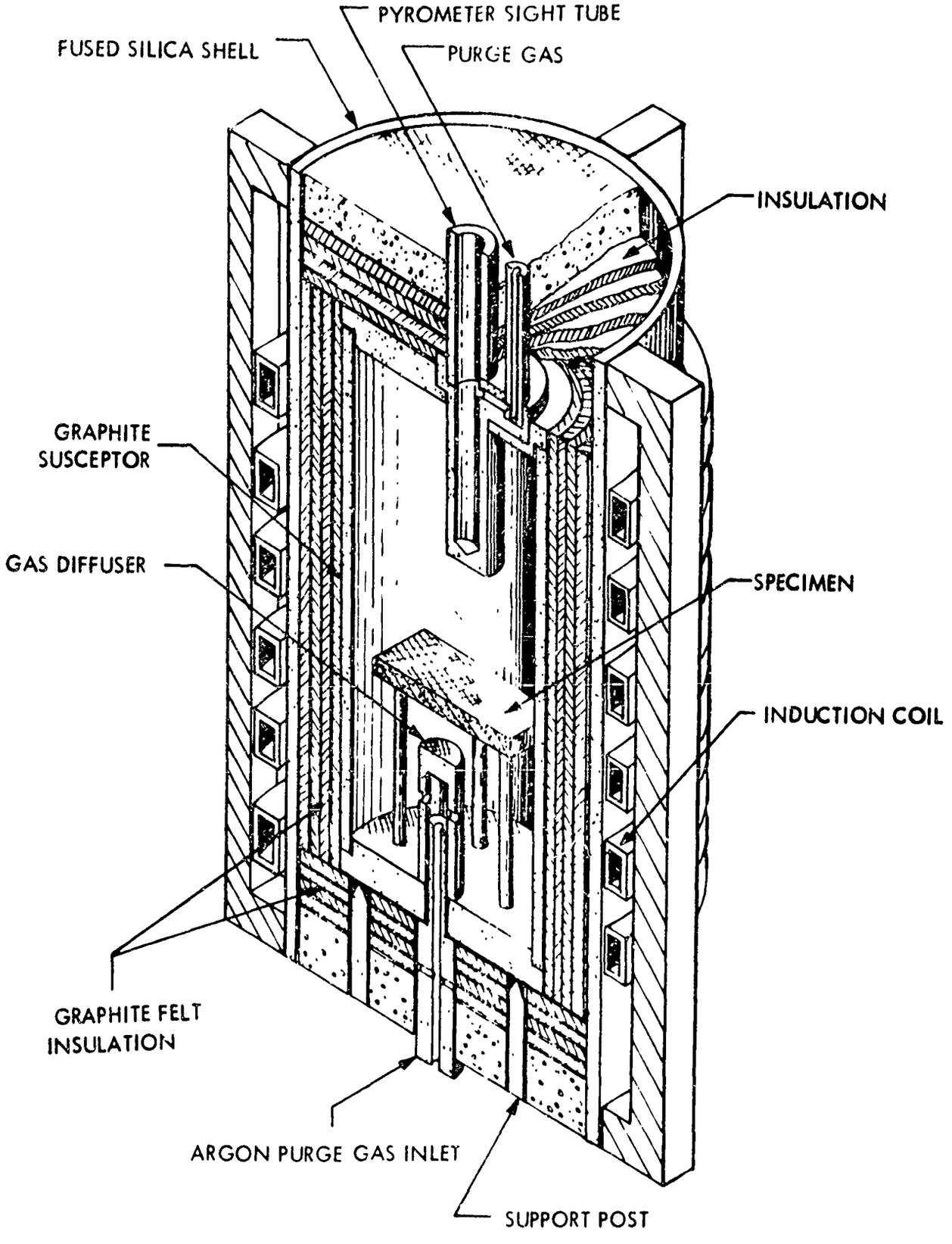

FIGURE 31 INDUCTION HEATED GRAPHITE RETORT

the behavior of conductivity during the early stages of pyrolysis where total porosity and pore size is low. 1800°F chars were selected to obtain fully pyrolyzed material that would have fully developed porosity, but no graphitization on the basis of previous studies [1]. 1800°F chars from low density virgin material were included to obtain data at the higher levels of porosity found in ablation chars. 3000°F and 5000°F chars were selected to provide stable samples having intermediate and high levels of graphitization or ordering. 5000°F represents the practical limit of current capability for steady state thermal conductivity measurements in vacuum. Measurements to the highest possible temperatures were desired to investigate behavior attributable to a radiation component of thermal conductivity. It was expected on the basis of previous results [1] that the effects of graphitization on thermal conductivity would not be linear with temperature, and that both graphitization effects and a radiation component could be affected by the level, size, and orientation of porosity. To cover these possibilities, maximum porosity 1800°F chars were included for runs to 5000°F at progressively higher temperatures as a direct measure of the effects of graphitization versus temperature at high porosity.

Initial furnace charring runs to 1800°F and 3000°F were made using the standard temperature-time cycle developed on the previous program [1] with a stopping point at 1800°F added and a 3000°F stopping point substituted for the previous 2500°F stopping point. This cycle gave excessive delamination in the 0-degree layup samples of FM-5055A. Previous experience with CCA-1 carbon reinforced phenolics had indicated that techniques such as heating under a cross ply compression load had no effect and that the only way to decrease delamination was to conduct the pyrolysis portion of the charring cycle at a slower rate. The standard cycle was extended by a factor of three in time to obtain good quality 0-degree layup charred samples. Zero-degree layup chars produced by this slower cycle had localized interlaminar cracks typical of phenolic-carbon but were physically intact and of uniform density. All 1800°F maximum porosity chars from the low density virgin material were produced using the slow cycle.

The 5000°F chars were obtained by heating two slabs for each orientation where one of each pair had been precharred at 1800°F and one had been precharred at 900°F in an early trial at producing partially pyrolyzed specimens. An interesting result was that the best uniformity was obtained on those specimens that had been only partially precharred to 900°F. Those precharred to 1800°F were therefore designated as No. 2 or spare specimens. All slabs were run simultaneously on a rapid heating cycle that slowed gradually to a 5 minute hold at 5000°F. Temperature versus time recorded with an automatic optical pyrometer gave the following 5000°F charring cycle record: RT to 3000°F, 20 minutes; 3000°F to 4000°F, 12 minutes; 4000°F to 4500°F, 8 minutes; 4500°F to 5000°F, 15 minutes; 5000°F hold, 5 minutes; 100°F/minute initial cooling rate after shutdown; 5000°F to 3000°F, 25 minutes; 3000°F to 2000°F, 40 minutes.

The uniformity of all specimens was checked by X-ray transmission density surveys using the set-up described in Reference 1. All samples had densities uniform within ±1.5% except at one edge of the spare 5000°F 0-degree layup specimen, on which no conductivity measurements were made, and except for the 90-degree layup maximum porosity chars produced from low density virgin material. These samples showed a 6% density gradient across the one inch wide center portion and a low density region at one edge outside the measurement zone. This non-uniformity conforms to the density gradient through the thickness of the low density FM-5055A virgin material described previously.

THERMAL STABILITY CHARACTERISTICS

All thermal conductivity specimens produced at 1800°F or above were assumed to be stable for high temperature exposures not exceeding the initial furnace charring heat treatment temperature. This assumption was valid on the basis of previous experience[1] and on the basis of thermal conductivity measurements made upon cooling from the highest temperatures reached during the conductivity measurements. For the incompletely pyrolyzed virgin and 825°F charred specimens, thermal stability was established on the basis of thermogravimetric analysis (TGA). TGA apparatus and procedures were discussed in Reference 1.

The maximum temperature for thermal conductivity measurements on virgin material was established to limit the total weight loss to less than 4% during the extended temperature exposures accompanying conductivity measurements. A 560°F constant temperature TGA measurement on virgin FM-5055A showed that a 4% weight loss was obtained at 3 hours exposure and the sample was stable thereafter. On this basis 500°F was adopted as a conservative temperature limit for virgin material thermal conductivity measurements.

The stability of the partially pyrolyzed specimens charred at 825°F was checked by comparing TGA measurements of total weight loss to 1800°F on a portion of the furnace charred slabs, representing the specimen condition before conductivity measurements, and on a portion of the tested conductivity specimens. The results, summarized in the following table, indicate that the specimens were sufficiently stable during the long thermal soak accompanying the thermal conductivity measurements.

TABLE V — REMAINING PYROLYSIS WEIGHT LOSS ON 825°F CHARS

	Percent Weight Loss to 1800°F, Dry Basis	
	Before k Test	After k Test
0-degree layup (800-0-H)	10.13	8.95
30-degree layup (800-30-H)	9.89	8.54

GRAPHITIZATION CHARACTERISTICS

As pyrolysis is completed during ablation of phenolic-carbon materials such as FM-5055A, additional ordering and crystallization occurs as temperature increases in the mature char layer. The term graphitization is used to describe the increase in carbon char crystallinity with temperature that approaches the characteristic crystal spacing of graphite. The complex temperature dependent ordering that occurs also effects the porosity of both the carbon fiber and pyrolysis residue constituents in the char. These changes are analogous to those that occur in hard or glasslike carbons (see Appendix I).

A quantitative measure of the relative concentrations of anisotropic or crystalline material corresponding roughly to graphite was provided by x-ray diffraction intensities at d-spacings, (002) interplanar spacing along the c axis, close to that of graphite. Polarized light photomicrographs provided a visual analysis of the location of crystalline material relative to amorphous material. The application of these techniques to chars has been discussed previously in Reference 1.

Portions of the furnace charred slabs were used for x-ray diffraction intensity measurements of the relative levels of graphitization in planes normal and parallel to the heat flow directions in pre-test thermal conductivity specimens. Table VI summarizes the average values of over 100 individual measurements, with the range of values in the principal directions indicated. Emphasis was placed on measurements in the laminate and cross-ply planes, the principal directions for correlation of thermal conductivity data, to note any directional effects in the graphitization cross sections.

TABLE VI PRE-TEST THERMAL CONDUCTIVITY SPECIMEN GRAPHITIZATION

Table I Item Number, Type Sample	X-Ray Diffraction Intensity, (002) Plane, counts/second			
	Laminate Planes (±17%)	Crossply Planes (±13%)	30° to Lam. Planes	60° to Lam. Planes
1. High density virgin	120	104	---	---
2. 1800°F Char (low density precursor)	122	120	---	---
3,6. 1800°F Char	120	1.2	122	115
5. 3025°F Char	236	216	234	---
7. 5000°F Char	835	470	524	488

No significant differences between specimens of a given type were found. High values in the laminate planes of the 5000°F chars are consistent with the tendency for graphitized material to occur in layers along yarns and interlaminar cracks. The dramatic increase in laminate plane values between 3024°F and 5000°F chars appears to be consistent with the very high temperature dependence found in Section VII for the thermal conductivity of the pyrolysis residue during initial heating in this temperature range. Similarly, the lower increase in cross-ply plane values with temperature, where fiber ends are exposed to the diffraction measurement, is consistent with the lower temperature dependence of the fiber constituent axial conductivity during initial ablation heating. All laminate plane diffraction intensity values agree well with values measured at depths corresponding to short exposures at the same temperatures in FM-5055A plasma test chars, Reference 1. This is taken as additional evidence that graphitization is primarily temperature-dependent and occurs at rapid rates[1].

The x-ray diffraction intensities in the planes normal to the heat flow in thermal conductivity specimens 5000-90-L and 5000-0-L were measured on a central portion of the post-test conductivity specimens. Measurements were made near the hot and cold faces and in the center of each sample to determine if there was a gradient in the final graphitization level corresponding to the conductivity measurement temperature gradient. The average diffraction intensities in both specimens were within 2.5% of the 5000°F values in Table IV. Data scatter was normal and there was no evidence of a gradient in graphitization level. However, these specimens were exposed to approximately a 200°F lower average temperature than the 5000°F chars in Table VI, which may indicate that some additional graphitization accompanied the thermal conductivity measurement. Similar post test measurements were made on sample 5000-90-H, which was pre-graphitized to 5000°F, and an average value 23% higher than recorded for the same specimen prior to conductivity testing was obtained. This is outside the normal data scatter and may indicate some additional ordering during the conductivity measurements. This post test sample was also uniformly graphitized. It was noted that post test specimens may have been contaminated during handling and sectioning by the graphite used in the conductivity measurement assembly. Considering this, together with the stability of the conductivity values during the extensive temperature cycling employed during the conductivity measurements on specimen 5000-90-H, it is believed that if further graphitization did occur during the conductivity measurements, it was insignificant in terms of any effect on measured thermal conductivities.

Approximate d-spacings were also obtained from the graphitization level measurements. In general, crystal density in the furnace chars increased with increasing heat treatment temperature; d-spacings range from 3.70Å on 1800°F chars to 3.39Å on 5000°F chars. Debye-Scherrer diffraction patterns were obtained on separated fiber and pyrolysis residue material from sample 5000-90-H after the conductivity measurements to investigate the relative crystal densities of the two major constituents. Fiber material, which included adhering pyrolytic deposits,

showed a denser and more highly ordered structure than pyrolysis residue material. Polarized light photomicrographs of these samples showed the same relative characteristics. The (002) crystal spacing on pyrolysis residue material alone was close to that measured on the composite material. Values on fiber and adhering deposits alone were as low as 3.34Å. These results, the behavior of porosity versus heat treatment temperature described in the next subsection, and the temperature dependence of predicted pyrolysis residue conductivities in Section VII, all suggest that the pyrolysis residue can be described as hard or glasslike carbon material. Similarly, at least at high temperatures, the carbon fiber and adhering pyrolytic deposits appear to be more like graphite.

Polarized reflected light photomicrographs were obtained of planes representing each heat flow direction at each charring temperature on portions of the furnace charred slabs. Anisotropic material appears as bright areas under polarized light, and the relative amounts of visible anisotropic material were roughly proportional to the measured x-ray diffraction intensities in the chars. This is illustrated by laminate plane views for each charring temperature in Figure 32. Some ordered material is visible in 1800°F chars even though x-ray diffraction intensities have not increased significantly above the levels for virgin material. No anisotropy is visible in the 825°F chars. Polarized light photomicrographs appear to be a better test for detecting low concentrations of ordered material than x-ray diffraction level measurements. The photomicrographic results are consistent with the predicted fiber axial conductivities in Section VII, where fibers exposed to 825°F appear to have the same conductivity as those in virgin material, but the conductivity of fibers exposed to 1800°F or higher has increased.

Figure 33 illustrates the location of the ordered or graphitized material in the chars. The highly anisotropic material visible at any charring temperature appears as pyrolytic deposits on the CCA-1 (1641) high purity carbon fiber surfaces. This is the same behavior noted in MX-4926 laminates utilizing CCA-1 standard fibers in Reference 1. There appears to be less graphitization in the FM-5055A pyrolysis residue than was noted for MX-4926 in Reference 1. The resin-carbon powder filler combination in FM-5055A is the same as in the FM-5014 phenolic-graphite described in Reference 1, which also showed little graphitization in the pyrolysis residue. It is not known if the resin-filler combination is the controlling factor in this behavior, however. Fiber surface deposits were not visible in FM-5014 phenolic-graphite, for example, indicating that at least the fiber surface deposits may depend strongly on the reinforcement. Also illustrated in Figure 33 is some visible evidence of graphitization in the fibers themselves at 5000°F. The fiber graphitization visible under polarized light is not as extensive as that visible for graphite fiber reinforcement in Reference 1, however. The appearance of graphitization in the fibers at 5000°F is consistent with a slight negative slope and high level of fiber conductivity predicted at this temperature in Section VII. The appearance and relative amounts of pyrolytic appearing material on the fiber surfaces seems consistent with the predicted fiber conductivities at all temperatures, however, and appears to be the most significant aspect of char graphitization influencing the conductivity of the combined fiber and fiber surface deposits.

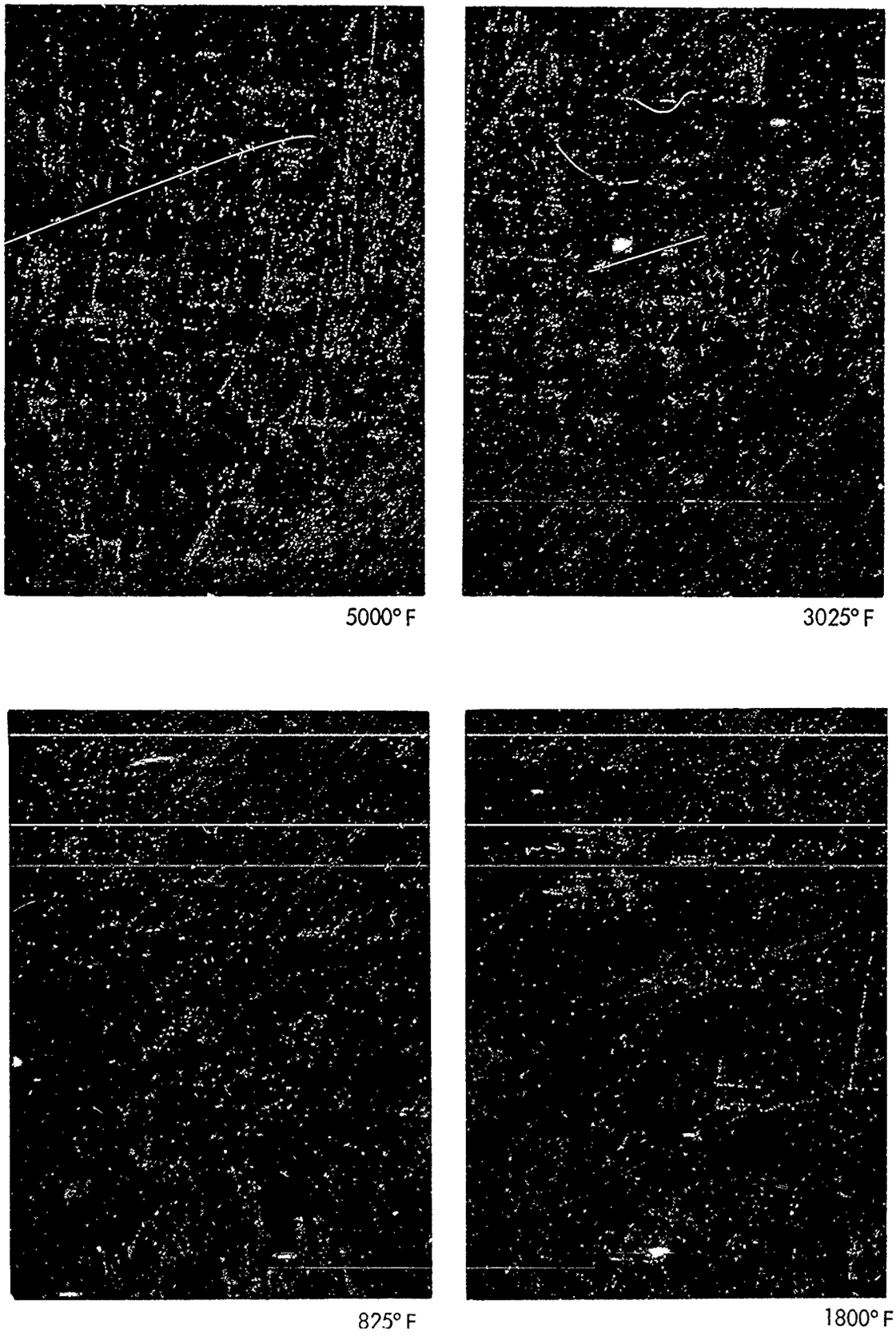

FIGURE 32 50X POLARIZED-REFLECTED LIGHT VIEWS OF ORDERED FIBER SURFACE DEPOSITS VERSUS CHARRING TEMPERATURE

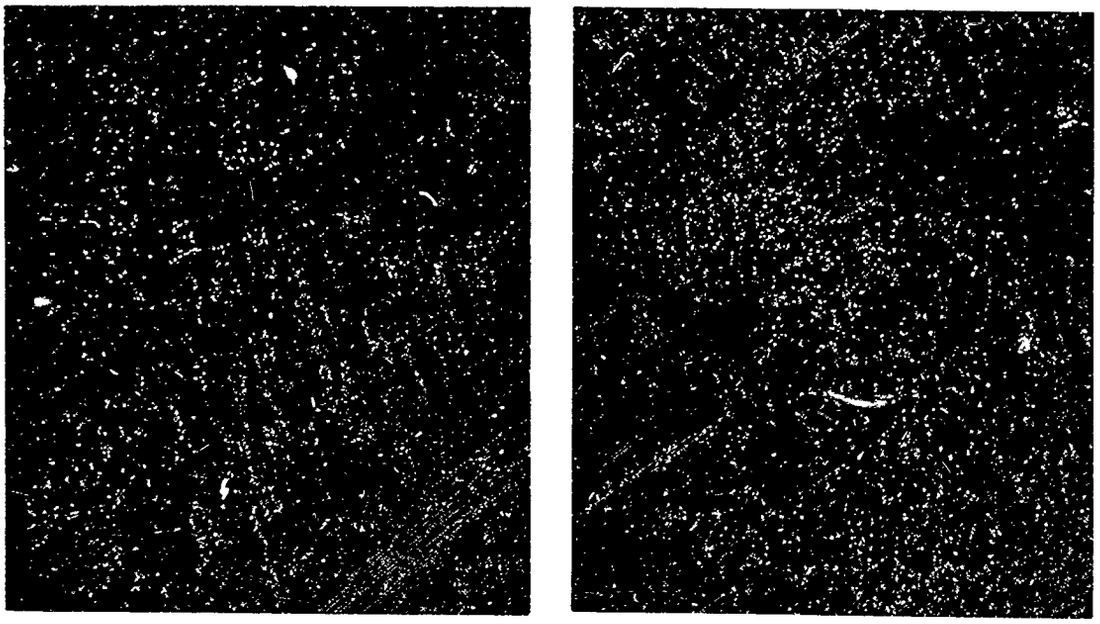

400X 1000X

5000°F char views showing that the most highly ordered (bright) material is at the carbon fiber surfaces

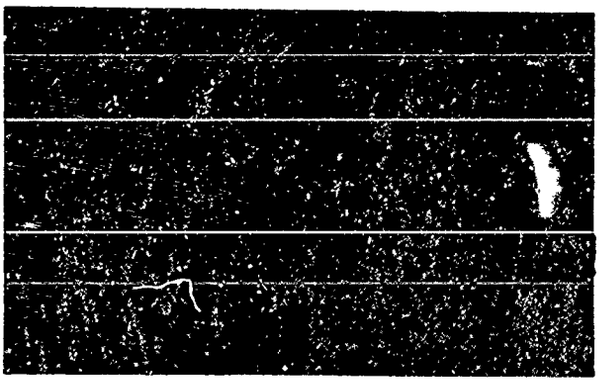

400X

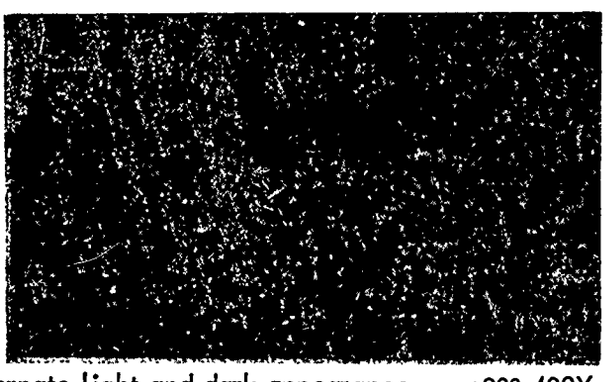

Alternate light and dark appearance of perpendicular 5000°F char fibers with 90° rotation in polarized light indicates some fiber ordering

+90° 400X

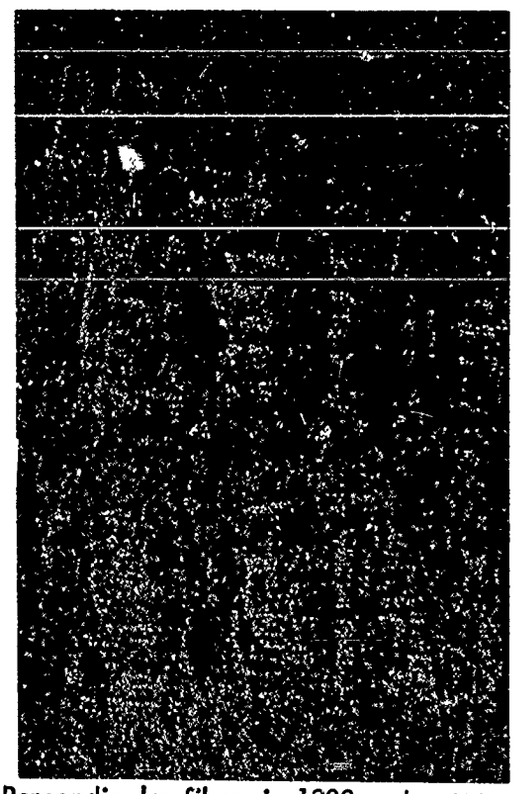

Perpendicular fibers in 1800 and 3000°F chars show little ordering but anisotropy in fiber surface ridges is visible

400X

FIGURE 33 LOCATION OF FM-5055A CHAR ANISOTROPY WITH POLARIZED-REFLECTED LIGHT

DENSITY, TOTAL POROSITY, AND SURFACE AREA CHARACTERISTICS

Experimental Results

Apparent and solid densities were measured on all charred thermal conductivity specimens before the conductivity measurements and on most specimens after the measurements. All measurements were made on dried samples, and there was good agreement between pre-test and post-test values on all specimens. Apparent density only was measured on virgin specimens. Approximate B.E.T. total surface areas were obtained for post-test chars. On all charred specimens, total porosity was computed from the measured apparent and solid density values. These characteristics have significant effect on thermal conductivity.

Pre-test apparent densities were obtained from weight and volume measurements on the rough machined specimens before shipping by Boeing and on the finished pre-test specimens by Battelle. These measurements had a nominal uncertainty of ±2%. Post-test apparent density values with a nominal uncertainty of ±1% were calculated from weight and mercury displacement volume measurements on a center portion of the conductivity specimen that was free of all laminations. Solid densities were calculated from powdered sample weight and helium displacement volume measurements using a Beckman Pychnometer at Boeing and a B.E.T. apparatus at Battelle. Pre-test solid densities were obtained at Boeing on a portion of the furnace charred slab from which the conductivity specimens were cut, and post-test values were obtained on a center portion of the conductivity specimen at Battelle. Experience with several remeasurements indicates that the nominal uncertainty of the helium solid density values was about ±8% due to variations among the char materials themselves.

Post test B.E.T. total surface area measurements were performed by Battelle on fractions of the samples used in the solid density measurements by means of nitrogen gas adsorption from a mixture of helium and nitrogen gas at liquid nitrogen temperature in a flowing stream apparatus. These measurements were performed only to investigate the effect of heat treatment on the relative B.E.T. surface area, so an approximate method having 15-20% uncertainty was employed. Solid density and B.E.T. surface area samples were taken by sectioning entirely through the thermal conductivity specimens to obtain an average sample including both hot and cold face material.

Table VII summarizes the density, porosity, and B.E.T. surface area data for all conductivity specimens. The independent pre-test and post-test density values are in agreement. The 1800°F chars appear to have densified slightly, with an accompanying lowering of porosity, during the measurement. Other chars behaved in the opposite manner. There is a fairly consistent increase in apparent density and decrease in total porosity with layup angle in each char class. Since the integrity of the char also generally improved with layup angle, this trend may reflect a decrease in void volume caused by delaminations.

TABLE VII THERMAL CONDUCTIVITY SPECIMEN DRY DENSITY, POROSITY AND SURFACE AREA VALUES

Specimen	Apparent Density, g/cc			Solid Density, g/cc [1]		Total Porosity [2]		Post Test B.E.T. Surface Area, M^2/g
	Roughcut	Pre Test	Post Test	Pre Test	Post Test	Pre Test	Post Test	
V-O-H	1.52	1.52	-	-	-	-	-	-
V-30-H	1.48	1.48	-	-	-	-	-	-
V-90-H	1.49	1.49	-	-	-	-	-	-
800-0-H	1.33	1.32	1.30	1.63	1.71	19.0	24.0	17.0
800-30-H	1.36	1.36	1.32	1.69	1.72	19.6	23.2	18.0
1800-0-H	1.21	1.22	1.25	2.14 (1.76)	2.11 2.25	43.0	40.7	199
1800-30-H	1.23	1.23	1.29	2.24 (1.63)	2.12	45.1	39.1	213
1800-90-H	1.25	1.25	1.29	2.18	1.94	42.7	33.5	-
1800-0-L	1.04	1.05	1.11	2.13	1.99	50.7	44.2	202
1800-90-L	1.17	1.19	1.25	2.09	1.98	43.1	36.9	217
3000-O-H	1.24	1.23	-	1.61	1.67	23.6	-	9.0
3000-30-H	1.25	1.25	1.21	1.61	1.67	22.3	26.2	-
3000-90-H	1.26	1.27	1.25	1.59	1.71	20.2	26.9	17.0
5000-O-H	1.19	1.17	-	(1.72) [3]	1.76	32.0	-	5.0
5000-30-H	1.25	1.25	-	(1.70) [3]	1.73	26.5	-	5.0
5000-90-H No. 1	1.32	1.32	-	(1.70)	1.70	22.4	-	10.6
5000-90-H- No. 2	1.32	-	-	1.66 1.67 (1.71)	-		-	-
5000-O-L	1.16	1.17	-	2.17	1.64	46.1	-	-
5000-90-L	1.16	1.18	-	2.27	1.59	48.0	-	8.5

[1] ⬭ indicates water saturated sample and

( ) indicates volume measurement in nitrogen gas rather than helium.

[2] Based on lowest solid densities from dry weight and helium displacement volume measurements: Total porosity = 1 - $\frac{\text{apparent density}}{\text{solid density}}$

[3] Values obtained from spare specimen slab.

Variation with Heat Treatment Compared to Glassy Carbon

A pronounced peak in B.E.T surface area values and in solid density and porosity occurs for the 1800°F chars. Figure 34 is a plot of the average values for the chars from high density precursor at each heat treatment level. The 1800°F chars, and to a lesser extent the 3000°F chars, were quite active in nitrogen. A special experiment where samples were saturated with a known amount of water gave solid density results on 1800°F chars similar to those on 5000°F chars and had no effect on values for the 5000°F chars. This behavior appears to be related to the presence of micro-voids in 1800°F chars that will admit gasses and water, but are no longer present in the higher temperature chars. The carbon reinforcement must be participating in these changes; there is insufficient volume of phenolic resin char to account for the solid density variations without the pyrolysis residue exceeding the theoretical density of graphite.

The same variations in helium solid density and B.E.T. surface area with heat treatment illustrated in Figure 34 have been observed on certain glasslike carbons prepared from non-melting resins (see Appendix I). Available information on glasslike carbons indicates that profound structural changes can be expected to occur within the temperature region 1100°F to 1900°F as a result of thermally activated processes of polymer condensation and subsequent crystallite formation and growth. In this temperature region the helium density reaches values close to theoretical crystallite density, while the concurrent order of magnitude increase in B.E.T. surface area suggests that conglomerates of the crystallites are surrounded by open or interconnected voids. If the char composites are viewed as powders composed of cubical particles, the effective particle sizes as computed from the helium solid densities and B.E.T. surface areas are as follows:

High density precursor chars:	0.20 micron at 800°F
	0.01 micron at 1800°F
	0.28 micron at 3000°F
	0.69 micron at 5000°F
Low density precursor chars:	0.01 micron at 1800°F
	0.44 micron at 5000°F

The effective particle size is extremely small at the 1800°F char level. Based upon Yamada's[9] summary of data for glasslike carbons, it may be expected that the permeability and water adsorbtion of the char matrix material also reaches maximum values in the temperature region 1100°F to 1900°F. As will be discussed in the following subsection, the micro-void (less than 3 microns) distribution in the carbonaceous chars shifts toward smaller, isolated voids with advancing heat treatment above about 1800°F.

Loch and Austin[10] investigated the micro-void structures of several types of carbons heat treated at about 4600°F, including one prepared from a phenol-formaldehyde resin. The microvoid fractions were computed from the measured x-ray densities and the apparent densities determined by the helium displacement

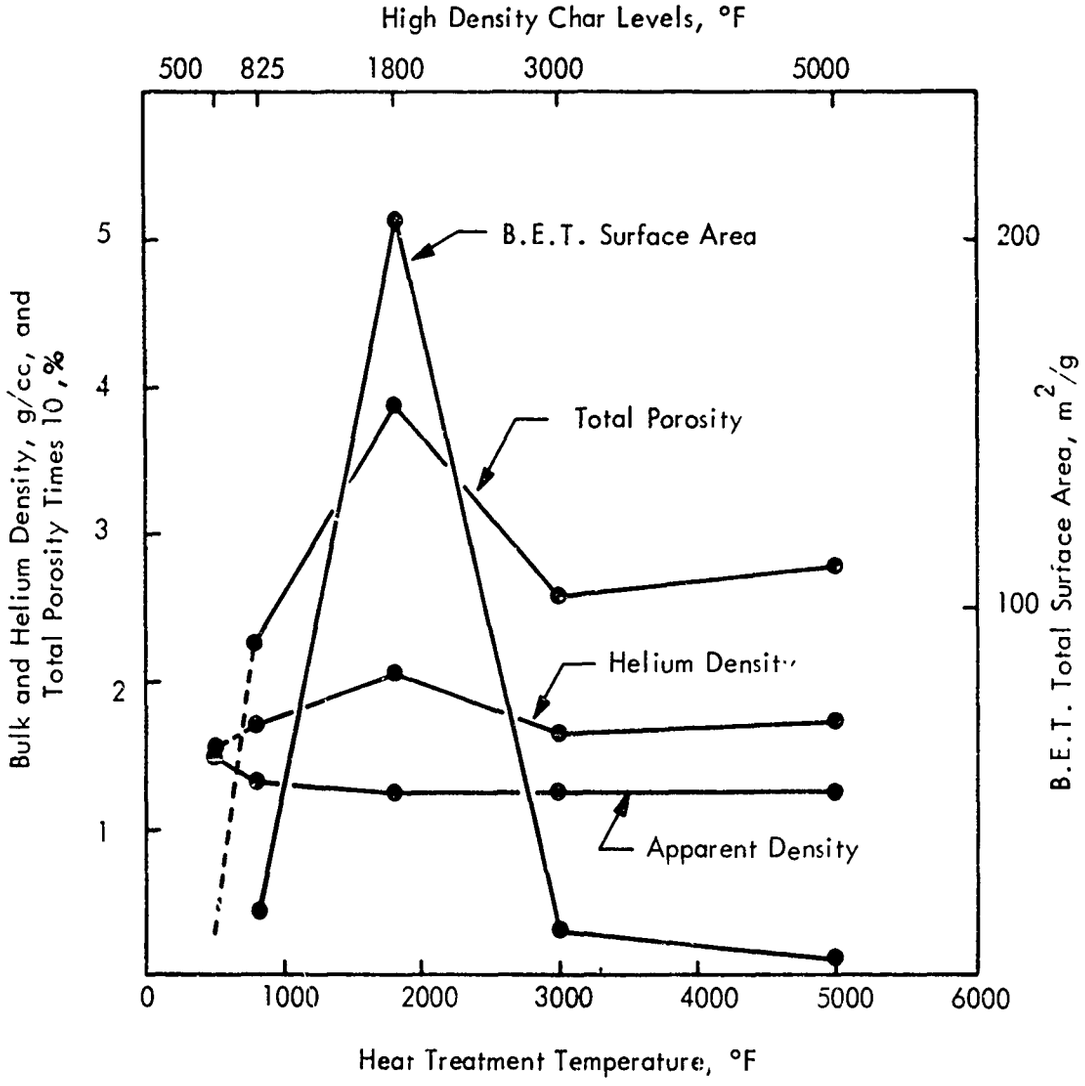

FIGURE 34 VARIATION OF AVERAGE DENSITY, TOTAL POROSITY, AND B.E.T. TOTAL SURFACE AREA OF HIGH DENSITY CHARS WITH HEAT TREATMENT

technique utilizing powdered samples. The x-ray densities ranged from 2.19 to 2.22 g/cc, while the corresponding calculated microvoid fractions ranged from 27 to 19 percent for the hard carbon samples. Average spacings between adjoining crystallites, estimated from measured crystallite size parameters and densities, were small enough (3 to 8 angstroms) to suggest that the voids were located between adjoining crystallites. The voids were estimated to be small enough and isolated enough to prevent liquid penetration and hinder helium penetration. The existance of intercrystalline voids was directly confirmed by electron micrographs.

Because a direct measure of the void fraction comprised of voids smaller than 3 microns was not obtained for the chars on this program, the total void fractions of the chars heat treated to temperatures greater than 1800°F must be considered uncertain; the helium densities may be in considerable error when regarded as a measure of the true density of the solid char material above this temperature. Kipling, et.al.[11] investigated the effects of ambient temperature on the apparent helium densities of a number of polymer carbons experiencing various levels of heat treatment. Their results confirmed an influence of void structure on the measured helium density values. In fact, the volume of helium displaced by the char specimens in the helium density measurements was noted to drift with time most severely in the case of the 1800°F chars. Such behavior may signify that a porosity resistant to accession by helium had begun to form at this heat treatment level.

Sanders, et.al.[30] did extensive characterization studies on phenolic-nylon chars (roughly analogous to the pyrolysis residue constituent in phenolic-carbon chars) with emphasis on investigation of the analogy to hard carbon-like behavior. It was concluded, on the basis of true density, sonic velocity, and electrical resistivity measurements, that the chars were more carbon-like than graphite-like for all heating rates to all temperatures below about 3300°F. High heating rates during ablation exposures to 5000°F resulted in more graphite-like behavior, but slow furnace heating resulted in carbon-like behavior to 5000°F. Carbon-like behavior was dependent only on charring temperature, consistant with the observations on porosity and x-ray diffraction intensities in this study, and in Reference 1 for both furnace chars and ablation chars. There was also a tendency for a lower porosity and larger mean pore size versus heat treatment temperature in the phenolic-nylon chars, but the trends were not as apparent in that material due to high initial porosity in the virgin state.

An estimate of the magnitude of the void fraction due to an intercrystalline porosity within the chars can be achieved from the data given in Figure 34 under a specific assumption about the value of the solid material density. The helium density values of 2.11 to 2.25 g/cc obtained for the 1800°F chars are equivalent to x-ray densities reported for various carbons heat treated to much higher temperatures. Assuming that the true average solid density of the chars remains constant at the 1800°F helium density value, the measured helium densities above 1800°F may be considered to be the apparent densities of carbon containing a distributed, isolated, intercrystalline porosity. The intercrystalline void fractions, as percentages of the true total void volume in the composite, are calculated from the assumed value of solid density,

2.1 g/cc, and the values of helium and composite apparent densities in Figure 34 to be 0 at 1800°F, 16 percent at 3000°F, and 12 percent at 5000°F. The true total void fraction including all voids is calculated from the assumed value of the solid density, 2.1 g/cc, and the measured apparent densities of the composites, 1.25 g/cc in Figure 34, to be 40 percent at 1800°F and constant above 1800°F. The void fractions calculated from the helium density and composite apparent density and given in Figure 34 as the "total" porosity encompasses only voids which are accessible to helium. It is these voids which are characterized in this subsection and the subsection to follow.

The apparent density of the char is directly influenced by the macrostructure of the composite. It will be shown in the subsection to follow that the void structure in the chars consists of two general groups of voids distinguished by the mechanisms by which they are generated: (1) pyrolysis generated microvoids distributed throughout the matrix whose development with heat treatment finds parallel in the heat treatment of hard carbons in bulk, and (2) fissures created by the differences in the expansion characteristics of the reinforcement fibers and rigid carbon matrix. Voids falling into the latter group are not observed in significant quantities in the virgin and 800°F chars, but are in the 1800°F and higher temperature chars. For this reason, the bulk density of the furnace charred composite, and therefore the computed total void fraction, depends essentially on the properties of the matrix only to some undefined heat treatment level between 800°F and 1800°F.

VOID STRUCTURE CHARACTERIZATION

Approach to Characterization of Voids

Porosity lowers the composite solid conductivity, oriented nonspherical pores contribute to anisotropy, and pore size is significant in evaluating a possible radiation contribution to thermal conductivity. For pore structure characterization, one or more samples from each of 12 thermal conductivity specimens were prepared by Battelle for examination in reflected light on the Quantimet Image Analyzing Computer. Basically, this instrument consists of optics to provide suitable magnification of the area of the specimen (or photomicrograph of the specimen) under study, and electronic circuitry to convert the magnified image into a television display which can be observed on a monitor. Areas of sufficient contrast can be counted, and mean lengths of the contrasted areas in the direction of scan as well as mean area ratios can be quickly determined. The analyzer is extremely useful in the study of the structure of materials comprised of discrete phases.

Ideally, the void structures of the chars could be characterized through definition and measurement of pore size, densities, shape, orientation, and homogeneity factors. In fact, however, the complex nature of the pore structure frustrated realization of the full potential of the Quantimet Analyzer in achieving measures of these quantities in this study. For this reason, idealization of the void structures had to be made in the characterization studies. The simplification consisted basically of two points: (1) reduction of the actual pore size distribution existing in the chars

to a distribution comprised of four distinct void classes defined by the size range and shape of the voids contained in each class, and (2) accounting for void orientation by specifying the average orientation of each pore class relative to the reinforcement fiber bundles. The characterization is made semi-quantitative by employing the Quantimet Analyzer to determine the fractions of the total void volumes which are attributable to each void class.

Study of prepared cross sections of the chars, illustrated in the photomicrographs, Figures 35 through 51, provided the basis for the definitions of the four general void classes. They are:

Class 1 Voids:

Extended voids or delaminations resembling thin disks with diameters significant compared to the thickness or diameter of the disk thermal conductivity specimen. This class of void occurred in its severest form in the 0-degree layup angle furnace-produced materials. The 6X macrographs, Figures 37, 38, 43 and 46, illustrate Class I voids.

Class 2 Voids:

Voids approximately 10 to 80 mils in length, generally aligned along the fiber bundles and located predominatly in the filler material between the fiber bundles.

The void structures of the chars produced from high density virgin material differ quite markedly from those of the chars produced from low density virgin material in the void shapes populating this void class. In the high density chars, the idealized shape of the voids approximately 8 to 80 mils in length is prolate ellipsoidal with major-to-minor axes ratios in the range of 5 to 50; the 6X macrographs in Figures 37 through 45 illustrate these voids. In the 0-degree layup angle chars, the nominal heat flux vector is normal to the major axes of the prolate ellipsoids, whereas in the 90-degree layup angle chars, the nominal heat flux vector lies approximately at the bias angle (45 degrees) of the cloth to the major axes of these voids.

The 6X macrographs in Figures 46 through 49 of the low density char sections show the voids in the length range of 10 to 80 mils to be composed of large, spheroidal voids as well as the elongated fissures found in the high-density chars. The filament-like voids appear to be prolate ellipsoids approximately 8 to 60 mils in length with major-to-minor axes ratios in the range 5 to 30. The spheroidal voids ideally approximate oblate ellipsoids (platelets) with the equal, longest axes in the length range of 5 to 35 mils and an axes ratio of about 1/2. The prolate ellipsoidal voids align with their major axes along fiber bundles; the oblate ellipsoidal voids are flattened in the plane of the cloth. The nominal heat flux vector is normal to

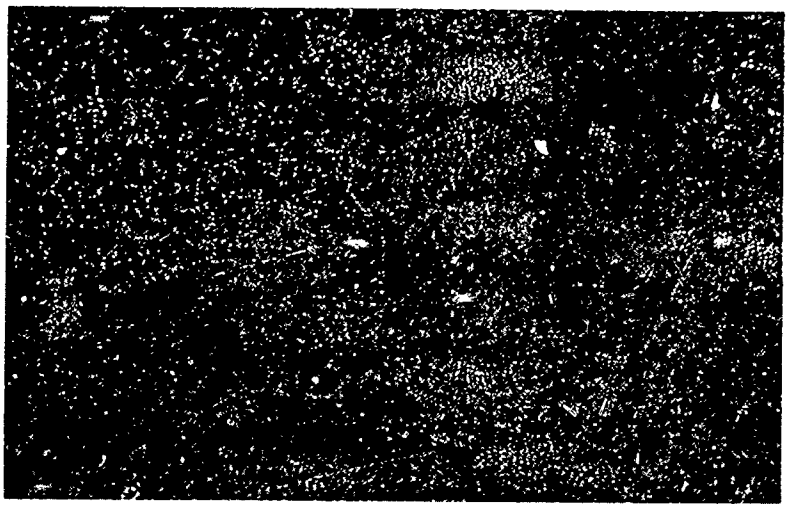

50X

FIGURE SPECIMEN V-90-H, CROSS PLY SECTION PARALLEL TO FLAT FACE

No porosity above 3 microns is detectable

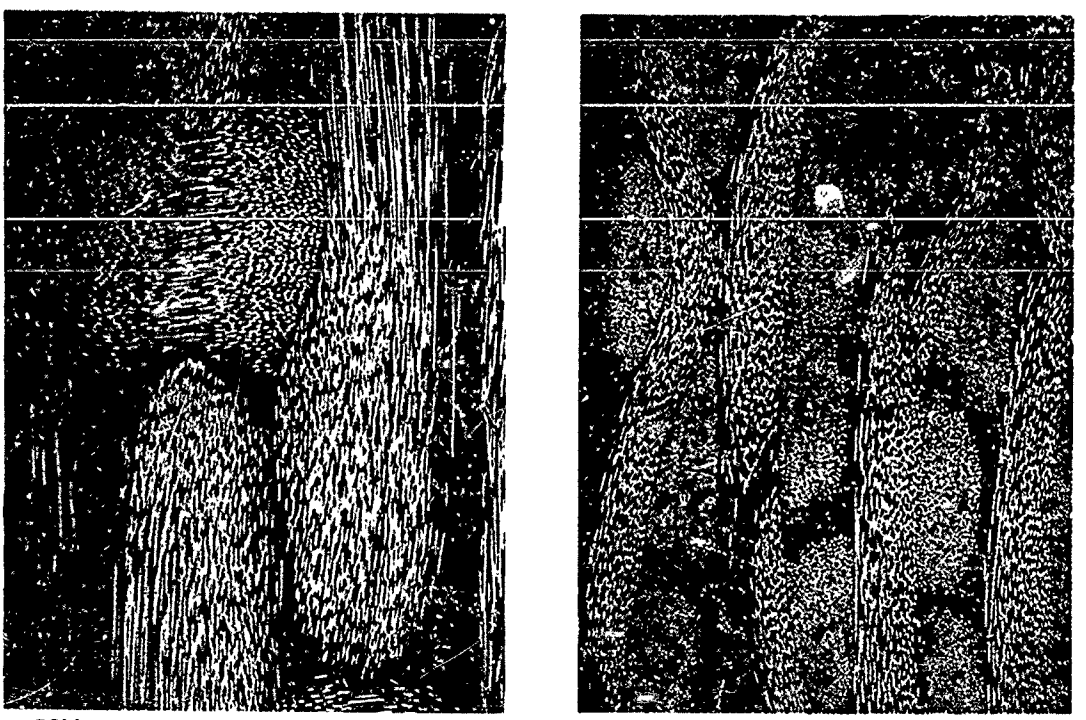

50X A 50X B

FIGURE 36 SPECIMEN 800-0-H, SECTIONS PARALLEL (A) AND PERPENDICULAR (B) TO THE FLAT FACE (CLOTH PLANE)

Note absence of large fissures.

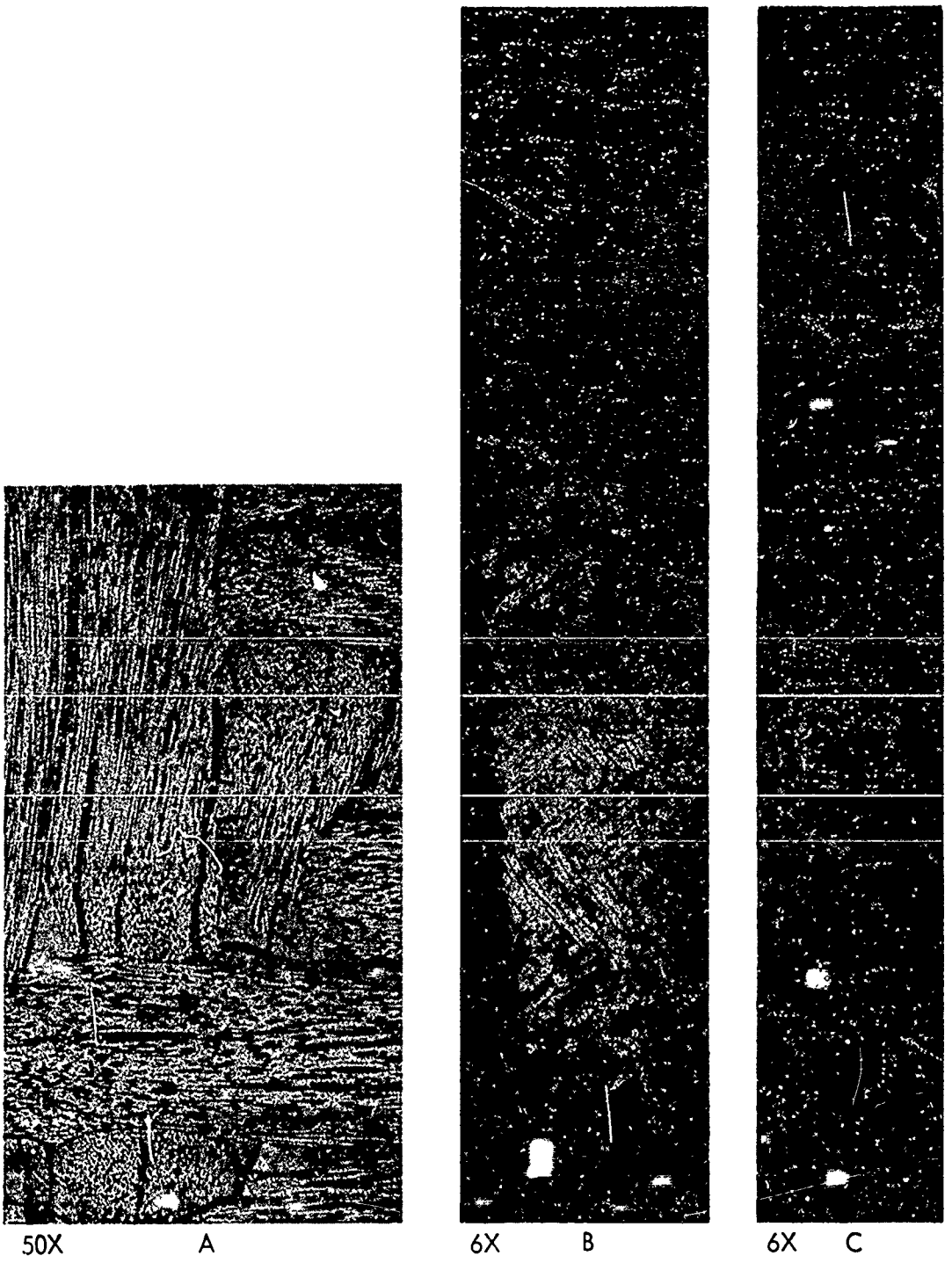

FIGURE 37 SPECIMEN 1800-0-H, SECTIONS PARALLEL (A&B) AND PERPENDICULAR (C) TO THE FLAT FACE (CLOTH PLANE)

The development of complex void structure is evident. Note delaminations. The large delamination probably resulted from sectioning.

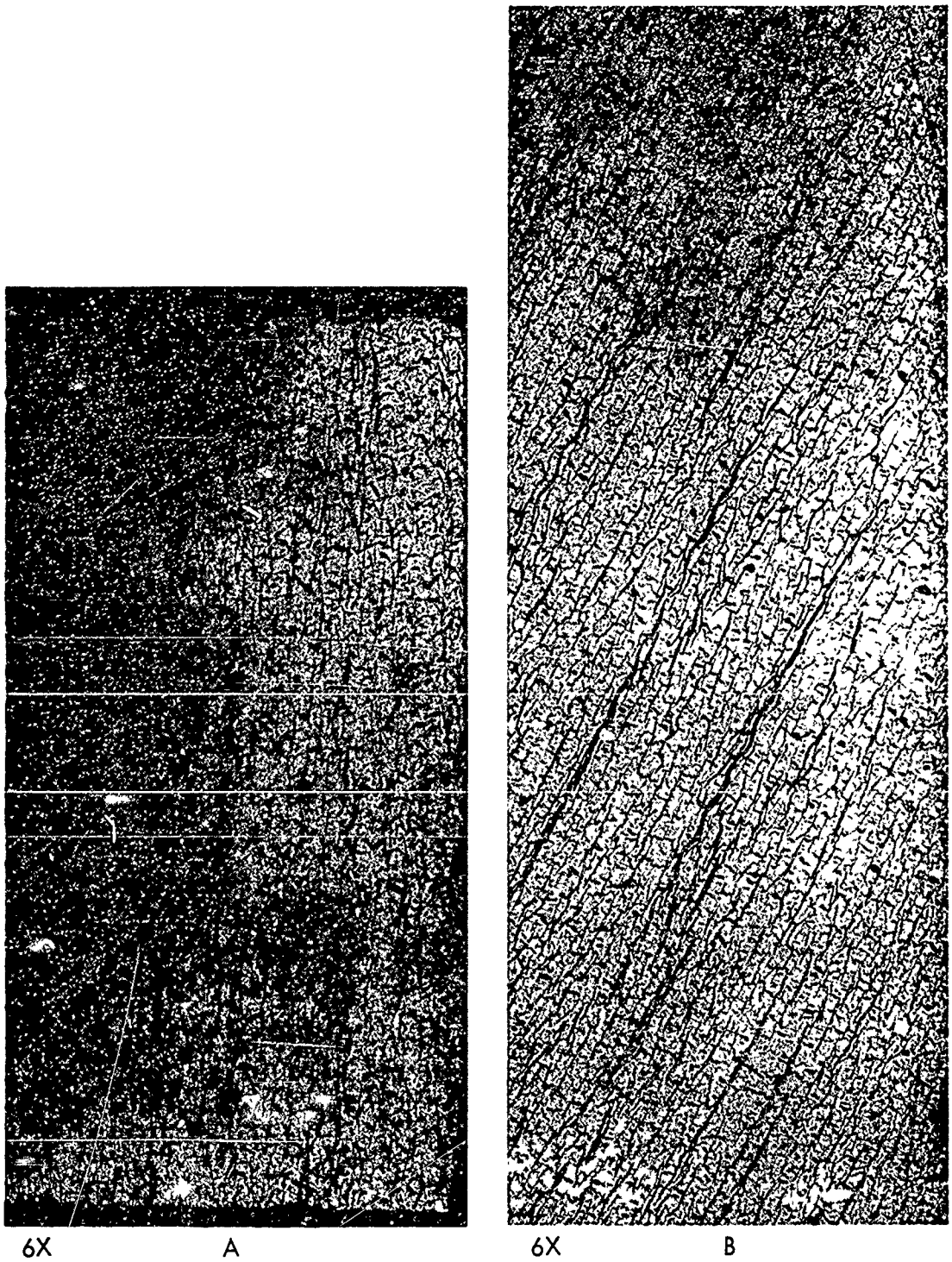

6X A 6X B

FIGURE 38 SPECIMEN 1800-30-H, SECTIONS PARALLEL (A) AND PERPENDICULAR (B) TO THE FLAT FACE

Several delaminations are apparent.

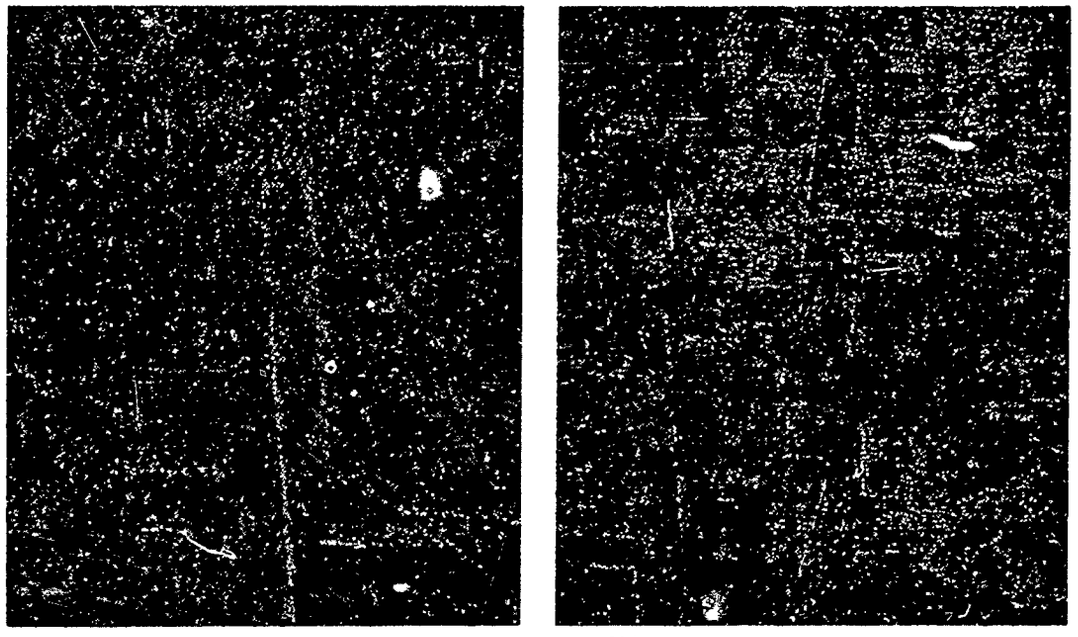

50X 50X

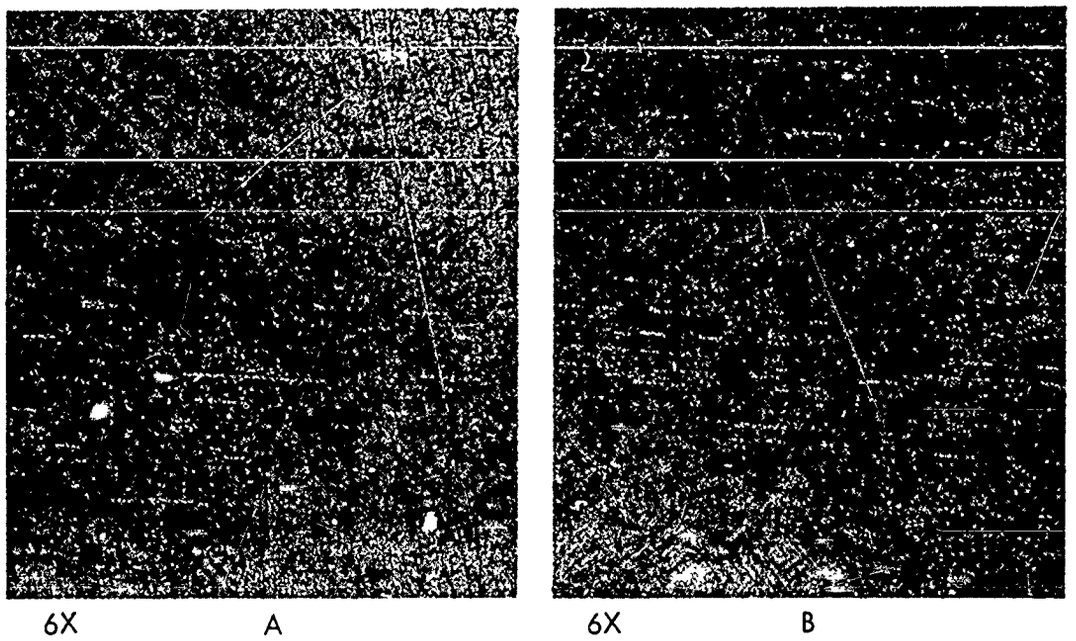

6X A 6X B

FIGURE 39 SPECIMEN 1800-90-H, SECTIONS PARALLED (A) AND PERPENDICULAR (B) TO THE FLAT FACE (CROSS PLY PLANE)

Note the shape and orientation of fissures relative to reinforcement yarns.

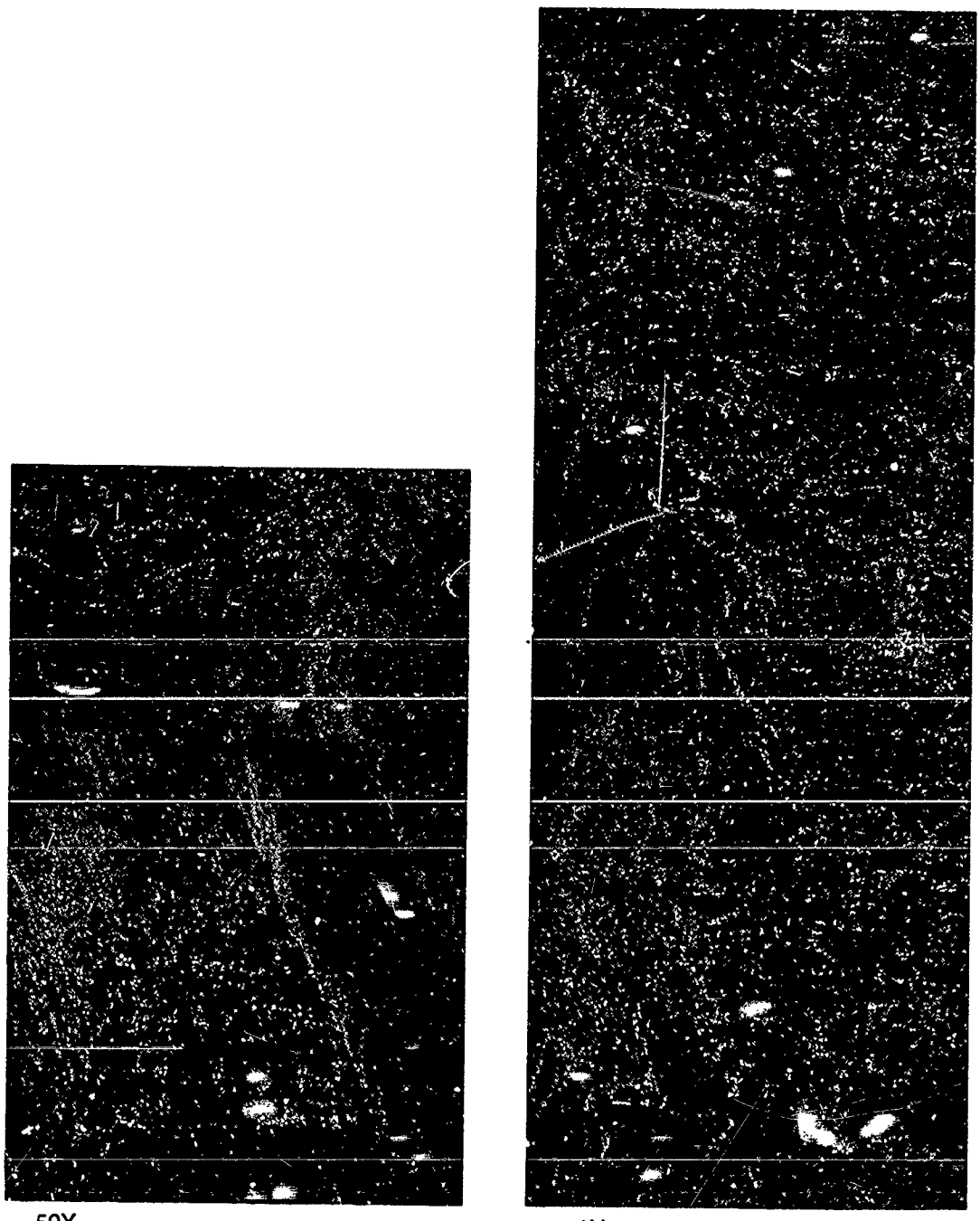

50X 6X

FIGURE 40 SPECIMEN 3000-0-H, CROSS PLY SECTIONS PERPENDICULAR TO FLAT FACE

Note the growth of fissures over the 1800 F char level.
Extended delaminations are not apparent in this specimen section.

50X 6X

FIGURE 41 SPECIMEN 3000-30-H, SECTIONS PERPENDICULAR TO FLAT FACE

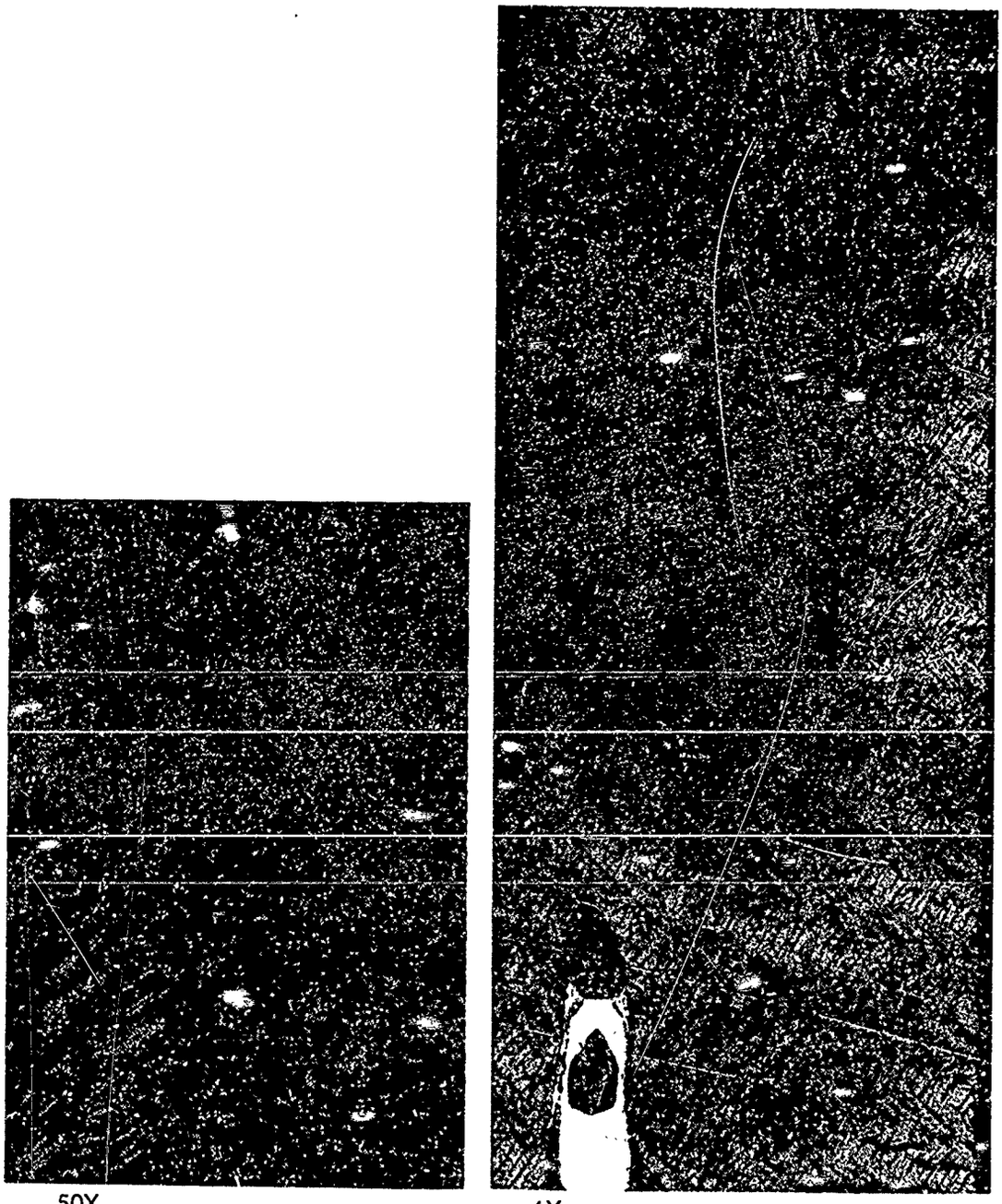

FIGURE 42 SPECIMEN 3000-90-H, CLOTH PLANE SECTIONS PERPENDICULAR TO FLAT FACE

The apparent porosity within the fiber bundles lying parallel to the specimen surface in the 50X photomicrographs probably resulted from polishing.

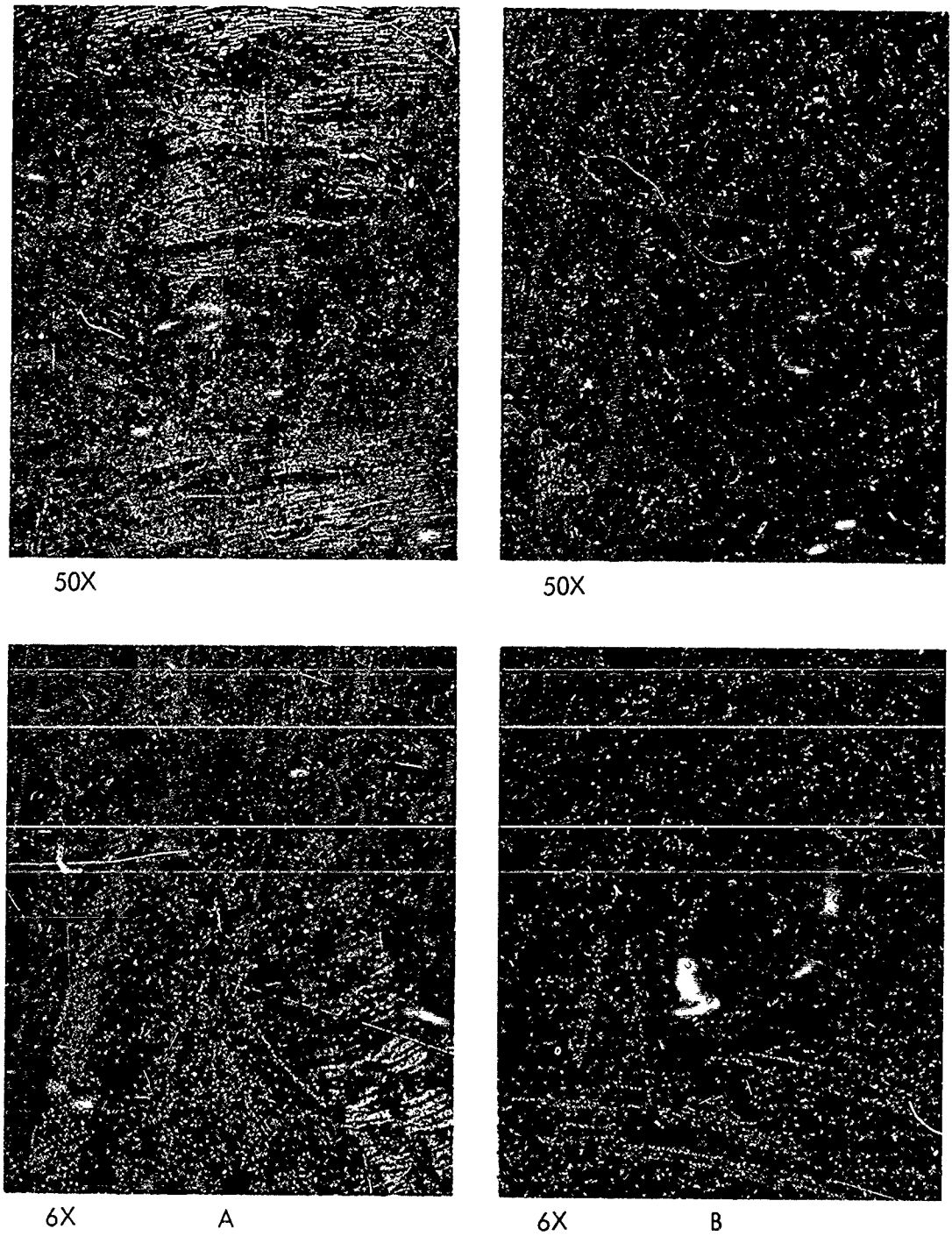

FIGURE 43 SPECIMEN 5000-0-H, SECTIONS PARALLEL (A) AND PERPENDICULAR (B) TO FLAT FACE (CLOTH PLANE)

Note the growth of fissures over the 3000 F char level. The extensive delamination shown in the normal view occured on sectioning. Also note that few small voids are apparent in the plane of the cloth

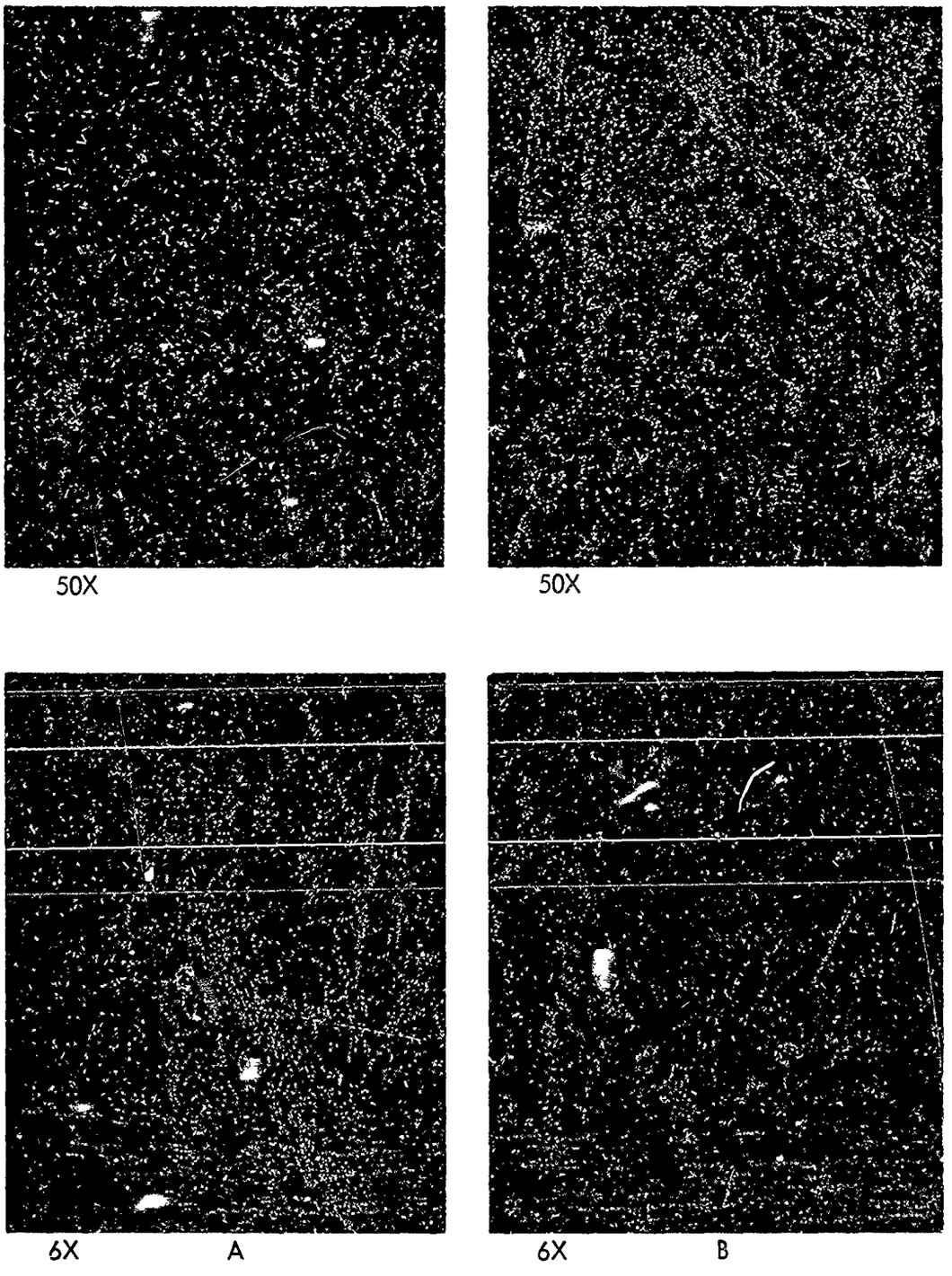

FIGURE 44 SPECIMEN 5000-30-H, SECTIONS PARALLEL (A) AND PERPENDICULAR (B) TO THE FLAT FACE

The cloth layup angle is not apparent in (B) because of the planar angle at which the section was taken.

50X

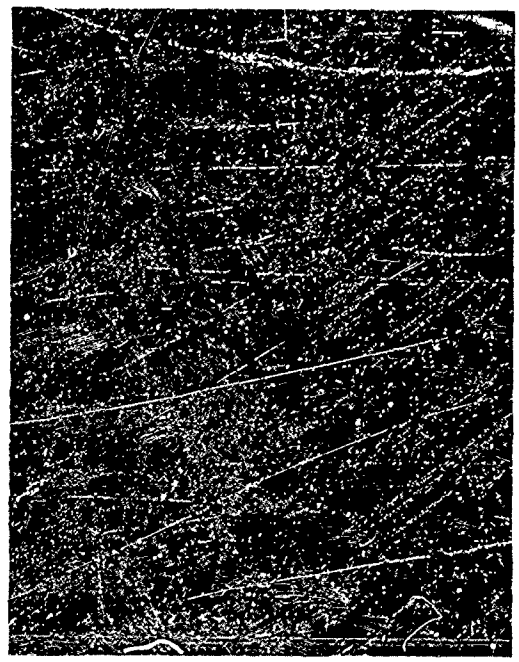

50X

6X A

6X B

FIGURE 45 SPECIMEN 5000-90-H, SECTIONS PARALLEL (A) AND PERPENDICULAR (B) TO THE FLAT FACE (CROSS PLY PLANE)

Note the growth of fisssures over the 3000 F char level.

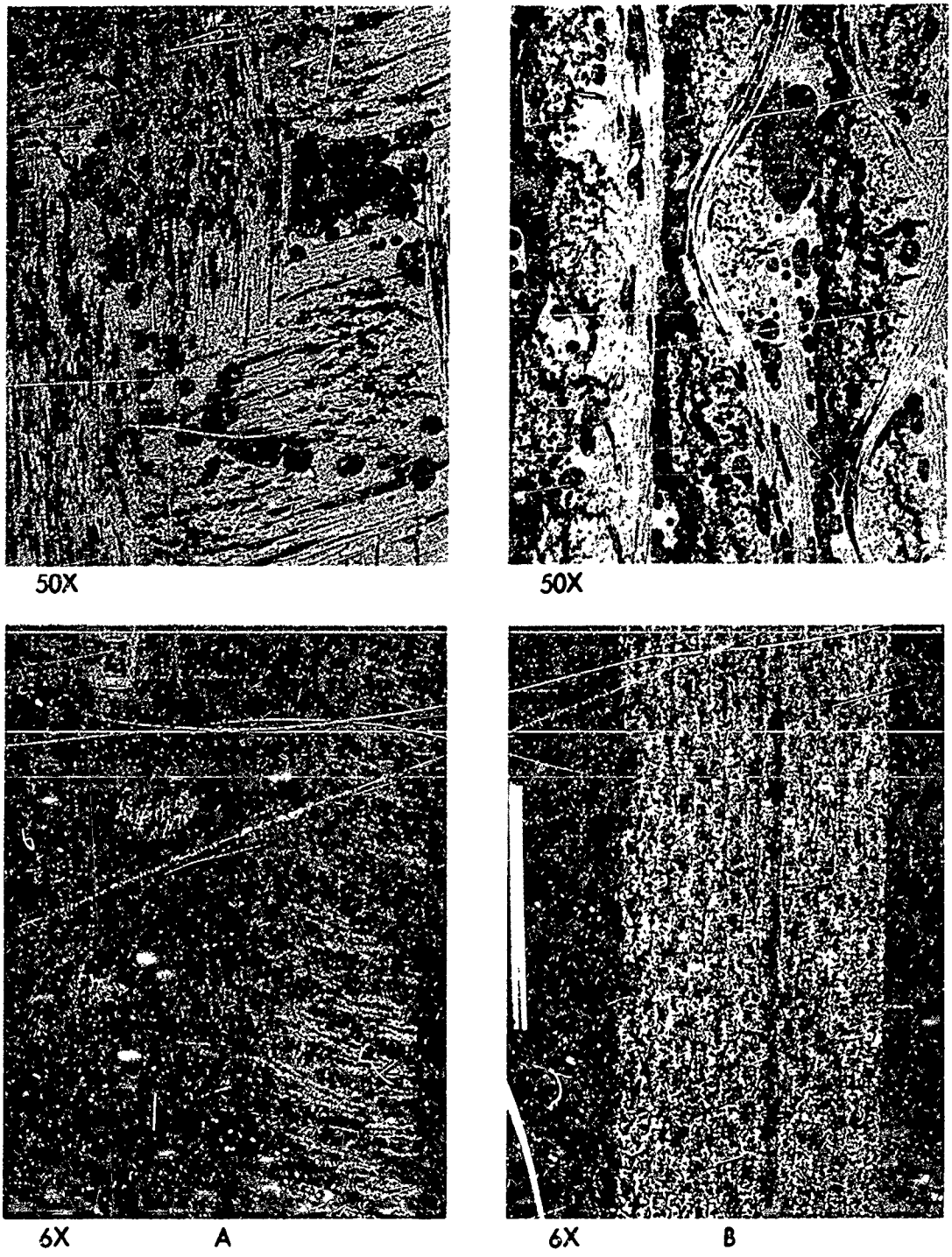

FIGURE 46 SPECIMEN 1800-0-L, SECTIONS PARALLEL (A) AND PERPENDICULAR (B) TO THE FLAT FACE (CLOTH PLANE)

The cloth plane is not parallel to the surface of specimen in (A). Note the single extended delamination in (B). Note the spheroidal shape of voids relative to those in the 1800 F high density chars.

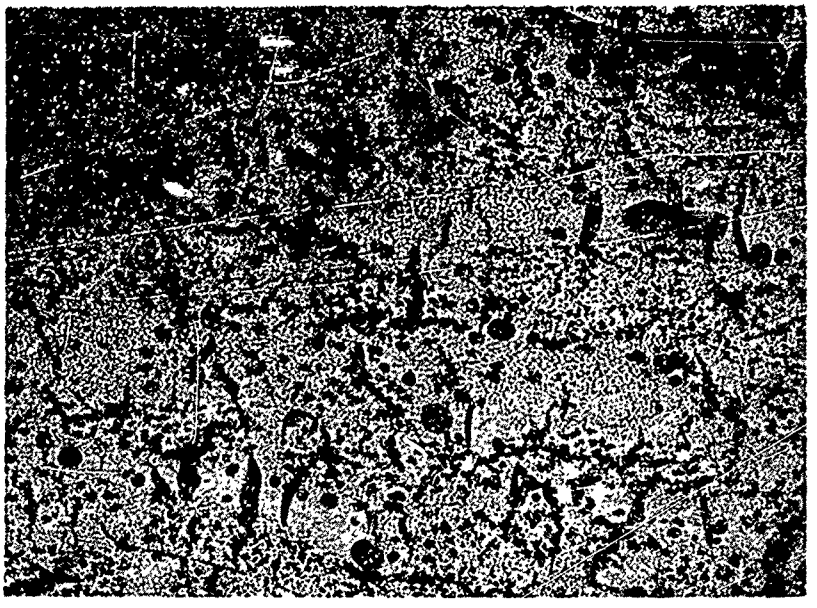

50X A

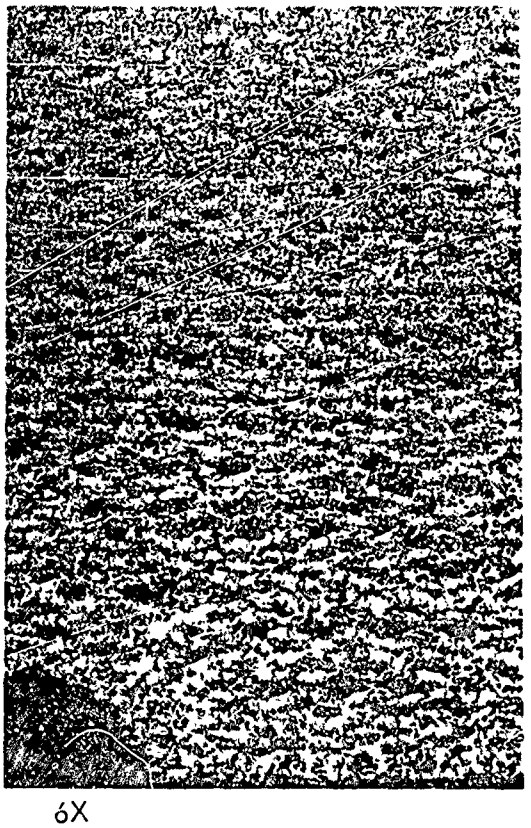

6X

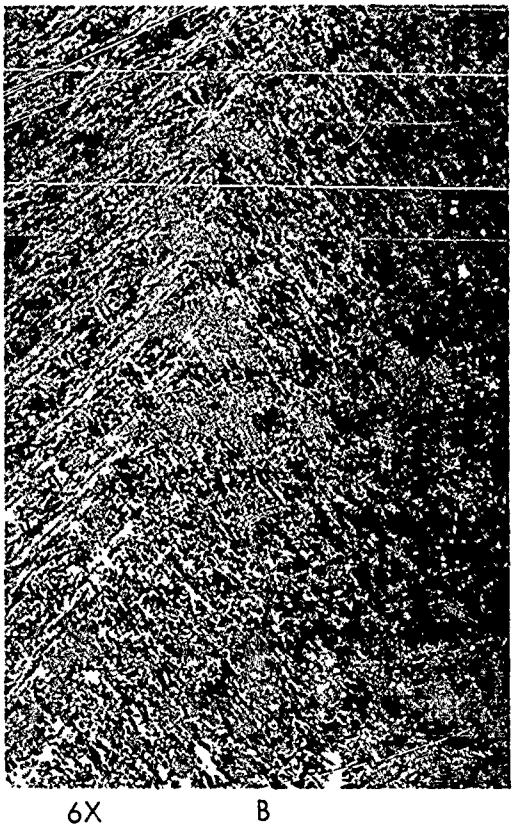

6X B

FIGURE 47 SPECIMEN 1800-90-L, SECTIONS PARALLEL (A) AND PERPENDICULAR (B) TO THE FLAT FACE (CROSS PLY PLANE)

Nonhomogeneity in the density of the large voids is apparent in (A).

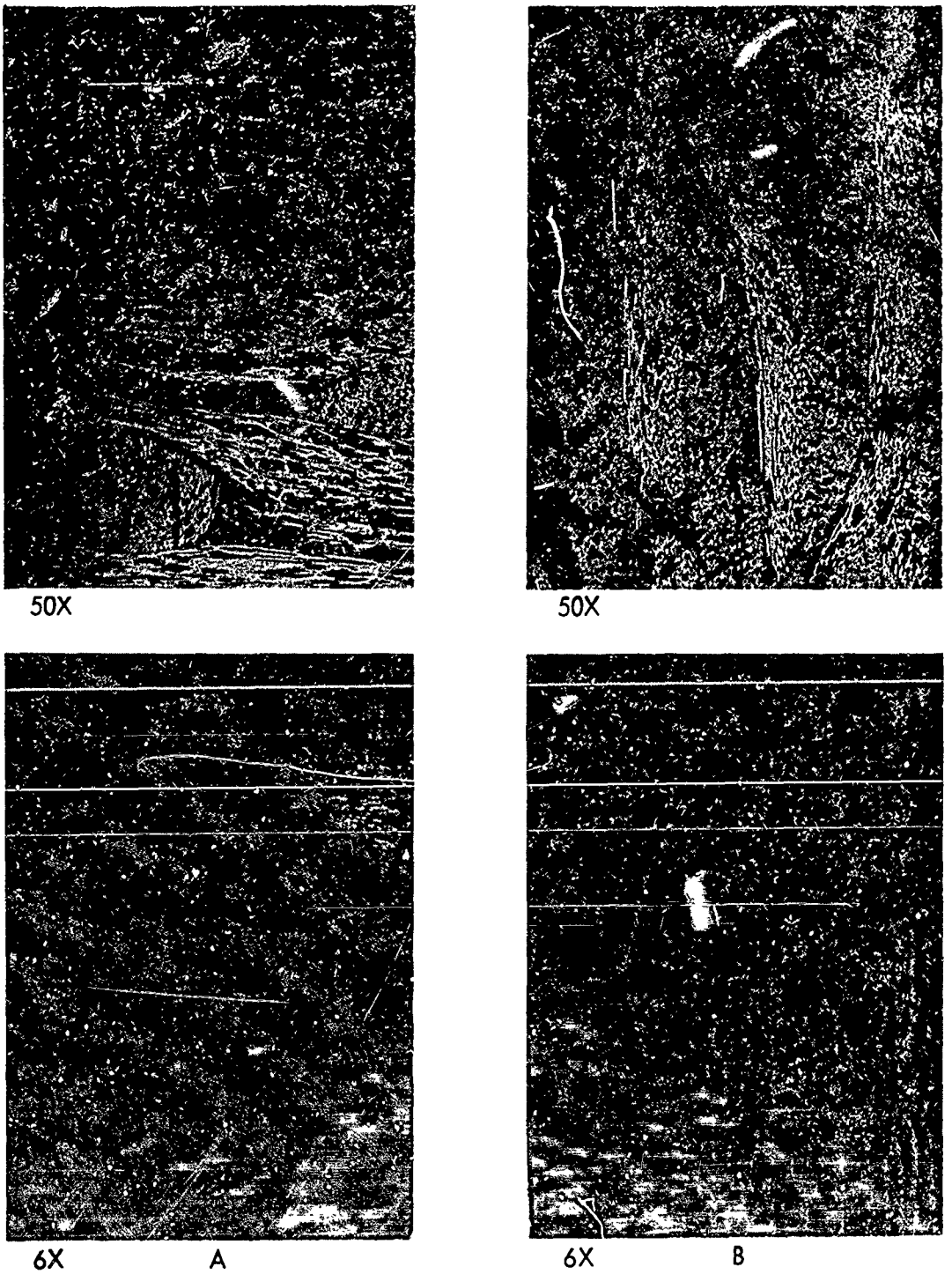

FIGURE 48 SPECIMEN 5000-0-L, SECTIONS PARALLEL (A) AND PERPENDICULAR (B) TO THE FLAT FACE (CLOTH PLANE)

The extreme delaminations shown in (B) occurred upon sectioning. Note much closer similarity in the void structures of the 5000 F low and high density chars than existed at the 1800 F char level.

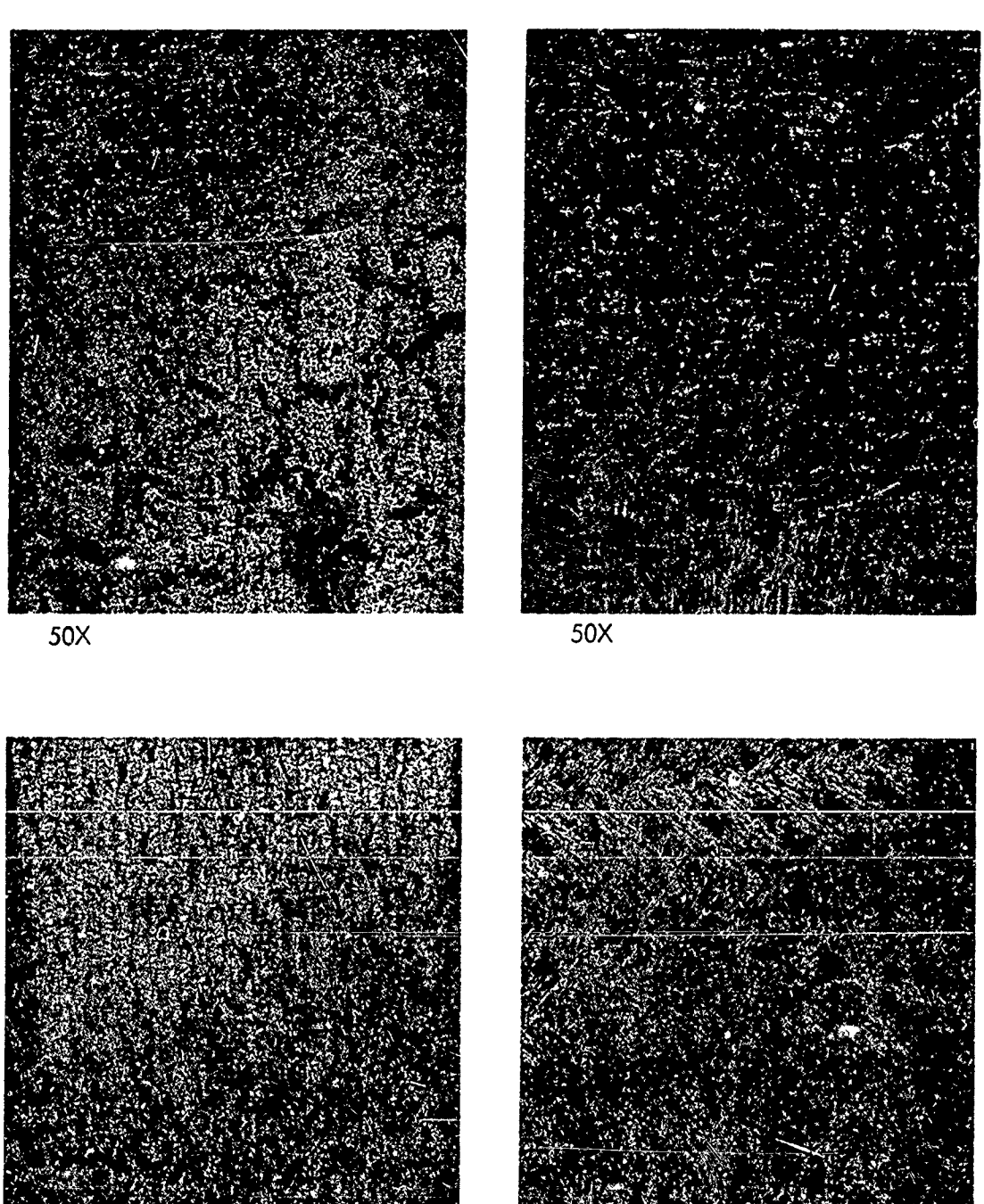

FIGURE 49 SPECIMEN 5000-90-L, SECTIONS PARALLEL (A) AND PERPENDICULAR (B) TO THE FLAT FACE (CROSS PLY PLANE)

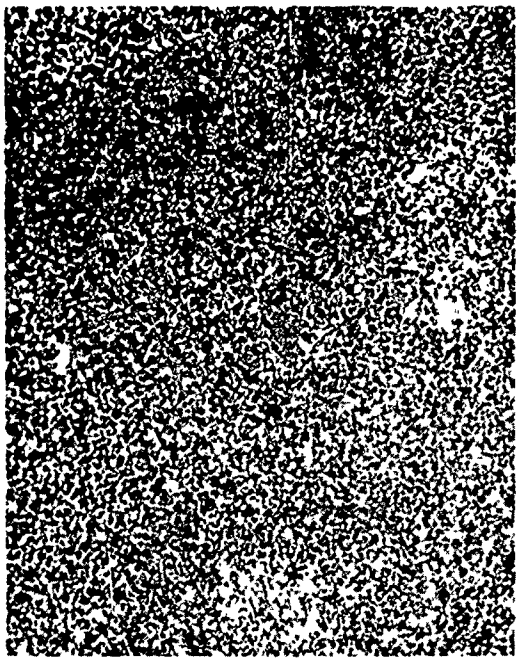

Specimen 800-0-H

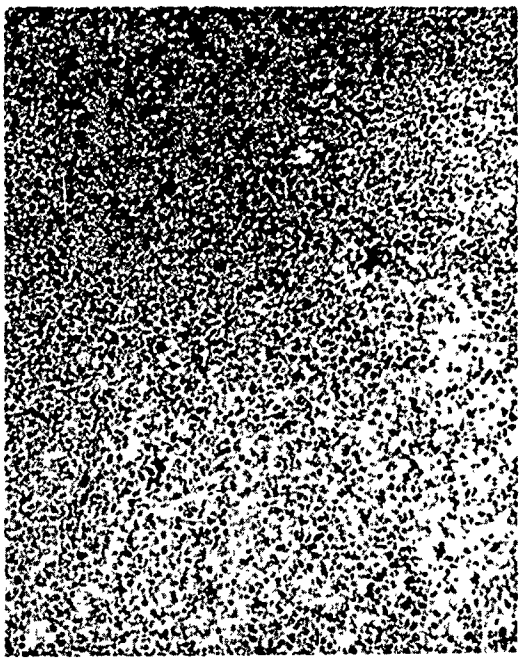

Specimen 1800-90-H

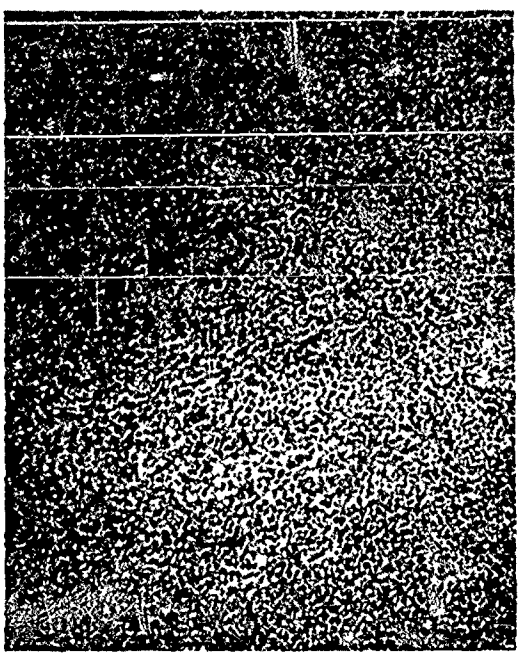

Specimen 3000-0-H

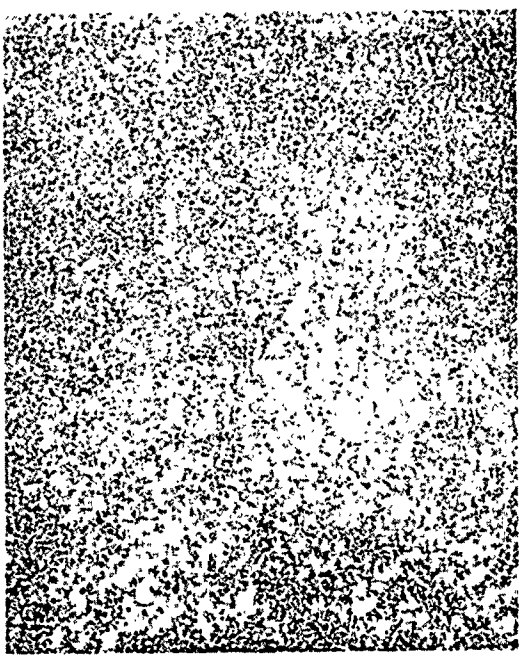

Specimen 5000-0-H

FIGURE 50 TYPICAL SITES IN HIGH DENSITY CHAR PYROLYSIS RESIDUE - 1000X

Note decrease in density of micro-voids with heat treatment above 3000°F
(0.12 inch on prints = 3 microns)

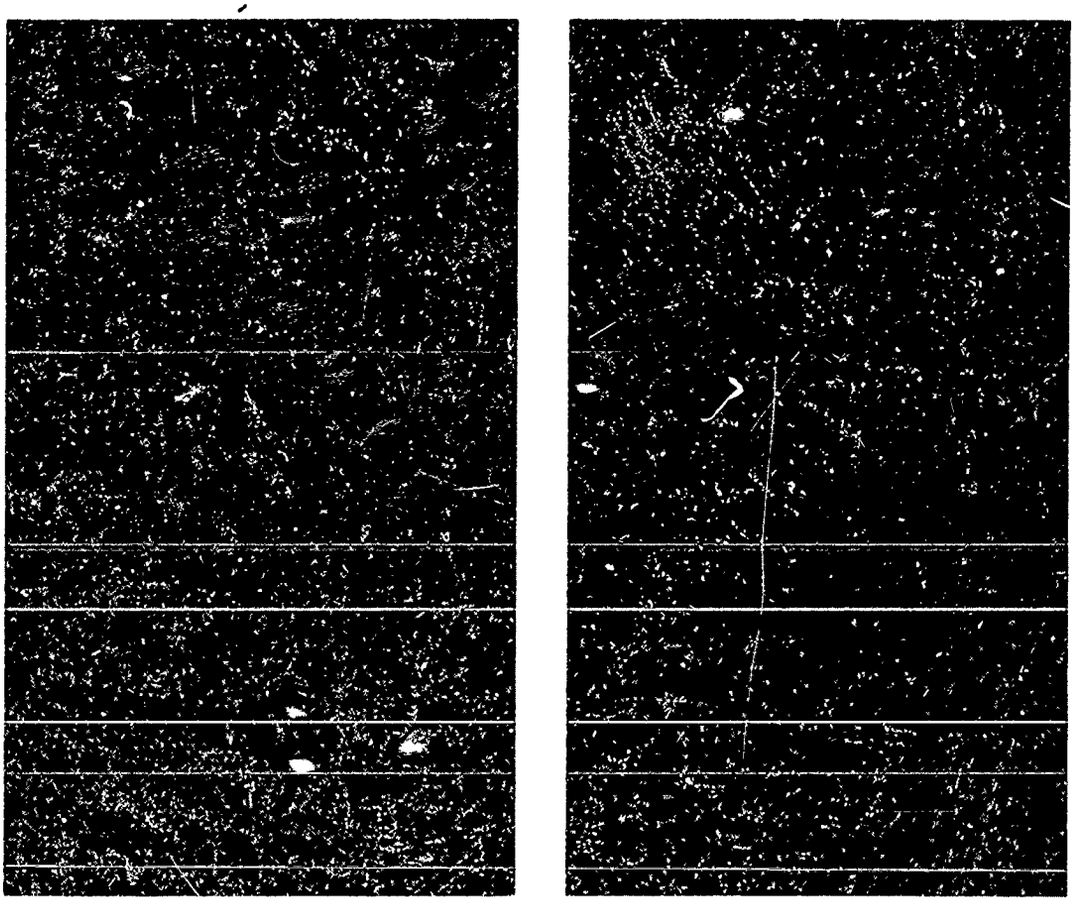

Specimen 1800-90-L

Specimen 5000-90-L

FIGURE 51 TYPICAL SITES IN LOW-DENSITY CHAR PYROLYSIS RESIDUE - 1000X

the major axes of the prolates and to the plane of the platelets in the 0-degree layup angle chars, and lies approximately at the bias angle (45 degrees) of the cloth to these references in the case of the 90-degree layup angle chars.

Class 3 Voids:

These are voids approximately 0.8 to 10 mils in length, occurring more frequently per unit volume than the Class 2 voids. They are located within and between fiber bundles and appear to orient with equal probability both along and normal to the fiber bundles so that their overall orientation relative to the plane of the reinforcement cloth is more random than in the case of the Class 2 voids.

The 50X photomicrographs, Figures 39, 40, and 44, illustrate the Class 3 voids in the chars produced from the high-density virgin material. The shapes of these voids may be described in a very general sense as prolate ellipsoidal. In contrast, the 50X photomicrographs of the low-density chars, Figures 46, 47 and 49, show a preponderance of nearly spherical void shapes in the length range 0.8 to 6 mils, with ellipsoidal shapes emerging for void lengths in the range of 6 to 10 mils.

Class 4 Voids:

These are nearly spherical voids smaller than about 0.8 mils (20 microns) in diameter, occurring both within the fiber bundles and the filler material between bundles. The larger of these can be observed in the 50X photomicrographs of the char sections, e.g., Figure 47.

The general approach taken in the following analyses is to describe the char structure in terms of "discrete" void Classes 2, 3 and 4, surrounded by a continuous, albeit complex, solid material comprised of the reinforcement fibers and carbon matrix. The Class 1 gross delamination type void is so large in comparison to at least one significant dimension of the total specimen volume that it is better described as a "continuous" void. Although interlaminar bonding is of concern in the relation between the performance of the furnace chars and active ablators, quantitative investigation of the extent of influence of Class 1 voids on the thermal properties of the chars requires an effort which was beyond the scope of the present program. For this reason, the gross delaminations were neglected in the quantitative studies which follow.

Results of Quantimet Studies

The void structures defined in terms of Class 2, 3 and 4 voids were not suited to direct microscopic evaluation from the prepared char sections. Consequently, representative polaroid photomicrographs were prepared and the porosity evaluations were performed on the Quantimet Analyzer at 16.1x the magnification of the

photomicrographs. Six X macrographs were utilized in the study of the Class 2 void fractions, and 50X photomicrographs for the Class 3 and 4 void fractions. The magnifications and sensitivity adjustments used on the Quantimet in the study of the Class 2, 3 and 4 voids produced the following approximate resolution limits for the various scans:

TABLE VIII RESOLUTION OF VOID OBSERVATIONS

Where Viewed	Total Magnification	Area of Specimen Observed sq. in.	Side of sq. of equiv. area, mils.	Range of Void Length, L, Detectable in Observed Area, mils
Photo	6	700×10^{-3} (Entire Section)	840	
6X Photo on Quantimet	96.6	10.0×10^{-3}	100	$8 < L < 80$ to 120
Photo	50	6.3×10^{-3}	80	$0.6 < L < 80$
50X Photo on Quantimet	805	0.14×10^{-3}	12	$0.12 < L < 10$ to 15

The 6X macrographs of each char cross-section were examined on the Quantimet with the sensitivity adjusted so that most of the void fraction determined in each scan was due to the voids which fell into the definition given above for the Class 2 voids. At least 10 fields were evaluated for Class 2 area void fractions in each macrograph. The minimum area void fraction observed for each cross section, the maximum, and the average for all the fields evaluated are given as the first numbers in the triplet in each column in Table IX.

In the determinations of Class 3 and 4 void fractions, 17 to 48 fields were evaluated within each 50X photomicrograph on the Quantimet; fewer were evaluated in the case of the 800°F chars where only slight variation was obtained in the results for each field because of the simpler pore structures found in these materials. Generally, the fields were chosen to exclude large Class 2 voids so that the desired Class 3 and 4 area void fractions were not unduly weighted. Each field of each 50X photomicrographs was scanned such that two area void fractions were obtained. The first was comprised predominatly of the Class 3 voids (0.8 mils to 10 mils in length) present in the field. Next, the maximum resolution of the Quantimet was utilized to obtain the total area porosity in the field (0.12 mils to 10 mils in length). The fractions so determined are given in Table IX for all of the chars examined as the second and third numbers of the triplet in each column respectively; the difference between these numbers is the Class 4 void fraction resolved at the magnification

TABLE IX QUANTIMET IMAGE ANALYZER AREA VOID FRACTION DETERMINATIONS

Specimen [1]	Average Area Void Fraction, % [2]	Minimum Observed, % [2]	Maximum Observed, % [2]
V-90-H // and ⊥	No porosity detected		
800-0-H //	1, 3.1, 3.9	0, 2.5, 3.8	0, 3.6, 4.0
⊥ [3]	1, 5.3, 10.	0, 2.0, 6.0	0, 14.0, 18.0
⊥	1, 4.3, 9.0	0, 1.0, 4.0	0, 11.0, 14.0
1800-0-H //	5.0, 11.8, 15.5	3.0, 5.0, 9.0	8.0, 36.0, 41.0
⊥	8.0, 12.4, 16.1	4.0, 4.0, 4.0	12.0, 26.0, 28.0
1800-30-H //	6.0, 15.7, 22.6	4.0, 3.0, 13.0	8.0, 28.0, 37.0
⊥	5.0, 14.4, 16.8	3.0, 7.0, 8.0	7.0, 28.0, 28.0
1800-90-H //	2.0, 10.6, 18.2	1.0, 7.0, 12.0	2.0, 22.0, 28.0
⊥	5.0, 12.0, 14.8	4.0, 5.0, 5.0	7.0, 20.0, 23.0
1800-0-L // [3]	8.0, 18.8, 36.0	3.0, 11.0, 22.0	14.0, 39.0, 60.0
⊥	16.0, 32.0, 37.0	12.0, 21.0, 23.0	18.0, 51.0, 53.0
⊥	16.0, 32.6, 38.1	12.0, 19.0, 16.0	18.0, 53.0, 60.0
1800-90-L //	9.0, 25.5, 27.6	5.0, 17.0, 18.0	18.0, 34.0, 34.0
⊥	14.0, 18.6, 19.5	10.0, 7.0, 7.0	21.0, 30.0, 40.0
3000-0-H ⊥ [4]	7.0, 12.0, 17.5	5.0, 1.0, 5.0	8.0, 28.0, 34.0
⊥	7.0, 9.5, 14.8	5.0, 2.0, 4.0	8.0, 20.0, 27.0
3000-30-H ⊥ [4]	11.1, 13.4, 19.3	10.0, 4.0, 6.0	17.0, 26.0, 32.0
⊥	– , 12.1, 23.0	– , 2.0, 10.0	– , 39.0, 44.0
3000-90-H ⊥ [4]	9.0, 11.8, 24.4	5.0, 3.0, 7.0	12.0, 30.0, 38.0
⊥	9.0, 11.0, 19.0	5.0, 2.0, 8.0	12.0, 28.0, 28.0
5000-0-H //	12.0, 21.0, 21.0	6.0, 10.0, 10.0	16.0, 42.0, 42.0
⊥	10.4, 21.7, 21.7	8.0, 12.0, 12.0	13.0, 38.0, 38.0
5000-30-H //	13.5, 24.0, 24.0	11.0, 14.0, 14.0	16.0, 35.0, 35.0
⊥	12.0, 20.0, 20.0	10.0, 14.0, 14.0	14.0, 36.0, 36.0
5000-90-H, //	10.7, 24.0, 24.0	8.0, 17.0, 17.0	13.0, 33.0, 33.0
No. 1 ⊥	10.8, 20.0, 20.0	6.0, 13.0, 13.0	15.0, 30.0, 30.0
5000-0-L //	15.6, 26.8, 26.8	10.0, 22.0, 22.0	20.0, 36.0,36.0
⊥	15.4, 28.3, 28.3	12.0, 20.0, 20.0	20.0, 45.0, 45.0
5000-90-L //	19.8, 31.9, 31.9	18.0, 28.0, 28.0	22.0, 45.0, 45.0
⊥	15.4, 28.7, 28.7	12.0, 20.0, 20.0	20.0, 37.0, 37.0

[1] // refers to metallographic section taken parallel to flat face of disk thermal conductivity specimen, and ⊥ refers to section taken normal to the flat face.

[2] First number of triplet is the Class 2 area void fraction, the second, the Class 3 area void fraction, and the third, the combined Class 3 and 4 area void fraction.

[3] Class 3 and 4 voids evaluated on two sections taken normal to the flat face.

[4] Class 3 and 4 voids evaluated on 50X photomicrographs of two areas on a section.

employed (0.12 mils to 0.8 mils). It may be noted that the Class 3 and combined Class 3 and 4 void fractions become equivalent at the 5000°F char level, suggesting complete disappearance of the Class 4 voids.

The standard deviations of the Class 3 and combined Class 3 and 4 area void fractions in each field ranged from about 2 percent in the case of the 800°F chars to about 6 percent in the higher temperature chars, with a maximum of about 10 percent occurring in the 1800°F chars produced from the low density virgin material. The relatively large variation in individual area void fractions from field to field indicates nonhomogeneity in the char material over the sample dimension utilized for the Quantimet porosity determinations. It should be noted that some of the fissures which appeared on the photomicrographs used in the area porosity determinations reported in Table IX very likely were created during polishing of the specimen section. This unavoidable occurrence is evident in Figure 42, for example, and is pronounced only in those sections wherein fiber bundles lay parallel, or nearly so, to the surface of the polished section. For these cases, at least some of the fissures due to polishing were included in the area porosity measurements. Inclusion of the artificial voids would tend to increase the standard deviation and value of the porosity attributed to the Class 3 voids.

The data in Table IX may be used to look for gross void orientation characteristics with respect to reinforcement cloth yarn direction. Comparison of the high density char void fractions for the sections taken parallel and normal to flat faces of the disk specimens reveals that they are essentially equivalent. Within the resolution achieved in the void structure characterization, no significant quantitative effects of layup angle on the measured void fractions of the high density chars were discernible. The Quantimet study of the low density chars, especially in regard to Class 2 voids, was complicated by the presence of oriented, oblate-like voids which caused the metallographic sections taken nearly parallel to the cloth layer to appear extremely nonhomogeneous, as can be seen in the 6X macrographs, Figures 46 through 49. These are voids at the weave crossovers described in Section III.

Variations of several percent in the various void fractions given in Table IX between individual fields evaluated, between individual specimen sections taken in the same direction, and between different 50X photomicrographs taken on the same section, are interpreted as resulting from the difficulty in adequately sampling the chars rather than reflecting true variations in the void distribution and orientation characteristics within a given char. Averaging of the results in the table is therefore appropriate. In addition, even though area void fractions are not directly comparable to volume void fractions except for specific combinations of void shapes, distribution and sampling, comparison of the two types of values gives information on the size composition of the total void volume.

TABLE X POST CONDUCTIVITY TEST AVERAGE VOID DISTRIBUTION

Specimen	Total Volume Void Fraction % [1]	Class 2 Voids [2] Area Fraction %	Class 2 Voids [2] % of Void Volume	Class 3 Voids [2] Area Fraction %	Class 3 Voids [2] % of Void Volume	Class 4 Voids [3] Area Fraction %	Class 4 Voids [3] % of Void Volume	Total Class 2,3&4 Voids [2] Area Fraction %	Total Class 2,3&4 Voids [2] % of Void Volume
800-0-H	24.0	0		4.2	17.5	19.8	82.5	7.7	32.1
1800-0-H	40.7	6.5	16.0	12.1	29.7	22.1	54.3	22.3	54.8
1800-30-H	39.1	5.5	14.1	15.0	38.4	18.6	47.6	25.2	64.4
1800-90-H	33.5	3.5	10.4	11.3	33.7	18.7	55.8	20.0	59.7
1800-0-L	44.2	12.0	27.1	27.8	62.9	4.4	9.9	50.3	114.0
1800-90-L	36.9	11.5	31.2	22.0	59.6	3.4	9.2	35.0	94.8
3000-0-H	26.3	7.0	26.6	10.7	40.7	8.6	32.7	23.1	87.8
3000-30-H	26.2	11.1	42.4	12.7	48.5	2.4	9.2	32.2	123.0
3000-90-H	26.9	9.0	33.5	11 4	42.4	6.5	24.2	30.7	114.0
5000-0-H [4]	33.5	11.2	33.4	21.4	63.9	0 9	2.7	32.6	97.3
5000-30-H [4]	27.7	12.7	46.0	22.3 22.0	66.6 79.4	0 0	0 0	33.5 34.7	100.0 125.0
5000-90-H [4]	22.4	10.8	48.2	15.0 22.0	54.0 98.2	0	0	27.7 32.8	100.0 146.0
5000-0-L [4]	28.6	15.5	54.2	11.6 27.5	51.8 96.3	0	0	22.4 43.0	100.0 150.0
5000-90-L [4]	25.8	17.6	68.2	13.1 30.3	45.8 117.0	0	0	28.6 47.9	100.0 186.0
				8.2	31.8			25.8	100.0

[1] Averate total volume porosity from Table VII ; post test values where available.

[2] Average of all Quantimet Image Analyzer values in Table IX.

[3] Calculated as the difference between the total volume void fraction and the combined Class 2 and Class 3 area void fractions.

[4] Underlined values are Class 3 void fractions calculated as the difference between the total volume void fraction and the Class 2 area void fraction.

Table X presents a comparison of the average Quantimet-determined area void fractions and the density-determined total volume void fraction for each char specimen. Also presented is a separate estimate of the Class 4 void fraction determined as the difference between the total volume void fraction and the sum of the Class 2 and 3 area void fractions. For the 5000°F chars, separate estimates of the Class 3 void fraction, the underlined values in Table X, were obtained as the difference between the total volume void fractions and the Class 2 area void fractions. To emphasize the composition of the total void volume, the individual area void fractions are also expressed as percentages of the total volume void fraction.

Because of the variability of void shapes and sizes, some overlap invariably occurred in the number of voids included in the Quantimet determinations of the Class 2, 3, and combined Class 3 and 4 void fractions. Inclusion of a fraction of the voids into more than one void class decreased the precision of the void distribution determination. Through the 1800°F char level, the void classes were relatively well defined and separable in the Quantimet studies so that a significance of about 6% may be attached to variations in the percent of total volume void fraction values in the last column of Table X for the fairly homogeneous, high density 800°F and 1800°F chars. However, in the 3000°F chars, the Class 3 fissures had grown in size to where the distinction between Class 2 and 3 voids was less apparent. For this reason, the level of significance in the variations in the percent of total volume void fraction figures in the last column of Table X increased to about 20 percent for the 3000°F chars. These errors in the cummulative Quantimet results may be evenly distributed over the individually determined Class 2, 3 and combined Class 3 and 4 void fractions.

At the 5000°F char level, distinction between Class 2 and 3 voids was difficult to achieve by the Quantimet technique employed, resulting in considerable overlap of the indicated void fractions. This is apparent in the results of the last column of Table X for the 5000°F chars, wherein the Quantimet-determined total void fractions are generally larger than those derived from the helium and bulk densities. At this char level, the Class 2 void fractions obtained from the 6X macrographs are the only relatively secure measures of an individual void class fraction. As will be discussed below, most of the Class 4 voids appear to be filled at the 5000°F char level. Therefore, within the definitions of the void classes applied in the characterization studies, the difference between the density-determined total void fraction and the Quantimet-determined Class 2 void fraction is predominantly due to the Class 3 voids. The void distribution derived in this manner is expressed as the underlined values in Table X, and is felt to represent the salient aspects of the void distribution in the 5000°F chars.

The Table X values show that the void distributions are quite consistent among the chars of different layup angle within each group defined according to the density

of virgin material (high or low), and heat treatment. These results may be applied to investigate the development of the void structure with heat treatment, and the effect of the virgin material density on char void structure.

The discussion of the helium displacement solid density results in the previous subsection admitted the possibility that the helium density may fail as a measure of the density of the solid char material above the 1800°F char level because of the development of a distributed, intercrystalline porosity inaccessible to helium. The Quantimet-determined void fractions in Tables IX and X are unaffected by the presence of a void distribution below the limit of resolution of the scans, and the total volume void fractions in Table X would represent only the fraction of the total void volume which is accessible to helium for the char levels above 1800°F. Therefore, the Class 4 void fractions as calculated in Table X would include only the voids in the size range 20 microns to the upper limit of the intercrystalline voids. An independent measurement, not included in the scope of the present program, would be required to resolve the intercrystalline porosity as a separate entity, e.g., a Class 5 void fraction.

Void Development with Heat Treatment

In order to illustrate the development of the void structure with heat treatment, the values in Table X for the high density chars, averaged over all the chars in each temperature class, are plotted as functions of the char heat treatment temperature in Figure 52. Linear variations between the discrete data points are assumed in the figure for discussion purposes. The solid curves indicate the data believed to give the most accurate description of the chars. The underlined values from Table X were plotted for the 5000°F chars.

The solid curves in Figure 52 show that about 82% of the total void fraction at 800°F is due to the small, Class 4 voids, with the remaining 18% due almost entirely to the intermediate size Class 3 voids. Between 800°F and 1800°F, the Class 4 void fraction remains constant while larger, Class 3 and 2 voids develop. At the 1800°F char level, the Class 4 voids account for about 52% of the total void fraction, Class 3 about 34%, and Class 2 about 14%. The delayed development of Class 2 and 3 voids with respect to the Class 4 voids between 500°F and 1800°F, considered in conjunction with the general orientations and locations of the three void classes with respect to the reinforcement cloth yarns, suggests that the Class 4 voids are formed in the resin-plus-filler matrix as the result of the evolution of gaseous products during the early stages of resin pyrolysis, while the Class 2 and 3 voids may be caused by differences in the expansion characteristics of the reinforcement fibers and the rigid, coke-like matrix.

Between 1800°F and 3000°F, the total volume void fraction decreases by about 30 percent, while the Class 3 void fraction remains almost constant and the Class 2 void fraction undergoes a 63 percent increase. These changes apparently occur at the expense of the Class 4 voids, whose void fraction decreases by about 68 percent over this temperature range. The possibility discussed previously

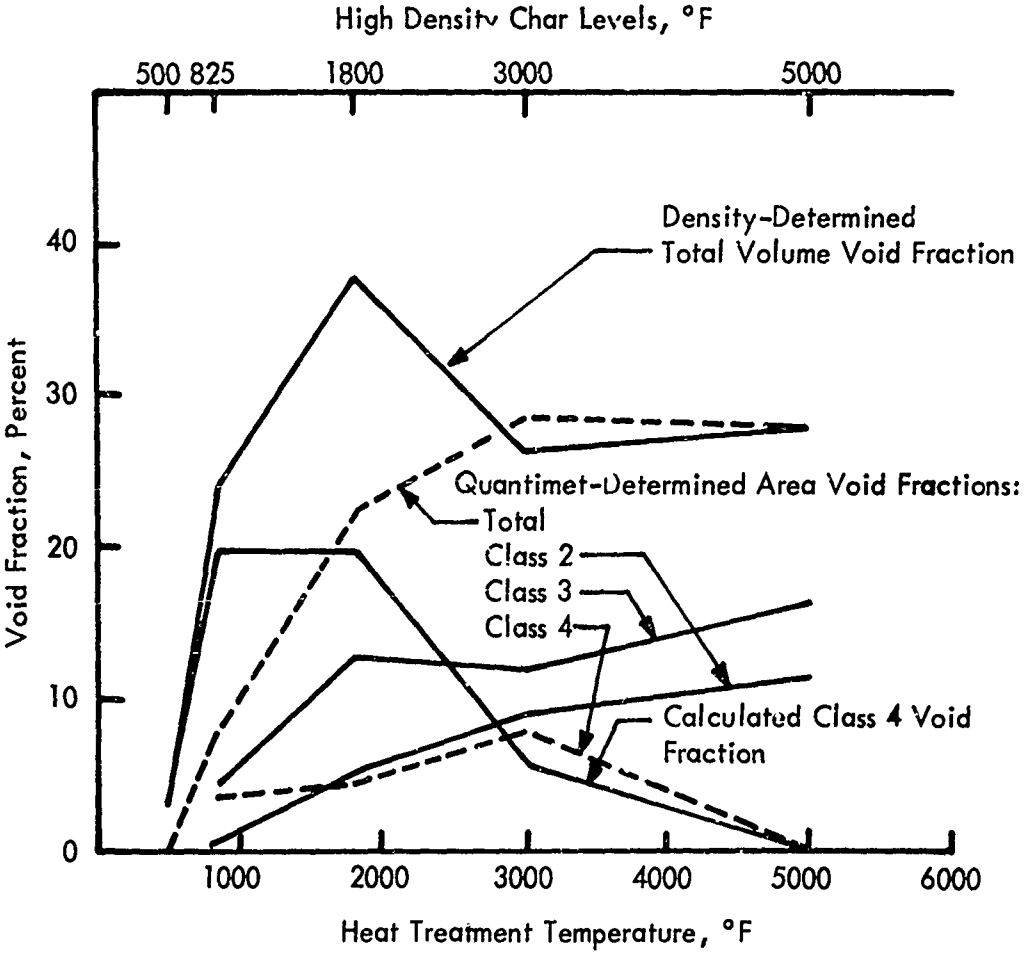

FIGURE 52 VARIATION OF AVERAGE CLASS 2, 3, 4 AND TOTAL VOID FRACTIONS OF THE HIGH DENSITY CHARS WITH HEAT TREATMENT

of the development of an isolated, intercrystalline porosity above about 1800°F affects the definition of the Class 4 void fraction plotted as a solid line in Figure 52. This quantity remains useful as a measure of the area fraction of voids encompassing the size range 20 microns down to the upper limit of the intercrystalline voids which are inaccessible to helium. Similarly, the total void fraction in Figure 52 represents only the fraction of the total void volume which is accessible to helium. The decrease in these two void fractions between 1800°F and 3000°F is attributed to either the actual disappearance, or closure to helium, of voids smaller than 3 microns.

Between 3000°F and 5000°F, the total void fraction increases by 5 percent while the Class 4 voids, exclusive of intercrystalline voids, apparently completely disappear. The increase in porosity over this temperature range is due to the progressive growth of the large Class 2 and 3 fissures, whose fractions exhibit increases of 35 percent and 40 percent, respectively.

The two dashed curves in Figure 52 represent the variation with heat treatment of the average Class 4 and total void fractions as determined directly from the Quantimet scans, for which the resolution limit was about 3 microns. The increase in the Quantimet-determined Class 4 void fraction between 1800°F and 3000°F implies that the density of Class 4 voids in the size range 3 to 20 microns is increasing with heat treatment up to the 3000°F char level. The fact that no Class 4 porosity was detected by the Quantimet in the 5000°F chars suggests that the voids in this size range vanished between 3000°F and 5000°F heat treatment.

It is seen that the Quantimet resolved only 18 percent of the Class 4 porosity given by the solid curve in Figure 52 in the 800°F chars, about 23 percent of the Class 4 porosity in the 1800°F chars, and virtually 100 percent of the Class 4 porosity in the 3000°F and 5000°F chars; the Quantimet-determined total void fraction correspondingly approaches the density-determined total void fraction with heat treatment. Further resolution of the Class 4 void fraction may be drawn from a comparison of the solid and dashed Class 4 void fraction curves in Figure 52 as follows: the void structure in the 800°F high-density chars is composed predominantly (82 percent) of open (to helium) voids smaller than about 3 microns; at the 1800°F char level, the Class 4 void fraction has about the same value as at 800°F, and 77 percent of it remains due to open microvoids smaller than 3 microns; between 1800° and 3000°F the voids smaller than 3 microns apparently vanish or develop into isolated voids which are inaccessible to helium. Between 3000°F and 5000°F the Class 4 void fraction, exclusive of intercrystalline voids, approaches zero, indicating disappearance of all voids smaller than 20 microns and larger than the isolated, intercrystalline voids.

The results described above are generally consistent with the trends in pore size distribution obtained by mercury porosimeter and helium pycnometer measurements in Reference 1 on both post-ablation chars and furnace chars. The mercury porosimeter data provided resolution of pore opening sizes in the range 0.012 to 75 microns. The data showed that the small voids developed early in both furnace

and ablation chars, with the proportion of large voids increasing with temperature. Data on furnace chars showed greater decrease in the relative fraction of very small voids (<3 microns) with heat treatment than did the data on post-ablation chars. Both post-ablation and furnace chars showed a decrease in helium displacement determined total void volume with heat treatment, consistant with the results of this study. The mercury porosimeter data did not suggest complete disappearance of Class 4 voids in measurements on furnace chars heated to 4000°F, but did show the disappearance of voids smaller than 0.012 microns between 2500°F and 4000°F. The analogy to glassy carbon behavior discussed previously is strong. The minor differences in behavior between furnace chars and post-ablation chars in Reference 1 are consistant with those noted for phenolic-nylon chars in Reference 30, where it was concluded that the higher heating rate post-ablation chars (analogous to the pyrolysis residue in the carbon cloth reinforced materials) showed a greater tendency toward graphite-like behavior, but only at the highest temperatures encountered during ablation.

Figure 50 presents 1000X photomicrographs of "typical" sites within the matrix of the high density chars at the 800°F, 1800°F, 3000°F, and 5000°F heat treatment levels. Microvoids on the order of 3 microns and larger are visible. The photomicrographs show that these microvoids persist into the 3000°F char level. However comparison of the 3000°F and 5000°F photomicrographs in Figure 50 reveals a striking reduction in micro-void density over this temperature interval. Of course, voids in the size range of intercrystalline voids are not resolved in these photomicrographs.

Effect of Density of Virgin Precursor on Void Distribution

An interesting comparison between the void structures of the high and low density chars is found in the results for the 1800°F chars in Table X. Whereas the total density-determined void fractions are about equal for the 1800°F low and high density chars, the Class 2 and 3 void fractions for the former are each about twice as great as those for the latter. Many of these voids were present initially in the virgin resin. In contrast to the high density char case, the total of the Quantimet scans accounts for essentially all of the porosity in the low density chars, indicating that voids smaller than 3 microns and open to helium exist in much lower densities in these chars than in the high density chars. Comparison of the 1000X photomicrograph of the 1800°F low density char matrix, Figure 51, with that of the 1800°F high density char matrix, Figure 50, lends visual support to this supposition.

At the 5000°F char level, the total void fractions for the low and high density chars are about equal. It will be seen in Section VII that one of the reasons that the porosities of the chars from both types of precursor are nearly equal is that the low density precursor had low resin content; hence a lower volume of material producing porosity during pyrolysis. Although the Class 2 and 3 void fractions for the two types of chars are more equal in this char level than at the 1800°F char level, the void distribution in the low density char remains more heavily weighted towards the Class 2 voids than that in the high density chars. The 1000X photomicrographs of

the 5000°F low density char matrix, Figure 51, indicates an almost complete absence of voids on the order of 3 microns and larger as in the case of the 5000°F high density char.

Because the apparent decrease in total void fraction between the 1800°F and 3000°F high density char levels is attributable to developments within the char matrix, the apparent low density char total void fraction can be expected to behave similarly with heat treatment over this temperature interval, the possible influence of a distributed, intercrystalline porosity being unresolved in both cases.

Void Size Distributions of Class 3 Voids for Several Selected Chars

To characterize the void size distribution in further detail, the Class 3 and the few Class 2 voids appearing in the 50X photomicrographs of several of the 800°F and 1800°F char sections were individually counted and catalogued according to the longest dimension of each pore. The numbers of voids in each size category and the corresponding percentage of the total number counted are given in Table XI.

Several general observations concerning the results of the void count and classification are:

(1) The majority of the voids counted in the high density chars lie at the smallest lengths measured, 0.6 to 2.5 mils, i.e., the void density is increasing towards the Class 4 void size range. This tendency is not so pronounced in the low density chars.

(2) Comparison of the figures for the parallel and normal samples in the 0- and 90-degree layup angle specimens does not suggest a preferred orientation for the Class 3 voids as they are here defined according to size and shape.

(3) The number of voids in the larger size categories increases with char heat treatment.

For the most part, the voids counted comprise the Class 3 void fractions given in Tables IX and X. Thus, an approximate void size distribution for the Class 3 voids, (the fraction of the total void volume due to Class 3 voids as a function of void length) between about 0.6 and 10 to 15 mils can be obtained by multiplying the appropriate percent values in a column of Table XI with the Class 3 void fractions given in Table X. The void size distribution so obtained may be expected to be more descriptive of the actual void structure than that obtained by the mercury porosimeter technique if the fraction of the voids which are closed is large or, as appears to be the case, many of the voids are larger than can be resolved by mercury porosimetry. However, the number of fields visually examined in establishing the fractions given in Table XI were not great enough to provide statistically reliable average values.

TABLE XI VOID COUNT AND CLASSIFICATION ACCORDING TO LONGEST DIMENSION

	Fissure Length, mils	800-0-H[a] ∥ No. pores, %	800-0-H[a] ⊥ No. pores, %	1800-0-H[a] ∥ No. pores, %	1800-0-H[a] ⊥ No. pores, %	1800-30-H[a] ∥ No. pores, %	1800-30-H[a] ⊥ No. pores, %	1800-90-H[a] ∥ No. pores, %	1800-90-H[a] ⊥ No. pores, %	1800-0-L[a] ∥ No. pores, %	1800-0-L[a] ⊥ No. pores, %	1800-90-L[a] ∥ No. pores, %	1800-90-L[a] ⊥ No. pores, %
Class 3 Voids	0.6	21, 39.0	30, 51.0	185, 51.0	226, 64.0	120, 42.3	138, 55.0	144, 43.6	265, 66.0	42, 15.0	163, 42.4	56, 25.0	165, 45.0
	1.25	8, 16.0	9, 16.0	66, 17.0	38, 11.0	41, 15.0	33, 14.0	35, 11.0	47, 11.6	107, 38.1	79, 20.6	48, 21.0	90, 24.0
	2.5	6, 12.0	2, 3.4	47, 13.0	20, 5.6	43, 15.0	25, 10.0	50, 15.0	41, 10.2	40, 14.2	59, 15.0	39, 17.0	53, 15.0
	5.0	3, 6.0	7, 12.0	26, 8.5	14, 4.0	21, 7.5	18, 7.0	45, 13.3	17, 4.2	26, 9.3	11, 3.0	22, 9.6	19, 5.0
	7.5	2, 3.6	2, 3.4	17, 4.0	16, 5.0	13, 4.6	8, 3.0	20, 6.3	5, 1.0	15, 5.4	27, 7.0	11, 5.0	11, 3.0
	10.0	5, 9.0	2, 3.4	8, 2.0	1, 0.3	7, 2.5	4, 1.5	9, 2.7	8, 2.0	16, 5.7	11, 3.0	8, 3.5	6, 1.6
Class 2 Voids	12.5	4, 7.0	1, 2.0	5, 1.3	2, 0.6	3, 1.0	2, 0.8	7, 2.1	1, 0.2	15, 5.4	11, 3.0	5, 2.2	10, 2.7
	15.0	2, 3.6	0	2, 0.5	4, 1.3	8, 2.8	2, 0.8	7, 2.1	2, 0.5	4, 1.4	6, 1.5	10, 4.4	5, 1.3
	17.5	1, 1.8	2, 3.4	0	8, 2.2	1, 0.3	3, 1.2	5, 1.5	1, 0.2	5, 1.8	3, 0.8	7, 3.0	3, 0.8
	20.0	1, 2.0	1, 2.0	2, 0.5	3, 0.9	5, 1.7	3, 1.2	1, 0.3	3, 1.0	1, 0.3	3, 0.8	5, 2.2	4, 1.0
	22.5	0	0	2, 0.5	1, 0.3	1, 0.3	1, 0.4	4, 1.2	1, 0.2	2, 0.7	4, 1.0	1, 0.5	2, 0.5
	25.0	0	0	1, 0.3	2, 0.6	6, 2.1	3, 1.2	0	1, 0.3	3, 1.0	2, 0.5	4, 2.0	0
	27.5	0	1, 2.0	0	0	0	3 1.2	1, 0.3	1, 0.3	2, 0.7	3, 0.8	2, 1.0	0
	30.0	0	0	1, 0.3	2, 0.6	5, 1.7	0	0	3, 0.7	1, 0.3	0	4, 2.0	0
	32.5	0	0	0	3, 0.9	1, 0.3	4, 1.5	1, 0.3	1, 0.3	2, 0.7	0	2, 1.0	0
	35.0	0	1, 2.0	0	3, 0.9	4, 1.4	1, 0.4	1, 0.3	2, 0.5	0	0	0	0
	37.5	0	0	1, 0.3	0	0	0	0	1, 0.3	0	0	1, 0.5	0
	40.0	0	0	2, 0.5	4, 1.2	0	0	0	0	0	1, 0.3	1, 0.5	0
	42.5	0	0	0	1, 0.3	0	0	0	1, 0.3	0	0	0	0
	45.0	0	0	0	0	0	0	0	0	0	0	0	0
	47.5	0	0	0	0	0	0	0	0	0	0	0	0
	50.0	0	0	0	1, 0.3	1, 1.5	2, 0.8	0	0	0	0	0	0
	55.0	0	0	1, 0.3	0	0	0	0	0	0	0	0	0
	57.5	0	0	0	0	0	0	0	1, 0.3	0	0	0	0
	62.6	0	0	0	0	0	0	0	0	0	1, 0.3	0	0
	Total	53, 100	58, 100	366, 100	349, 100	280, 100	250, 100	330, 100	402, 100	281, 100	384, 100	226, 100	368, 100

(a) The symbols ∥ and ⊥ are defined in footnote (a) of Table IV

Photomicrographs similar to those used to obtain the results given in Tables IX, X and XI were presented in Figures 35 through 49. These figures present an interesting history of the development of the void structure with heat treatment, and clearly reveal the extremely complex nature of the char structure. The salient factors which limited detailed evaluation of pore size distribution and orientation parameters with the Quantimet were:

(1) The void shapes within the pyrolyzed chars are extremely variable in shape and size.

(2) An optimum contrast between all voids and surrounding matrix proved difficult to obtain.

(3) Meaningful magnifications at which to analyze the void structure require further definition.

(4) The chars are nonhomogeneous over sample dimensions which were required for use in the structure studies, necessitating large numbers of samples in order to obtain representative average quantities.

Experience in this program has convincingly demonstrated that quantitative characterization of the void structure in terms of void size factors, densities of voids, void orientation factors relative to reinforcement cloth, and homogeneity of void groups within the specimen volume is a formidable task. Although the approach applied utilizing the Quantimet Image Analyzer holds promise for detailed, quantitative characterization, additional effort is required to alleviate the difficulties summarized above.

SIGNIFICANCE OF CHARACTERIZATION RESULTS FOR THE CORRELATION OF THERMAL CONDUCTIVITY DATA

It is apparent from the extensive characterization of the thermal conductivity samples conducted on this program that very substantial changes occur in charred phenolic carbon as a function of heat treatment. In a previous correlation of thermal conductivity data[1], the total volume void fraction based on apparent density and helium displacement solid density measurements was used as the major variable accompanying pyrolysis, and all other effects such as graphitization were presented as an empirical function of temperature in the char. The more detailed study of behavior of porosity and other changes such as graphitization as a function of heat treatment level in this program indicate that all of these changes are coupled in a behavior analogous to that of hard carbon. An analogy to hard or glassy carbon behavior has also been noted for unreinforced phenolic chars[30] The new characterization results, as well as consideration of the behavior of measured thermal conductivities relative to the proposed thermal model for phenolic-carbon type materials, suggests the previous correlation[1] based on density determined total void fractions is too great a simplification of the phenomena accompanying ablation, even though the overall behavior of conductivity was correctly described.

The characterization results of this study indicate that all temperature dependent changes in charred material should be lumped together in correlation of the conductivity data. In particular, it has been shown that even with extensive effort, it is very difficult to sufficiently describe porosity for use as a major variable in data correlation. Also, lack of evidence of a significant radiation component of thermal conductivity in the chars removes the need for detailed consideration of porosity to correlate radiation heat transfer. Therefore, correlation of conductivity data on the basis of porosity characteristics, the original reason for extensive porosity characterization, has been abandoned in favor of use of the new theory outlined in Section III and correlation of data using the overall behavior of the major constituent conductivities. Correlation of the conductivity data on this basis is presented in the next section.

Porosity remains a major variable affecting the thermal conductivity, particularly of the continuous phase resin and pyrolysis residue during pyrolysis. One advantage of data correlation in terms of constituent properties is that as further information on the nature of porosity in ablation chars becomes available, it may be possible to reintroduce porosity as a major correlation variable separately for each constituent. In this way, it is much more likely that the variation of the effects of porosity with layup angle in the anisotropic composite will be correctly estimated. It was shown in Section III that anisotropy in the continuous phase due to oriented non-spherical pores can be neglected in charred material. The problem then reduces to that of a correct determination of the behavior of total porosity neglecting pore shape, both in the discontinuous fiber phase and in the continuous resin or pyrolysis residue phase. The current results indicate that even this is a more formidable task than previously expected. However, as will be seen in the next section, the behavior of conductivity during pyrolysis is still not well described, and this may justify further study of the porosity effects which dominate in the pyrolysis stage of ablation.

SECTION VII

PREDICTION AND CORRELATION OF CONSTITUENT THERMAL CONDUCTIVITIES FOR FM-5055A PHENOLIC-CARBON AND RELATED MATERIALS

In this section the FM-5055A phenolic-carbon thermal conductivity data presented in section IV are used to predict the conductivities of the high purity CCA-1 reinforcement and the conductivities of the filled resin and pyrolysis residue. The procedure for obtaining constituent conducrivities from the measured composite conductivities outlined in Section III is employed to obtain constituent conductivity versus temperature for each type of conductivity sample. The constituent conductivities are then correlated versus temperature for use during both heating and cooling in ablation analysis, where constituent conductivities are recombined to obtain composite thermal conductivities using equations 33 through 35 from Section III. Constituent conductivities are also predicted for the virgin and charred ablative composites studied on a previous program[1]; MX-4926 phenolic-carbon, which contains a standard purity form of the CCA-1 reinforcement used in FM-5055A, and FM-5014 phenolic-graphite, which has the same carbon powder filled resin system as FM-5055A.

Additional virgin material constituent conductivities were obtained from composite conductivity data on several laminates with the same reinforcements that were reported in Reference 31 along with the required material descriptions. Reinforcement data was obtained for standard CCA-1 carbon (material i-2 in Reference 31), WCB graphite which is essentially identical to the WCA graphite in FM-5014 (materials a-1, -2 and -3 in Reference 31), and Pluton B-1 (material i-3 in Reference 31), the reinforcement in R-6300 ablative composites discussed separately in Section VIII. The composites selected from Reference 31 all include unfilled SC 1008 phenolic resin, and an independent measurement of the conductivity of the unreinforced cast resin was also reported. It was noted in Section III that any errors in the theoretical procedure are reflected in the predicted continuous phase resin conductivities. Therefore, resin conductivities predicted from the composite conductivities in Reference 31 can be compared to the independently measured resin conductivities to provide a test of the theory relating constituent and composite conductivities. The data from Reference 31 provides a test of the theory over a range of reinforcement volume fraction from 0.41 to 0.64 and for values of the ratio of fiber to resin conductivity from 12 to 86. These data also provide a test of the applicability of the thermal model in Figure 1 to both the eight-harness satin weave (CCA-1) and the square weave (WCB and Pluton B-1).

DETERMINATION OF REINFORCEMENT VOLUME FRACTION

The theory in Section III that relates constituent and composite conductivities requires a knowledge of the volume fraction of the reinforcement, P_f. This is not normally specified for laminated materials and must be obtained indirectly using

the weight fractions of resin and resin filler to obtain the reinforcement weight fraction as the remainder, and using constituent densities to convert weight fractions to volume fractions. The results are shown in Table XII for both the high and low density virgin and charred FM-5055A phenolic carbon materials studied on this program. Similar results for all other composites employed on the constituent property predictions are given in Appendix V.

The total relative volume of virgin material in Table XII is adjusted to give the known values for virgin material density, with the adjustment (increase) in total volume shown as virgin material porosity. The predicted virgin material porosities are reasonable for all materials with the possible exception of the graphite reinforced materials in Appendix V, where predicted porosities are low.

Predicted virgin material porosities obtained in the manner described above can be viewed as a reflection of the accumulated errors in the prediction of constituent volume fractions. Constituent weight fractions are not known to better than 3 percent, and accurate density values are not available for all constituents. The constituent densities selected represent a consensus of available information. For example, 1.19 g/cc was selected as the phenolic resin density on the basis of extensive studies in Reference 32, but a value of 1.21 g/cc was measured on cast phenolic in Reference 31, so this value was used in the prediction of constituent volume fractions for the data from Reference 31. Both of these values probably include some porosity; values up to 1.3 for phenolic resin density have been reported. Density may also vary slightly with phenol content, extent of cure, and other variables. Standard Hitco CCA-1 carbon reinforcement has a density of 1.8 g/cc while the high purity version has a density of 1.85 g/cc. Standard and high purity Pluton B-1 apparently have the same density, 1.86 g/cc. Reported carbon fiber densities have a range of about ±0.05 g/cc. Reported densities for the graphite reinforcements range all the way from 1.42 to 1.7 g/cc but the lower values seem inconsistent with the final composite densities. A value of 1.6 g/cc is used. The carbon powder filler density of 1.9 g/cc is based on the reported values for Sterling R used in MX-4926[1]. Resin char density is estimated at 1.9 g/cc.

Note that in Table XII and in Appendix V where charred material conductivities are analyzed, the shrinkage that accompanies furnace charring is accounted for by adjusting the total volume of the charred composite. This bulk shrinkage does not apply for active ablation chars attached to virgin material. Therefore the reinforcement volume fraction for furnace chars, required for the data reduction, is slightly higher than for virgin material, while active ablators have a constant reinforcement volume fraction.

Table XII shows that while there was a substantially higher porosity in the low density virgin material, as planned, there was also a lower resin content in the fabricated blocks. The result was that when the resin was converted to pyrolysis

TABLE XII THEORETICAL VOLUME FRACTIONS OF CONSTITUENTS IN FM-5055A PHENOLIC-CARBON **

Constituent Description	Wt % of Virgin Mat'l	Density g/cc [1]	Relative * Volume	Volume Percent Virgin	Ablation Char	Furnace Char [5]
91 LD Phenolic Resin	35.4	1.19	29.7	44.7	-	-
	31.9	1.19	26.8	34.8	-	-
USP-6 Carbon Powder	13.0	1.9 [2]	6.8	10.3	10.3	10.6
	13.0	1.9	6.8	8.8	8.8	9.2
CCA-1(1641) Reinforcement	51.6	1.85	27.9	42.0	42.0	43.5
	55.1	1.85	29.8	38.8	38.8	40.2
Resin Char (Carbon)	17.2 [3]	1.9 [2]	9.0	-	13.5	14.0
	16.0	1.9	8.4	-	10.9	11.3
Voids	-	-	2.0 [4]	3.0 [4]	34.2	31.9
	-	-	13.5	17.6	41.5	39.3
Virgin Totals	100.0	1.50	66.4	100.0	-	-
	100.0	1.3	76.9	100.0	-	-
Char Solids Totals	81.8 [3]	1.87	43.7		65.8	68.1
	84.1	1.87	45.0		58.5	60.7
Ablation Char Totals	81.8	1.23	66.4	-	100.0	-
	84.1	1.09	66.9	-	100.0	-
Furnace Char Totals	81.8	1.28	64.1 [5]	-	-	100.0
	84.1	1.13	74.2	-	-	100.0
% Voids in filled resin or Pyrolysis Residue	-	-	-	5.2	59.0	56.4
	-	-	-	28.7	67.8	65.7

* Relative volume = weight %/Density

** Upper and lower values for high and low density virgin material respectively

[1] Resin density from reference 32 .

[2] Estimated

[3] Based on TGA total wt. loss

[4] Virgin porosities selected to give correct virgin density

[5] Adjusted for 3.5% shrinkage during charring

residue having 50% of the resin weight and high density, the porosity of the charred low density composite was much closer to that of charred high density composites than originally expected. The last item in Table XII is the porosity of the continuous phase assuming that it includes all porosity, and the low density furnace char pyrolysis residue is only 17% more porous than that of the high density chars. Reinforcement volume fractions are also much closer than would have been obtained if the resin contents had been the same. These considerations explain the fact that there was little difference between the measured composite conductivities for the two types of chars in Section IV.

It is clear that if the conductivity of a laminate containing high conductivity reinforcement must be closely specified, it would be desirable to develop methods for the direct determination of the reinforcement volume fraction and include this parameter in the composite specification. Fortunately for the prediction and use of constituent properties, if the reinforcement volume fraction is predicted incorrectly, the resulting errors in predicted constituent conductivities, which are in the same direction but greater for the continuous phase constituent, are cancelled when constituent conductivities are recombined. There is a resulting uncertainty and scatter in the predicted constituent conductivities, however, that is in addition to that originating from the composite conductivity data. The additional uncertainty is about ±5% for fiber conductivity and up to ±20% for continuous phase resin or pyrolysis residue conductivity. The nominal ±10% uncertainty on all of the composite conductivity data used in these predictions carries over directly to the predicted constituent properties.

PREDICTION OF CONSTITUENT CONDUCTIVITIES

Smoothed composite conductivity data from 0-degree and 90-degree layup conductivity specimens was used to predict constituent conductivities by the procedure presented in Section III. The smoothed composite conductivity data was obtained from the lines plotted through independent measurements in Section IV for the measurements made on this program and from plotted lines in References 1 and 31 for previously published data. The smoothed conductivities and the corresponding predicted constituent properties are tabulated versus temperature in Appendix IV for FM-5055A and in Appendix V for the other materials. In some cases the smoothed conductivities were extrapolated slightly to obtain constituent conductivities over the largest possible range of temperatures.

One departure from the above procedure was that 90-degree layup composite conductivities were predicted for the 825°F chars using the measured 0-degree and 30-degree layup values in equation (1). Only values up to 900 R, where the data departed from normal temperature dependence, were used to obtain fiber

conductivities for use in correlations. 90-degree layup values were not measured on these chars. Fiber conductivities were estimated directly from the 90-degree layup angle measurements during graphitization (between the Zone II and I conditions) in MX-4926 and FM-5014 using the fact that K_f/K_{90} is nearly constant in the chars. To eliminate the large scatter attributable to partial delaminations in some 0-degree layup chars, 0-degree layup conductivities were predicted from the 90-degree and intermediate layup angle values to obtain a supplementary set of pyrolysis residue conductivity values; fiber conductivity values were not affected. These supplementary values were not tabulated but are shown plotted along with plots of all of the other constituent conductivity values in the following subsections. The plotted constituent properties were used to obtain a correlation versus temperature for both heating and cooling conditions accompanying ablation.

CORRELATION OF CARBON AND GRAPHITE REINFORCEMENT FIBER AXIAL CONDUCTIVITIES

In Section III it was noted that regardless of uncertainties due to the effect of delaminations or possible constituent anisotropy in the charred materials, fiber conductivities would be predicted to within 20% of true values. There would be an additional data scatter of about 10% carried over from the measured composite conductivities. It was also shown that the values obtained in chars are the conductivity of the fiber in the axial direction, which controls the charred composite conductivity at all but the lowest layup angles. Prediction of constituent conductivities for virgin materials required that the constituents be isotropic, a condition that was expected to be met.

Figure 53 shows all of the predicted fiber conductivity values obtained from virgin or partially pyrolyzed material. The correlation equations describing the data except for Pluton B-1, given later, are also plotted. A line through the data is plotted for Pluton B-1. All individual values are within 13% of the correlation curves, which is excellent agreement when it is considered that the predictions are based on data from several sources obtained over a seven year period. There is no trend in the data versus reinforcement volume fraction of the various laminates to indicate a failure of the theory. The reinforcement thermal conductivities appear to be quite reproducible and the values in Figure 53 are stable for both heating and cooling. The carbon fibers show a decreasing positive slope of conductivity versus temperature up to about 1200 R but the graphite fiber data is represented by a straight line above 450 R. No attempt was made to match closely the limited data below 450 R. Values for standard and high purity CCA-1 carbon and for WCA and WCB graphites are indistinguishable. The slopes for both carbon and graphite fibers are positive, indicating that hard carbon temperature dependence is dominant at low temperatures in both types of materials.

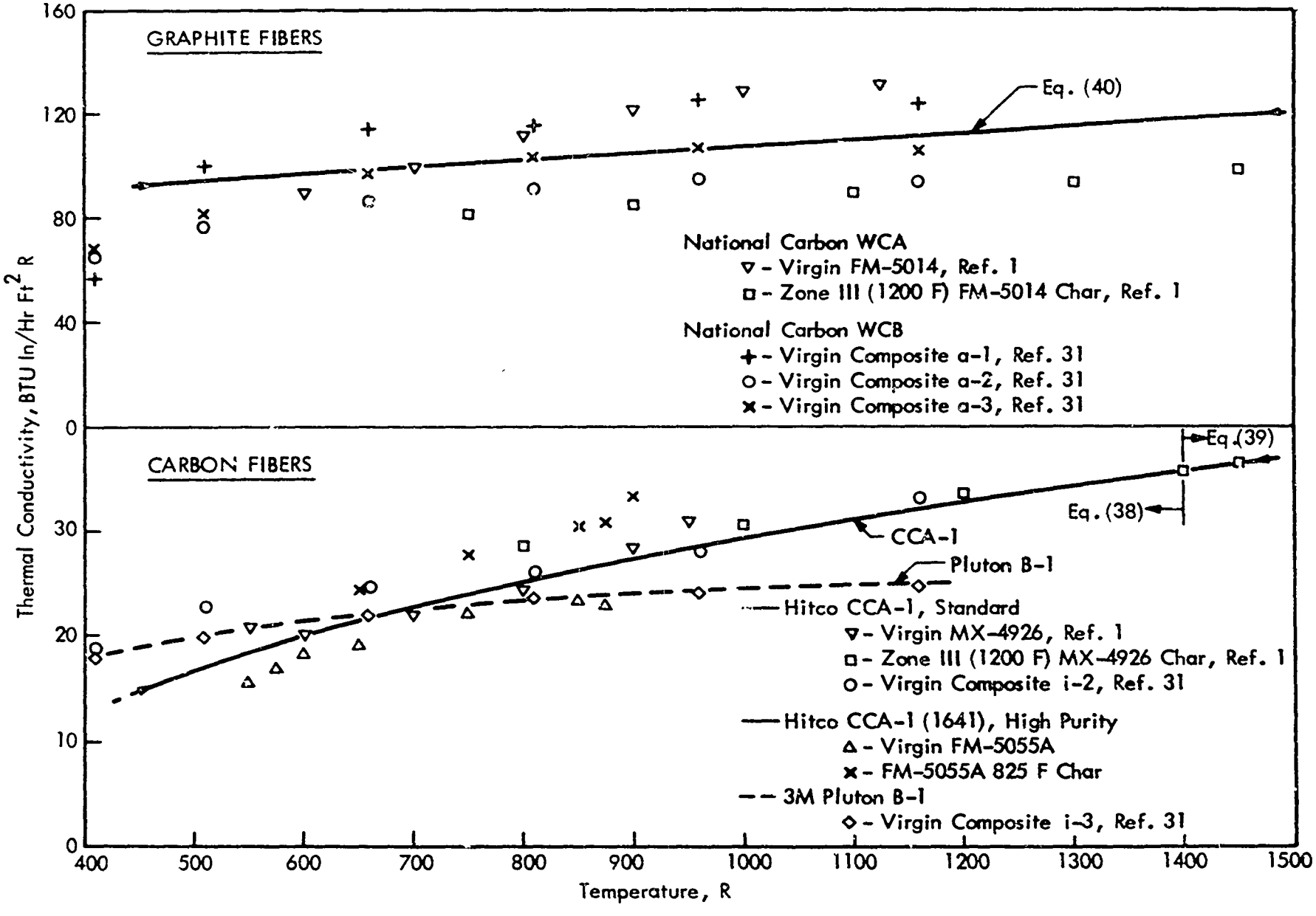

FIGURE 53 REINFORCEMENT FIBER THERMAL CONDUCTIVITIES TO 1500 R

All of the high temperature values for CCA-1 carbon fiber axial conductivity in reinforced phenolic chars are summarized in Figure 54, along with a plot of the correlating equations. Each curve is identified by the 90-degree layup composite specimen which established the value of the fiber conductivity. Figure 54 also illustrates how the correlation was selected considering all of the data and the relationship between artifically charred conductivity specimens and high heating rate ablation chars. Fiber conductivity values predicted from measurements on furnace chars, or chars cooled from the highest heat treatment experienced during conductivity measurements above the initial furnace charring temperature, give the temperature dependence applicable to cooling conditions during ablation. Extrapolation of these curves to the heat treatment temperature gives a value applicable to initial heating at low rates. An additional extrapolation to temperatures predicted in post-ablation chars where the same X-ray diffraction intensities were found in the Reference 1 characterization studies is also shown. These higher temperatures give an initial estimate of the extent of any rate effects during high heating rate ablation. Extrapolation off the end of the curves into a region of unstable material is somewhat uncertain, and the approximate range of this uncertainty, which includes the uncertainty in the X-ray diffraction data, is indicated. The uncertainty is increased by a tendency for the data to curve up versus temperature near the highest previous heat treatment, but this behavior does tend to show that there is a smooth transition into additional heat treatment effects.

The temperature dependence of the fiber conductivity versus heat treatment at low heating rates is given directly by the measurements above initial furnace charring temperatures where graphitization accompanied heating during the conductivity measurements. Values measured versus heat treatment temperature are in good agreement with furnace char values versus ambient temperature extrapolated to the furnace heat treatment temperature. Therefore the correlation applicable to heating periods during ablation, was selected to follow the measured values versus heat treatment temperature with some weighting toward the higher temperatures estimated for the same material characteristics in ablation chars. This gives a correlation that is an average over any graphitization rate effects that may be included in the comparison between furnace and ablation chars. Since any graphitization rate effects will be neglected in ablation analysis for lack of information, the correlation established is appropriate.

High temperature CCA-1 fiber axial conductivities predicted from data on both MX-4926 and FM-5055A are in good agreement. As was the case at low temperatures, the values for standard CCA-1 in MX-4926 and high purity CCA-1 (1641) in FM-5055A are indistinguishable. The slope of fiber conductivity versus ambient temperature below the heat treatment temperatures range from slightly positive to slightly negative versus increasing heat treatment temperature The highly negative slope of the cooling cycle data from specimen 5000-90-L has been ignored in the correlation, since it is not found in any of the other conductivity data or in the diffusivity data (Section IV) obtained specifically to investigate this behavior.

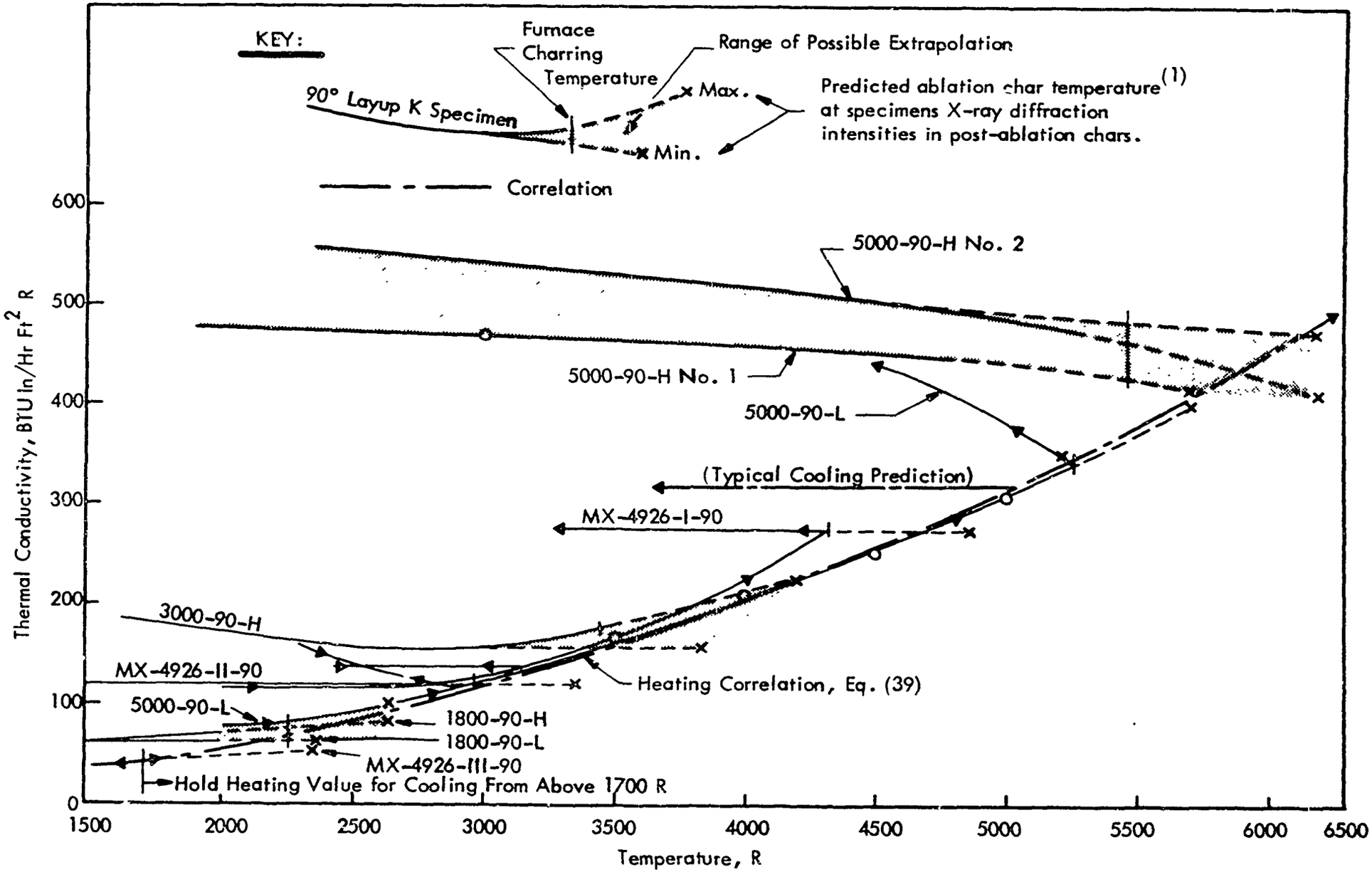

FIGURE 54 CCA -1 CARBON REINFORCEMENT AXIAL THERMAL CONDUCTIVITY ABOVE 1500 R

A simple correlation of the results applicable to cooling conditions during ablation was obtained by holding the highest value of fiber conductivity reached during the permanent changes accompanying heating to any temperature above about 1700 R. This procedure will underpredict the conductivity slightly on return from high temperatures, but is believed to be adequate for ablation analysis and certainly preferred over the past procedure of returning along the heating correlation curve.

The high temperature values of predicted WCA graphite fiber axial conductivity, believed to be applicable to WCB fibers also, are shown in Figure 55. The results were correlated by the same procedures used for CCA-1 carbon fibers in Figure 54. The correlation for heating during ablation is a straight line for all temperatures above 450 R in the virgin material. The carbon fiber correlation shown for comparison in Figure 55 indicates that the carbon fibers are more affected by graphitization accompanying heat treatment than are the graphite fibers. The differences in fiber conductivity at high temperature are greater than are apparent in the corresponding composite conductivities because graphite composites usually have a compensating, higher fiber volume fraction due to lower fiber density and surface area. Graphite fiber conductivity values applicable to cooling are estimated in the same way as for carbon fibers for simplicity. Both types of fiber show a hard carbon-like behavior versus heat treatment and a graphite-like behavior versus ambient temperature below heat treatment temperatures above about 1700 R. This is the same behavior noted in Section IV for the 90-degree layup FM-5055A composite data, which is controlled by the fiber conductivity. The temperature dependence versus heat treatment above 2000 R is practically identical for the CCA-1 fibers (equation 39) and the 90-degree layup FM-5055A composites.

The fiber conductivity correlations have been expressed as equations for substitution in equation (33) which recombines constituent properties for use in ablation computer programs. The plotted correlations are values obtained from the following equations written in terms of the units commonly employed in ablation computer programs: Btu in/sec-ft^{2}R conductivity units and degrees R temperature units.

Hitco CCA-1 and CCA-1(1641):

For 450 R < T < 1400 R; both heating and cooling

$$K_f = 50.3 \times 10^{-4} \ln T - 266 \times 10^{-4} \qquad (38)$$

For T > 1400 R; hold local values for cooling and reheating from T > 1700 R.

$$K_f = 26 \times 10^{-4} (T/1400)^{-5.0} + 146 \times 10^{-4} (T/2000)^{1.95} \qquad (39)$$

National Carbon WCA and WCB:

For T > 450 R; hold local values for cooling and reheating from T > 1700 R.

$$K_f = 216 \times 10^{-4} + 0.08125 \times 10^{-4} T \qquad (40)$$

K = BTU-in/sec-ft^{2}R; T = R

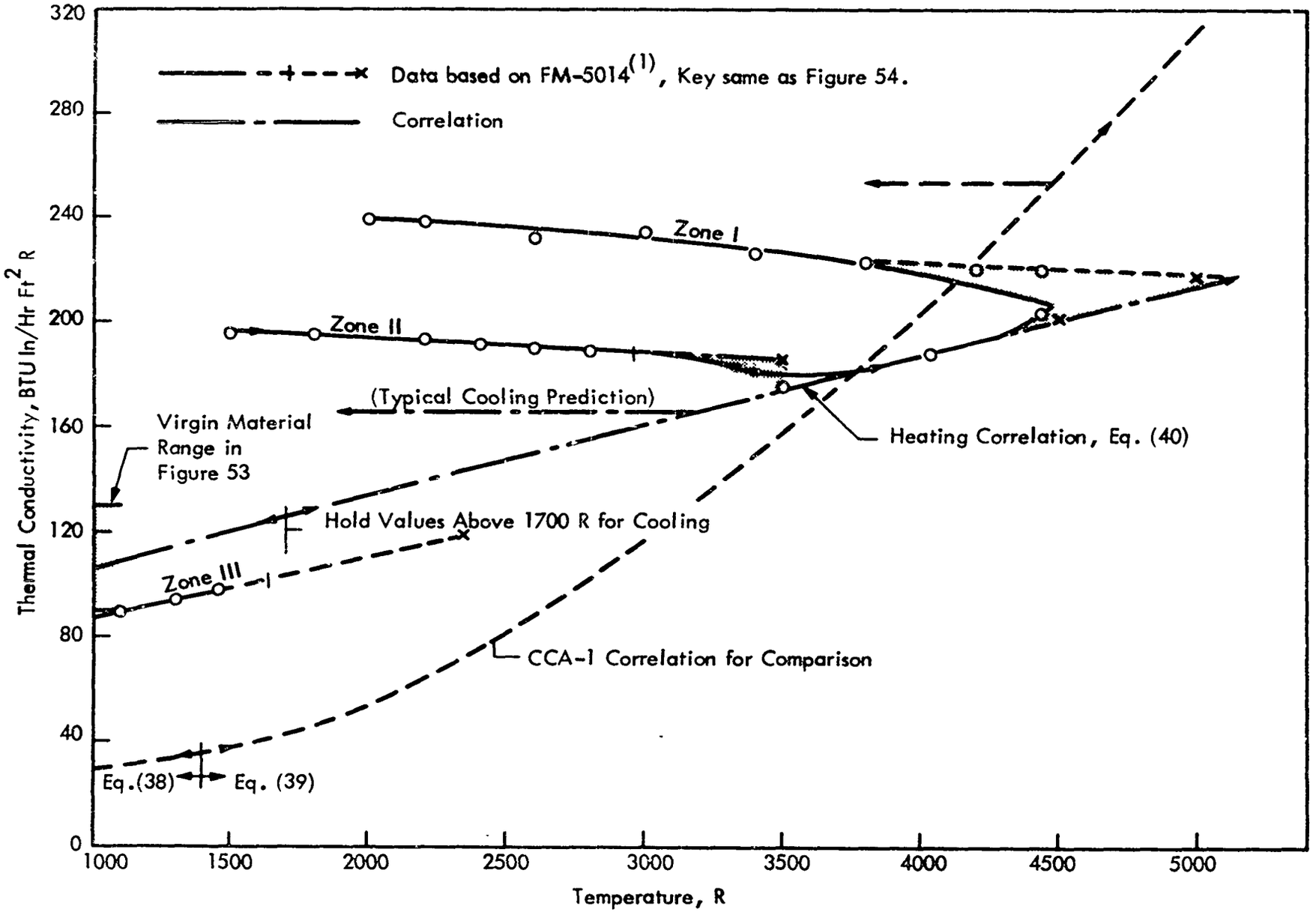

FIGURE 55 WCA (AND WCB) GRAPHITE REINFORCEMENT AXIAL THERMAL CONDUCTIVITY ABOVE 1000 R

CORRELATION OF CARBON POWDER FILLED AND UNFILLED VIRGIN PHENOLIC RESIN CONDUCTIVITIES

The available composite conductivity data provides predictions of the thermal conductivity of carbon powder filled 91-LDand SC 1008 resins plus unfilled SC 1008 resin. As discussed previously, the predicted conductivities for unfilled SC 1008 are compared to independently measured values[31] to provide a test of the theory relating constituent and composite conductivities. All of the virgin resin conductivity values are shown in Figure 56, along with plots of the correlating equations.

All values for carbon filled resins in Figure 56 are within 11% of the correlation line. Good agreements between the two sets of values for filled 91-LD resin indicates success of the theory employed for both eight-harness satin weave CCA-1 carbon reinforced composites (FM-5055A) and square weave WCA graphite reinforced composites (FM-5014). The fact that the same results were obtained for the filled SC 1008 reinforced with CCA-1 was surprising considering the lower carbon filler content in this resin. Values for this combination would be expected to be lower if the conductivities of the two types of carbon powder filler employed were the same. There is no basis for definite conclusions on the relative conductivities of the fillers, however. If the full range of the prepreg specifications for these materials are considered[1], it is possible for both resins to have had the same filler content of about 32% by weight. It appears that the conductivity of both of the carbon-filled resin systems studied, which are used in many other composite systems as well, can be represented by a single line.

Actual filler contents are not reported by prepreg suppliers, and this would appear to be one source of variability in the thermal conductivities of composites. The resin content is the constituent fraction specified, so if filler content varies the difference is made up by fiber content, and the overall composite crossply conductivity remains in a relatively narrow range, independent of the amount of carbon powder filler. Conductivity in the ply direction would vary in proportion to the actual fiber content. This is an additional arguement for direct specification of fiber content (and filler content) if conductivity is to be closely controlled in the composite.

All of the data for unfilled SC 1008 resin in Figure 56 is represented by a straight line above 450 R that very closely follows the independently measured values on an unreinforced resin casting. This is a significant substantiation of the theory, since predictions from composites representing the full range of reinforcement volume fractions and conductivities are included, and all uncertainties in the theoretical procedure are reflected in the continuous constituent predictions. The requirement that both the resin and fiber be isotropic for accurate constituent property predictions on virgin materials appears to have been met. All of the data that is more

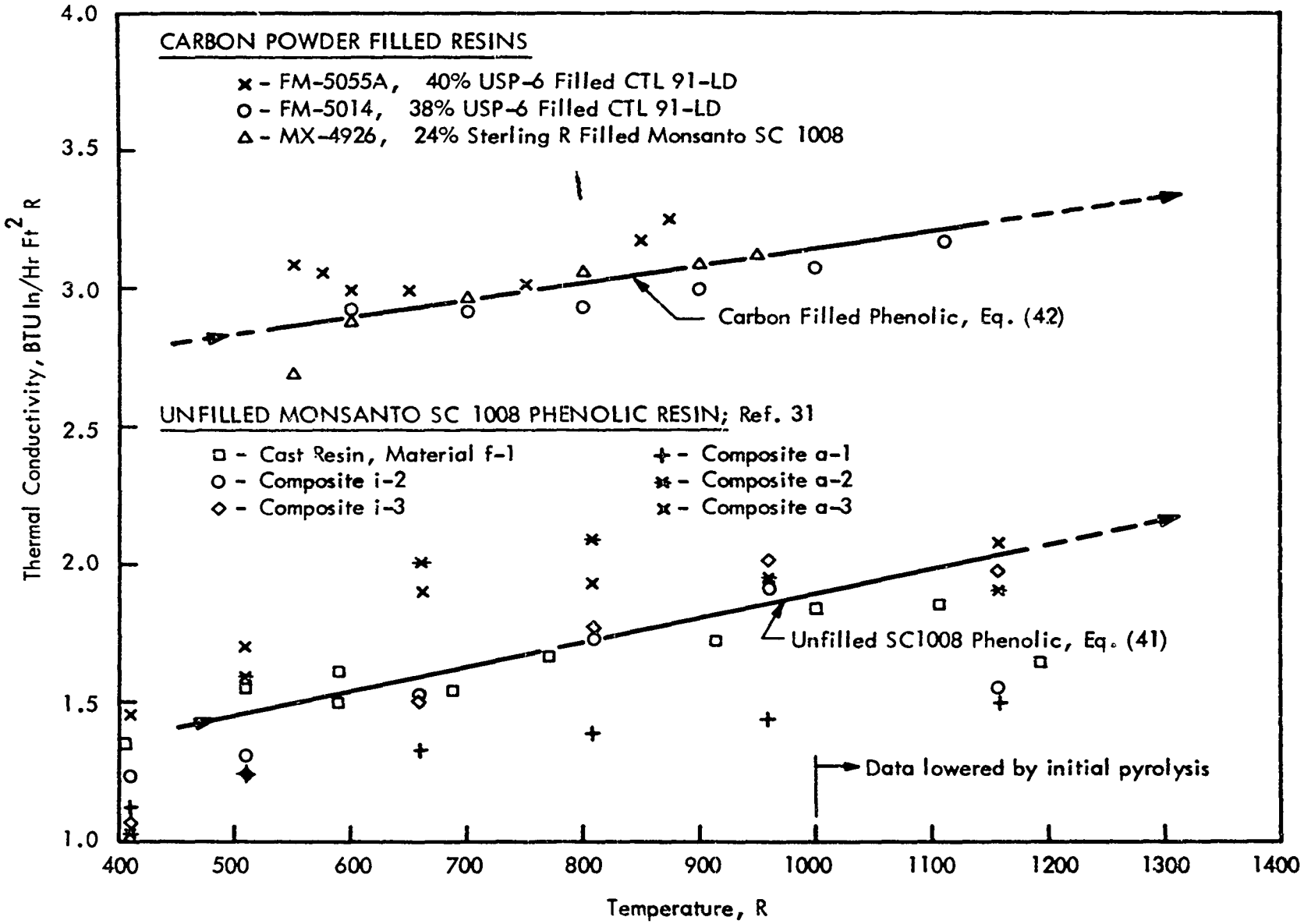

FIGURE 56 UNFILLED AND CARBON POWDER FILLED VIRGIN PHENOLIC RESIN THERMAL CONDUCTIVITIES

than 11% from the correlation line between 450 R and 1000 R is from composites incorporating the square weave graphite reinforcement. These data are up to ±25% from the correlation line. Values above 1000 R are not included in the correlation, since they have been lowered by varying amounts due to initial pyrolysis and the accompanying development of increased porosity. The results may signal the breakdown of the thermal model as applied to the square weave when the ratio of fiber to resin conductivity is high. The fact that good agreement was obtained for the filled resin-graphite composite (FM-5014) and for the square weave Pluton B-1 carbon-SC 1008 composite (material i-3), except for one point, suggests that uncertainties are limited to square weave composites with very high fiber to resin conductivity ratios. The data for materials a-1 through a-3 are for increasing resin content, and there is no constant trend versus this parameter. The values from material a-1 are low, possibly due to high porosity in this high reinforcement content composite.

The correlation for the virgin phenolic resins, filled and unfilled, are written below for the units used in ablation computer programs; K = BTU-in/sec-ft^{2}R, T = R.

Unfilled Monsanto SC 1008 resin:

For T > 450 R; both heating and cooling

$$K_v = 2.8 \times 10^{-4} + 0.00245 \times 10^{-4} T \qquad (41)$$

Carbon powder filled CTL 91-LD and SC 1008 resins:

For T > 450 R; both heating and cooling

$$K_v = 6.99 \times 10^{-4} + 0.00174 \times 10^{-4} T \qquad (42)$$

Equations (41) and (42) assume that the virgin resin conductivity can be extrapolated to very high temperatures where pyrolysis would begin at high heating rates. This behavior is assumed to be independent of the behavior of the reinforcement conductivity. The independent behavior of fiber and resin conductivities is supported by the fact that the same fiber conductivities are predicted from both virgin and low temperature charred composites that are not graphitized. The assumption that the resin conductivity can be extrapolated indefinately is consistent with current practice in ablation analysis, but has not been independently substantiated.

CORRELATION OF CARBON POWDER FILLED PHENOLIC RESIN PYROLYSIS RESIDUE CONDUCTIVITIES

The data for charred FM-5055A composites of this study, and for charred MX-4926 and FM-5044 studied previously, provide predicted pyrolysis residue conductivities for the same filled resin systems evaluated above in the virgin state. Pyrolysis residue conductivity below the maximum temperatures experienced by the composite conductivity samples represents the temperature dependence of conductivity for

cooling conditions during ablation. Correlation of values at the heat treatment temperatures gives the temperature dependence for ablation heating, including the effect of progressive graphitization, in the same manner employed in the correlation of fiber conductivities. Pyrolysis residue conductivities act in the same manner as 0-degree layup composite conductivities discussed in Section IV, since the pyrolysis residue controls composite conductivity in this direction.

Predicted pyrolysis residue conductivities are plotted in Figure 57 along with the correlating relationships. Data curves are identified by the 0-degree layup composite specimen which established the value of the pyrolysis residue conductivity. There is a very wide scatter in the results, which is a reflection of the uncertainties introduced by 0-degree layup conductivity specimen delaminations and possible constituent anisotropy, as predicted from theoretical considerations in Section III.

To reduce the effect of these uncertainties, and to insure a data correlation applicable to layup angles above 20-degrees that are of the most practical interest, adjusted 0-degree layup angle composite conductivities were obtained from the available data at 90-degrees and intermediate layup angles using equation (1) solved for K_0. This was done to replace the data from specimens 3000-0-H and MX-4926-I-0, the only 0-degree layup composite data at high temperatures that did not yield intermediate layup angle conductivities within 20% of measured values when used in equation (1). The adjusted values of K_0 were used to obtain new values of pyrolysis residue conductivity for use in obtaining a correlation. These values, also plotted in Figure 57, are identified by the intermediate layup angle data used to estimate K_0. Since the intermediate and 90-degree layup angle conductivity specimens were relatively free of delaminations, the adjusted pyrolysis residue conductivities show less scatter and are believed to better reflect the actual behavior of the constituent conductivity as well as the actual behavior of the composites during ablation at all but the lowest layup angles. It is clear that the conductivity for chars in heat shields having layup angles lower than 20-degrees remains uncertain by at least a factor of ±2. This uncertainty was also reflected in the comparative diffusivity measurements presented in Section IV.

The correlation for heating conditions in Figure 57 indicates that the permanent changes due to graphitization in the pyrolysis residue become significant at higher temperatures and develop a greater temperature dependence than was the case for the reinforcements. This same relative behavior versus heat treatment was noted for the 0-degree and 90-degree composite conductivities in Section . The temperature dependence of the pyrolysis residue conductivity during heating at high temperatures is generally greater than noted for the 0-degree layup composites, however, which is a reflection of the procedure used to lessen the influence of delaminations on the predicted pyrolysis residue conductivities.

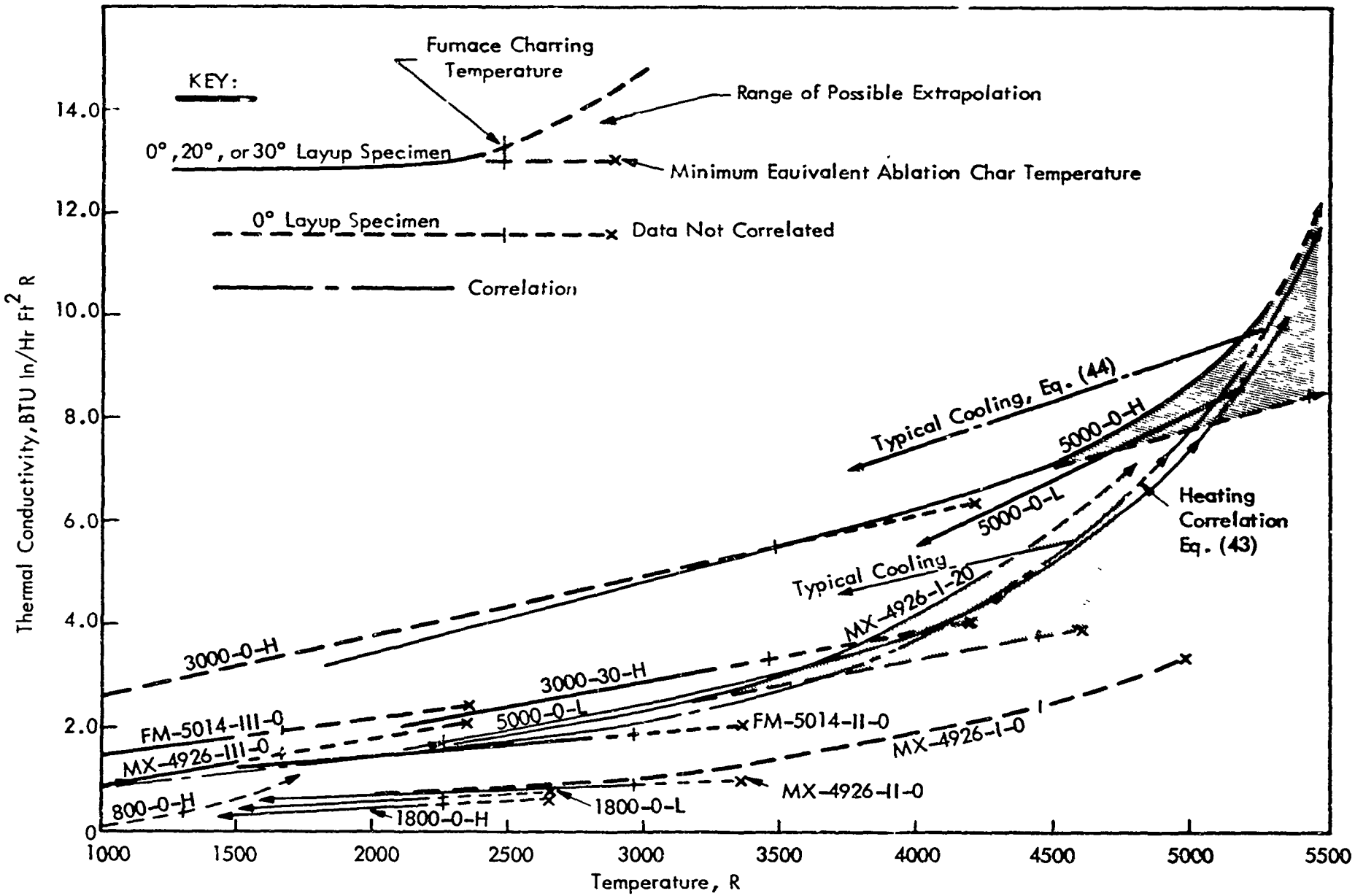

FIGURE 57 CARBON POWDER FILLED PHENOLIC PYROLYSIS RESIDUE THERMAL CONDUCTIVITY

The correlation for cooling conditions is a very approximate, simple representation of the behavior of the pyrolysis residue conductivity below maximum heat treat temperatures. The correlation assumes that local cooling values return on a straight line from the highest value reached during heating to an intercept of 0.288 BTU-in/hr-ft^{2}R at 0-degrees R. This simple correlation gives an approximate fit to all of the cooling data, properly reflects the increasing slope of the cooling data versus heat treatment, and is believed adequate for ablation analysis while offering an improvement over returning along the heating curve from high temperatures. Additional, more consistent data, would be required to justify any more complicated correlation of pyrolysis residue conductivities applicable to cooling. The temperature dependence of pyrolysis residue conductivity remains analogous to that of hard or glasslike carbon to over 5000 R. The very steep rise in values versus heat treatment near 5000 R may indicate that conversion to graphite-like behavior would occur at higher temperatures.

The correlation relationships for pyrolysis residue thermal conductivity are written below for the units used in ablation computer programs; K = BTU-in/sec-ft^{2}R, T = R.

Carbon filled phenolic pyrolysis residue:

For $450 < T < 2800$ R, heating and cooling; and $2800 \leq T$, heating only.

$$K_{pr} = 0.8 \times 10^{-4} + 0.0015 \times 10^{-4} T + 10^{-4} (T/3250)^6 \qquad (43)$$

For $T > 450$ R, cooling and reheating only.

$$K_{pr} = 0.8 \times 10^{-4} + \left[\frac{\text{Eqn (43) value} - 0.8}{\text{Maximum T in Eqn (43)}}\right] T \times 10^{-4} \qquad (44)$$

Note that below 2800 R, the results from equations (43) and (44) are the same (the last term in equation (43) is negligible), so equation (44) need not be employed below 2800 R if desired. In addition, for ablative composites having layup angles at or near 90-degrees, the simple procedure of holding the heating value for cooling from any heat treatment temperature above 2800 R would overpredict K_{pr} for cooling, but would partially compensate for neglecting the negative slopes of high temperature heat-treated fiber conductivity and increase the accuracy of the correlation.

THERMAL CONDUCTIVITY IN THE PYROLYSIS ZONE

While correlated fiber conductivities were affected only by graphitization, the continuous phase conductivity is obviously affected by both pyrolysis and graphitization. Only graphitization is accounted for in the temperature dependence of the correlations. In Section III it was proposed that pyrolysis be accounted for by the accepted procedure of using the pyrolysis fraction weighed average of extra-

polated virgin resin conductivity and pyrolysis residue conductivity at any temperature in the pyrolysis zone (equations 34 and 35). This procedure may overpredict the conductivity of the continuous phase during the first half of the pyrolysis. The predicted pyrolysis residue conductivities for 825°F chars are very low relative to the correlation, while the conductivities of 1200°F Zone III chars that are about 90% pyrolyzed are higher and the conductivities of 1800°F and 2500°F (Zone II) chars are low relative to the correlation. These values were not greatly affected by specimen delaminations. It is possible that the effective continuous phase conductivity decreases markedly due to porosity generation in the early stages of pyrolysis, then increases as the proportion of carbon becomes very high in the latter stages of pyrolysis, followed by a decrease related to loss of thermal bonding to the fibers. However, the 825°F pyrolysis residues have a relatively high temperature dependence and the composite data suggests that this increases near the point where pyrolysis would continue. If the thermally active material during pyrolysis has higher conductivity, the suggested procedure for the high temperature pyrolysis zone during ablation may be a better approximation than a more complicated procedure that attempts to follow the variations listed above. Also, the high temperature pyrolysis zones accompanying active ablation require a relatively severe extrapolation of both the resin and partially pyrolyzed residue data obtainable only at low temperatures. Low temperature fully pyrolyzed material would be encountered only during cooling, so precise correlation of these data is not too important for most applications. However it is interesting to note that if the correlation had been obtained using only values for FM-5055A, the portion below 3500 R would have indicated much lower values. It is not known if some of this data scatter reflects real differences in the material.

Considering all of the uncertainties, pyrolysis zone conductivities can be no better than gross estimates, and additional information would be required to justify departure from the suggested procedure that at least is known to yield successful ablation predictions. Ablation prediction results using this pyrolysis fraction weighted averaging procedure applied to continuous phase constituent conductivities as suggested, and to composite conductivities as commonly done previously, are demonstrated in Section IX.

ACCURACY OF COMPOSITE CONDUCTIVITIES OBTAINED FROM CORRELATED CONSTITUENT CONDUCTIVITIES

There are three major factors to be considered in estimating the accuracy of composite conductivities obtained from predicted constituent conductivities for use in ablation analysis. The first is the accuracy of the basic theory relating composite and constituent conductivities for the principle layup angles, 0- and 90-degrees. The second factor is the accuracy of equation (1) for the effect of layup angle, into which the theory relating composite and constituent conductivities is substituted for predicting the thermal conductivity at all intermediate layup angles. The third factor is whether or not the results based on furnace chars actually represent active ablation chars. These factors are discussed in order below.

The closed form solutions developed in Section III relating constituent and composite conductivities for use in ablation predictions represent the exact theory to better than 1% for the full range of composites considered in this study. The theory as applied to predict constituent conductivities from composite conductivities is correct within experimental error on the basis of the comparison between predicted and independently measured values for unfilled phenolic resin. All large uncertainties in the predicted constituent conductivities are confined to the pyrolysis residue, but any systematic error is cancelled out when constituent conductivities are recombined to obtain charred composite conductivities. Therefore, the theoretical approach employed results in no greater error in final constituent conductivities than that associated with the experimental measurements. The fact that many sources of data may be combined for correlating constituent properties increases the statistical confidence in the results, demonstrates their applicability to many composite systems, and demonstrates that the effect of composite variables on thermal conductivity can be predicted.

The use of equation (1) to generalize the results for all layup angles can be substantiated using the measured composite conductivities, since measurements on 30° layup angle material were included for this purpose. Equation (1) was shown in a previous study[1] to predict intermediate layup angle conductivities to within about 25% of measured values. Results using the FM-5055A data of this study are similar. Average prediction errors over the measurement temperature range when K_{30} is calculated from corresponding measured values of K_0 and K_{90} are +6% for virgin material, -5% for 1800°F chars, +25% for 3000°F chars, and +12% for 5000°F chars. An alternate relationship that is sometimes used, where $\sin^2 \theta$ is replaced by $\sin \theta$ [1], gives prediction errors larger than +70% for all 30-degree layup chars. Equation (1) is an adequate expression for the influence of layup angle. Errors larger than 20% are found only in high temperature chars where the measured values of K_0 are highly variable due to the influence of delaminations. The procedure used to adjusted K_0 and predicted pyrolysis residue conductivity showed that K_0 values giving the largest errors from equation (1) were out of line with the other available data. These values could then be eliminated from the correlation, which insures that measured composite conductivities for all layup angles greater than 20-degrees will be accurately reflected by the correlated results. Predicted K_0 values will not reproduce the measured data that appeared to be out of line. The variability in K_0 is real, and the range of the results suggest that actual K_0 values could differ from predicted values by a factor of ±2, the apparent range between sound and extensively delaminated material.

The final correlation, using equations (33) through (35) and the expressions for correlated constituent properties, represents all virgin material data to within about 12% and all char data for layup angles above 20-degrees to within about 25%. A large uncertainty in the thermal conductivity of very low layup angle chars remains. The results for chars correspond to material including some partial delaminations. In general, the correlation will give results that are as good as the

thermal conductivity measurements and the ability to establish the reinforcement volume fraction and interlaminar integrity in the ablative composites.

The applicability of the results to actual ablation chars must be estimated on the basis of the comparative characteristics of low heating rate furnace chars used for conductivity measurements and high heating rate ablation chars. All of the charred conductivity specimens used for the data correlations have known relationships to post-test ablation chars characterized in detail in Reference 1. This relationship was illustrated in the correlation of constituent properties and the correlations were established to represent both furnace and ablation chars. None of the char characteristics data, nor the rapid heating rate electrical resistivity results, indicate that the material graphitization at high temperatures is significantly rate dependent. If this major possible material variable is negligable, the correlation should be applicable to active ablation chars. Comparative diffusivity measurements on furnace chars and ablation chars support this conclusion. Conductivity in the high temperature pyrolysis zone accompanying active ablation is obtained by accepted extrapolation procedures that have historically yielded accurate ablation predictions, but have not been otherwise substantiated.

The remaining questions regarding the applicability of the conductivity results to active ablation are the possibility of heretofore undetected rate dependent graphitization and a significant radiation component accompanying very high heating rate ablation with associated steep temperature gradients. The available data does not indicate the presence of a significant radiation component, which would be expected to be apparent in the predicted conductivities of the porous pyrolysis residue. Any minor radiation component is included in the predicted pyrolysis residue conductivity. Lackof a large radiation component is consistent with the results on porous phenolic-nylon chars in Reference (30). Delineation of both graphitization rate effects and radiation component effects requires specialized investigations at very high temperatures. If both effects occur, they would be self-compensating, so their combined influence on high temperature char thermal conductivity is not necessarily large.

SECTION VIII

PRELIMINARY CHAR CHARACTERIZATION AND THERMAL CONDUCTIVITY CORRELATION FOR R-6300 PHENOLIC CARBON

Nominal R-6300 phenolic-carbon composites[35] consist of 35% by weight unfilled Monsanto SC 1008 phenolic resin and 3M Pluton B-1 square weave carbon cloth. The designation R-6300 HP is used for the high purity composite containing high purity Pluton B1-HP. Charred material from exposure to a simulated reentry ablation environment was to be characterized versus depth by techniques developed previously[1] to insure that any material changes associated with a severe environment were taken into account in correlating thermal conductivity data. Available thermal conductivity data on R-6300 was then to be correlated by the techniques developed on this program. These efforts were only partially successful due to lack of intact chars exposed to a severe environment and the limited availability of accurate thermal conductivity data on fully described specimens as required for correlation purposes.

R-6300 CHAR CHARACTERIZATION

Charred wedge models from Aerospace Corporation tests in the Cornell Wave Superheater were provided by the Air Force for characterization on this program. Details of the model construction and ablation tests are given in Reference 34. The wedge test surfaces were slightly curved to give an increasing angle of attack downstream from the leading edge. This curvature was varied among models to obtain specified surface pressure gradients in the Superheater expanding free jet tests. Four half-models consisting of 3M Pluton B1-HP cloth laminated with 44% SC 1008 resin and two half-models consisting of unidirectional Pluton PX-505 yarn bonded with Ironside L8 phenolic resin for comparison were provided. The half-models had been cut off at the model streamwise centerline by Aerospace Corporation, providing a charred section of each model about 0.7 inches wide by 1.7 inches long.

Table XIII summarizes the information provided with the Cornell Wave Superheater models by Aerospace Corporation together with centerline char depth estimates by direct visual measurements, estimates of the degree of surface spalling, and surface X-ray diffraction measurements. The chars were too thin to obtain good resolution of char depth by X-ray transmission measurements, but X-ray tests did indicate that the models were otherwise uniform. The yarn and cloth warp were oriented at approximately a 35 to 40 degree layup angle, slanting downstream, to the slightly curved final surfaces of the primary test area in the first inch from the model leading edge.

Only the Pluton PX-505/L8 phenolic model shaped to give a zero pressure gradient, Model #6, shows what might be considered a meaningful improvement in erosion resistance relative to the other models provided. This model showed the least

TABLE XIII CORNELL WAVE SUPERHEATER MODEL DATA

		PLUTON REINFORCED PHENOLIC MATERIALS						
		BI-HP Cloth/SC1008 Resin				PX-505 Yarn /L8 Resin		
Run No/ Model No.		280/5	286/3	287/4	278/1	281/6*	288/8	270* [1]
Pressure Gradient-ATM/in.		0	-10	-10	-20	0	-10	-20
Pressure-ATM		31	33	33	29	31	32	29
Enthalpy-BTU/lb		2250	2280	2280	2270	2190	2220	2230
Test Time-Sec		1.58 [2]	1.62	1.68	1.77	1.77	1.71	1.73
0.5 inches from L.E.	℄ Recession-in	0.210	0.252	0.260	0.248	0.194	0.290	0.260
	℄ Char-mils	10-20	10-15	15	10	35-40	15-20	--
	Max Temp-°R	5,900	5,930	6,000	5,880	6,130	5,600	6,050
1.0 inches from L.E.	℄ Recession-in	0.252	0.256	0.236	0.218	0.190	0.295	0.216
	℄ Char-Mils	10-20	10-15	15	10	15-20	10-15	--
	Max. Temp.-°R	5,820	5,700	5,680	5,720	5,750	5,620	5,600
1 4 inches from L.E.	℄ Recession-in	0.253	0.212	0.182	0.158	0.186	0.173	0.10
	℄ Char-Mils	15	15	15	10-15	15-20	10	--
Maximum Recession-in		0.254	0.265	0.263	0.255	0.197	0.303	0.265
Maximum-in from L.E.		1.2	0.6	0.6	0.6	0 8	0.8	0.6
Amt. Spalls to Virgin Mat.		moder.	exten.	exten.	exten.	few	none	--
X-ray Diff:char/virgin-count/sec.		114/80	108	76	68	94/120	68	--

* Leading edge gouged out.

[1] This model not provided for characterization.

[2] Maximum erosion occurred in the center area.

erosion, the highest surface temperature, and the greatest char depth, all of which are consistent with lower mechanical erosion. The significance of these results is uncertain, however, due to the lack of a clear trend as the pressure gradient is increased.

PX-505 yarn reinforced material showed substantially less spalling in the char than the B1-HP cloth reinforced material. This appears to be related to the orientation of the B1-HP cloth reinforcement, which was laid up with the fill yarns parallel to the surface so that spalled areas appear to coincide with the removal of these yarns. The data does seem to indicate that the B1-HP cloth reinforcement spalling tendency is reduced for the zero pressure gradient case. The slightly greater char depth is consistant with this, since pressure gradient shear is roughly proportional to char depth. The zero pressure gradient models of both materials show more uniform erosion versus distance from the leading edge, indicating that this may be a desirable model design for material evaluation. The extensive spalling on the B1-HP models and the high erosion of the PX-505 models exposed with a pressure gradient left only the zero pressure gradient models for further characterization.

The X-ray diffraction results on the last line of Table XIII showed a surprisingly low level of graphitization at the char surfaces considering the measured surface temperatures, which were within a few hundred degrees of the peak temperatures listed throughout the indicated test times. Since surface roughness causes scattering that lowers the results, char values are even below the virgin values for the PX-505 yarn reinforced material. The B1-HP cloth reinforced material shows some evidence of graphitization. The values are assumed to be much lower than would have been obtained if there had not been extensive spallation of the high temperature surface material. Because of these irregularities there should be no attempt to assign any trends to these data. It is known from RESEP TASK II[36] results that furnace chars of the B1-HP reinforced material show significant graphitization and that graphitization is visible under polarized light in chars from RESEP ablation tests. Polarized light photomicrographs of both zero pressure gradient chars from 50X to 1000X were made for comparison. Evaluation of these photomicrographs indicated the presence of graphitization near the surface in the B1-HP char and confirmed the lack of graphitization in the PX-505 char. Graphitization appeared greatest on pore surfaces parallel to the surface in the B1-HP char, and lack of pores parallel to the surface in the PX-505 char may be related to the apparent lack of graphitization in this material. Unlike char from RESEP TASK II ablation tests, the graphitization in B1-HP Superheater char is not widely distributed. In addition, graphitization at the surface in the B1-HP char is lacking, possibly due to mechanical removal, which would tend to give low values of graphitization by X-ray diffraction. Photomicrographs indicated that unpyrolyzed resin existed up to the char surface in both materials, so the pyrolysis zone extended up to 6000 R under the severe test conditions[34]; heat flux = 6000 BTU/ft^{2}sec and shear stress = 300 lb/ft^2.

the zero pressure gradient chars were sectioned by progressive removal of layers a few mils thick. These sections were measured and weighed after the removal of each slice to provide data for calculation of the density gradient through the chars. There was insufficient material for any other measurements such as porosity determinations. Bulk densities at the char surface were very low, from 0.2 to 0.4 g/cc, which reflects the extensive mechanical loss of material in the char sections. Density gradient results were very erratic and not considered meaningful due to this spalling behavior. Virgin density was 1.45 g/cc in the B1-HP material and 1.35 g/cc in the PX-505 material.

The characterization results suggest the possibility that graphitization does not occur in the high temperature pyrolysis zone during very rapid ablation. If this is true, the effect would be to suppress the increases in fiber and pyrolysis residue conductivities related to graphitization until pyrolysis was nearly complete. An alternate possibility is that there was insufficient time for graphitization to occur during the short test exposures. However, this is contrary to experience with other ablation chars[1], and the visible graphitization appeared to be of normal thickness and structure but located only where the resin was depleted. This was particularly true for deposites on fibers. If graphitization requires completion of pyrolysis, this is an additional arguement for specific studies on the behavior of properties in the pyrolysis zone.

R-6300 THERMAL CONDUCTIVITY

The only available thermal conductivity data on fully described specimens similar to nominal R-6300[35] was the virgin material data for material i-3 in Reference 31. Constituent conductivities predicted from this data are tabulated in Appendix V and were included on Figures 53 and 56 in Section VII. The standard Pluton B-1 reinforcement had a conductivity similar to CCA-1 but slightly lower at high temperatures consistent with the lower carbon content of Pluton B-1 fibers. Predicted SC 1008 resin conductivities agreed well with the other results in Figure 56. Virgin and charred (to 2000°F) composite conductivities for 20-, 70-, and 90-degree layup materials described as nominal R-6300 are summarized in Reference (35). Data on 18-degree[37] rosette layup virgin and 4000°F charred composites having a 48% resin content (material STP-PBHP-RA04) are given in Reference (36). These data are not reproduced here since they were not successfully correlated, as discussed below.

When virgin material data in Reference (35) was used to predict constituent properties, fiber conductivities up to 30% lower than predicted for material i-3 were obtained. The 90-degree layup results are believed to have been obtained by standard guarded hot plate techniques, which would be expected to be about 20% low for the level of conductivity measured[31]. If this assumed 20% error is removed, virgin constituent conductivities predicted from the Reference (35) data are in excellent agreement with those predicted from material i-3 data. However, if the resin content was actually higher than 35%, which is often the case,

this could also bring the data in Reference 35 into agreement. The necessary material and conductivity test descriptions to resolve this uncertainty were not available to the authors. The char conductivity data in Reference 35 did not appear suitable for correlation. 70-degree layup material had lower conductivity than 20-degree layup material, for example, and specific specimen descriptions required to establish the reinforcement volume fractions were not available.

Trial predictions were made to determine if the phenolic resin and CCA-1 fiber conductivities could be used to estimate R-6300 composite conductivities, since CCA-1 and Pluton B-1 had similar constituent conductivities in Figure 53. Results for 20-degree layup angle virgin material were in good agreement with the data in Reference 35. Results at 70- or 90-degree layup angles were high, reflecting the discrepancies discussed above. Predictions for 18-degree layup angle virgin material having a 40 percent volume fraction of reinforcement were 12% low at 100°F to 25% low at 300°F compared to the data on similar material containing Pluton B1-HP in Reference 36. Predictions for 4000°F chars using CCA-1 fiber and carbon powder filled pyrolysis residue conductivities were a factor of 3.4 lower than the measured values on 18 degree layup chars, material STP-PBHP-RA04 in Reference 36.

The above results indicate that the thermal conductivity for R-6300 composites is not well established, especially on chars. A new series of accurate thermal conductivity measurements similar to those obtained for FM-5055A on this program is required. There is some evidence that new measurements should consider the effect of the laminate processing method on thermal conductivity of materials using square weave reinforcements such as Pluton B-1. Photographs[37] of the 18-degree rosette layup material for which high conductivity values were reported in Reference 36 indicated that the cloth was not flattened in the manner of press laminated material, and that weave crossovers occurred with almost 90-degree bends in the fibers. This would tend to raise composite conductivity at low layup angles and lower it at high layup angles. The theory relating composite and constituent properties would have to be modified, possibly by an empirical processing parameter, to take this into account.

SECTION IX

EXAMPLE REENTRY ABLATION PREDICTIONS USING CORRELATED FM-5055A THERMAL CONDUCTIVITY

Application of the new thermal conductivity correlation was demonstrated by in-depth ablation response predictions for a 20-degree layup FM-5055A phenolic-carbon heat shield on a high performance ballistic reentry vehicle. Computer predictions were performed using both suggested procedures for inputing correlated thermal conductivities. One prediction was carried out by writing equations (33) through (35) into the program and using the correlated constituent conductivities, equations (38), (39), (42), (43), and (44) and the related logic, to generate the composite thermal conductivity during the run. A second prediction was done using 20-degree layup composite virgin and mature char conductivities obtained from these equations and fitted with cubic equations for input to the program.

Thermal conductivity was added to the printout of internal conditions versus depth in the ablator to provide a direct comparison of the two procedures. No cooling was encountered in the example predictions, so the differences in thermal conductivity for heating and cooling conditions were not investigated. The remaining difference between the two procedures is in the pyrolysis zone, where the pyrolysis fraction weighted average of the virgin resin and pyrolysis residue constituent conductivities, or of the virgin and fully-charred composite conductivities is used. There is also a small error in the cubic equation representation of composite conductivities that gives slightly high values for virgin or fully charred material.

The ablation analysis was performed using the Boeing Convective Heating and Ablation Program (CHAP) described in Reference 33. The inputs to the program were vehicle configuration, reentry trajectory, and material properties for 20-degree layup FM-5055A phenolic-carbon. Table XIV gives all of the composite properties used, including the expressions for composite thermal conductivity. The analysis was performed for a location 3 feet aft on a sharp conical vehicle of 9 degrees half angle, assuming turbulent flow. A constant ballistic coefficient of 3000 lb/ft^2 was used for reentry from 300,000 feet altitude at an initial velocity of 24,900 ft/sec and an entry angle of -19 degrees.

Table XV gives the details of the material response after initiation of ablation. Inspection of this table shows that the calculations using the two procedures for incorporating thermal conductivity gave nearly identical overall ablation performance, with all individual material consumption responses less than 1 percent different except for some values of sublimation and erosion rates that reflect a few degrees difference in surface temperature. There is a tendency for the pyrolysis zone to be thicker for the most severe ablation conditions using the constituent conductivities.

TABLE XIV PROPERTIES OF U.S. POLYMERIC FM-5055A, 20° LAYUP

Virgin Plastic	
Density, lbm/ft^3	93.5
Emissivity	0.9
Conductivity, BTU in/ft^{2}sec°R	(a)
Specific Heat, BTU/lbm°R	(b)
Heat of Decomposition, BTU/lbm	1000.
First Term Decomposition Constants	
Collision Frequency, 1/sec	7.9×10^{-4}
Activation Temperature, °R	3880.
Reaction Order	2.0
Second Term Decomposition Constants	
Collision Frequency, 1/sec	2.6×10^{4}
Activation Temperature, °R	27000.
Reaction Order	2.0

Gas	
Ablation Gas Specific Heat, BTU/lbm°R	(e)
Char Combustion Products	
Specific Heat, BTU/lbm°R	(f)

Char	
Density, lbm/ft^3	76.5
Emissivity	0.9
Conductivity, BTU in/ft^{2}sec°R	(c)
Specific Heat, BTU/lbm°R	(d)
Arrhenius Decomposition Constants	
Effective Collision Frequency, lbm/ft^{2}sec	286
Activation Temperature, °R	20100.
Reaction Order	0.5
Char Combustion Parameter	0.75
Heat of Combustion, BTU/lbm	4300.
Sublimation Constants	
Effective Collision Frequency, lbm/ft^{2}sec	1.6×10^{7}
Activation Temperature, °R	1.11×10^{5}
Reaction Order	0.67
Heat of Sublimation, BTU/lbm	25300.

Erosion Constants	
Constant A, lbm/ft^{2}sec/lbf/in^2	8.0×10^{4}
Constant B, °R	77000.

(a) $k_v = 12.5 \times 10^{-4} + 7.5 \times 10^{-7}\ T$

(b) $c_{p_v} = 0.60 \times 10^{-3}\ T - 0.246 \times 10^{-6}\ T^2 + 0.035 \times 10^{-9}\ T^3$

(c) $k_c = 8.0 \times 10^{-4} + 5.5 \times 10^{-14}\ T^3$

(d) $c_{p_c} = 0.094 + 0.271 \times 10^{-3}\ T - 0.059 \times 10^{-6}\ T^2 + 4.42 \times 10^{-12}\ T^3$

(e) $c_{p_g} = 0.60 + 4.0 \times 10^{-8}\ T^2$

(f) $c_{p_{c,g}} = 0.235 + 2.5 \times 10^{-5}\ T$

ALL TEMPERATURES ARE IN °R.

TABLE XV PREDICTED BALLISTIC REENTRY ABLATION OF FM-5055A [1]

(20° Layup, 3 ft. Aft on a Sharp 9° Half-Angle Cone, $W/C_DA = 3000$ lb/ft^2)

Altitude, 10^3 ft.	Time From 3×10^5 ft, Seconds	Blocking Function	Gas Trans. Rate lb x 10^2 / ft^2 sec	Char Surface Recession Rates: Combust. lb x 10^2 / ft^2 sec	Sublim. lb x 10^3 / ft^2 sec	Erosion lb x 10 / ft^2 sec	Total in x 10^2 / sec	Virgin Plastic Thick. Inches	Char Thick. Inches	Pyrolysis Zone Thick. Inches	Total Thick. Inches
153.2	18	.92342	.0336	.0267	.0000	6.7×10^{-15}	.0032	.5988	.0001	.0012	.6000
		.92219	.0342	.0270	.0000	7.2×10^{-15}	.0032	.5988	.0001	.0012	.6000
136.8	20	.61302	.4328	.0904	.0000	1.3×10^{-11}	.0121	.5797	.0001	.0201	.5998
		.61281	.4336	.0899	.0000	1.2×10^{-11}	.0120	.5797	.0001	.0201	.5998
120.4	22	.50304	1.028	.1633	.0000	1.9×10^{-8}	.0243	.5642	.0003	.0350	.5995
		.50066	1.041	.1621	.0000	1.5×10^{-8}	.0241	.5642	.0003	.0350	.5995
104.1	24	.54294	1.453	.3461	.0000	4.5×10^{-5}	.0531	.5444	.0140	.0403	.5987
		.54056	1.472	.3445	.0000	4.0×10^{-5}	.0528	.5443	.0139	.0405	.5987
87.8	26	.61663	1.724	.7487	.0107	.01148	.1331	.5242	.0371	.0357	.5970
		.61837	1.711	.7509	.0113	.01191	.1340	.5240	.0371	.0359	.5970
71.8	28	.70351	2.029	1.598	.9273	.4467	.9591	.4991	.0548	.0352	.5891
		.70414	2.025	1.600	.9140	.4359	.9422	.4990	.0546	.0354	.5891
56.3	30	.73403	2.893	2.937	4.454	2.1505	3.901	.4690	.0467	.0260	.5417
		.73644	2.916	2.948	4.296	2.0676	3.761	.4648	.0475	.0301	.5425
41.8	32	.69347	5.726	4.477	3.923	2.5508	4.747	.4140	.0240	.0159	.4539
		.69551	5.599	4.490	3.998	2.5381	4.718	.4100	.0247	.0199	.4546
28.9	34	.72491	6.333	6.195	3.010	2.3101	4.630	.3244	.0179	.0155	.3577
		.72666	6.330	6.208	3.066	2.3332	4.667	.3242	.0183	.0156	.3581
18.0	36	.78062	4.938	7.259	1.604	1.2961	3.192	.2440	.0202	.0157	.2799
		.78130	4.936	7.265	1.603	1.3011	3.199	.2439	.0204	.0158	.2801
9.1	38	.83620	3.159	7.585	.4429	.4230	1.862	.1783	.0264	.0262	.2309
		.83616	3.162	7.583	.4481	.4245	1.864	.1782	.0263	.0264	.2309
2.0	40	.86978	2.097	7.304	.0464	.06612	1.254	.1386	.0320	.0306	.2013
		.86995	2.092	7.305	.0468	.06655	1.255	.1384	.0319	.0308	.2012

[1] Upper value of pair gives results from inputing composite conductivities and lower value gives results from inputing constituent conductivities and the new theory.

Figure 58 illustrates the behavior of thermal conductivity and density in the pyrolysis zone for the extremes of the ablation conditions. Values at 24 seconds in the reentry are for the thickest, lowest temperature fully developed pyrolysis zone. Values at 34 seconds are for the thinnest, highest temperature pyrolysis zone. For both conditions, use of pyrolysis fraction weighted continuous constituent conductivities predicted a higher thermal conductivity in the pyrolysis zone. The density gradient results in Figure 58 are not significantly affected. The other property that is estimated by using the pyrolysis fraction weighted average of virgin and char values is specific heat. Specific heat values were also printed out, and no differences greater than 0.2 percent were found.

The ablation prediction results show that both suggested methods for inputing the correlated thermal conductivity results from this program can be used with equal confidence. Differences in predicted pyrolysis zone thermal conductivities are probably not significant, particularly since the values obtained by either procedure are estimates.

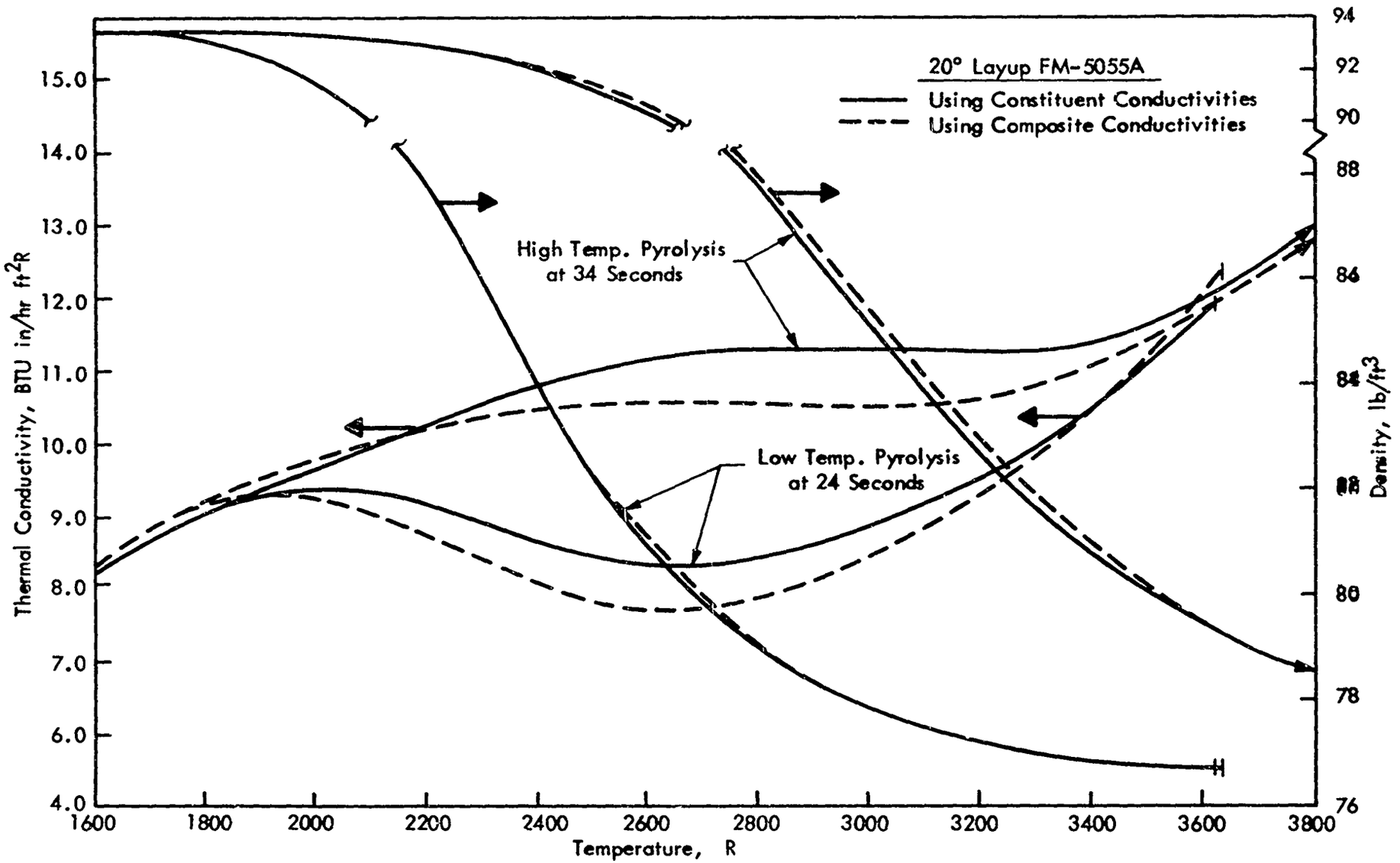

FIGURE 58 REENTRY PYROLYSIS ZONE CONDUCTIVITY AND DENSITY

SECTION X

CONCLUSIONS

A correlation that will predict the thermal conductivity to over 5000°F during ablation of several phenolic-carbon and phenolic-graphite composites has been obtained. Thermal conductivity is provided for both heating and cooling conditions at all stages of ablation in heat shields of normal reinforcement content constructed at any layup angle. Results are obtained within the accuracy of measured values and the reproducibility of thermal conductivity specimens; ±12% for virgin material and ±25% for chars having layup angles greater than 20 degrees. Large uncertainties in the thermal conductivity of very low layup angle charred composites remain, due primarily to the variable influence of delaminations.

New theory that relates composite and constituent (fiber and matrix) thermal conductivities for all layup angles has been successfully demonstrated and applied to correlate thermal conductivity for use in ablation analysis. Using the new theory, constituent conductivities were predicted from all of the composite conductivity data obtained in this contract, and from accurate literature data, with good agreement. Constituent properties were successfully correlated for both heating and cooling conditions during ablation, and expressed as equations for substitution into a simplified expression for their recombination into correlated composite conductivities used in ablation analysis. It was shown that the same overall results were obtained in predicted ballistic reentry ablation on phenolic-carbon when the correlation relationships were incorporated directly into the computer program or when they were used to predict composite virgin material and char conductivities for substitution into ablation computer programs as currently written.

The conductivity correlation procedure based on constituent conductivities should enable prediction of the conductivity of any composite for which the constituent conductivities have been established. Constituent properties for Hitco CCA-1 carbon cloth (from FM-5055A and MX-4926 data), National Carbon WCA and WCB graphite cloth (FM-5014 and others), carbon powder filled CTL 91-LD (FM-5055A and FM-5014), and Monsanto SC 1008 (MX-4926) phenolic resins and their pyrolysis residues, and unfilled SC 1008 resin (R-6300 and others) have been established. Attempts to establish the behavior of 3M Pluton B-1 carbon cloth used in R-6300 composites were unsuccessful due to lack of suitable literature data. The fiber and matrix conductivities were shown to behave independently during pyrolysis. Conductivity in the pyrolysis zone can be estimated from the pyrolysis fraction weighed average of either the resin and pyrolysis residue or the virgin and charred composite conductivities. The first procedure predicts somewhat higher composite conductivities in the pyrolysis zone.

The thermal conductivity of all carbon or graphite cloth reinforced phenolic ablators increases versus layup angle and reinforcement volume fraction, is reduced by pyrolysis generated porosity, and increases in the mature char versus temperature and the degree of graphitization. The temperature dependence of both thermal and electrical conductivity in composites was similar to that of hard or glass-like carbon. Both the correlated conductivity and the characteristics of pyrolysis residue showed hard carbon behavior at all temperatures. The reinforcements became graphite-like at high temperatures. Extensive graphitization of CCA-1 carbon fiber raised its conductivity above that of WCA or WCB graphite fibers at high temperatures. No evidence of rate controlled graphitization was obtained, and no significant radiation component of thermal conductivity was detectable in the data.

SECTION XI

RECOMMENDATIONS

1. Thermal conductivity measurements on refractory fiber reinforced ablators should be conducted at temperatures above 5500 R to verify conductivity predictions at the highest possible temperatures.

2. Thermal conductivity should be obtained and correlated for virgin and charred ablative composites representing all of the most common constituents, including silica, to provide thermal conductivity for ablation predictions.

3. Thermal conductivity values for both the fiber and resin constituents of ablators should be measured independently to further validate the theory developed herein.

4. The behavior of the fiber and resin conductivity versus temperature and graphitization during pyrolysis should be studied to reduce the extrapolation required for the ablation pyrolysis zone.

5. The influence of the method of construction of composite heat shields on thermal conductivity should be determined, particularly when square weave reinforcements are used.

6. Special studies should be conducted to determine if rate controlled graphitization exists to influence the thermal conductivity in chars exposed to high ablation heating rates.

7. High temperature char thermal conductivity and optical property measurements should be conducted to verify the apparent absence of a significant radiation component of thermal conductivity.

8. The influence of delaminations on thermal conductivity should be studied by controlled experiments to establish the significance of this phenomena quantitatively.

9. Procedures for the direct determination of the cloth reinforcement volume fraction in ablative composites should be developed and used for composite specifications when it is desired to control the thermal conductivity.

APPENDIX I

HARD, OR GLASSLIKE CARBONS

The so-called hard (glasslike) carbons normally do not easily graphitize even at extremely high temperatures. The changes in density, void size distribution, and electrical and thermal properties as a function of heat treatment temperature are described over temperature intervals roughly equivalent to those defined by the four high density char states of this program.

The following summary of hard carbon properties is based upon work reported in the following references: Pinnick[16], Castle[17], Warren[18], Loch and Austin[10], Winslow, et al[19], Jamieson and Mrozowski[20], Davidson and Lostz[12], Yamada, et al[13], Yamada[9], and Kipling, et al[11].

This discussion emphasizes observed property variations with heat treatment found for those carbons which appear to behave similarly to the carbon formed through pyrolysis of the non-melting type phenolic used in the FM-5055A chars. Starting materials for the hard carbons treated in the above references include non-melting resins, cellulose, and various combinations of fillers and resins. The general criteria for the starting material is a high degree of cross linking which stabilizes the solid phase and inhibits molecular mobility and ordering during heat treatment.

The initial decomposition of the starting material involving the greatest weight loss, shrinkage, and evolution of gaseous products becomes essentially complete between 800°F and 1100°F. In this temperature range, the electrical resistivity can be very high, on the order of 10^6 ohm-cm, and the thermal conductivity is lower than that for the virgin material.

Major changes in structure and properties take place between 800°F and 1900°F. The bulk density increases due to continued shrinkage of the material without loss in mass. The content of disorganized carbon decreases by about a factor of 2. Relatively larger, aromatic ring structures condense and stack to form crystallites similar in structure to graphite but much smaller in size. The crystallites, being separated by a disorganized carbon phase, lack the rotational orientation between planes that is found in graphites; the average lattice spacing is large by comparison. The helium density maximizes within this temperature region at a value close to theoretical crystallite density. The total void fraction, B.E.T. surface area, void size, water adsorption and helium permeability also reach maxima. Over this temperature region, the electrical resistivity decreases by perhaps 8 to 10 orders of magnitude and exhibits the dependence on ambient temperature characteristic of intrinsic semiconductors. The thermal conductivity increases by perhaps a factor of 3.

Above 1900°F, crystallite size continues to increase, and average lattice spacing decreases. The bulk density remains constant while the helium density decreases toward the value of the bulk density, reaching a constant value between 3000°F and 3600°F. Between these temperatures the micron size voids are filled by local expansion and sintering of crystallite domains, and the material becomes impermeable. Differences between theoretical and helium densities are attributed to the existence of isolated, intercrystalline voids in the size range 2 to 50 angstroms.

Above 3600°F, lattice spacing and crystallite size do not change further with temperature. In general, glasslike carbons are isotropic and do not readily graphitize, even at temperatures up to 5000°F, although changes toward graphitic structure may be induced by the catalytic action of certain additives. Nakamura[21] has reported that the presence of artifical and natural graphite within glassy carbon enhanced the tendency for the carbon to graphitize while not affecting the isotropy of the carbon; Yokokowa, et al[6, 7], have reported on the ability of metallic compound additives to effect a further degree of graphitization than would normally occur in certain hard carbons at temperatures as low as 2700°F; Noda, et al[5] have demonstrated the catalytic effects of oxygen in accelerating the graphitization process in a calcined petroleum coke. The crystallite size and lattice spacing the hard carbons are reported to be sensitive to heating rate and time at temperature.

APPENDIX II

STRUCTURAL INTEGRITY OF THERMAL CONDUCTIVITY SPECIMENS

The overall structural integrity of the thermal conductivity specimens varied. In the worst cases, structural flaws appeared to be extensive enough to influence results of the thermal conductivity measurements. Delamination of the reinforcement cloth layers was the most troublesome flaw; the 0-degree layup angle specimens were most subject to delamination, the 30-degree specimens were less inclined to delaminate, and the 90-degree specimens were highly resistant to delamination. It is difficult to judge the integrity of the interlaminar bonds in the 0-degree specimens as they existed during the conductivity measurements, but generally these specimens were quite fragile and came apart during post-test sectioning prior to characterization. This is illustrated in the 6X macrographs in the text. The possibility that interlaminar bond integrity may have varied between the various 0-degree specimens introduced an unpredictable influence on the thermal conductivity results.

Although delaminations also occurred to some extent in the 30-degree layup angle specimeans, they were not as extensive as in the 0-degree layup angle specimens, and, due to the layup angle, should have influenced the conductivity measurements to a much lesser degree.

Another aspect of overall structural integrity involves the homogeneity of the specimens produced from the low density virgin precusor. These specimens tended to be of poorer quality with respect to homogeneity of void structure throughout the specimen volume than did the chars produced from the high density virgin precursor. In the case of Specimen 1800-90-L, a density variation of about 6 percent across the one inch diameter central core (the measurement volume in the thermal conductivity measurements) was observed by Boeing in X-ray transmission density surveys. A density gradient would upset the normal heat flow pattern through the specimen in the thermal conductivity measurement, an effect which, in this case, was verified by measured variations in heat fluxes in the measurement and guard sections of the heat-flow meter.

A final source of difficulty involves precise definition of the reinforcement cloth layup angle. Since conductivity is sensitive to layup angle, uncertainty in the value of the layup angles limits the certainty with which correlation of the data with layup angle can be performed. It also makes comparison of the data for chars of nominally identical layup angles, but different heat treatments, subject to greater uncertainty. Several of the 0-degree layup angle chars exhibited rather ill-defined layup angles because of variation of apparent angle within the individual specimen.

APPENDIX III

THERMAL CONDUCTIVITY DATA FOR FM-5055A PHENOLIC-CARBON

In the data lists to follow, the first number of doublet is the measured conductivity in BTU in/hr ft^2 R, the second is the temperature of the data point in degrees, R. The data are identified by specimen number and are given in the order in which they were obtained.

V-O-H[a]	V-30-H[a]	V-90-H[a]	800-0-H[a]	800-30-H[a]
5.7, 566	5.9, 566	7.3, 568	0.25, 639	2.8, 954
6.0, 636	6.2, 631	8.0, 636	0.38, 919	1.8, 616
6.1, 744	6.4, 744	8.4, 748	0.25, 759	2.3, 947
5.5, 564	5.6, 562	9.2, 875	0.64, 1124	1.9, 789
6.5, 866	6.9, 862	8.8, 794	0.31, 863	3.6, 1052
6.3, 773	6.4, 683	6.8, 571	0.41, 1000	1.7, 705
		8.8, 875	0.24, 708	
		7.9, 690	0.49, 1075	

1800-0-H[a]	1800-30-H[a]	1800-90-H[a]
0.39, 782	2.7, 678	14.8, 1499
0.60, 1131	4.1, 1018	16.0, 1849
0.99, 1538	4.9, 1543	15.7, 1995
1.21, 1848	4.9, 1801	16.4, 2117
0.64, 1293[d]	5.2, 2049	11.4, 861
1.03, 1680[d]	3.8, 1297	13.0, 1223
0.37, 790[d]	3.0, 991	14.5, 1813
		10.6, 847

(Continued)

3000-0-H[b]	3000-30-H[b]	3000-90-H[b]
8.1, 1059[c]	13.5, 1343[c]	48.6, 1160[c]
9.7, 1693[c]	13.8, 1739[c]	46.9, 1428[c]
11.3, 2186[c]	16.3, 2245	44.8, 1847[c]
11.9, 2182	16.6, 2654	44.6, 2287
12.4, 2598[c]	18.1, 3178	41.7, 2197
12.9, 2591	16.4, 2944	41.3, 2665
12.3, 2908		42.3, 2902
14.8, 3354		46.0, 3383
		42.3, 2598

5000-0-H[b]	5000-30-H[b]	5000-90-H No. 1[b]	5000-90-H No. 2[b]
10.6, 1991	42.4, 1794	108.9, 2598	132.8, 2582
11.3, 2323	38.8, 2120	97.0, 3057	135.0, 3158
13.2, 2668	37.1, 2647	100.7, 3539	119.4, 3865
15.2, 3149	36.5, 3097	110.4, 4123	112.3, 4778
12.3, 2495	36.3, 3524	118.3, 4672	117.8, 5134
15.5, 3268	37.8, 2375	109.3, 1950	127.6, 3563
18.4, 3932	36.0, 3201	122.6, 2527	126.3, 4083
22.0, 4637	37.4, 4128	100.8, 2918	126.0, 5327
26.2, 5087	39.3, 4852	112.8, 2695	129.7, 3613
	41.9, 5098	105.7, 1525[a]	
		107.2, 1768[a]	
		102.0, 1929[a]	

(Continued)

1800-0-L[a]	1800-90-L[a]	5000-0-L[b]	5000-90-L[b]
0.38, 747	13.2, 1064	3.5, 2070	17.2, 1897
0.64, 1034	13.3, 1368	3.9, 2107	18.0, 2036
1.08, 1431	13.3, 1821	4.7, 2333	19.1, 2267
0.89, 1259	12.9, 1596	5.8, 2584	21.5, 2468
1.47, 1854	13.7, 2044	7.1, 2843	27.3, 2897
0.45, 843	13.7, 951	4.8, 2290	34.7, 2294
		5.7, 2656	29.4, 2670
		7.8, 3476	37.0, 3448
		11.7, 4288	52.7, 4288
		22.0, 5199	81.5, 5235
		18.1, 4481	89.7, 4940
		11.9, 3532	101.8, 4342
		7.8, 2447	

(a) Low Temperature Apparatus
(b) High Temperature Apparatus
(c) Thermocouples used for temperature measurements in high temperature apparatus.
(d) Specimen cut to about 1/2 original thickness.

APPENDIX IV

SMOOTHED CONDUCTIVITY DATA AND PREDICTED CONSTITUENT PROPERTIES FOR FM-5055A PHENOLIC-CARBON

In these data lists all conductivity values are given in BTU in/hr ft^2 R. Measured conductivities are identified by specimen number and predicted conductivities by the designations used in the report.

Temp. R	Virgin Material Conductivities					800°F Char Conductivities				
	Measured			Predicted		Measured		Predicted		
	V-O-H	V-30-H	V-90-H	K_f	K_v	800-0-H	800-30-H	K_{90}	K_f	K_{pr}
550	5.7	5.8	7.0	15.5	3.08					
575	5.8	5.8	7.3	16.9	3.05					
600	5.8	5.9	7.6	18.2	2.95					
650	6.0	6.1	8.0	19.0	2.95	0.23	1.6	5.7	24.4	0.071
750	6.2	6.4	8.6	22.0	3.01	0.25	1.8	6.5	27.6	0.077
850	6.5	6.8	9.0	23.1	3.17	0.30	2.0	7.1	30.4	0.092
875	6.6	6.8	9.0	22.8	3.25	0.32	2.1	7.4	30.7	0.098
900						0.34	2.2	7.8	33.3	0.104
1000						0.44	2.9	10.3	40.4	0.132
1050						0.50	3.4	12.1	50.7	0.153

Temp. R	1800°F High Density Char Conductivity					Low Density Char Conductivity			
	Measured			Predicted		Measured		Predicted	
	1800-0-H	1800-30-H	1800-90-H	K_f	K_{pr}	1800-0-L	1800-90-L	K_f	K_{pr}
700						0.31		62.0	0.112
800	0.38	3.3	10.7	48.5	0.123				
1000	0.49	3.6	11.7	52.3	0.159	0.61	13.0	63.5	0.223
1200	0.62	3.9	12.7	55.3	0.205				
1400	0.78	4.2	13.7	61.7	0.254				
1600	0.96	4.6	14.6	64.8	0.313	1.21	13.2	61.1	0.447
1800	1.16	4.9	15.4	67.7	0.379				
1900	1.25	5.0	15.7	68.7	0.409	1.51	13.2	61.4	0.561
2000	1.36	5.2	16.0	70.4	0.446		13.3	61.6	0.598

3000°F Char Conductivities

Temp. R	Measured 3000-0-H	3000-30-H	3000-90-H	Predicted K_f	K_{pr}
1000	7.7		49.3	206.4	2.59
1200	8.4	13.1	48.3		
1400	9.0	13.6	47.2	192.2	3.06
1600	9.6	14.1	46.1		
1800	10.2	14.6	45.1	179.2	3.52
2000	10.8	15.0	44.0		
2200	11.4	15.5	43.0	166.7	3.98
2400	12.0	16.0	42.3		
2600	12.6	16.5	41.7	157.0	4.48
2800	13.2	17.0	41.8	156.0	4.72
3000	13.8	17.5	42.4	156.4	4.97
3200	14.4	18.0	43.6	161.0	5.20
3400	15.0	18.5	46.4	171.5	5.39

5000°F High Density Char Conductivities

Temp. R	Measured 5000-0-H	5000-30-H	5000-90-H #1	5000-90-H #2	Predicted Using K_{90} No. 1 K_f	K_{pr}	Using K_{90} No. 2 K_f	K_{pr}
1900	9.9	40.8	110	-	479	3.25		
2200	11.2	38.7	110		474	3.69		
2600	12.8	37.1	110	128	471	4.24	552	4.22
3000	14.6	36.2	110	126	468	4.87	540	4.83
3400	16.2	36.1	110	125	461	5.43	527	5.40
3800	17.8	36.6	110	124	458	5.99	521	5.96
4200	19.6	37.3	110	123	452	6.64	511	6.59
4600	21.7	38.4	110	121	447	7.41	497	7.36
4800	23.2	39.3	110	120	442	7.96	488	7.90
5000	25.2	40.8		120			482	8.63
5100	26.3	41.9		120			481	9.04
5200	27.7	43.3		119			472	9.58
5300	29.3	44.6		119			468	10.18

Temp. R	5000°F Low Density Char Conductivities[a]			
	Measured		Predicted	
	5000-0-L[a]	5000-90-L[a]	K_f	K_{pr}
2000	3.5	17.6	76.8	1.34
2100	3.8	18.1	77.6	1.46
2200	4.4	19.1	82.0	1.70
2500	5.4	21.3	89.9	2.10
2800	6.1	25.3	107.6	2.36
2200	4.4	36.2	168	1.64
2500	5.4	31.5	141	2.04
2800	6.1	28.0	121	2.34
3000	6.6	29.0	125	2.54
3500	8.0	37.9	165	3.07
4000	9.9	47.2	206	3.79
4500	13.3	57.5	246	5.13
5000	19.0	72.2	303	7.43
5200	22.0	80.0	334	8.62
5200	22.0	82.5	344	8.60
5000	20.9	88.1	377	8.07
4600	18.6	96.9	427	7.08
4400	17.3	101	451	6.54
4300	16.6	102	459	6.26
3400	11.2			4.13
2400	7.7			2.82

(a) Smoothed data from the initial heating cycle, intermediate cooling cycle, and the cooling cycle subsequent to the highest char heat treatment experienced during measurement.

APPENDIX V

CONSTITUENT VOLUME FRACTIONS AND THERMAL CONDUCTIVITIES PREDICTED FROM LITERATURE DATA

TABLE V-1 THEORETICAL VOLUME FRACTIONS OF CONSTITUENTS IN MX-4926 PHENOLIC-CARBON **

Constituent Description	Wt % of Virgin Mat'l	Density g/cc [1]	Relative * Volume	Volume Percent Virgin	Ablation Char	Furnace Char [5]
SC1008 Phenolic Resin	33.3	1.19	28.0	40.9	-	-
Sterling R Carbon Powder	8.0	1.9	4.2	6.1	6.1	6.6
CCA-1 Reinforcement	58.7	1.80 [2]	32.6	47.6	47.6	51.0
Resin Char	15.8 [3]	1.9 [2]	8.3	-	12.1	13.0
Voids	0	0	3.7 [4]	5.4 [4]	34.2	29.4
Virgin Totals	100.0	1.46	68.5	100.0	-	-
Char Solids Totals	82.5 [3]	1.83	45.1	-	65.8	70.6
Ablation Char Totals	82.5	1.2	68.5	-	100.0	-
Furnace Char Totals	82.5	1.29	63.9 [5]	-	-	100.0
% Voids in fitted resin or Pyrolysis Residue	-	-	-	10.3	65.2	60.0

** All notes except [5] same as table XII . Material described in Reference 1.

[5] Adjusted for 6.6% shrinkage during charring.

TABLE V-2 PREDICTED CONSTITUENT CONDUCTIVITIES IN MX-4926 PHENOLIC-CARBON*

Reference/ Designation	Temperature, R	Measured Composite Conductivity (BTU in/hr ft^2 R)		Predicted Constituent Conductivity (BTU in/hr ft^2 R)	
		K_o	K_{90}	K_f	K_c
VIRGIN	550	6.3	8.8	20.8	2.69
	600	6.5	8.8	19.9	2.89
	700	6.8	9.4	21.9	2.96
	800	7.2	10.2	24.4	3.05
	900	7.6	11.3	28.1	3.09
	950	7.8	12.0	30.9	3.12
ZONE III	800	2.53	8.6	28.6	0.723
	1000	3.08	9.5	30.5	0.898
	1200	3.62	10.4	33.6	1.06
	1400	4.15	11.4	35.5	1.20
	1450	4.30	11.5	36.2	1.29
ZONE II	1000	1.85	31.0	122	0.477
	1200	2.00	"	122	0.517
	1400	2.15	"	120	0.558
	1800	2.43	"	120	0.633
	2400	2.71	"	119	0.748
	2800	3.16	"	119	0.829
ZONE I	2000	3.0	70.0	277	0.768
	2400	3.4	"	269	0.822
	2800	3.8	"	276	0.977
	3200	4.3	"	280	1.14
	3600	5.8	"	271	1.52
	4400	9.0	"	261	2.37

*Material description and smoothed composite conductivity data from Reference 1, except new K_{90} values from Section IV used for Zones II and I.

TABLE V-3 THEORETICAL VOLUME FRACTIONS OF CONSTITUENTS IN FM-5014 PHENOLIC-GRAPHITE**

Constituent Description	Wt. % of Virgin Mat'l	Density g/cc	Relative* Volume	Volume Percent		
				Virgin	Ablation Char	Furnace Char [5]
91LD Phenolic Resin	32	1.19 [1]	26.9	38.7	-	-
USP-6 Carbon Powder	13	1.9 [2]	6.8	9.8	9.8	10.2
WCA Reinforcement	55	1.6	34.4	49.5	49.5	51.4
Resin Char	16.0 [3]	1.9 [2]	8.4	-	12.1	12.6
Voids	0	0	1.4 [4]	2.0 [4]	28.6	25.8
Virgin Totals	100	1.44	69.5	100.0	-	-
Char Solids Totals	84.0 [3]		49.6		71.4	74.2
Ablation Char Totals	84.0		69.5	-	100.0	-
Furnace Char Totals	84.0		66.9 [5]	-	-	100.0
% Voids in Filled Resin or Pyrolysis Residue	-	-	-	4.0	58.6	53.1

**All notes except [5] same as Table XII . Material described in Reference 1.

[5] Adjusted for 3.8% shrinkage during charring.

TABLE V-4 PREDICTED CONSTITUENT THERMAL CONDUCTIVITIES IN FM-5014 PHENOLIC-GRAPHITE*

Reference/ Designation	Temperature R	Measured Composite Conductivity (BTU in/hr ft^2 R)		Predicted Constituent Conductivity (BTU in/hr ft^2 R)	
		K_o	K_{90}	K_f	K_c
VIRGIN [1]	600	9.60	27.5	89.7	2.92
	700	9.75	28.8	98.4	2.91
	800	9.96	33.2	112	2.94
	900	10.2	35.8	121	2.99
	1000	10.5	37.6	129	3.07
	1125	10.8	38.5	131	3.17
ZONE III	750	4.64	23.0	81.6	1.26
	900	5.00	24.1	84.7	1.37
	1100	5.50	25.4	88.9	1.51
	1300	6.00	26.8	93.4	1.65
	1450	6.37	28.2	98.6	1.76
ZONE II	1500	4.6	51.0	195	1.20
	1800	5.1	"	195	1.34
	2200	5.8	"	194	1.52
	2400	6.1	"	191	1.61
	2600	6.5	"	191	1.71
	2800	6.8	"	188	1.79
ZONE I [2]	2000	10.5	66.0	239	-
	2200	11.2	"	239	-
	2600	13.0	"	233	-
	3000	14.5	"	235	-
	3400	16.0	"	226	-
	3800	17.5	"	223	-
	4200	19.0	"	219	-
	4460	20.2	"	205	-

*Material description and smoothed composite conductivity data from Reference 1, except new K_{90} values from Section IV used for Zones II and I.

[1] Virgin K_o values corrected for plotting error in Reference 1.

[2] Linearized Zone I K_o estimates from Section IV of this report. No independent K_c values are obtained.

TABLE V-5 THEORETICAL VOLUME FRACTIONS OF CONSTITUENTS IN SC-1008/CCA-1 PHENOLIC-CARBON*

Constituent Description	Wt.% of Virgin Mat'l.	Density g/cc	Relative Volume	Vol % of Virgin Mat'l.
SC1008 Phenolic Resin	32.5	1.21	26.9	38.2
CCA-1 Reinforcement	67.5	1.80	37.5	53.3
Virgin Voids	0	0	6.0	8.5
Virgin Totals	100.0	1.42	70.4	100.0

TABLE V-6 PREDICTED CONSTITUENT THERMAL CONDUCTIVITIES IN SC-1008/CCA-1 PHENOLIC-CARBON*

Temperature R	Measured Composite Conductivity (BTU in/hr ft^2R) K_0	K_{90}	Predicted Constituent Conductivity (BTU in/hr ft^2R) K_f	K_v
410	3.92	7.2	18.8	1.22
510	4.34	8.45	22.8	1.30
660	4.92	9.3	24.7	1.49
810	5.5	10.0	26.0	1.71
960	6.05	10.8	27.8	1.89
1160	5.35	11.6	32.9	1.52

* Material Description and Smoothed Composite Conductivity Date for Material i-2 in Reference 31

TABLE V-7 THEORETICAL VOLUME FRACTIONS OF CONSTITUENTS IN SC-1008/WCB PHENOLIC-GRAPHITE *

Reference Designation	Constituent Description	Wt % of Virgin Mat'l	Density g/cc	Relative Volume	Vol. % of Virgin Mat'l
a-1	SC 1008 Phenolic Resin	29.0	1.21	24.0	34.6
a-2	"	38.2	1.21	31.6	45.0
a-3	"	52.0	1.21	42.9	58.9
a-1	WCB Reinforcement	71.0	1.6	44.3	63.9
a-2	"	61.8	1.6	38.6	55.0
a-3	"	48.0	1.6	30.0	41.1
a-1	Virgin Voids	0	0	1.1	1.5
a-2	"	0	0	0	0
a-3	"	0	0	0	0
a-1	Virgin Totals	100	1.44	69.4	100
a-2	"	100	1.43	70.2	100
a-3	"	100	1.37	72.9	100

* Material Description In Reference 31 .

TABLE V-8 PREDICTED CONSTITUENT THERMAL CONDUCTIVITIES IN SC-1008/WCB PHENOLIC-GRAPHITE *

Reference Designation	Reinf. Vol. Fraction	Temperature R	Measured Composite Conductivity (BTU in/hr ft^2 R)		Predicted Constituent Conductivity (BTU in/hr ft^2 R)	
			K_o	K_{90}	K_f	K_V
a-1	0.64	410	6.90	22.0	57.4	1.12
a-2	0.55	410	4.60	21.0	66.6	1.03
a-3	0.41	410	3.90	16.5	68.2	1.45
a-1	0.64	510	8.20	36.0	99.2	1.24
a-2	0.55	510	6.80	25.0	77.2	1.59
a-3	0.41	510	4.6	19.8	81.7	1.70
a-1	0.64	660	8.90	41.4	114	1.33
a-2	0.55	660	8.40	28.2	86.0	2.00
a-3	0.41	660	5.12	23.0	96.4	1.89
a-1	0.64	810	9.30	42.0	115	1.39
a-2	0.55	810	8.84	29.7	90.8	2.09
a-3	0.41	810	5.24	24.8	104	1.93
a-1	0.64	960	9.70	45.2	125	1.44
a-2	0.55	960	8.26	30.4	94.0	1.93
a-3	0.41	960	5.25	25.8	106	1.93
a-1	0.64	1160	10.0	44.8	123	1.50
a-2	0.55	1160	8.15	30.3	93.5	1.90
a-3	0.41	1160	5.58	25.0	105	2.06

* Material Description and Smoothed Composite Conductivity Data From Reference 31 .

TABLE V-9 THEORETICAL VOLUME FRACTIONS OF CONSTITUENTS IN SC-1008/PLUTON B-1 (R-6300) PHENOLIC-CARBON

Material Designation	Constituent Description	Wt. % of Virgin Matl.	Density g/cc	Relative Volume	Vol. % of Virgin Matl.
i-3 in Ref. 31	SC 1008 Phenolic Resin	30	1.21	24.8	35.7
R-6300	SC 1008 Phenolic Resin	35	1.21	28.9	41.1
i-3 in Ref. 31	Pluton B-1 Reinf.	70	1.86	37.6	54.2
R-6300	Pluton B-1 (HP)	65	1.86	35.0	49.7
i-3 in Ref. 31	Virgin Voids	0	0	7.0	10.1
R-6300	Virgin Voids	0	0	6.5	9.2
i-3 in Ref. 31	Virgin Totals	100	1.44	69.4	100
R-6300	Virgin Totals	100	1.42	70.4	100

TABLE V-10 PREDICTED CONSTITUENT THERMAL CONDUCTIVITIES IN SC 1008/PLUTON B-1 PHENOLIC-CARBON *

Temperature, R	Measured Composite Conductivity (BTU in/hr-ft^{2}R)		Predicted Constituent Conductivity (BTU in/hr-ft^{2}R)	
	K_0	K_{90}	K_f	K_v
410	3.58	6.8	18.3	1.06
510	4.12	7.6	19.9	1.24
660	4.90	8.6	21.9	1.51
810	5.60	9.45	23.7	1.77
960	6.16	9.9	23.8	2.01
1160	6.10	10.0	24.6	1.97

* Material Description and Smoothed Composite Conductivity Data for Material i-3 in Reference 31. Nominal R-6300 Composites are Described in Reference 35.

APPENDIX VI

ELECTRICAL RESISTIVITY DATA FOR FM-5055A CHARS
GRAPHITIZED DURING MEASUREMENT

Electrical Resistivity in Cross Ply Direction			Electrical Resistivity in Ply Direction		
Temperature, K	Resistivity, ohm-cm x 10^2	Symbol Used in Figure	Temperature, K	Resistivity, ohm-cm x 10^3	Symbol Used in Figure
1041	2.48	●	1108	5.72	●
1061	2.39	●	1225	5.59	●
1093	2.34	●	1385	5.31	●
1174	2.26	●	1631	4.91	●
1191	2.23	●	1710	4.73	●
1234	2.14	●	1790	4.59	●
			1846	4.39	●
1131	2.22	□	1902	4.21	●
1234	2.12	□	1984	3.98	●
			2058	3.78	●
1505	1.84	□	2099	3.53	●
1536	1.79	□			
1563	1.79	□	1585	4.20	△
1635	1.75	□	1703	4.02	△
1665	1.75	□	1788	3.90	△
			1941	3.70	△
1155	2.05	△	2088	3.45	△
1266	1.96	△			
1277	1.96	△	2201	3.23	△
1612	1.78	△	2301	2.95	△
			2437	2.73	△
1766	1.71	△			
1873	1.61	△	1707	3.21	+
1998	1.51	△	1813	3.11	+
2108	1.39	△	2037	2.91	+
			2173	2.80	+
1561	1.56	○	2435	2.62	+
1866	1.50	○			
2100	1.37	○			
2240	1.24	○			
2438	1.08	○			
1695	1.31	◇			
1910	1.22	◇			
2094	1.15	◇			
2392	1.06	◇			
2607	0.956	◇			
2725	0.907	◇			

APPENDIX VII

THEORETICAL RELATIONSHIPS BETWEEN COMPOSITE AND CONSTITUENT THERMAL CONDUCTIVITIES

$\frac{K_f}{K_c}$	$P_f = 0.35$		$P_f = 0.40$		$P_f = 0.45$		$P_f = 0.50$	
	$\frac{K_0}{K_c}$	$\frac{K_{90}}{K_0}$	$\frac{K_0}{K_c}$	$\frac{K_{90}}{K_0}$	$\frac{K_0}{K_c}$	$\frac{K_{90}}{K_0}$	$\frac{K_0}{K_c}$	$\frac{K_{90}}{K_0}$
2.	1.268	1.032	1.313	1.033	1.359	1.034	1.407	1.033
3.	1.440	1.090	1.520	1.092	1.606	1.092	1.697	1.089
5.	1.655	1.225	1.789	1.226	1.938	1.223	2.101	1.214
7.	1.787	1.367	1.960	1.367	2.155	1.358	2.376	1.342
10.	1.912	1.585	2.126	1.582	2.374	1.564	2.660	1.534
14.	2.013	1.879	2.264	1.869	2.560	1.838	2.911	1.788
20.	2.101	2.321	2.387	2.301	2.731	2.249	3.147	2.168
32.	2.189	3.207	2.513	3.166	2.911	3.068	3.404	2.924
72.	2.282	6.164	2.650	6.047	3.112	5.794	3.701	5.431
100.	2.305	8.234	2.684	8.063	3.163	7.701	3.779	7.182
170.	2.330	13.409	2.721	13.103	3.220	12.466	3.866	11.559
300.	2.346	23.021	2.745	22.464	3.256	21.315	3.922	19.686
540.	2.355	40.766	2.760	39.744	3.278	37.650	3.956	34.686
1000.	2.360	74.777	2.768	72.864	3.291	68.959	3.976	63.437

	$P_f = 0.535$		$P_f = 0.57$		$P_f = 0.60$		$P_f = 0.63$	
2.	1.442	1.032	1.477	1.031	1.509	1.030	1.541	1.029
3.	1.765	1.087	1.835	1.083	1.898	1.080	1.963	1.076
5.	2.225	1.206	2.359	1.195	2.480	1.185	2.609	1.175
7.	2.547	1.326	2.734	1.308	2.908	1.291	3.095	1.272
10.	2.888	1.507	3.141	1.476	3.381	1.447	3.644	1.415
14.	3.195	1.745	3.517	1.696	3.827	1.650	4.174	1.601
20.	3.491	2.099	3.889	2.021	4.279	1.949	4.723	1.873
32.	3.821	2.801	4.314	2.664	4.809	2.538	5.384	2.406
72.	4.215	5.124	4.839	4.785	5.485	4.474	6.262	4.151
100.	4.320	6.746	4.982	6.264	5.674	5.823	6.514	5.364
170.	4.439	10.798	5.146	9.956	5.893	9.188	6.811	8.390
300.	4.517	18.319	5.255	16.810	6.041	15.431	7.014	14.000
540.	4.564	32.202	5.322	29.458	6.132	26.953	7.139	24.352
1000.	4.592	58.809	5.361	53.700	6.185	49.035	7.214	44.191

APPENDIX VIII

DERIVATION OF THE GENERALIZED VARIABLE DISPERSION EQUATION

One general form for the dilute dispersion equation is:

$$\frac{K - K_c}{K + X K_c} = P \left(\frac{K_d - K_c}{K_d + X K_c} \right)$$

A general form for the variable dispersion equation was derived[22] following the method used by Bruggeman[27] for the special case of spheres. Differentiating the above equation using $d \frac{u}{v} = \frac{vdu - udv}{v^2}$:

$$\frac{(X + 1) K_c \, dK}{(K + X K_c)^2} = \frac{dP \, (K_d - K_c)}{K_d + X K_c}$$

If a particle having conductivity K_d is introduced into a medium of conductivity, K, then K_c can be considered to be K, so, for a small additional P, the above result may be written:

$$\frac{dK}{(X + 1) K} = \frac{dP}{1 - P} \left(\frac{K_d - K}{K_d + XK} \right)$$

The factor 1-P in this equation adjusts the reference volume for using K in place of K_c. This result is decomposed into partial fractions and integrated between the limits $K = K_c$ at $P = 0$ and $K = K_d$ at $P = 1$. Rearranging:

$$\frac{K_d \, dK}{(K_d - K)(X + 1) K} + \frac{X d K}{(K_d - K)(X + 1)} = \frac{dP}{1 - P}$$

Integrating:

$$\frac{-1}{(X+1)} \log \frac{(K_d - K)}{K} - \frac{X}{(X+1)} \log (K_d - K) + \log C = -\log (1-P)$$

Writing the antilog:

$$\left(\frac{K}{K_d - K} \right)^{\frac{1}{X+1}} \cdot \left(\frac{1}{K_d - K} \right)^{\frac{X}{X+1}} \cdot C = \frac{1}{1 - P}$$

At $P = 0$ and $K = K_c$:

$$\frac{K_c^{\frac{1}{X+1}}}{K_d - K_c} \cdot C = 1 \; ; \; C = \frac{K_d - K_c}{K_c^{\frac{1}{X+1}}}$$

At $P = 1$ and $K = K_d$:

$$\frac{K_d^{\frac{1}{X+1}}}{K_d - K_d} \cdot C = \frac{1}{0} \; ; \; C \text{ is unrestricted}$$

Substituting the value for C and rearranging:

$$1 - P = \frac{K_d - K}{K_d - K_c}\left(\frac{K_c}{K}\right)^{\frac{1}{X+1}} \qquad \text{(Eqn. (6) in text)}$$

For the case of interest where reinforcement fibers are considered as cylinders perpendicular to the heat flow, $X = 1$. Substituting this value and forming the ratio K_d/K_c in the denominator gives:

$$1 - P = \frac{K_d - K}{\left(\frac{K_d}{K_c} - 1\right)K_c}\left(\frac{K_c}{K}\right)^{\frac{1}{2}}$$

Substituting $K_d = K_c \; (K_d/K_c)$ and combining terms:

$$1 - P = K_c\left(\frac{K_d}{K_c}\right) - K\left(\frac{K_d}{K_c} - 1\right) K_c^{\frac{1}{2}} \; K^{\frac{1}{2}}$$

Solving for K to the first power and dividing through by K_c gives:

$$\frac{K}{K_c} = \frac{K_d}{K_c} - (1 - P)\left(\frac{K_d}{K_c} - 1\right)\left(\frac{K}{K_c}\right)^{\frac{1}{2}} \qquad \text{(Eqn. (23) in text)}$$

This result is quadratic in $(K/K_c)^{1/2}$. Solving by the quadratic equation gives:

$$\left(\frac{K}{K_c}\right)^{\frac{1}{2}} = \frac{\left[(1-P)^2\left(\frac{K_d}{K_c}-1\right)^2 + 4\,\frac{K_d}{K_c}\right]^{\frac{1}{2}} - (1-P)\left(\frac{K_d}{K_c}-1\right)}{2}$$

(Eqn. (8) in text)

This last result is the form that yields a direct solution for dispersed cylinders perpendicular to the heat flow.

REFERENCES

1. Clayton, W. A., and Fabish, T. J., et al, "Thermal Properties of Ablative Chars", Technical Report AFML-TR-67-413, January 1967
2. Unpublished data and private communications from D. R. Flynn, H. E. Robinson, and I. L. Martz, Heat Transfer Section, National Bureau of Standards, Washington, D.C.
3. Lucks, C. F., "Armco Iron as a Thermal Conductivity Reference Material", to be published, Battelle Memorial Institute, Columbus Laboratories, Columbus, Ohio.
4. Wechsler, A. E., et al., "Development of High Temperature Thermal Conductivity Standards", Technical Report, AFML-TR-69-2, June 1969.
5. Noda, T., Inagaki, M., and Sekiya, T., "Kinetic Studies of the Graphitization Process - I Effect of Ambient Gas Phase on the Rate of Graphitization", Carbon Volume 3, 1965, pp. 175-180.
6. Yokokawa, C. Hosokawa, K., and Takegami, Y., "Low Temperature Catalytic Graphitization of Hard Carbon", Carbon, Vol. 4, pp. 459-465.
7. Yokokawa, C., Hosokawa, K., and Takegami, Y., "A Kinetic Study of Catalytic Graphitization of Hard Carbons", Carbon, Vol. 5, 1967, pp. 475-480.
8. Carslaw, H. S., and Jaeger, J. C., Conduction of Heat in Solids, Second Edition, Oxford, Clarendon Press, 1959, pp. 46-48.
9. Yamada, S., "A Review of Glasslike Carbons", DCIC Report 68-2, April 1968.
10. Loch, L. D., and Austin, A. E., "Fine Pore Structure - Crystallite Size Relationships in Carbons", Proceedings of the First and Second Conferences on Carbon, Buffalo, New York, 1956, pp. 65.
11. Kipling, J. J., et al., "The Helium Densities of Some Polymer Carbons", Carbon, Vol. 4, 1966, pp. 5-11.
12. Davidson, H. W., and Lostyz, H. H. W., "Impermeable Cellulose Carbon", G.E.C. Journal, Vol. 30, No. 1, 1963, pp. 22-30.
13. Yamada, S., Sato, H., and Ishii, T., "Properties and Use of Glassy Carbon", Carbon, Vol. 2, No. 2, 1964, pp. 253-260.
14. Powers, A. E., "Conductivity in Aggregates", Proceedings of the Second Conference on Thermal Conductivity, N.R.C., Ottawa, Canada, October 1962, pp. 280-309.
15. Eucken, A., "Thermal Conductivity of Ceramics Refractory Materials", Forsch. Gebiete Ingeneiur, B-3, Forschung Sheft No. 353, 16 pp. March-April, 1932.
16. Pinnick, H. T., "Electronic Properties of Carbons and Graphites", Proceedings of the First and Second Conferences on Carbon", Buffalo, New York, 1956, pp. 3.

17. Castle, J. G., Jr., "Heat Conduction in Carbon Materials", Proceedings of the First and Second Conferences on Carbon, Buffalo, New York, 1956, pp. 13.

18. Warren, B. E., "X-Ray Study of the Graphitization of Carbon Black", Proceedings of the First and Second Conferences on Carbon, Buffalo, New York, 1956, pp. 49.

19. Winslow, F. H., Baker, W. O., and Yager, W. A., "The Structure and Properties of Some Pyrolysed Polymers", Proceedings of the First and Second Conferences on Carbon, Buffalo, New York, 1956, pp. 93.

20. Jamieson, C. F., and Mrozowski, S., "Thermal Conductivities of Polycrystalline Carbons and Graphites", Proceedings of the First and Second Conferences on Carbon, Buffalo, New York, 1956, pp. 155.

21. Inokuchi, H., and Akamatu, H., "Electrical Conductivity of Organic Semiconductors", Solid State Physics, Vol. 12, Academic Press, N.Y., 1961.

22. Clayton, W. A., "Analytical Correlation of the State Dependent Thermal Conductivity of Phenolic-Carbon and -Graphite Chars", Masters Thesis for Department of Mechanical Engineering, Seattle University, Seattle, Washington, June 1969.

23. Clayton, W. A., Fabish, T. J., and Denman, G. L., "Effect of Ablation on Thermal Conductivity to 5000 R in Phenolic-Carbon and Phenolic-Graphite", AIAA/ASME 10th Structures, Structural Dynamics and Material Conference, April 1969, pp. 48-56.

24. Wang, L. S., and Tien, C. L., "A Study of Various Limits in Radiation Heat-Transfer Problems", Int. J. Heat and Mass Transfer, Pergammon Press Ltd., London, Vol. 10, November 1967, pp. 1327-1338.

25. Rayleigh, Lord, "On the Influence of Obstacles Arranged in Rectangular Order Upon the Properties of a Medium", The Philosophical Magazine and Journal of Science, Vol. 34, December 1892, pp. 481-502.

26. Belle, J., and Berman, R. M., et al., "Thermal Conductivity of Bulk Oxide Fuels", AEC Research and Development Report WAPD-TM-586, February 1967.

27. Bruggeman, D.A.G., "Dielectric Constant and Conductivity of Mixtures of Isotropic Materials", Annalen Physik, Vol. 24, 1935, pp. 636-679.

28. Cowan, R. D., "Pulse Method of Measuring Thermal Diffusivity at High Temperatures", J. of Applied Physics, Vol. 34, 1963.

29. Denman, G. L., "Thermal Diffusivity of Tantalum and Tantalum Alloys", Proceedings of the Sixth Conference on Thermal Conductivity, Dayton, Ohio, 1966.

30. Sanders, H. G., et al., "An Investigation of Some Thermal and Mechanical Properties of a Low-Density Phenolic-Nylon Ablation Material", NASA CR-66731, February 1969.

31. Pears, C. D., "The Thermophysical Properties of Plastic Materials from -50°F to Over 700°F", Technical Documentary Report No. ML-TDR-64-87, Part I, August 1964, and Part II, April 1965.

32. Farmer, R. W., "Thermogravimetry of Phenol-Formaldehyde Polycondensates, Part II — Empirical Kinetic Parameters", Technical Report AFML-TR-65-246, Part II, March 1967.

33. Hillberg, L. H., "The Improved Convective Heating and Ablation Program (CHAP)", Boeing Document D2-126104-1, June 1969.

34. Barry, W. T., and Fisher, E. G., "Design and Testing of Ablation Models with Controlled Pressure Gradients", AIAA/ASME 10th Structures, Structural Dynamics and Materials Conference, April 1969, pp. 89-95.

35. "Reentry Materials Handbook", Aerospace Corporation, Report No. TOR-1001 (S2855-20)-3, December 1967.

36. "Reentry Systems Environmental Protection (RESEP) Program, Task 2 — High Performance Heat Shields", Semiannual Report, SAMSO TR-68-85, October 1967.

37. Private communications from C. M. Pyron, Thermodynamics Section, Southern Research Institute, Birmingham, Alabama.

UNCLASSIFIED
Security Classification

DOCUMENT CONTROL DATA - R&D

(Security classification of title, body of abstract and indexing annotation must be entered when the overall report is classified).

1. ORIGINATING ACTIVITY (Corporate author)
The Boeing Company, Aerospace Systems Division
P.O. Box 3999
Seattle, Washington 98124

2a. REPORT SECURITY CLASSIFICATION
Unclassified

2b. GROUP

3. REPORT TITLE

Thermal Conductivity of Phenolic-Carbon Chars

4. DESCRIPTIVE NOTES (Types of report and inclusive dates)
Final Report (1 April 1968 to 30 September 1969)

5. AUTHORS (First name, middle initial, last name)
Clayton, Wilson A., Fabish, Thomas J., Lagedrost, John F.

6. REPORT DATE	7a. TOTAL NO. OF PAGES	7b. NO. OF REFS
December 1969	192	37

8a. CONTRACT OR GRANT NO.	9a. ORIGINATOR'S REPORT NUMBERS
AF33615-68-C-1416	none
b. Project No. 7831	
c Task No. 783106	9b. OTHER REPORT NO(S) (Any other numbers that may be assigned this report)
d.	AFML-TR-69-313

10. DISTRIBUTION STATEMENT
Distribution of this document is unlimited.

11. SUPPLEMENTARY NOTES	12. SPONSORING MILITARY ACTIVITY
	Air Force Materials Laboratory Air Force Systems Command Wright-Patterson Air Force Base, Ohio 45433

13. ABSTRACT

The thermal conductivity of several phenolic-carbon and phenolic-graphite ablative composites was established as a function of layup angle and temperature for ablation heating or cooling from -10°F to over 5000°F. Conductivity was measured on virgin and charred FM-5055A phenolic-carbon as a function of layup angle and heating or cooling temperature to 5000°F. These measurements, plus new measurements on charred MX-4926 phenolic-carbon and FM-5014 phenolic-graphite were made by the steady-state, unidirectional, comparative disk method. Furnace charred conductivity specimens were shown to represent ablation chars by detailed characterization and by comparative thermal diffusivity measurements. Theory relating the constituent (cloth and matrix) and composite conductivities was used to correlate the new conductivity data and literature data on composites having the same reinforcements. The procedure provides correlated constituent conductivities for CCA-1 standard and high purity carbon cloth, WCA and WCB graphite cloth, and carbon powder filled and unfilled 91-LD and SC 1008 virgin or charred phenolic resins, from which the conductivity of virgin or charred composites is obtained within the accuracy of composite conductivity measurements. All results are expressed as equations for direct substitution in ablation computer programs, which was demonstrated for ballistic reentry ablation of FM-5055A phenolic carbon. The thermal conductivity of all carbon or graphite cloth reinforced phenolics increases versus layup angle and reinforcement volume fraction, is reduced by pyrolysis generated porosity, and increases in the mature char versus temperature and the degree of graphitization.

DD FORM 1 NOV 65 1473
U3 4802 1030 REV 7/66
PART 1 OF 3

UNCLASSIFIED
Security Classification

14. KEY WORDS	LINK A		LINK B		LINK C	
	ROLE	WT	ROLE	WT	ROLE	2 T
THERMAL CONDUCTIVITY						
CHAR						
ABLATION						
PHENOLIC-CARBON						
PHENOLIC-GRAPHITE						